SCHOOL OF ENGINEERING

The Department of Civil engineering and Industrial Design

Lateral Impact Responses of Steel End Plate Beam-to-Column Connections

Thesis submitted in accordance with the requirement of the University of Liverpool for the degree of Doctor of Philosophy in Civil and Structural Engineering

By

Ali Al-Rifaie

B.Sc. Building and Construction Engineering

M.Sc. Structural Engineering

January 2018

DEDICATION

To the spirit of that strong and gentle soul who spent his life for me….

My father;

To my mother for her deep love;

To the spirit of my brother, Ibrahim;

To my wife Ayat Al-zubaidi for her support and encouragement;

Finally, to my beloved children, Hasan and Ayat;

I dedicate this work.

ACKNOLEDGMENTS

I would like to express my sincere gratitude to my primary supervisor, Dr. Zhongwei Guan for his guidance, support, encouragement and positive feedback in every step of the PhD research. I also would like to express my thankfulness to my second supervisor, Dr. Steve Jones for his positive advice and suggestions. I am also grateful to Dr. Robert Birch and Dr. Alaa Al-Husainy for their assistance with using the laser Doppler equipment and the processing of the experimental data.

I would like to acknowledge the financial support given by the Ministry of Higher Education and Scientific Research in Iraq. The efforts given by Al-Muthanna University to nominate me for this scholarship are really appreciated.

I would like to thank the staff of the School of Engineering at the University of Liverpool, especially Mr. Marc Bratley, Mr. Derek Neary, Mr. John Curran and Mr. Glen Friel for their assistance in the experimental work.

I would not have been able to accomplish my goals had it not been for the support from my wife, Ayat Al-Zubaidi, whose patience is infinite throughout the ups and downs in my study.

LIST OF PUBLICATIONS

Journal Papers:

A. Al-Rifaie, Z.W. Guan, S.W. Jones, Q. Wang (2017). Lateral impact response of end-plate beam-column connections. Engineering Structures, 151, 221-234

A. Al-Rifaie, S.W. Jones, Q. Wang, Z.W. Guan (2017). Experimental and numerical study on lateral impact response of concrete filled steel tube columns with end plate connections. (Submitted to International Journal of Impact Engineering)

Conference Papers:

A. Al-Rifaie, Z.W. Guan, S. Jones (2017), Quasi-Static Analysis of End Plate Beam-to-Column Connections. World Academy of Science, Engineering and Technology, International Science Index 127, International Journal of Civil, Environmental, Structural, Construction and Architectural Engineering, 11(7), 936 - 941.

A. Al-Rifaie, Z. Guan, S. Jones (2017), A Methodology of Testing Beam to Column Connection under Lateral Impact Load, World Academy of Science, Engineering and Technology, International Science Index 127, International Journal of Civil, Environmental, Structural, Construction and Architectural Engineering, 11(7), 942 - 945.

ABSTRACT

This thesis provides an investigation on the lateral impact response of the standard end plate beam-column connections using ordinary bolts and the end plate beam to CFST column connections using a long bolt technique.

A series of full-scale beam-to-column connection specimens are fabricated and tested under lateral quasi-static and lateral impact loading. The material properties of concrete and steel profiles involved in the experimental work are also tested. A stiff reaction frame is designed and fabricated to mount the specimens against floor during the test. The most common types of beam-to-column connections, named flush plate connection (FPC) and partially depth end plate connection (PDEPC), are selected to be studied in this thesis. The effects of impact loading location and end plate thickness on the connection response for the aforementioned connection types with ordinary and long bolts are firstly investigated experimentally.

The experimental observations show that the deformation modes are not significantly influenced by changing the loading type (quasi-static or impact loading) and the loading location. However, changing the plate thickness has a significant effect on the deformation mode. Comparing the experimental results obtained for connections with long bolts with the standard connections has demonstrated the validity of using the long bolt technique against lateral impact loading, but bearing mind the potential reduction in the axial capacity of the impacted CFST due to the cracks produced in the concrete infill.

Three-dimensional finite element (FE) models are developed using the commercial code ABAQUS/Explicit to simulate the quasi-static and impact response of the specimens tested. All the FE modelling outputs are validated against the corresponding experimental results, with a good agreement. The finite element models on both the impact and the quasi-static tests have produced accurate predictions of the force-displacement relationships, strain time histories and deformation modes of the connections investigated. The validated FE models are further used to perform full-range analyses and parametric studies to obtain more

knowledge on the response of the end plate connections to both loading regimes. It is found that ABAQUS/ explicit is an effective tool to simulate the behaviour of end plate connections under quasi-static, provided using loading rate less than 0.67 mm/s and a mass scaling factor of 10^6. The full-range analyses have emphasized the validity of using the end plate with the long bolt technique under lateral impact loading, as the CFST column helps alleviate the internal forces in the connection. Based on the parametric studies performed, the deformation modes of connection are not changed even using different projectile shapes. Also, increasing the number of bolts delays the tearing failure of the partial depth end plate connection but does not alleviate the tensile forces in the first bolt. The validated models are also employed to predict the lateral impact response of another type of connections, namely extended end plate. It shows that it has a higher impact moment capacity than FPC and PDEPC by 25 and 61 %, respectively. Finally, based on the experimental results, the dynamic increase factors (DIFs) proposed varies between 1.25 and 1.38, whilst, the numerical results show that the maximum DIFs are 1.21, 1.16, 1.36 and 1.45 for first bolt, second bolt, axial capacity and moment capacity of both connections investigated, respectively.

NOTATIONS

$\dot{\varepsilon}^*$	strain rate ratio
$\dot{\varepsilon}_0$	reference quasi static strain rate
$\dot{\varepsilon}_p/\ \dot{\varepsilon}_{ref}$	ratio of equivalent plastic strain rate to a reference strain rate
$\bar{\varepsilon}_o^{pl}$	equivalent plastic strain
$A_\circ$	original cross sectional area of the tensile specimen tested
A_f	cross sectional area of the tensile specimen tested after fracture
DIF_{JC}	Dynamic increase factor of strain rate based on Johnson-Cook constitutive model
Q_i	hardening constants of the extended Voce hardening rule
T_h	homogenous temperature
θ_i	hardening constants of the extended Voce hardening rule
σ_{eng}	engineering stress
σ_{true}	true stress
σ_y	yield stress
$\dot{\varepsilon}$	current strain rate
ε_{eng}	engineering strain
$\varepsilon_{p,plate}$	equivalent plastic strain at the end of the yield plateau
ε_p	equivalent plastic strain
E_i	energy dissipated under impact load
ε_{true}	true strain
E_s	energy dissipated under quasi-static load
A_e	area of the contact element
C	strain rate constant.
c	Vertical distance away from the neutral axis

D	damage parameter
d_c	damage variable in compression
DIF	Dynamic increase factor
d_t	damage variable in tension of confined concrete
E	Modulus of elasticity of steel
E_0	elastic stiffeners
ε_{cc}	confined concrete strain
E_{cc}	elastic modulus
ε_{ck}	corresponding strain with the *fcc*
ε_u	corresponding strain with *fu*
f_{cc}	cylinder compressive strength for the confined concrete
f_{cd}	dynamic compressive strength of the concrete
f_{ck}	cylinder compressive strength of the concrete
f_{ck}	cylinder compressive strength of the concrete
f_{cs}	static compressive strength of the concrete
f_{cu}	cube compressive strength of the concrete
fi	field variable
f_{tc}	static tensile strength of the concrete
f_{td}	dynamic tensile strength of the concrete
f_u	ultimate force for the confined concrete
f_{yd}	dynamic yield strength of the steel
f_{ys}	static yield strength of the steel
I	Moment of inertia around the neutral axis
k	contact stiffness
K_B	bulk modulus
L	CFST column length
L_c	element size

m	constant
M	bending moment at the strain gauge location
M_p	Dynamic plastic moment of the CFST column
P_f	penalty stiffness factor
r	radius of the tube
u^{pl}	effective plastic displacement of element after damage onset
V	velocity
V_e	volume of contact element
w_c	crack width
w_{cc}	critical crack width
x	penetrated distance
δ_{max}	maximum displacement
$\theta^{'}$	Rotation angle at the end of tube
Θ	temperature
σ_{co}	compression failure stress
σ_{cu}	ultimate stress
σ_{to}	tensile failure stress
$\dot{\varepsilon}$	Strain rate
ε_{cp}	equivalent plastic strain in tension
$\dot{\varepsilon}_s$	static strain rate of the steel
ε_{tpl}	equivalent plastic strain in compression

Table of Contents

1 Chapter 1 : Introduction 1

1.1 Overview 2

1.2 Research objectives 6

1.3 Scope of the thesis 7

2 Chapter 2: Literature Review 9

2.1 Introduction 10

2.2 Steel connections types and classification 10

2.2.1 Connection to open sections 10

2.2.2 Connections to Concrete filled steel tube (CFST) columns 16

2.3 Structures under impact loads 18

2.3.1 Columns under impact loads 18

2.3.2 Connections under impact loads 26

2.4 Remarks and research originality 33

3 Chapter 3: Experimental Procedure 34

3.1 Introduction 35

3.1.1 The motivation of the proposed experimental work 35

3.2 Material testing 36

3.2.1 Concrete 36

3.2.2 Steel 37

3.3 Specimens preparation 39

3.3.1 Specimen designs through initial tests 39

3.3.2 Parameters to be investigated 41

3.3.3 Final design of test specimens 43

3.4 Test setup 49

3.4.1 Loading rigs 49

3.4.2 Mounting stiff frame 50

3.4.3 Final test setup 52

3.1 Instrumentations 55

3.1.1 Instrumentation used in impact test 55

3.1.2 Instrumentations used in quasi-static test 61

3.2 Summary 61

4 Chapter 4 : Experimental Results and Discussion 62

4.1 Introduction 63
4.2 Material test results 63
4.2.1 Concrete 63
4.2.2 Steel 64
4.3 Impact test results of connections to steel columns 67
4.3.1 The Effect of impact loading locations 68
4.3.2 The effect of plate thickness 74
4.3.3 Comparison between response of FPC and PDEPC 79
4.4 Quasi-static test results of the connection to steel columns 82
4.4.1 Deformation modes 82
4.4.2 Force-displacement relationships 83
4.5 Dynamic increase factors 85
4.6 Impact test results of connections to CFST columns 87
4.6.1 Deformation modes 88
4.6.2 Force-displacement relationships 93
4.7 Summary 101
5 Chapter 5: Numerical Procedure 102
5.1 Introduction 103
5.1 Modelling of the end plate connection under lateral impact loading 103
5.1.1 Geometries and boundary conditions 103
5.1.2 Element type and mesh size 106
5.1.3 Contact interactions 109
5.1.4 Material modelling 111
5.1.5 Simulation of impact loading 121
5.2 Modelling of end plate connection under quasi-static loading 121
5.2.1 Geometries and boundary conditions 122
5.2.2 Element type and mesh size 122
5.2.3 Contact interactions 126
5.2.4 Material modelling 126
5.2.5 Simulation of quasi-static loading 127
5.3 Summary 131
6 Chapter 6: Numerical Results and Discussion 132
6.1 Introduction 133
6.2 Modelling outcomes of end plate connections to steel columns 133

6.2.1 Validation of the modelling of impact results 133
6.2.2 Validation of the modelling of quasi-static results 145
6.2.3 The full range analyses of the structural response 150
6.2.4 Dynamic increase factors (DIFs) based on internal forces 158
6.2.5 Strain-rate distribution 161
6.2.6 Energy dissipation 162
6.2.7 Parametric study 164
6.3 Modelling outcomes of end plate connections to CFST columns 179
6.3.1 Validation of numerical results against experimental results 179
6.3.2 Full range analyses of the structural response 189
6.4 Summary 200
7 Chapter 7: Conclusions and Future Work 203
7.1 Introduction 204
7.2 The proposed future work 210

List of figures

Figure 1.1. Progressive collapse of Ronan Point Building in London 2

Figure 1.2. Catenary action due to column removal scenario in structural frames. 4

Figure 2.1. Classification of connections 11

Figure 2.2. Survey results of preferred method of connecting an open section beam to an open section column 12

Figure 2.3. Identification of the T-stub in the extended end plate connection. 13

Figure 2.4. Moment resistance connections. 14

Figure 2.5. Typical partial depth end plate connection. 14

Figure 2.6. Typical double web-angle connection. 15

Figure 2.7. Typical fin plate connection. 15

Figure 2.8. Typical cross section shapes for the CFST columns. 16

Figure 2.9. Traditional solutions to connect steel beams to CFST column. 17

Figure 2.10. Failure modes of the deformed specimens after lateral impact 20

Figure 2.11. Specimens under lateral impact load with different velocities 20

Figure 2.12. The validation of the numerical results against the experimental results for MDF1 specimen 22

Figure 2.13. Boundary conditions used by Qu et al. 24

Figure 2.14. The possible cause of lateral impact. 27

Figure 2.15. Experimental test setup adopted by Tyas et al. 28

Figure 2.16. Beam-to-column configuration adopted by Kang et al. 29

Figure 2.17. Impact analysis results of 2D frame with different vehicle speed 29

Figure 2.18. Test setup and connection details adopted by Grimismo et al. 32

Figure 3.1. Compressive test of concrete cubes. 37

Figure 3.2. Tensile test of steel specimens 38

Figure 3.3. Full details of the fabricated coupons of the steel materials (Dimensions in mm). 38

Figure 3.4. Steel structural frame of Beijing Corning LCD. 39
Figure 3.5. First proposal of test specimen. 40
Figure 3.6. Second proposal of test specimen. 40
Figure 3.7. Typical connection configuration used in the experimental investigation. 42
Figure 3.8. Details of parts used in the test specimens (dimensions in mm). 46
Figure 3.9. Welding of end plate to beam 47
Figure 3.10. Full details of specimens to be tested (dimensions in mm). 49
Figure 3.11. Impact rig components: (1) Drop hammer, (2) Quick release pin, (3) Switch panel (4) driven winch. 50
Figure 3.12. Mounting stiff frame: (1) Vertical mounted support (2) Bracer (3) Detachable clamp (4) Cross members (5) Floor mounted rail. 51
Figure 3.13. Schematic diagram of the test setup. 53
Figure 3.14. Details of detachable clamp. 53
Figure 3.15. Quasi-static test setup: (1) Loading ram (2) Steel sphere (3) Loading frame (4) Detachable clamp (5) Bracer (6) M20 thread bars (7) Box sections (8) Rigid steel beam 54
Figure 3.16. Quasi-static loading arrangement (1) Loading ram (2) steel sphere (3) column of specimen (4) LVDT. 54
Figure 3.17. Schematic arrangement of the Laser Doppler Velocimeter 56
Figure 3.18. Typical filtered velocity-time histories of the impact test. 57
Figure 3.19. Strain measurement system. 60
Figure 3.20. Locations of strain gauges on a specimen to be tested (Dimensions in mm). ... 61
Figure 4.1. Engineering stress-strain relationships for steel components. 65
Figure 4.2. Failure mode of steel coupons under uniaxial tensile loading. 66
Figure 4.3. Bending of the end plate under lateral impact load in specimens connected to steel columns 69
Figure 4.4. Bending of the first bolt pair 69

Figure 4.5. Fracture of the end plate close to the weld toe. (a) Specimen PFI8. (b) Specimen PNI8. 69
Figure 4.6. Typical stages of Load-displacement traces of selected specimen (FNI8). 72
Figure 4.7. Effect of impact load location on load-displacement traces of FPC to steel column. 72
Figure 4.8. Force-displacement traces of selected test specimens under impact load obtained by Grimsmo et al. 73
Figure 4.9. Effect of impact load location on load-displacement traces of PDEPC to steel column. 73
Figure 4.10. Slight bending of PDEPC with thick plate. 76
Figure 4.11. Flange crippling of steel column in PDEPC specimen with thick plate. 76
Figure 4.12. Flange crippling of steel column in FPC with thick plate. 76
Figure 4.13. Strain time history of SG2 located at end plate. 76
Figure 4.14. Strain time history of SG3 located at end plate. 77
Figure 4.15. Strain time history of SG1 located at column. 77
Figure 4.16. Effect of end plate thickness on load-displacement traces of FPC to steel column. 78
Figure 4.17. Effect of end plate thickness on load-displacement traces of PDEPC to steel column. 79
Figure 4.18. Comparison between the load-displacement traces of FPC and PDEPC to steel column loaded with lateral impact at L_1 with 8 mm end plate thickness. 81
Figure 4.19. Comparison between the load-displacement traces of FPC and PDEPC to steel column loaded with lateral impact at L_2 with 8 mm end plate thickness. 81
Figure 4.20. Comparison between the load-displacement traces of FPC and PDEPC to steel column loaded with lateral impact at L_1 with 15 mm end plate thickness. 82
Figure 4.21. Tearing failure close to the weld toe of specimen PNI8S under quasi-static load. 83

Figure 4.22. Force-displacement curves of the specimens loaded near the connection (FNI8S and PNI8S) under quasi-static load. 84
Figure 4.23. Force-displacement curves of the specimens loaded far away from the connection (FFI8S and PFI8S) under quasi-static load. 84
Figure 4.24. Force-displacement curve of specimen PNI8 under impact load and PNI8S under quasi-static load. 85
Figure 4.25. Dissipated energy of specimens tested under quasi-static load. 87
Figure 4.26. Bearing failure of first bolt row in specimen connected to CFST. 88
Figure 4.27. Bending of the end plate failure in specimens connected to CFST columns. 89
Figure 4.28. Tearing failure of PDEPC. 89
Figure 4.29. Bending failure of PDEPC specimen with thick plate. 90
Figure 4.30. Punching shear failure of CFST column around first bolt row. 91
Figure 4.31. Failure mode of FPC with thick plate. 91
Figure 4.32. Tearing failure of end plate of PDEPC connected to hollow tube. 91
Figure 4.33. Concrete cracks in CFST column. 92
Figure 4.34. Force-displacement relationships of specimen with hollow column (PF68) and CFST column (PFC8). 95
Figure 4.35. Effect of impact loading location on load-displacement traces of FPC to CFST column. 96
Figure 4.36. Effect of impact loading location on load-displacement traces of PDEPC to CFST column. 96
Figure 4.37. Effect of end plate thickness on load-displacement traces of PDEPC to CFST column. 97
Figure 4.38. Effect of end plate thickness on load-displacement traces of PDEPC to CFST column. 98
Figure 4.39. Comparison between the load-displacement traces of FPC and PDEPC to CFST column loaded with lateral impact at L_1 with 8 mm end plate thickness. 99

Figure 4.40. Comparison between the load-displacement traces of FPC and PDEPC to CFST column loaded with lateral impact at L_2 with 8 mm end plate thickness. 100
Figure 4.41. Comparison between the load-displacement traces of FPC and PDEPC to CFST column loaded with lateral impact at L_1 with 15 mm end plate thickness. 100
Figure 5.1. Geometries and boundary conditions of beam-to-column connection (dimensions in mm). 104
Figure 5.2. Modelling of the bolt (dimensions in mm). 105
Figure 5.3. The mesh of specimens connected to I-section steel columns..... 108
Figure 5.4. The element size effect on the accuracy of the FE model under impact loading. 108
Figure 5.5. The mesh of concrete infill. 109
Figure 5.6. Master and slave configuration in surface to surface contact 110
Figure 5.7. The contact penetration of the master surface into the slave surface 110
Figure 5.8. The formulation of the contact using Penalty method 112
Figure 5.9. Stress-strain curve with progressive damage degradation 114
Figure 5.10. Equivalent plastic strain-tri-axial stress state envelope developed by Ribeiro et al. 115
Figure 5.11. Concrete response under uniaxial loading in tension (a) and compression (b)117
Figure 5.12. Stress-strain relationship of confined and unconfined concrete 117
Figure 5.13. Stress-strain relationship of confined concrete used in the modelling. 120
Figure 5.14. Concrete material behaviour in tension. 120
Figure 5.15. The element size effect on the accuracy of the FEA model under quasi-static loading. 124
Figure 5.16. The modelling of tensile test of 8 mm steel plate and the validation of using the adopted mesh size. 125
Figure 5.17. The mesh of specimen PFI8C connected to I-section steel columns under quasi-static loading. 126

Figure 5.18. The adopted procedure to select the optimum loading rate and mass scaling factor in quasi-static modelling using Abaqus/Explicit. 129
Figure 5.19. Deformation mode with a mass scaling factor of 10^8 and different loading rates. 130
Figure 5.20. The dynamic effect with a loading rate of 0.5 mm/s and different mass scaling factors..... 130
Figure 5.21. Typical smooth step amplitude used in quasi-static analysis. 131
Figure 6.1. Force-displacement traces of specimen FNI8 subjected to lateral impact load: comparison of experimental data with FE simulation..... 134
Figure 6.2. Force-displacement traces of specimen PNI8 subjected to lateral impact load: comparison of experimental data with FE simulation..... 135
Figure 6.3. Deformation mode of the specimen FNI8 under lateral impact load. 135
Figure 6.4. Validation of prying deformation of end plate in specimen PNI8. 135
Figure 6.5. Predicted the first crack location of the specimen FNI8 under lateral impact load. 136
Figure 6.6. Bearing deformation of first bolt under lateral impact load. 136
Figure 6.7. Comparison between the experimental and FE results of strain time histories of specimen FNI8. 137
Figure 6.8. Comparison between the experimental and FE results of strain time histories of specimen PNI8. 138
Figure 6.9. Force-displacement traces of specimen FFI8 subjected to lateral impact load: comparison of experimental data with FE simulation..... 139
Figure 6.10. Force-displacement traces of specimen PFI8 subjected to lateral impact load: comparison of experimental data with FE simulation..... 140
Figure 6.11. Comparison between the experimental and FE results of strain time histories of specimen FFI8..... 140
Figure 6.12. Comparison between the experimental and FE results of strain time histories of specimen PFI8..... 141

Figure 6.13. Force-displacement traces of specimen FFI15 subjected to lateral impact load: comparison of experimental data with FE simulation..... 142
Figure 6.14. Force-displacement traces of specimen PFI15 subjected to lateral impact load: comparison of experimental data with FE simulation..... 142
Figure 6.15. Validation of crippling of column flange in specimen PFI15. 143
Figure 6.16. Validation of crippling of column flange in specimen FFI15. 143
Figure 6.17. Validation of prying deformation of end plate in specimen PFI15. 143
Figure 6.18. Comparison between the experimental and FE results of strain time histories of specimen FFI15..... 144
Figure 6.19. Comparison between the experimental and FE results of strain time histories of specimen PFI15..... 144
Figure 6.20. Force-displacement traces of specimen FNI8S and PNI8S subjected to quasi-static load: comparison of experimental data with FE simulation. 146
Figure 6.21. Force-displacement traces of specimen FFI8S and PFI8S subjected to quasi-static load: comparison of experimental data with FE simulation. 146
Figure 6.22. Deformation mode of specimen PNI8S under quasi-static load: comparison between experimental observations and numerical results. 147
Figure 6.23. Comparison between the experimental and FE results of strain time histories of specimen FNI8S..... 148
Figure 6.24. Comparison between the experimental and FE results of strain time histories of specimen FFI8S. 148
Figure 6.25. Comparison between the experimental and FE results of strain time histories of specimen PNI8S..... 149
Figure 6.26. Comparison between the experimental and FE results of strain time histories of specimen PFI8S. 149
Figure 6.27 Internal tensile force time histories of the first bolt row of specimens with thin plate connected to steel columns under impact load..... 151

Figure 6.28. Internal tensile force time histories of the second bolt row of specimens with thin plate connected to steel columns under impact load. 151
Figure 6.29. Internal tensile force time histories of the first bolt row of specimens with thick plate connected to steel columns under impact load. 153
Figure 6.30. Internal tensile force time histories of the second bolt row of specimens with thick plate connected to steel columns under impact load. 153
Figure 6.31. Internal bearing force time histories of the first bolt row of specimens connected to steel column using ordinary bolts under impact load. 154
Figure 6.32. Free body cut section 155
Figure 6.33. Internal axial resistance time histories of the specimens with thin plate connected to steel columns under impact load. 155
Figure 6.34. Internal axial resistance time histories of the specimens with thick plate connected to steel columns under impact load. 156
Figure 6.35. Internal moment resistance time histories of the specimens with thin plate connected to steel columns under impact load 157
Figure 6.36. Internal moment resistance time histories of the specimens with thick plate connected to steel columns under impact load. 158
Figure 6.37. The locations of critical places selected to investigate the effect of strain rate. 162
Figure 6.38. Average strain rate distribution at the selected critical places 162
Figure 6.39. Plastic energy dissipation of connection components. 163
Figure 6.40. Force-displacement traces of FPC with different masses and impact velocities. 165
Figure 6.41. Force-displacement traces of PDEPC with different masses and impact velocities. 166
Figure 6.42. Projectile configurations used in the parametric study. 167
Figure 6.43. Effect of projectile shape on force-displacement traces. 168

Figure 6.44. Displacement time histories for a selected specimen (PFI8) with different projectile configurations. 168
Figure 6.45. Effects of projectile shape on the internal forces of bolts..... 169
Figure 6.46. Three bolts configurations adopted to predict the effect of increasing number of bolts on the lateral impact response of connection. 170
Figure 6.47. Effect of increasing number of bolts on tearing failure in PDEPC. 170
Figure 6.48. Extended end plate connection geometry with three bolt rows. 171
Figure 6.49. Predicted failure mode of extended end plate under lateral impact load. 172
Figure 6.50. Predicted force-displacement traces of EEPC with different impact velocities. 173
Figure 6.51. Predicted internal forces produced in the bolts of EEPC under lateral impact load..... 173
Figure 6.52. Predicted internal moment resistance time histories of different connection configurations. 174
Figure 6.53. Energy dissipation of end plate in different connection configurations. 174
Figure 6.54. Stiffened EEPC configuration. 175
Figure 6.55. Failure mode of stiffened EEPC under lateral impact load. 175
Figure 6.56. Predicted internal forces produced in the bolts of stiffened and unstiffened EEPC under lateral impact load. 176
Figure 6.57. Model geometry adopted to investigate the effect of boundary conditions. 177
Figure 6.58. Predicted force-displacement traces of a steel column connected from its both end and impacted in the middle by a flat projectile with different velocities. 178
Figure 6.59. Predicted internal force time histories of first bolt row for PDEPC and FPC with different boundary conditions. 178
Figure 6.60. Predicted internal force time histories of second bolt row for PDEPC and FPC with different boundary conditions. 179
Figure 6.61. Bearing deformation of first bolt row. 181
Figure 6.62. Prying deformation of PDEPC with thin plate. 181

Figure 6.63. Prying deformation of FPC with thin plate..... 181
Figure 6.64. Tearing failure of PDEPC with thin plate..... 181
Figure 6.65. Prying deformation of PDEPC with thick plate. 182
Figure 6.66. Punching shear of CFST around first bolt row. 182
Figure 6.67. FPC with thick plate after impact event. 182
Figure 6.68. Cracks of concrete infill around long bolts..... 182
Figure 6.69. Force-displacement traces of specimen PF68 subjected to lateral impact load: comparison of experimental data with FE simulation..... 183
Figure 6.70. Force-displacement traces of specimen FFC8 and FNC8 subjected to lateral impact load: comparison of experimental data with FE simulation. 184
Figure 6.71. Force-displacement traces of specimen PFC8 and PNC8 subjected to lateral impact load: comparison of experimental data with FE simulation. 184
Figure 6.72. Force-displacement traces of specimen FFC15 and PFC15 subjected to lateral impact load: comparison of experimental data with FE simulation. 185
Figure 6.73. Comparison between the experimental and FE results of strain time histories of specimen FNC8. 186
Figure 6.74. Comparison between the experimental and FE results of strain time histories of specimen FFC8 186
Figure 6.75. Comparison between the experimental and FE results of strain time histories of specimen PNC8. 187
Figure 6.76. Comparison between the experimental and FE results of strain time histories of specimen PFC8. 187
Figure 6.77. Comparison between the experimental and FE results of strain time histories of specimen FFC15. 188
Figure 6.78. Comparison between the experimental and FE results of strain time histories of specimen PFC15. 188
Figure 6.79. Comparison between the experimental and FE results of strain time histories of specimen PF68. 189

Figure 6.80. Internal tensile force time histories of the first bolt row of specimens connected to CFST column using long bolts under impact load..... 191
Figure 6.81. Internal tensile force time histories of the second bolt row of specimens connected to CFST column using long bolts under impact load. 192
Figure 6.82. Comparison between the internal tensile forces generated in the first bolt of both bolt techniques under lateral impact load. 192
Figure 6.83. Comparison between the internal tensile forces generated in the second bolt of both bolt techniques under lateral impact load. 193
Figure 6.84. Comparison between plastic energy dissipated in steel and CFST column..... 193
Figure 6.85. Internal tensile force time histories of the second bolt row of specimens connected to CFST column using long bolts under impact load. 195
Figure 6.86. Comparison between the bearing forces generated in the first bolt of both bolt techniques under lateral impact loading..... 195
Figure 6.87. Internal tying force time histories of specimens connected to CFST column using long bolts under impact loading. 197
Figure 6.88. Comparison between the internal tying forces of connections under lateral impact loading..... 197
Figure 6.89. Internal moment time histories of specimens connected to CFST column using long bolts under impact load..... 198
Figure 6.90. Comparison between the internal bending moment of connections under lateral impact load..... 199
Figure 6.91. Plastic dissipation energy of connection components. 200

List of tables

Table 2.1. Comparison between the theoretical and experimental results 23

Table 3.1. Concrete mix proportions. 36

Table 3.2 Matrix of parameters to be investigated in the experimental investigation. 44

Table 3.3. General settings of BSA..... 56

Table 3.4 Validation of measured strain using the strain measurement system developed and the theoretical strain. 59

Table 4.1. The equivalent cylinder compressive strength of concrete used in CFST specimens. 64

Table 4.2. Summary of material properties of steel profiles used in the experimental tests.. 65

Table 4.3. Summary of dissipated energies under-quasi-static and impact load and proposed DIFs. 87

Table 4.4. Failure modes of test specimens connected to CFST columns. 93

Table 5.1 Mesh sizes selected to be investigated in mesh sensitivity study. 107

Table 5.2. Plasticity parameters for CDP model. 119

Table 5.3. Proposed mesh configurations for quasi-static analysis..... 123

Table 6.1. Summary of extreme internal forces under impact and quasi-static loads of connections and proposed DIFs. 160

Table 6.2. Summary of details and results of both connections with different masses and impact velocities. 165

Chapter 1 : Introduction

1.1 Overview

The behaviour of structural members under static loading conditions has been studied extensively. Design regulations have also been provided in several design codes to help structural engineers to estimate the resistance of such members. Ronan point, which was a 22-storey building constructed in 1966 and completed on 11 March 1968 [1] in London, was one of the buildings that designed according to the design regulations in that time. A gas-stove leak occurred on the 18th floor in the apartment 90 of this building and the force of explosion knocked out the walls of this apartment, which represents the sole support for the walls directly above. Chain reaction was then created, in which floor 19 collapsed followed by the collapse of floor 20, and so on, propagating upward. The collapse of these floors then generated a sudden impact loading on floor 18 caused it to smash floor 17, progressing until it reached the ground floor [2], as can be seen in Figure 1.1.

Figure 1.1. Progressive collapse of Ronan Point Building in London [Source: https://en.wikipedia.org].

This catastrophic event warned structural engineers to update the design regulations in order to prevent such collapse. Subsequently, building codes in some countries such as the United Kingdom, the United States and Canada were modified to include structural integrity or "robustness" provisions as an attempt to prevent progressive collapse. Unfortunately, these updates seem to be insufficient to totally prevent progressive collapse of a building particularly with the increasing of terrorist attacks to buildings. Hence, the collapse of Ronan point was followed by more catastrophic events such as the collapse of World Trade centre (WTC) in September 2001, terrorist's bomb trains in Madrid in 2004 and Mumbai attack in 2008. The researchers realised the importance of understanding the response of structural members under accidental loads such as impact, blast and fire. Therefore, a considerable amount of studies were published to investigate the response of structural members under such loads. Most of these studies were focused on fire [3] or seismic hazard [4]. For the past decade, research on the study of the behaviour of structural members under impact and blast loads is increasing. It was indicated that connections subjected to impact loads needs to be understood to improve the performance of this critical component in structural frames. Also, reports issued after the WTC collapse [5, 6] noted that a lack of knowledge on the dynamic behaviour of connections still need to be covered.

It is worth mentioning that most research related to progressive collapse was based on column removal scenario [7, 8]. In this scenario, it is assumed that a column lose its capacity in a certain time duration producing which is called catenary action, as can be seen in Figure 1.2. Due to the catenary action, the beam-to-column connection would be under dynamic loading with different loading rates according to the time required for the removed column to lose its full capacity. Another important scenario that may cause the progressive collapse is called falling floor impact [9, 10] at which the debris of falling floor attempt to hit the floor underneath producing dynamic stresses on the members that form the floor underneath.

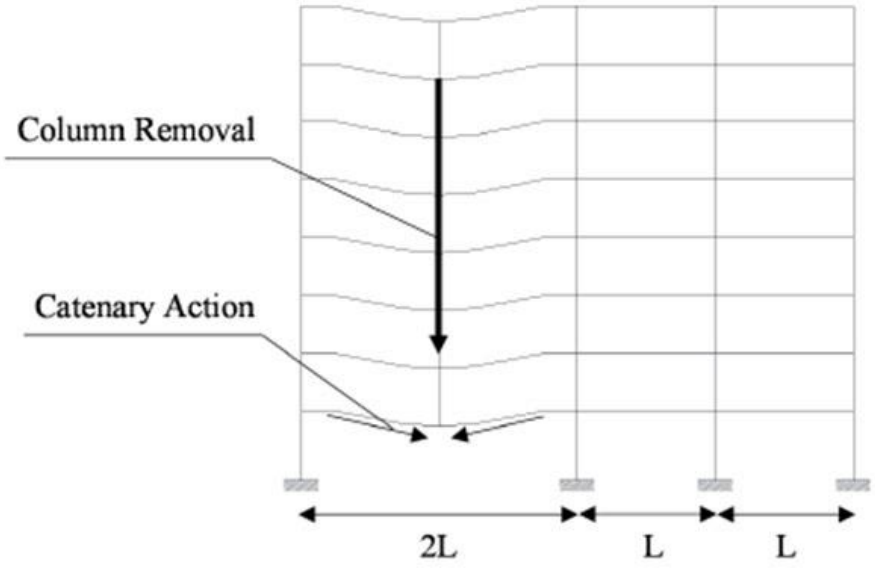

Figure 1.2. Catenary action due to column removal scenario in structural frames.

During the service life, structural members may experience impact loading due to vehicle, airplane or flying debris impact which may lead the column to lose part or all of its loading carrying capacity, which may be followed by a progressive collapse. Therefore, studies were carried out to investigate the response of columns under the lateral impact loading scenario. Different types of columns including steel and concrete filled steel tube (CFST) [11-13] were investigated under lateral impact load. It was found that the energy absorption and ductility were enhanced if the CFST column were used [14, 15]. As the columns in a structural frame must be connected to beams using an appropriate connection, it will be necessary to investigate the connection response to lateral impact loading, particularly if the connection strength is lower than column strength as in the cases of simple and semi-rigid connections. In spite of the numerous researches that were dedicated to investigate the lateral impact response of columns, there is hardly any study to investigate the connection response to such loads. This will be presented in more details in the next chapter to show this gap of knowledge. Therefore, attention should be given to study and understand the response of beam-to-column connections to lateral impact loading, particularly for connections with no

full-strength. It is therefore decided to investigate the end plate connection in the current study amongst the other types as it is the most common connection type used in practice.

For the past two decades, concrete filled steel tube (CFST) columns have been increasingly used in structural frames as an alternative option to steel and reinforced concrete columns. CFST columns have a better fire resistance than steel and reinforced concrete columns, which results in a reduction in the use of fireproof materials [16]. Also, CFST columns provide a high load carrying capacity due to the interaction between the concrete infill and the steel tube [17]. In addition to these features, CFST columns provide a lower cost and time of construction than those required for reinforced concrete column, as the labour of formwork and reinforcing bars is omitted. Despite the advantages of using CFST columns in construction, there are some difficulties to connect them to steel beams using the ordinary bolts. Some techniques were developed in order to sort this disadvantage out such as reverse channel, long bolts and flow-drill techniques. It was found that the end plate connection with long bolt provides a good resistance to static and even seismic loads, which will be discussed in the next chapter. To expand the work in the current study, it will be valuable to evaluate the resistance of beam-to-CFST column connection to lateral impact load, particularly with the confirmation of its good performance against seismic loading [18-20]. The evaluation of using the long bolts technique under lateral impact load can be achieved by comparing their behaviour with the standard connection using ordinary bolts.

It will also be useful if the current study enters the structural design field to help the engineers to predict the dynamic effect that the connections experience due to the lateral impact loading. This will be achieved by comparing the response of connection under quasi-static and impact loading followed by proposing dynamic increase factors (DIFs). It should be mentioned that undertaking this work experimentally needs considerable cost, which is not available in the budget of the current study, particularly with adopting using full scale specimens in the tests. Therefore, the finite element analysis can be employed to minimize the cost by reducing the number of specimens tested. If the finite element models are

validated properly against the experimental results, these models will provide better understanding to the entire response of connections. Also, different parameters can be investigated using the validated models. Here, the finite element code ABAQUS is employed to simulate all the experimental tests and to investigate the effect of different parameters.

1.2 Research objectives

This research is focused on the following objectives

i) To experimentally investigate the lateral impact response of standard end plate connections that used to connect steel beam to steel columns using ordinary bolts.

ii) To experimentally evaluate the lateral impact resistance of end plate connections that used to connect steel beams to CFST column using the long bolt technique by comparing with the experimental results of the standard connections.

iii) To develop the finite element models to assist with predicting the structural response of such connections subjected to quasi-static and low velocity lateral impact as well as to validate the models with the experimental results.

iv) To use the validated finite element models for further investigation of the lateral impact response of the end plate connection with ordinary bolts.

v) To use the validated finite element models for further evaluation of the use of end plate connections that used to connect steel beams to CFST column using the long bolt technique.

vi) To use the validated finite element models for further parametric studies to predict the effect of other parameters that might affect the lateral impact response of beam-to-column connections rather than the parameters investigated experimentally.

vii) To use the experimental and finite element results to propose dynamic increase factors in which the dynamic effect can be estimated.

1.3 Scope of the thesis

The scope of this thesis includes investigating the lateral impact response of beam-to-column connections with end plate experimentally and numerically. Also, it includes evaluating the use of long bolts technique to resist the lateral impact loading.

The review of previous studies related to columns and connections under impact loadings is presented in Chapter 2. The experimental investigations and numerical studies relevant to the current study are included.

In Chapter 3, the experimental work procedures are described, including the materials tests, preparations of structural testing samples and concrete mix design. This chapter also includes the test setup and the description of instrumentations used for both lateral impact and quasi-static tests conducted in this study.

The experimental results obtained from impact and quasi-static tests are presented and discussed in Chapter 4. The load-displacement traces and the deformation/failure modes of all specimens tested are also presented in this chapter. Moreover, effects of various parameters on the connection response to lateral impact are discussed. The dynamic increase factors are also proposed based on the experimental force-displacement traces.

Chapter 5 presents the development of the finite elements models to simulate the structural behaviour of the steel column and CFST column connected to beams with an end plate connection under quasi-static and lateral impact loading. This chapter describes the constitutive models of steel and concrete in the elastic, plastic and damage stage. The assumptions used to model the interactions between various components, as well as the boundary conditions are also presented.

After selection of the suitable modelling approaches in Chapter 5, the finite element models developed are rigorously validated in Chapter 6 against the experimental results obtained from Chapter 4. The validated models are then employed to investigate the internal forces generated in the connection zone such as the bolt forces, axial capacity and moment

capacity. Also, the dynamic increase factors are proposed in this chapter based on the internal forces obtained. Parametric studies are also conducted in this chapter based on the validated models to investigate effects of other parameters on the lateral impact response of the connections.

Finally, Chapter 7 presents conclusions drawn from the experimental and numerical results, and recommendations for future work.

Chapter 2: Literature Review

2.1 Introduction

In this chapter, the most common beam-to-column connection types currently used in practice are presented. Also, the difference between the connections to steel columns and CFST columns is discussed. Then, the previous work relevant to the current research is reviewed. The previous studies related to the response of steel columns and CFST columns to lateral impact load are presented first. Following on that, the studies on the response of beam-to-column connection are presented. The gap of knowledge is then specified based on the previous studies and the originality of the current study is then stated.

2.2 Steel connections types and classification

The beam-to-column connection is an important part of any steel building, since it provides the strong link between the other structural components and contributes to overall building integrity. The first attempt to fabricate steel connections was realised by using rivets, which however rarely been used since the 1950's. Nowadays, steel connections are fabricated mainly using bolts and/or welding. The behaviour of the connection of a structural frame is complex as a wide range of parameters involved. Consequently, many studies were carried out to investigate the behaviour of beam-to-column connections. The relevant research is still continuous to improve understanding of the behaviour of such connections and design methods. Glenn et al. [21] mentioned that the first study on the behaviour of beam-to-column connections was conducted on riveted connections by Wilson and Moore [22]. Since then many studies into the behaviour of beam-to-column connections have been reported. However, different types of connections were developed and their design procedures were presented in the code practices. The following sections are briefly reviewing the most common connections that used in practice.

2.2.1 Connection to open sections

Open sections refer to sections that are not hollow. Hence, I, H, channel and angle sections can be classified as open sections. Structural engineers have always distinguished two types of steel connections as either simple (pin) connections or moment resistance connections.

The simple connection is designed to resist shear and tension only, assuming no moment resistance. However, the moment resistance connections are designed to resist moment in addition to shear and tension. The studies showed that all connections, even for those that are considered to have no moment resistance (simple connections), have some capacity to resist bending moment [23-25].

2.2.1.1 Moment connections

Beam-to-column connections are classified by stiffness (as rigid, semi-rigid or nominally pinned) based on elastic analysis or by strength (as full strength, partially strength or nominally pinned) based on plastic analysis [26]. Figure 2.1 shows classification of connections. As long as the connection can resist at least 90% of the fixed-end moment, it can be classified as rigid. Whilst, if it cannot resist more than 50% of the fixed-end moment, it can be classified as semi-rigid [27]. Hence, both of rigid and semi-rigid connections are classified as moment resistance connections as they show considerable moment resistance. The semi-rigid and nominally pinned connections are the focus of this research as they are weaker and more vulnerable than rigid connections.

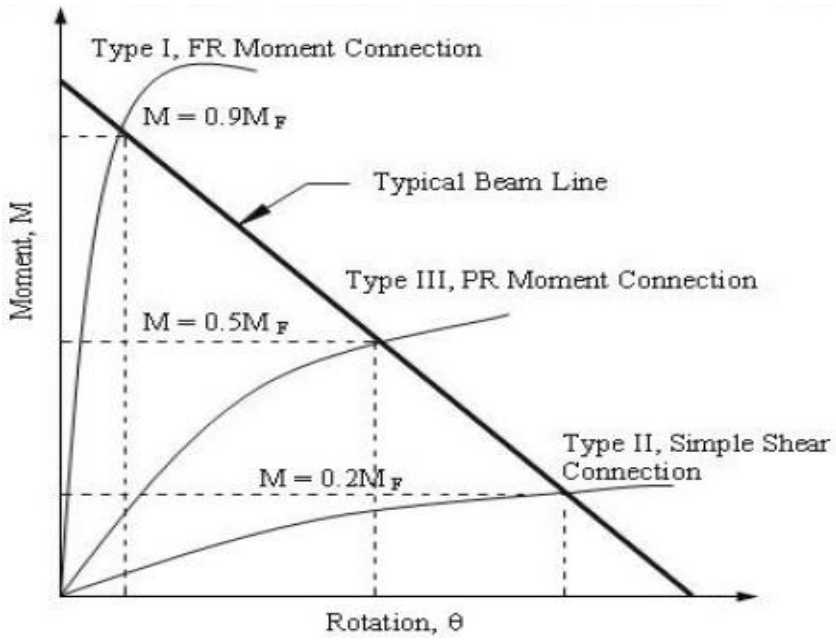

Figure 2.1. Classification of connections [27].

- Flush plate connections

It is called sometimes full depth end plate. In this type, an end plate is shop welded to the beam end along both the flanges and web, and then bolted to the column on site, as shown in Figure 2.4 (a). Number of bolt rows in tension zone may be increased and steel stiffeners may be added to increase the moment capacity of the flush plate connections [28]. It is the most popular connection currently used in the UK. This fact is recently emphasized by Kidd et al. [29] who conducted an online questionnaire, in which one of its targets was to specify the preferred method to connect a beam to a column using open sections. The questionnaire included the academic and steel industry communities. The results showed that 39% preferred using flush plate connections and 29% preferred the use of partial depth end plate connection as shown in Figure 2.2. Due to the popularity of this type of connections, many studies were conducted to investigate their behaviour under different loading regimes with different geometries [30-35].

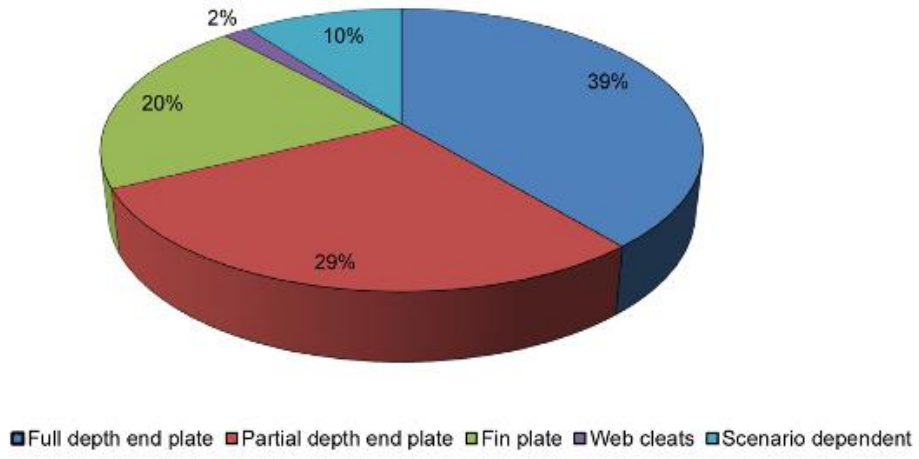

Figure 2.2. Survey results of preferred method of connecting an open section beam to an open section column [29].

- Extended end plate connections

Extended end plate connection is used to sustain high moments. Its configuration is similar to the flush plate connection but the end plate is extended to the tension side only, as shown

in Figure 2.4 (b) or to both the tension and compression sides. At least two bolt rows should be provided in the tension zone with one bolt row in the compression zone in extended end plate. Also, steel stiffeners may be added to enhance its moment capacity. Extended end plate connection is stronger than flush plate and it is classified as rigid and full strength connection [36].

- T-stub connections

This type of connection is fabricated by using T sections bolted to both the column and the beam flange as shown in Figure 2.4 c. This type of connection is no longer used in the UK but T-stub configuration is used by Eurocode to facilitate the analysis and design of end plate connections [37] as shown in Figure 2.3.

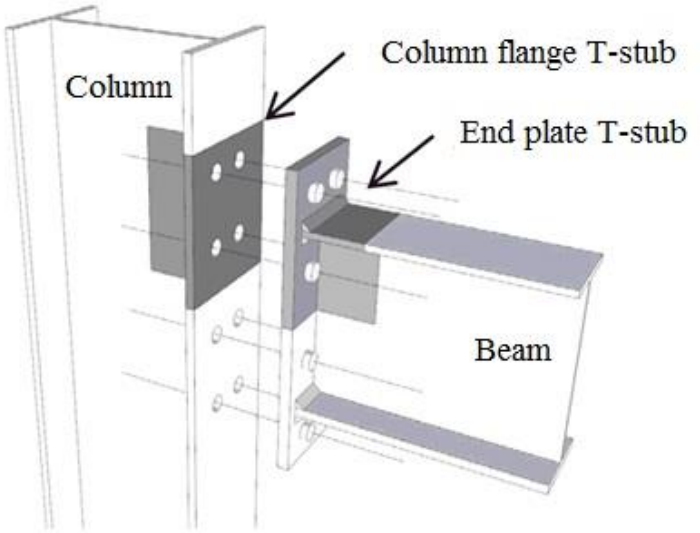

Figure 2.3. Identification of the T-stub in the extended end plate connection.

All of the above types could be used to connect a steel I-beam to steel an H-column section using ordinary bolts. However, ordinary bolts cannot be used if the column has hollow section such as circular and rectangular sections as no access is available to tighten the nuts.

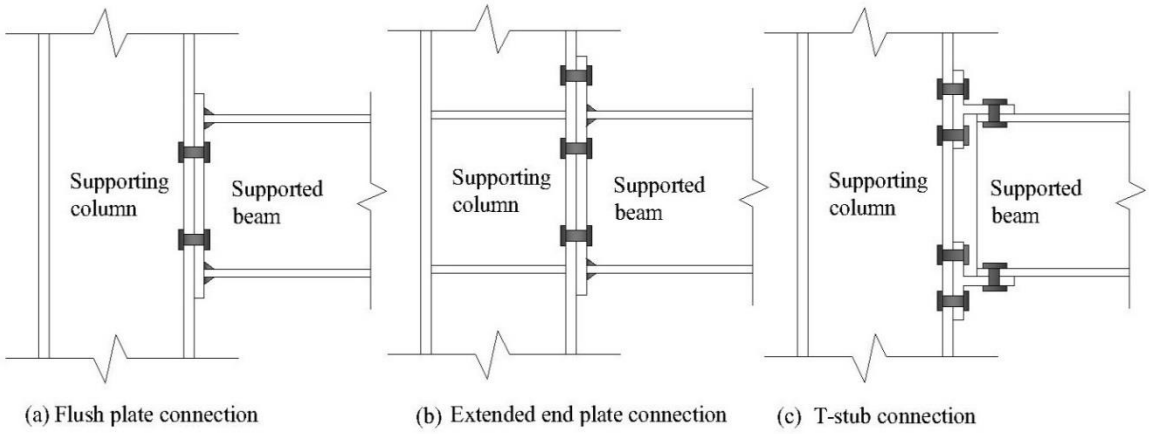

Figure 2.4. Moment resistance connections.

2.2.1.2 Simple connections

- Partial depth end plate connection

This type of connections is also classified as end plate connection. It contains an end plate, whose depth is less than the depth of the beam, welded to the beam web then bolted to the column, as shown in Figure 2.5. Accordingly, this type of connection is used mainly to transfer the vertical loads from the beam to the column.

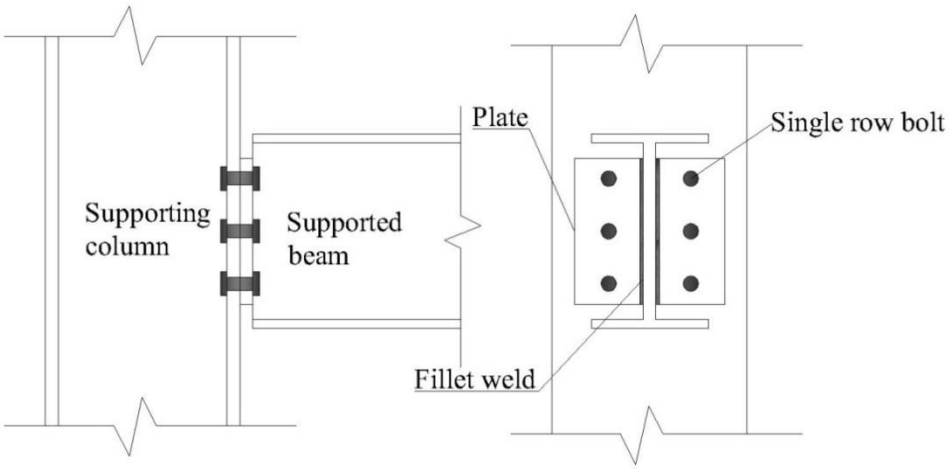

Figure 2.5. Typical partial depth end plate connection.

- Double web-angle (web-cleat) connection

In this type of the connections, two angles are bolted to both the column and the beam web, as shown in Figure 2.6. This type is no longer deemed as a standard connection as it requires

special surface treatment before assembly. Also, it cannot be used with skewed beam as in the end plate connection.

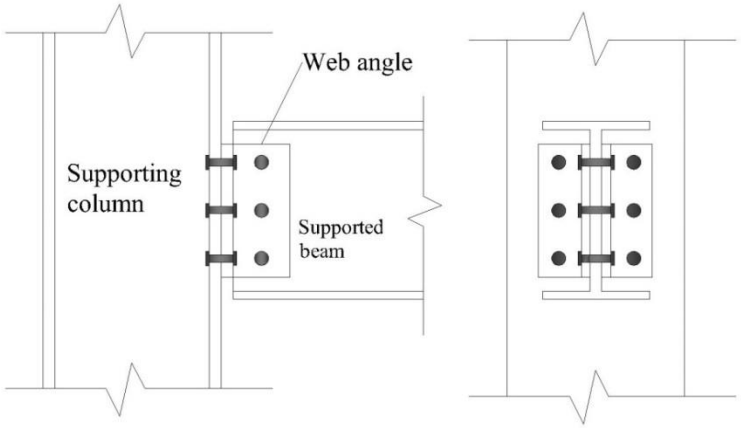

Figure 2.6. Typical double web-angle connection.

- Fin plate connection

In this type of connections, a single plate is welded to the column flange or web in work shop and then bolted in the field to the beam web, as shown in Figure 2.7. This type can easily accommodate off-centred and skewed beams and present no erection problems. Fin plate can be considered as the second best option after the end plate connection to provide a simple connection between beam and column.

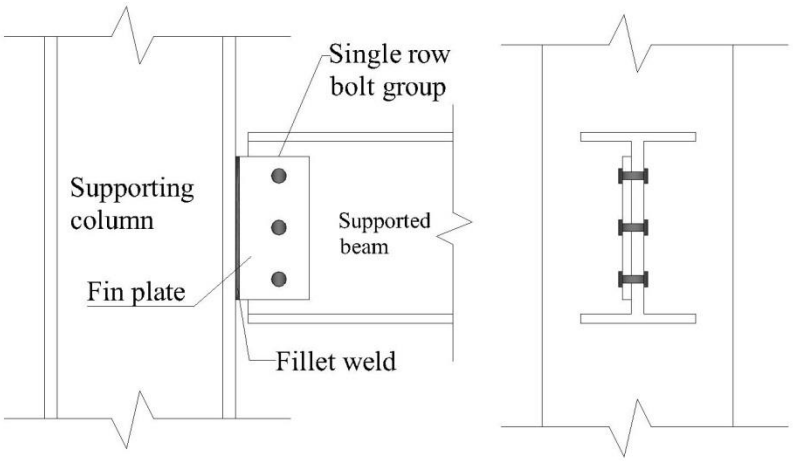

Figure 2.7. Typical fin plate connection.

2.2.2 Connections to Concrete filled steel tube (CFST) columns

The Concrete Filled Steel Tube is a system in which steel tube is filled with concrete. This system is used increasingly in many structural applications such as high rise buildings, bridges piers and offshore structures in addition to buildings in seismic zones [38-40].The stiffness and strength of CFST would increase due to confinement provided by steel tube. Meanwhile, the restraint of concrete delays the local buckling of tube wall. Also, the column formwork would be eliminated during construction leading to reduction in construction cost and time [16, 41]. Different cross sections of the tube could be used in CFST such as circular, square and rectangular, as shown in Figure 2.8 (a). However, some researchers have conducted studies on other section types such as hexagonal sections [42], elliptical sections [43, 44] and X section [45], as shown in Figure 2.8 (b).

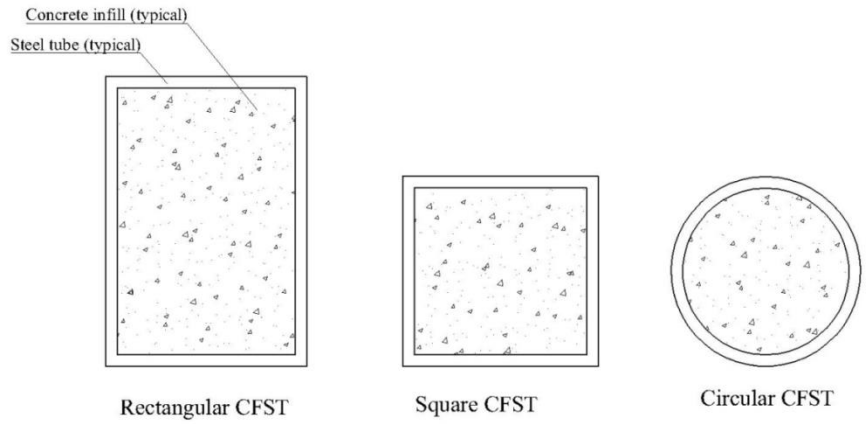

(a) The most widely used cross section shapes.

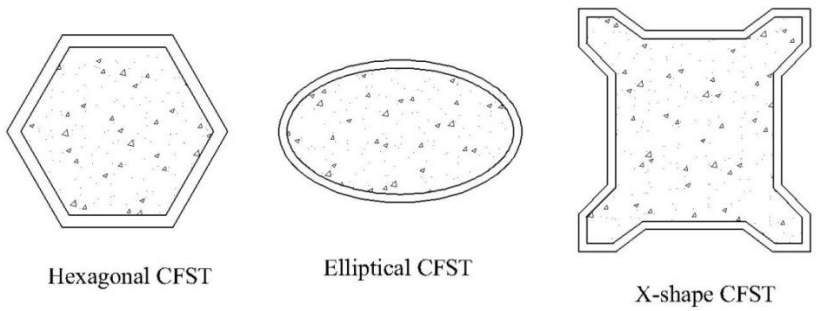

(b) Rarely used cross section shapes.

Figure 2.8. Typical cross section shapes for the CFST columns.

The main disadvantage of CFST columns is the inability to connect them to beams using ordinary bolts, as there is no access available like in open sections to tighten bolt nuts. For this reason, some of conventional connections used to connect open steel beam to open steel column using the ordinary bolts (discussed in Section 2.2) were modified to connect CFST columns to steel beams. However, the end plate connection as the most common type is modified by some researchers to connect a CFST column to beam. The following modifications are usually adopted in construction, as displayed in Figure 2.9, i.e. (1) the use of blind bolts or flowdrill connection, (2) the use of reversed U channel in addition to the use of long (through) bolts. Hoang et al. [46] found that using long bolts to connect the end plate connection to CFST column is the best solution comparing with the others. The fabrication cost is reduced using this solution and the flexural strength and stiffness is improved. Ikhlas et al. [47] investigated the end plate connection to CFST column using long bolts under cycling loading. The results demonstrated that the connections showed a good ductility up to large displacements. Several researches were performed on the application of using long bolts in composite structures, such as connections of steel-reinforced concrete column to steel beam and reinforced column to steel beam. The results showed its promising performance to resist seismic loads [18-20].

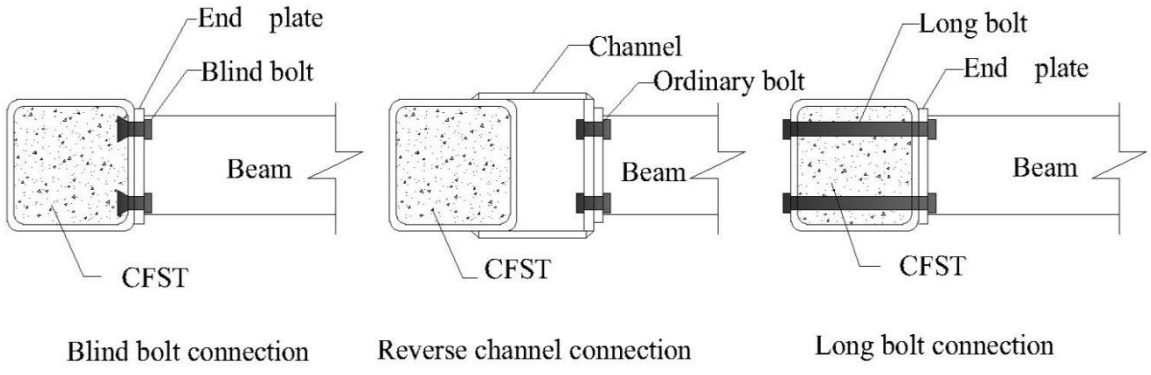

Figure 2.9. Traditional solutions to connect steel beams to CFST column.

2.3 Structures under impact loads

The behaviour of structural members under static loading conditions has been investigated extensively in the open literature, and several design procedures have been presented to determine their resistance. On the other hand, the behaviour of such members to severe impulsive loading like impact and blast is less documented. In the past four decades, structural engineers have given considerable attention on investigating the response of structural members subjected to such loads. These loads may be resulted from faulty practice, terrorist attack, explosions or vehicle impact, etc. The collapse of Ronan point in 1968 alerted structural designers to the problem of progressive collapse. Here, the local failure of primary structural elements led to the collapse of the connected members [48], which resulted in a disproportionate collapse. However, all structural members are likely to expose to high speed loading in various locations. Researchers realised the importance of exploring the response of structural members under these extreme loads. Hence, many studies have been carried out to compare between the behaviour of structural members under static and high speed loading regimes. The first part of these studies focused on the column response under impact loads by investigating different types of columns such as steel, reinforced concrete and CFST column, as is discussed in Section 2.3.1.

Nevertheless, the structural aspects of steel frames require columns to be connected to beams using suitable connections. Then, studying the columns response with ignoring the connection contribution would lead to incomplete understanding of the overall steel frame behaviour. However, the second part of studies focused on the response of connection to high speed loadings which is discussed in Section 2.3.2.

2.3.1 Columns under impact loads

Structural columns are used to support the vertical loads transferred from the slab to beam then to columns. In addition to these loads, column may expose to lateral impulsive loads such as terrorist attack, internal explosions, flying debris or vehicle impact. However, considerable amount of studies was carried out to investigate the lateral response of columns

under impulsive loads. Due to the difficulty to apply the impulsive loads using blast loads, most of the researchers preferred to apply an impact load using drop hammer which is available in laboratories. Also, the safety requirements of using drop hammer are much less than those required for blast loading experiments.

2.3.1.1 Steel columns

A considerable amount of experimental and numerical studies has been published on the behaviour of structural columns under lateral impact. In particular, the behaviour of axially restrained columns under lateral impact has been studied intensively [49-54]. Menkes and Opat [49] identified three modes of failure in their experiments on clamped aluminium beams subjected to lateral impulsive load. These failure modes are

a) large plastic deformation of the whole beam corresponding to a plastic hinge mechanism,

b) tensile tearing failure, and

c) transverse shear failure near the supports.

Some research studies were undertaken to investigate the effect of different parameters on the aforementioned failure such as material type and impact location [50-53], the speed of impact load [54] and the influence of pre-tensioning [55]. Of these three failure modes, shear failure and global failure may occur in axially compressed columns under lateral impact.

Few studies have been carried out on the behaviour of axially compressed columns under lateral impact. Amongst these studies, Zeinoddini et al. [11, 56, 57]conducted experimental and numerical investigations to study the behaviour of axially pre-compressed steel tubes under low velocity lateral impact. The experimental results showed two failure modes. The first one was plastic global buckling under high axial compression load and the second mode was local damage of the impact zone by applying lower axial load on thinner tube, as shown in Figure 2.10.

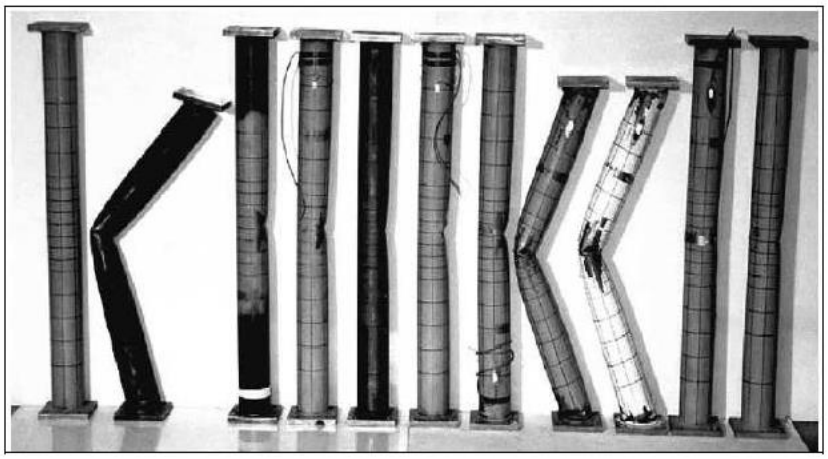

Figure 2.10. Failure modes of the deformed specimens after lateral impact [56].

Experimental studies were carried out by Adachi et al. [58] to investigate the buckling and post buckling behaviour of small scale axially compressed aluminium columns under lateral impact loads. It was found that the velocity of the column deformation increased as the lateral impact velocity increased even if the applied axial force was low. Therefore, the deformation during post-buckling process could be controlled by controlling the transverse impact. Hence, plastic hinges were not formed on the specimens loaded by impact velocity between 1.5 m/s to 2.2 m/s, while plastic hinges were formed when a velocity between 2.5 m/s and 3.0 m/s was applied, as shown in Figure 2.11.

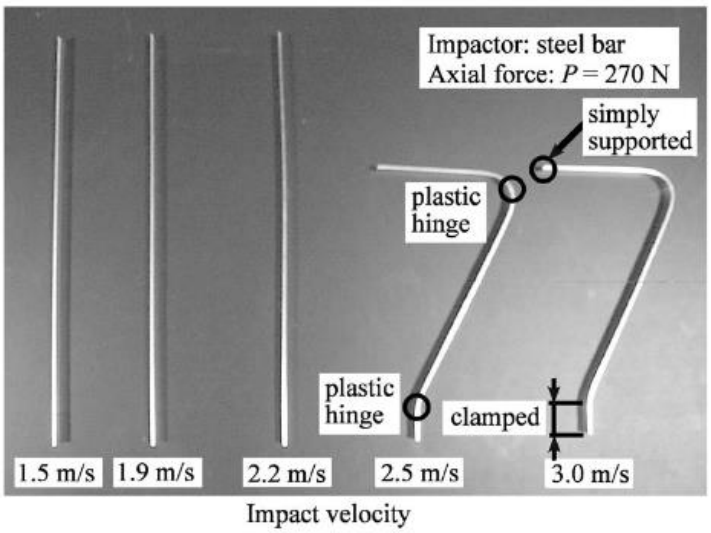

Figure 2.11. Specimens under lateral impact load with different velocities [58] .

Al-Thairy [13] conducted a numerical study to investigate the response of axially loaded steel columns under vehicle impact. The finite element analysis was performed and validated against some of the existed experimental results [11, 52, 53, 56, 59]. Intensive parametric studies were also performed using the validated FE models and the results show that the global buckling is the predominant failure mode of such columns under vehicle impact. The parametric studies have also indicated that strain rate has a minor effect on the response of steel columns under such loads.

It could be seen that the earlier studies started to understand the response of columns under pure lateral impact without loading the column axially as in the real situation. After that, the axially loaded column behaviour under lateral impact was investigated. The presented experimental and theoretical studies reflect the attention of the researchers to understand the response of steel columns under lateral impact loading.

In addition to steel columns, structural frame may be constructed using concrete filled steel tube (CFST) columns for their advantages that were discussed in Section 2.2.2. Therefore, considerable efforts were made to examine the response of these types of columns under impact load. The next section is to display the studies that were conducted to investigate the response of CFST column under lateral impact load.

2.3.1.2 CFST columns

Here, an overview on the studies that performed on the CFST column under lateral impact load is presented to obtain good insight into their behaviour and to show the importance of investigating their response under such loads.

Experimental studies were carried out to investigate the response of the unfilled and filled tubes under lateral impact loading. Xiaoqing and Stronge [60] studied the impact response on hollow, water and sand filled steel tubes hit by spherical projectile. The results showed that the specimens with water and sand filling exhibited lower deflection and higher stiffness than hollow specimens. Nishida and Tanaka [61] examined the perforation and cracking of

aluminium tubes filled with water and impacted by six steel spherical projectiles with various diameters. It was found that the strength of the tube wall reduced if the tube filled with water which reduced the impact velocity. An experimental and numerical study was conducted by Remennikov et al. [62] to study the response of hollow tube filled with rigid polyurethane foam (RPF) and concrete under impact load. Mild and stainless steel square sections were used in this study. The experimental results indicated that the strength of the specimens filled with concrete was higher than those filled with RPF. The numerical results obtained were in a good agreement with experimental results, as shown in Figure 2.12, which shows the comparison between the numerical and experimental results for the mild steel hollow tube filled with RPF (MDF1).

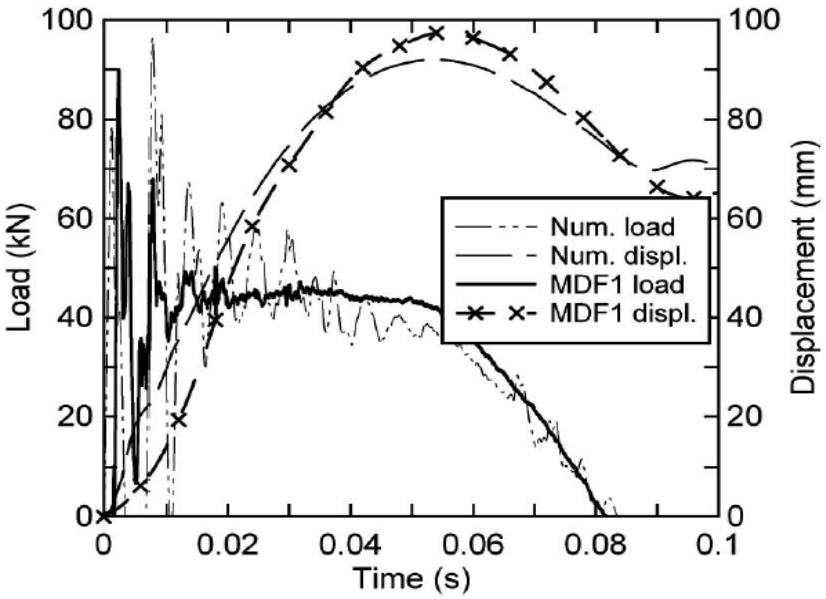

Figure 2.12. The validation of the numerical results against the experimental results for MDF1 specimen [62].

In recent years, a number of studies on the impact behaviour of concrete filled steel tube members have been carried out. The behaviour of the concrete filled square steel tube subjected to low velocity impact was studied by Bambach et al. [59]. The experimental work included testing a fully fixed beam with three different sizes under lateral impact load. However, rigid plastic analysis was used to predict the maximum force for the CFST

member with fixed ends under both static and impact loadings. It was found that the moment capacity of the CFST section was higher than the hollow section. Good correlation was obtained between the experimental results and those predicted from the proposed relationships, as can be seen in Table 2.1.

Table 2.1. Comparison between the theoretical and experimental results [59].

	F (kN) static-test	F (kN) impact-test	F (kN) theo.	F static theo./test	F impact theo./test
50 x 50 x 1.6 hollow	32.8	40.2	38.8	1.18	0.97
50 x 50 x 1.6 concrete filled	39.5	42.6	41.3	1.05	0.97
35 x 35 x 1.6 hollow	22.9	22.6	27.3	1.19	1.21
35 x 35 x 1.6 concrete filled	19.3	20.6	23.8	1.23	1.15
20 x 20 x 1.6 hollow	12.7	11.8	13	1.02	1.1
20 x 20 x 1.6 concrete filled	10.6	12.7	12.5	1.18	0.98

A numerical study using LS-DYNA on the behaviour of a circular CFST under lateral impact load was presented by Qu et al. [63]. Fixed-simple supported end boundary conditions was assumed to represent a column located on the first floor hit by rigid body as shown in Figure 2.13. The FE model is validated and used to develop a simplified analytical model to predict the maximum total displacement (δ_{max}) at the mid-span. The local deformation of the CFST column is ignored in this model and the maximum displacement can be predicted as follows:

$$\delta_{max} = \frac{L\theta'}{2} \tag{2.1}$$

where L is the CFST column length and Θ' is the rotation angle at the end of tube, which can be obtained from

$$\theta' = \frac{EI}{3Mp} \tag{2.2}$$

Here, *Mp* is the dynamic plastic moment of the CFST column section which is calculated from the experimental impact force based on the bending moment diagram with consideration of the strain rate effect for both steel tube and concrete infill by using a

dynamic increase factor. A variation of less than 7% between the predicted and experimental maximum deflection was obtained for different drop heights.

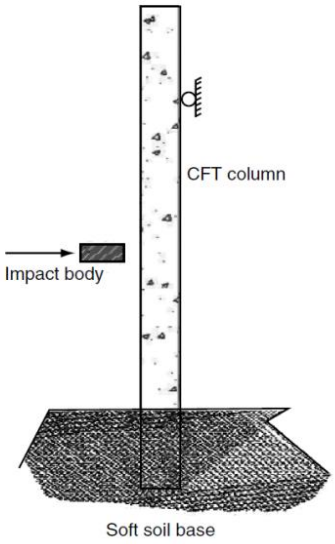

Figure 2.13. Boundary conditions used by Qu et al. [63].

An experimental investigation was carried out by Deng et al. [64] to study the behaviour of simply supported CFST members under lateral impact loading. The test included nine CFSTs, two post-tensioned CFSTs and one steel fibre CFST. The main findings indicated that the specimens failed with tensile fracture or circumferential rupture. Also, it was found that the concrete reinforcement with steel fibre and pre-stressing strands enhanced the impact resistance.

Wang et al. [65] presented an experimental and numerical study to investigate the impact performance of the CFST members. Three test parameters were investigated, i.e. the impact energy, the axial force level and the constraining factor. A finite element model was developed using the commercial code, ABAQUS. The concrete was modelled with concrete damage plasticity model, while an elasto-plasticity model was used to model the steel tube. It was demonstrated that the axial load did not affect the lateral displacement and the impact force. On the contrary, Yousuf et al. [12, 66, 67] found that the impact strength of the

stainless steel hollow and concrete filled columns with pre-axial load was 10-22% higher than those of the stainless steel columns without pre-axial load.

Han et al. [68] studied the impact behaviour of hollow and CFST columns. The main test parameters were the tube length, boundary conditions, the dropped mass and the impact velocity. It was found that the ductility increased if the hollow section filled by concrete and the deformation resistance enhanced by reducing the local buckling and the tube deflection.

A numerical study was presented by Aghdamy et al. [69] on the impact behaviour of the CFST columns. The finite element model was developed using LS-DYNA code and the model was in a good agreement with the experimental tests. The validated models were employed to perform parametric studies and the results showed that the maximum force and the maximum deflection were significantly affected by the ratio of the diameter to thickness of tube, slenderness ratio, impact location and the dropped mass.

Intensive experimental study was carried out by Shakir et al. [70] to investigate the lateral impact response of steel tube filled by recycled aggregate concrete reinforced with Carbon Fiber Reinforced Polymer (CFRP). The test parameters were the tube length, projectile shape, concrete type and reinforcement ratio of CFRP. The results showed that the strength of tubes filled with recycled aggregate concrete (RACFST) is comparable to those filled with normal aggregate concrete (NACFST). Also, it was found that the additional confinement of the CFRP reduced the total displacement for RACFST and NACFST.

From the series of researches presented above, it could be seen that considerable effort was made to understand the structural behaviour of CFST columns under lateral impact. It was found that these columns are more ductile than the steel columns under lateral impact. Also, the energy absorption of these columns was found to be higher than steel columns. This review gives valuable insight into the experimental and numerical studies which will help to achieve the current study. Also, it emphasizes the importance of studying the behaviour of structural members under lateral impact load.

2.3.2 Connections under impact loads

It was mentioned in Section 2.3 that the collapse of Ronan point in 1968 alerted structural engineers to the problem of progressive collapse. Therefore, the engineers realised that more knowledge was needed to present the solutions to prevent this collapse. SCI publication P391 [7] that presents the structural robustness of steel framed buildings in accordance with the Eurocode and UK National Annexes states that " In essence, the objective is to ensure that buildings do not suffer disproportionate collapse under accidental loading. Largely, this is assured in steel framed buildings by designing connections appropriately". Also, after the World Trade Centre (WTC) collapse in US, it was reported that the connection response against impact and fire needs to be understood and quantified as critical components of structural frame [5]. Hence, it will be beneficial to investigate the dynamic behaviour of this critical part on structural frames particularly for connections with a low moment resistance. For steel framed structures having simple or semi-rigid beam-to-column connections, the connections are likely to be weaker than the columns and beams. However, in this case, any local failure developed in the connection due to the accidental loading may likely be followed by a partially or entirely progressive collapse of the steel frame. Hence, connection response should be investigated prior to other steel frame components to prevent or reduce the possibility of progressive collapse occurrence.

Generally the impact loading could be transferred to any structural beam-to-column connection by either striking the beam or the column connected. However, columns are more likely to expose to such forces than beams such as vehicle impact, flying debris or internal explosion as shown in Figure 2.14. Consequently, intensive studies were carried out to investigate the response of different types of columns under such loads as presented in Section 2.4.1. In those studies, axially and non-axially loaded columns were investigated experimentally and numerically under lateral impact loads. It was mentioned in Section 2.3 that the structural aspects of steel frames require columns to be connected to beams using suitable connections. Then, studying the columns response without taking into account the

connection contribution would lead to incomplete understanding of the overall steel frame behaviour. Izzuddin et al. [71] realized this fact and concluded that progressive collapse failure of buildings is largely dominated by the maximum deformation allowed on the connections in relation to their built-in ductility.

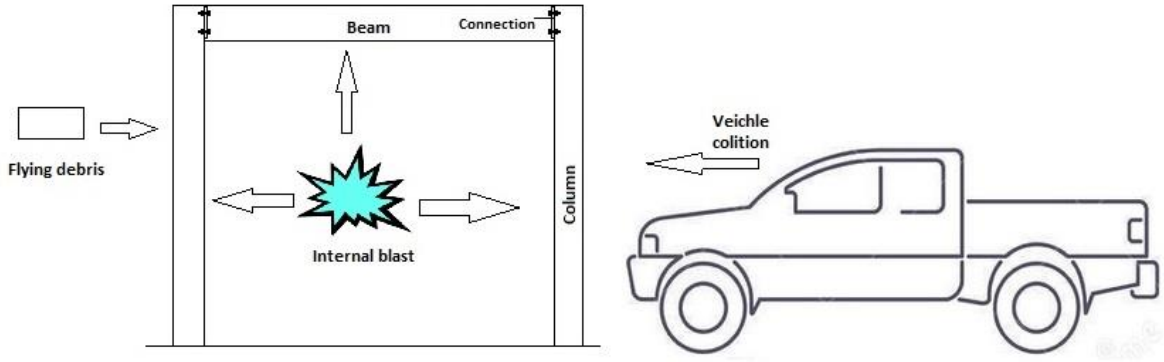

Figure 2.14. The possible cause of lateral impact.

The lack of knowledge on the dynamic capacities of steel connections indicates that limited studies were conducted. Tyas et al. [72] found that no published data existed on the connection behaviour under rapid and non-cyclical loading. However, their work was started to cover this gap by developing a novel experimental rig at which full-scale steel beam-to-column connections could be tested to failure over time scales varying between milliseconds (for dynamic loads) and several minutes (for quasi-static loads), as shown in Figure 2.15. The developed system was validated against some experimental tests on the partial depth end plate connection. The results showed a clear increase in peak resistance corresponding to a reduction in ductility of the connection when loaded to failure in around 40 ms compared to the behaviour under quasi-static loading.

An experimental and numerical study on fin-plate connections under static and dynamic conditions was undertaken by Stoddart et al. [73] with a loading time to failure less than 32 ms. The test setup adopted by Tyas et al. [72] was employed to simulate the complex conditions experienced by connections during catenary action. The study verified the ability

of the modified component method to predict the connection response under high strain rate loading [73].

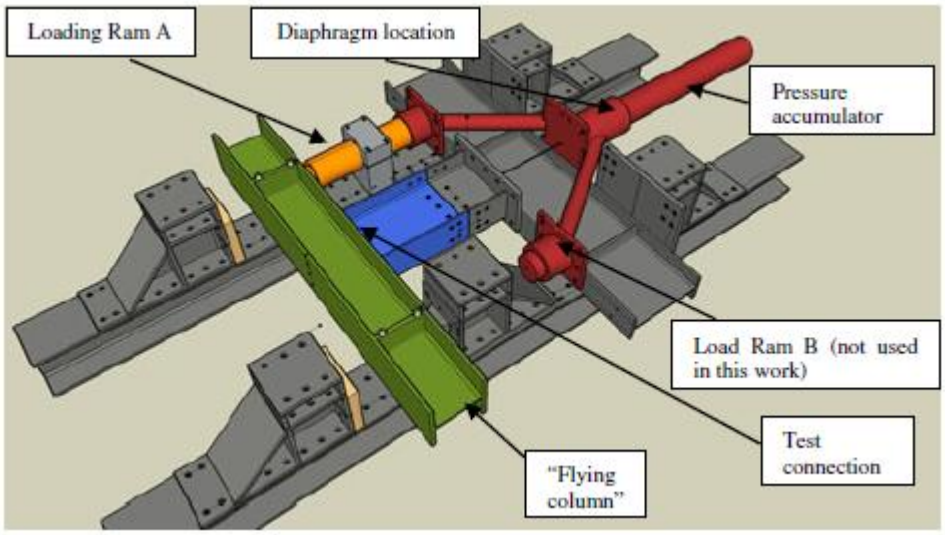

Figure 2.15. Experimental test setup adopted by Tyas et al. [72].

Wang et al. [9] also numerically investigated the response of a fin-plate connection due to falling floor impact loads. In the study, the impact load was applied on the beam and combined dynamic shear force and bending moment is generated on the connection. ANSYS/ LS_DYNA software was employed to establish detailed three dimensional finite element models. These models were validated against some existed experimental results [74, 75]. Six groups of numerical simulations were performed to study the influence of various parameters on impact resistance. The parameters included, impact location, impact energy, strength of material, distance between bolt holes and fin plate thickness. Parametric studies showed that a higher impact velocity could slightly improve the energy dissipation rate. Also, steel beams showed different impact resistance while they were impacted at different locations. Besides, it was found that the total displacement could be reduced using high strength steel.

Angle cleat connections were investigated as another type of connection under high loading rate by Rahbari et al. [76]. The test setup developed by Tyas et al [72] was employed, with

dynamic axial force and bending moment being applied on the connection. A total of ten tests were carried out and finite element models were developed and validated against the experimental tests. The comparison between quasi-static load and dynamic load results indicated that such connections are relatively insensitive to the strain rate.

A numerical study was presented by Kang et al. [77] as an attempt to investigate the response of entire steel frame with moment resisting connections against vehicle impact. Here, a 2D and a 3D steel moment frames subjected to vehicle collision at a first storey were modelled using LS-DYNA software. The impact simulation was conducted with three different vehicle speeds of 40, 80 and 120 km/h and fully welded beam to column connection was assumed between beams and columns connected, as shown in Figure 2.16. The results showed that the frame remained stable under 40 km/h (11.1 m/s) car hitting speed, while the frame was severely damaged in a progressive manner when the car speed reached more than 80 km/hr, as indicated in Figure 2.17.

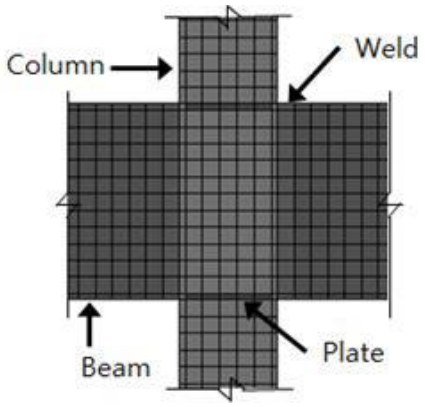

Figure 2.16. Beam-to-column configuration adopted by Kang et al. [77].

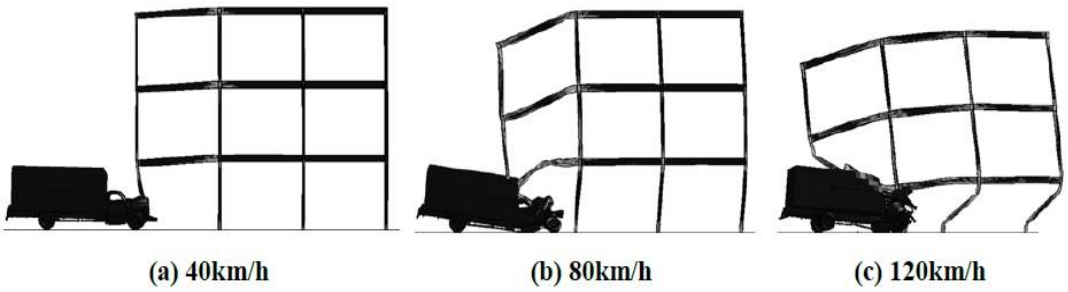

Figure 2.17. Impact analysis results of 2D frame with different vehicle speed [77].

Grimsmo et al. [78] conducted an experimental study in which extended end plate connections were tested under quasi-static and impact load hitting the column axially (i.e. shear and bending moment produced on the connection). Four tests were carried out under quasi-static loading, while eight specimens were tested under impact load. Six of the specimens were loaded so that the bending moment acted in the direction the connections were designed for, and the other six specimens were loaded in the opposite direction as shown in Figure 2.18 (a) and (b).The details of the connection used in this study are shown also in Figure 2.18 (c). The results showed that the connections tested behaved in a preferable manner and became more ductile under impact loads. However, Tyas et al. [72] showed that the connection became less ductile under dynamic test compared to that under quasi-static one. This contradiction in the results from Tyas et al. [72] and Grimsmo et al. [78] indicates that more research needs to be carried out on both connection types to improve the knowledge on this issue.

The experimental study that carried out by Grimsmo et al. aforementioned at reference [78] was followed by a numerical study conducted by the same authors using finite element modelling [79]. An elastic-thermoviscoplastic constitutive model was developed to model the steel up to failure as expressed below:

$$\sigma_{eq} = \begin{cases} \sigma_y & \text{if } \varepsilon_p \le \varepsilon_{p,plate} \\ \left[\sigma_y + \sum_{i=1}^{2} Q_i \left(1 - \exp\left(-\frac{\theta_i}{Q_i}\left(\varepsilon_p - \varepsilon_{p,plate}\right)\right)\right)\right]\left[1 + \frac{\dot{\varepsilon}_p}{\dot{\varepsilon}_{ref}}\right]^C \left[1 - T_h^m\right] & \text{if } \varepsilon_p > \varepsilon_{p,plate} \end{cases} \quad (2.3)$$

Where

σ_y is the yield stress, Q_i and $\theta_i$are the hardening constants of the extended Voce hardening rule, ε_p is the equivalent plastic strain, $\varepsilon_{p,plate}$ is the equivalent plastic strain at the end of the yield plateau, $\dot{\varepsilon}_p/\ \dot{\varepsilon}_{ref}$ is the ratio of equivalent plastic strain rate to a reference strain rate, C is a strain rate constant, T_h is homogenous temperature and m is a constant.

The FE models were validated against the experimental results and a good agreement was

obtained. The validated models were further employed to investigate the energy dissipated by the connection, the effect of using different plate thickness, the effect of axial forces in the beam in addition to the effect of increasing the inertia of the beam. The main findings were that the energy dissipated by the connection was significantly increased by reducing the end plate thickness, whilst marginal effect on the response of the connection was found by applying different axial forces on beam. Also, it was indicated that taking the additional mass from structural members such as floor slabs into account could change the failure mode.

A study with the aim of evaluating the response of a T-stub component subjected to static loading at ambient and elevated temperatures was carried out at the university of Coimbra [80]. This study was enlarged to investigate the behaviour of T-stub under impact loading [37, 80]. Rebeiro et al. [81] conducted a numerical study to investigate the behaviour of the end plate connection under impact load. The analysis was performed by assuming that the end plate is behaves as a T-stub. ABAQUS software was used to model the impact and quasi-static tests.

A relationship between the tri-axial stress state and the equivalent plastic strain was developed to predict the onset of ductile damage of bolts and end plate. The results showed that the force-displacement curves were enhanced under impact load compared with those under quasi-static. Also, it was concluded that the force displacement enhancement was less prominent for thicker T-stub.

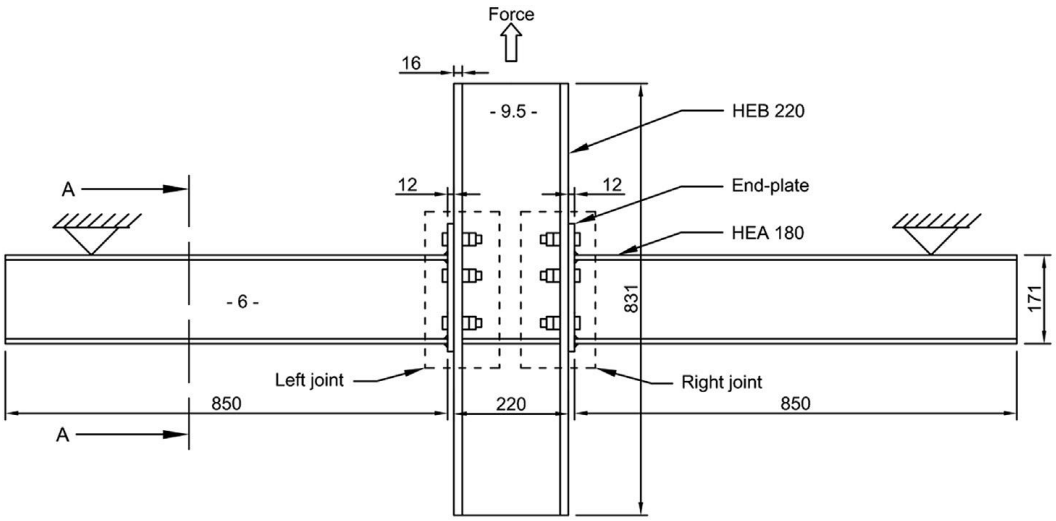

a) Elevation view of the Design Load Direction (DLD) specimen

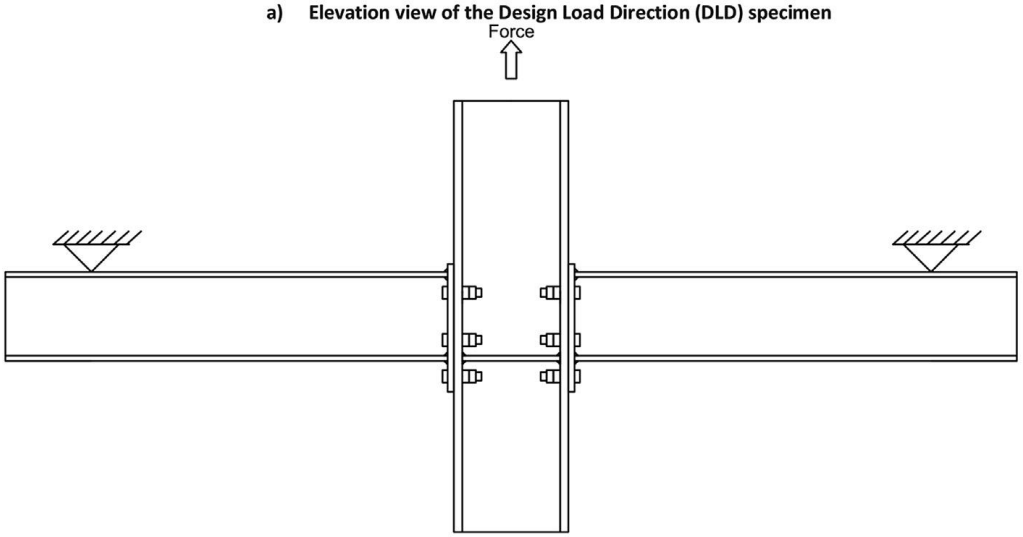

b) Elevation view of the Reverse Load Direction (RLD) specimen, which is similar to the specimen in a), just rotated 180 degrees in the plane and the stiffeners at the web of the column is moved.

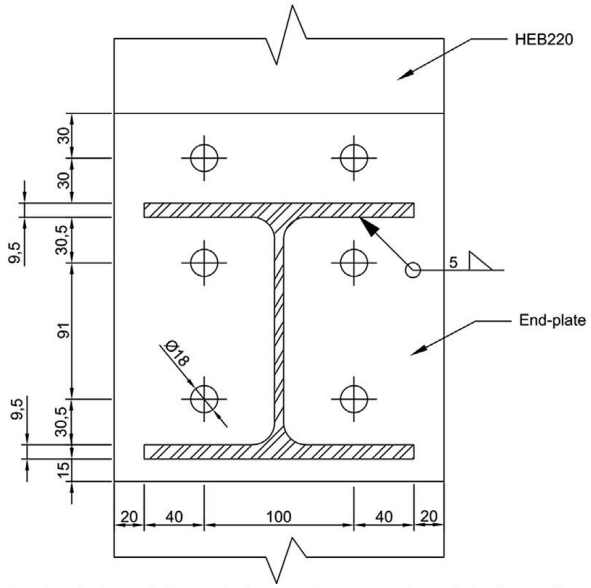

c) Section (A-A) view of the end-plate and cross-section of the beam for DLD specimen

Figure 2.18. Test setup and connection details adopted by Grimismo et al. [78].

2.4 Remarks and research originality

The previous studies presented in this chapter showed that the focus has been made on investigating the behaviour of different types of columns under lateral impact loading. Different parameters were examined such as impact energy, boundary conditions, CFST cross section, ratio of tube length to tube diameter (L/D) and ratio of tube diameter to tube thickness (D/t).

It is clear that the researchers realised the importance of investigating the connection behaviour under impulsive or impact loads during the last decade. Hence, the studies relative to beam-to-column connections presented in this chapter were started from 2012 until the writing of these words. However, this field still needs to be covered well, particularly with taking into account the variation of connection types and parameters that affect connection behaviour such as connection geometries, impact loading locations, boundary conditions in addition to using different material properties as well as dynamic increase factor. Also, the modelling of beam-to-column connections under impact load still unclear as limited studies are presented up to date. Hence, it will be beneficial to investigate the response of beam-to-column connections under such loads. However, it is decided in the current study to investigate the impact response of the most common beam-to-column connection type named the end plate connection. This type is chosen as it is used widely in practice as discussed in Section 2.2.1.1.

In addition to open sections, the end plate may be used to connect CFST column to steel open beam sections as discussed in Section 2.2.2. The best solution was found to be using long bolt to connect the CFST column to open steel beam sections particularly under seismic loads. However, no study is available in public domain on the performance of such connection under impulsive or impact load. Therefore, the second task of the current study is to investigate the performance of the end plate connection to CFST column using long bolt technique.

Chapter 3: Experimental Procedure

3.1 Introduction

In this chapter, an experimental investigation adopted to study the structural response of the end plate connections under impact and quasi-static loading was presented. Firstly, the motivation of the proposed experimental work is presented. The specimen preparations and the materials testing were then described in details. Test setup includes the loading rigs used and the fabrication of the stiff frame mounted required to support the specimens. Then, the structural tests, including impact and quasi-static tests, were conducted. All information on the instrumentations used in the impact and quasi-static tests are also presented in this chapter. It should be mentioned that the experimental tests were carried out at the University of Liverpool using the existing facilities. Specimens were also fabricated in the University of Liverpool, except for the welding which was done by a private company named Wren Industrial &Marine Fabrications LTD (Sandon Industrial Estate-Liverpool-L5 9YN).

3.1.1 The motivation of the proposed experimental work

In Chapter two, a literature review was presented on the behaviour of columns and connections under lateral impact loads. This review shows that no experimental investigation was conducted to study the lateral impact response of end plate connections. Consequently, the main aim of the experimental investigation is to experimentally investigate the response of end plate beam-to-column-connections subjected to lateral impact.

As mentioned in Chapter one, three dimensional (3D) finite element analysis (FEA) and the validated models would be employed to have a deep insight into the behaviour of end plate beam-to-column-connections. Finite element tools could be used to investigate different parameters that could not be measured experimentally. Nevertheless, FEA models should be verified first prior to be used to investigate these parameters. The best way to validate the FEA models is to validate the simulation results with the experimental results obtained. This could be considered also as the second motivation of performing the experimental work.

3.2 Material testing

The static material properties of concrete, steel sections, steel plates and bolts were obtained from various material tests. For concrete, the compressive strength was obtained using a uniaxial compression test and a four-point flexural test, respectively. Also, tensile test was carried out for steel materials to obtain the engineering stress-strain curves which are further processed to obtain the true-stress strain curves as will be discussed in the next chapter. All these materials were tested in accordance to the relevant BS and EN standards.

3.2.1 Concrete

Concrete is a material produced by mixing cement, gravel (coarse aggregate) and sand (fine aggregate) with water. These materials were supplied locally by Travis Perking Trading Company. Compressive strength class C25/30 was used for all specimens in this study. To obtain the characteristic cylinder strength (f_{ck}) of this class, general purpose Ordinary Portland Cement (OPC) complied with the requirements of British Standard BS EN 197-1 (2011) [82] was used. Also, crushed coarse aggregates used were with a maximum size of 10 mm and graded according to British Standard BS EN 12390-3: 2009 [83]. Normal river sand which complies with the British Standard BS 882: 1992 [84] was used as fine aggregates. Three trial concrete mixes were carried out with different mixing proportions to select a mix that is corresponding to the concrete compressive strength required. The concrete mix proportions to be used in this study are shown in Table 3.1.

Table 3.1. Concrete mix proportions.

Cement ($kg/m^{3)}$	Coarse aggregate (kg/m^3)	Fine aggregate (kg/m^3)	Water (kg/m^3)
460	1100	590	255

In order to obtain the compressive strength of concrete, nine 100 mm cubes were prepared and casted with each concrete batch to determine the concrete compressive strength at 7, 14 and 28 days to monitor the growth of the strength. The tests were performed using Tonipact

loading machine with a capacity of 3000 kN, as shown in Figure 3.1. The compressive strength was determined as the average of the three cube tests after 28 days. Finally, cubes strength (f_{cu}) was converted to cylinder strength (f_{ck}) using the conversion equation below [85] :

$$f_{ck} \approx 0.83\ f_{cu} \quad (3.1)$$

Figure 3.1. Compressive test of concrete cubes.

3.2.2 Steel

Standard tensile coupon tests were performed based on British Standard BS 10002-1: 2001 [86] for all steel sections involved in the specimens, in addition to the high strength bolts. The tests were performed using Instron universal test machine, as shown in Figure 3.2. Figure 3.3 shows the dimensions and details of coupons taken from the base components. It can be seen that the gauge length of all coupons is taken as 90 mm, except for the ordinary bolt which is taken as 15 mm due to its limited length. Circular section of coupons were used for parts that experienced high deformation such as bolts and plates in order to estimate fracture strain using Bridgman equation [87], which requires a circular cross section, as will be discussed in Chapter five. However, the rectangular cross sections were used for beams and columns as no plastic deformation was produced in these parts. The coupons were also taken from web and flange of both the beam and column to be tested separately as their properties may be varied. All the tests were repeated three times and the replicated tests

showed excellent repeatability. The corresponding engineering stress-strain curves were obtained for all constituent materials under quasi-static load and will be presented in Chapter four in details.

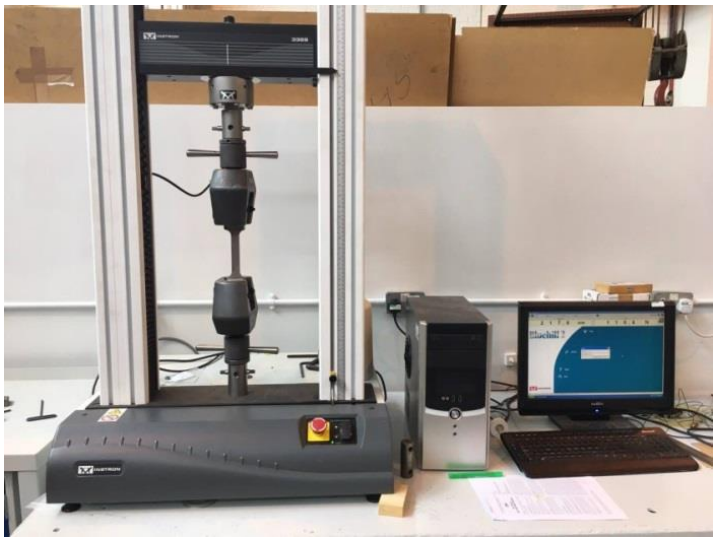

Figure 3.2. Tensile test of steel specimens.

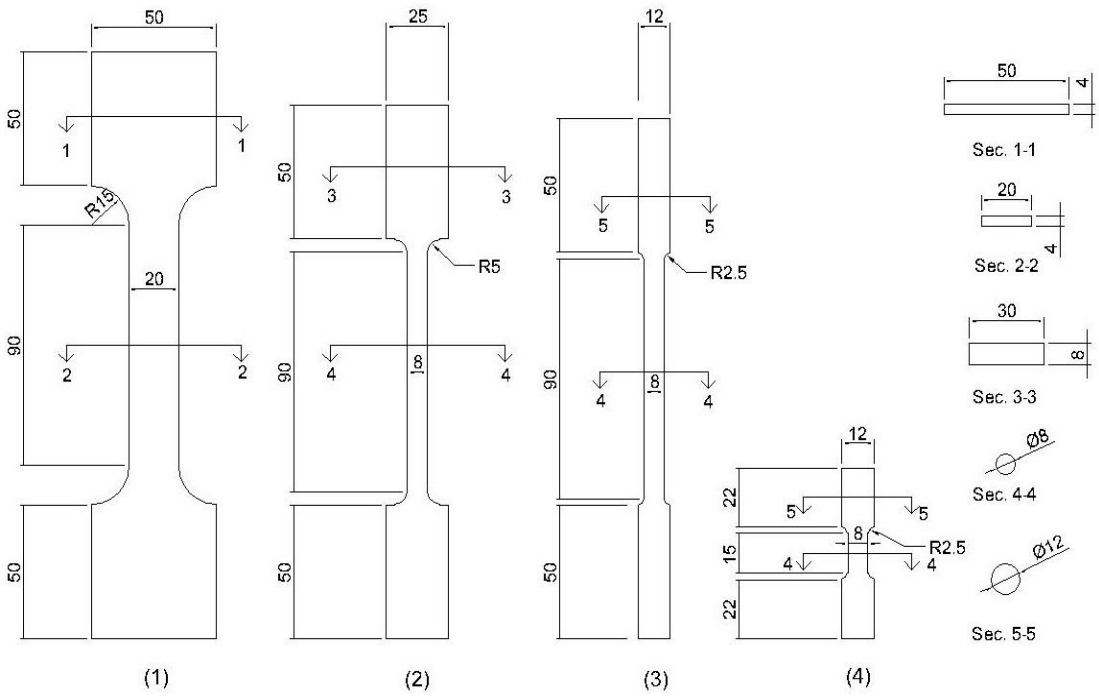

Figure 3.3. Full details of the fabricated coupons of the steel materials (Dimensions in mm).

3.3 Specimens preparation

The specimens preparation plan could be divided into three consecutive stages. The first stage was to design the test specimen. Then, the required parameters to be obtained from the experimental investigation were specified. Finally, full details of specimens are presented including the fabrication and assembly. These stages are discussed in details in the following sections.

3.3.1 Specimen designs through initial tests

Specimens on beam-to-column connection could be considered as one of the more complicated specimens if compared with other structural members. This is because an assembly of three structural members represented by beam, column in addition to their connection has to be fabricated and assembled before testing. Test specimens of other structural members such as beam, column or slab do not require the similar assembly in connections. In the real situation, structural frames of a building contain a considerable number of beam-to-column connections as shown in Figure 3.4.

Figure 3.4. Steel structural frame of Beijing Corning LCD.

This study focuses on the local response of beam-to-column connections rather than the response of the entire frame. Therefore, the possibility of using one column connected with two beams by two connections could be adopted as a first proposed test specimen, as shown in Figure 3.5.

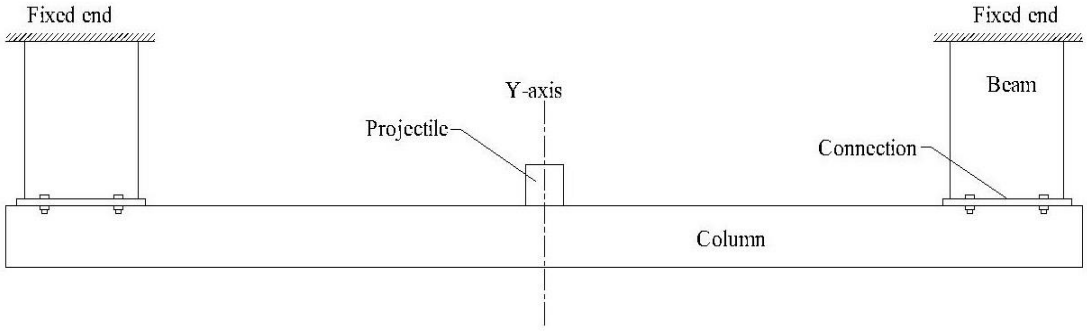

Figure 3.5. First proposal of test specimen.

It should be mentioned that the impact load could be applied in the vertical direction using a drop hammer only available in the laboratory. This limitation required the column to be located in the horizontal direction which is the opposite to the real situation. Since most of structural frames are braced, the horizontal translation of beams could be fixed and small portion of the beams could be used instead of long beam to save the cost and time of fabrication. With this test setup, each connection would be subjected to a dynamic tensile force and a dynamic bending moment. Moreover, due to symmetry, the response of both connections is similar in terms of resistance and failure mode. Therefore, the symmetry in y-axis could be employed to simplify the test specimen to have one beam, one column and one connection only, which represents the second proposal of the designed specimen, as shown in Figure 3.6.

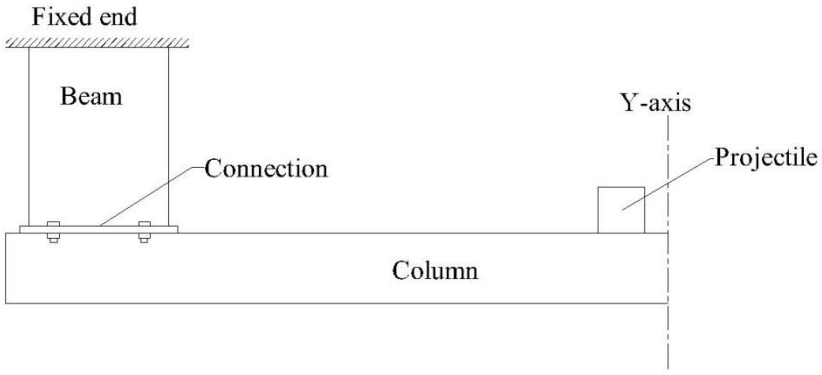

Figure 3.6. Second proposal of test specimen.

Many advantages could be obtained using the second proposal. Firstly, the connection still subjected to dynamic tensile force and dynamic bending moment as required, but with less materials and fabrication time. Secondly, by adopting the first proposal the connection may not have high deformation as the applied energy needs to be resisted by two connections. However, the setup of the second proposal increases the deformations in the connection significantly, as there is only one connection provided in the system which relaxes the limitation of the maximum impact energy offered by the drop hammer available, as is discussed in Section 3.4.1. It is important to obtain considerable deformations to investigate the maximum connection capacity and also to employ the deformed shape as one of the measures to validate the FEA models later. Moreover, a stiff mounting system should be designed and fabricated to provide a fixed end in the beam as discussed in Section 3.2.4. Using the second proposal only one stiff frame needs to be fabricated, which is a better option to significantly save the time and cost of the project. Finally, it could be concluded that the specimen based on the second proposal can be used in this study due to the aforementioned reasons.

3.3.2 Parameters to be investigated

The experimental investigation consisted of different parameters to be examined, i.e.

(1). Loading type: quasi-static loading and impact loading are applied to obtain the static and the impact response of the connections. This is to investigate the dynamic effect on the connections by comparing their response under the two aforementioned loading regimes. This would assist to suggest a dynamic increase factor (DIF) at which the static analysis could be used to predict the dynamic response. This approach is used by many researchers such as Wang et al. [88] to estimate the dynamic resistance capacity of concrete filled double steel tubular members under lateral impact. Also, it was used by Liu et al. [89] to address the appropriate DIF for the design of structures against progressive collapse.

(2). Type of connections: two types of end plate connections were selected and designed according to EC3 in terms of e_1, e_2, p_1, p_3, b_p, t_p [90]. The first one was the partial depth end

plate connection (PDEPC) which is used in practice to resist shear and tensile forces only. However, the second type was the flush plate connection which is classified as a moment resisting connection which is capable to resist bending moment in addition to tensile and shear forces. Figure 3.7 shows the typical configuration of both types as used in practice.

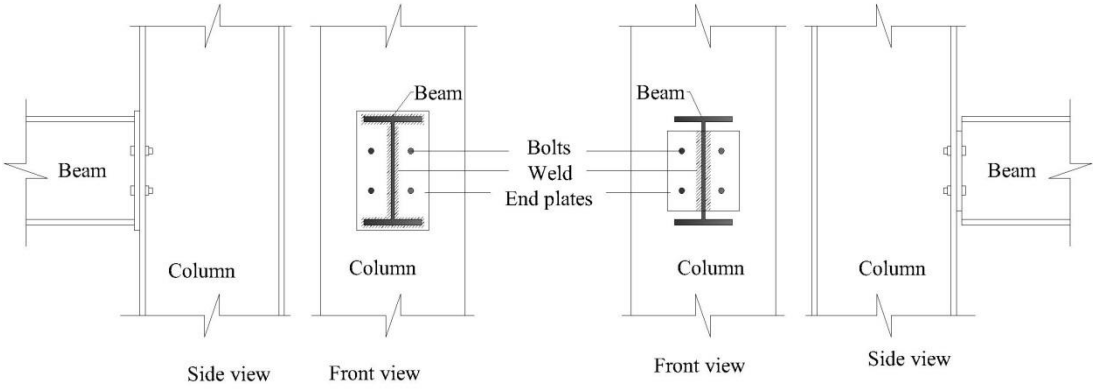

Figure 3.7. Typical connection configuration used in the experimental investigation.

(3). Types of columns: End plate connection may be connected to concrete filled steel tube columns (CFST) or steel I-sections. The previous studies presented in Chapter two indicate that CFST columns has many advantages compared with steel columns, such as the high strength and high ductility under impact load. However, it is interested to investigate connection response due to impact loading as it is usually the weak part of the system.

Also, it is a good opportunity to investigate the performance of using long bolts with CFST connection as the best solution available, as discussed in the Chapter two, to connect the CFST columns to steel beams using end plate connections. Both I-section and CFST columns were designed to have approximately similar bending capacity for comparison purpose. It should be mentioned that quasi-static tests were not performed for specimens connected to CFST columns as the aim is to investigate their impact response only as discussed in chapter one.

(4). Load Location: the column may expose to lateral impact in different locations. However,

two extreme load locations were selected in this study to be investigated. The first one was far away from the connection which was named as L_1 in this study, whilst the second location was selected to be closed to the connection and named as L_2. L_1 and L_2 were measured from the centre of projectile to the centre of connection. L_1 and L_2 were selected to be 0.374 m and 1.124 m, respectively. The column of specimens that was impacted at L_2 were cut for some setup limitations as the location of the existed impact rig impeded the column to be extended using the same length of specimens impacted at L_2.

(5). Plate thickness: changing the plate thickness leads to change the connection behaviour and the failure mode under quasi-static loading as discussed in Chapter two. Hence, two thicknesses of 8 mm and 15 mm were selected in this study to investigate the effect of plate thickness on the impact response of the connection.

(6). Concrete infill: in order to investigate the difference between the responses of connection to hollow columns and CFST column, one additional specimen having PDEPC was tested under lateral impact without concrete infill.

Finally, the matrix of parameters was arranged to contain 17 specimens as shown in

Table 3.2.

3.3.3 Final design of test specimens

The final design of the specimens to be tested was based on the initial design and the parameters to be investigated. Thus, the individual parts of the specimens were selected as follows.

(1). Beam: UK beam 305 x 127 x 27 was used with a length of 400 mm. Six holes with a diameter of 18 mm were drilled in each beam web to connect the beam to the mounting stiff frame using 16 mm high strength bolt, as shown in Figure 3.8 (a).

(2). Column: UK column 152 x 152 x 37 was used as an I-section column, while a square hollow section of 150 x 150 x 4 was used as CFST column. To investigate the effect of

Table 3.2 Matrix of parameters to be investigated in the experimental investigation.

Specimen Designation	Type of Loading	Type of connections	Type of column	Load location	Plate thickness (mm)	Concrete infill
PFI8	Impact	PDEPC*	I-section	L_1	8	-
FFI8	Impact	FPC*	I-section	L_1	8	-
PNI8	Impact	PDEPC	I-section	L_2	8	-
FNI8	Impact	FPC	I-section	L_2	8	-
PFI15	Impact	PDEPC	CFST	L_1	15	-
FFI15	Impact	FPC	CFST	L_1	15	-
PFI8S	Quasi-static	PDEPC	I-section	L_1	8	-
FFI8S	Quasi-static	FPC	I-section	L_1	8	-
PNI8S	Quasi-static	PDEPC	I-section	L_2	8	-
FNI8S	Quasi-static	FPC	I-section	L_2	8	-
PFC8	Impact	PDEPC	CFST	L_1	8	Yes
FFC8	Impact	FPC	CFST	L_1	8	Yes
PNC8	Impact	PDEPC	CFST	L_2	8	Yes
FNC8	Impact	FPC	CFST	L_2	8	Yes
PFC15	Impact	PDEPC	CFST	L_1	15	Yes
FFC15	Impact	FPC	CFST	L_1	15	Yes
PF68	Impact	PDEPC	CFST	L_1	8	No

impact loading location on the impact response, both columns were cut into two lengths of 1422 mm, and 672 mm as discussed in Section 3.2.2. Figure 3.8 (b).

(3). End plate: As mentioned before in Section 3.3.2, two plate thickness of 8 and 15 mm were used. End plate width and thickness of 150 x 8 mm were selected according to the recommended geometry by Eurocode 3 [90]. Using a plate with a thickness more than 12 mm is not recommended but this recommendation was adopted by the Eurocode based on static analysis. Hence, it is interested to investigate a plate thicker than the recommended one to examine its efficiency under dynamic load, particularly no test results available as indicated in the previous chapter. Thus, a plate of 15 mm thickness was used for this purpose. Figure 3.8 (c) shows the details of the two types of connections to be investigated in this study.

(4). Bolts: to connect the end plate to the I-section columns, ordinary bolts of 16 mm diameter and 65 mm length were used. Whilst, long bolts of the same diameter and a length of 220 mm were used to connect the end plate to the CFST columns. Figure 3.8 (d).

After completing the final design drawings of each individual part of the specimens to be tested, the fabrication then started with the following four consecutive processes:

(1). Cutting to length: All individual parts of connection were cut into lengths by the supplier and delivered to the laboratory, except for long bolts which were fabricated by cutting 1 m length thread bar into four 220 mm lengths according to the design adopted. The sharp edges of all individual parts were then deburred for safety requirements.

(2). Drilling: Plates, beams and columns were drilled to provide access for the bolts to pass through. All specimens were provided with 18 mm clearance holes to provide access for 16 mm bolt diameter with 2 mm clearance as recommended by BS EN ISO 4014 [91].

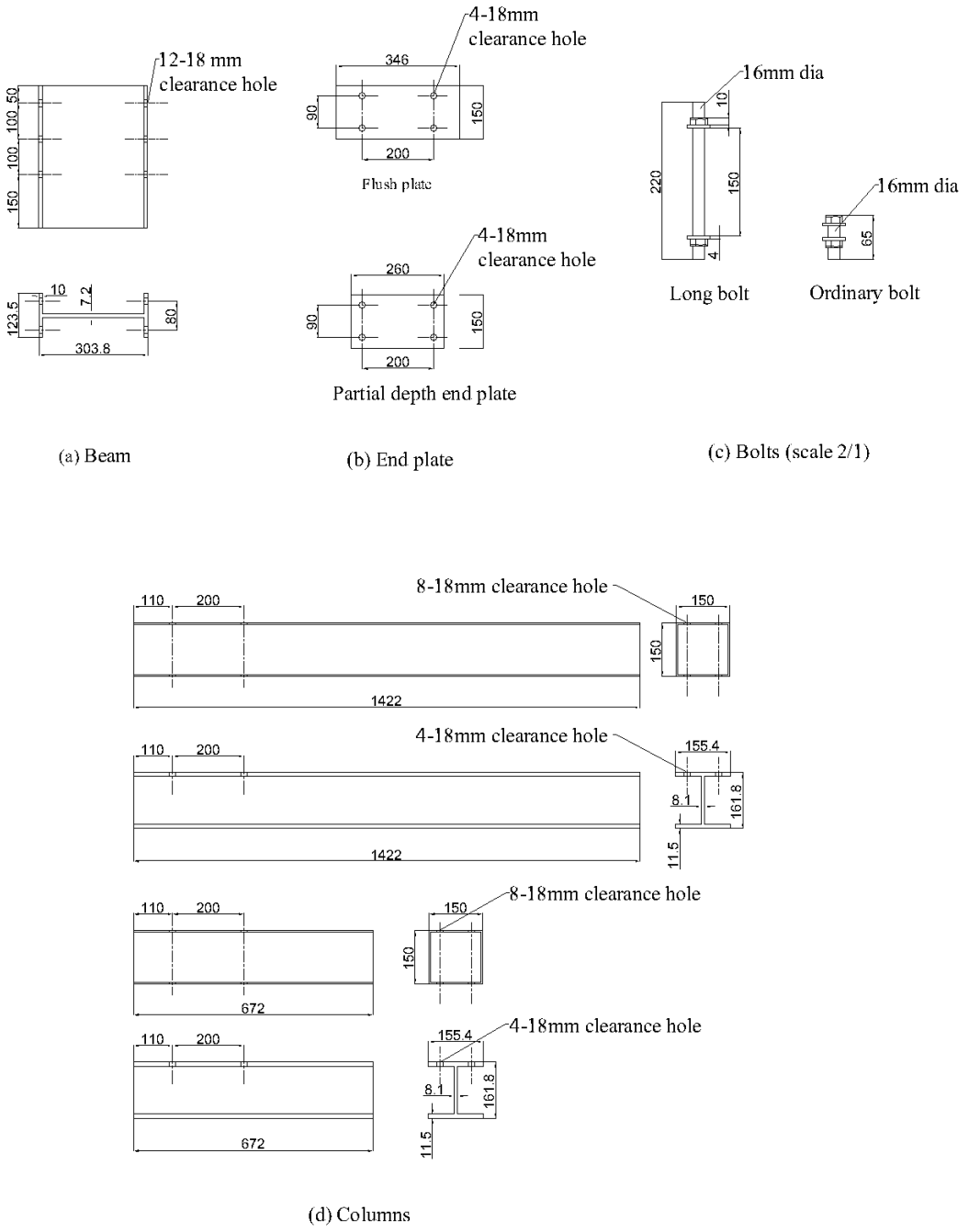

Figure 3.8. Details of parts used in the test specimens (dimensions in mm).

(3). Welding: Figure 3.9 shows the beam and end plate assembly after welding. All welding work was carried out by a licensed welder on a private company (WREN Industrial & Marine Fabrication LTD., Sandon Industrial Estate-Liverpool- L5 9YN) and special care was taken to avoid plate bowing due to high welding temperature. First, the welding area in both

plate and beam were grinded and then the beam was placed on its right location on the plate using previously lines marked. Stitch welding was used then to connect the beam to the plate and the plate to the welding table temporarily. After that, 4 mm full fillet weld was applied to connect the beam to the end plate using MIG welding machine. The sample then was left for one day to cool and the stitch welding between the plate and welding table was then taken off. This procedure was to avoid the plate distortion due to high temperature produced from the welding.

(4). Assembly: Figure 3.10 (a) to (e) show the final design of the specimens to be tested for both loading locations selected (L_1 and L_2), type of columns and type of connections. For beams to I- section specimens, the welded end plate to beam was connected directly to the I-section column by four ordinary bolts. However, for beams to CFST column specimens, the long bolts were placed in the holes provided in the column first, the column then was filled by concrete. After the concrete gained its full strength after 28 days, the end plate to beam assembly was connected to the CFST columns using the embedded long bolts, as shown in Figure 3.10 (c). The twelve holes provided in the beam were then used to connect the specimen to the mounting stiff frame, as discussed in Section 3.2.4.

Figure 3.9. Welding of end plate to beam

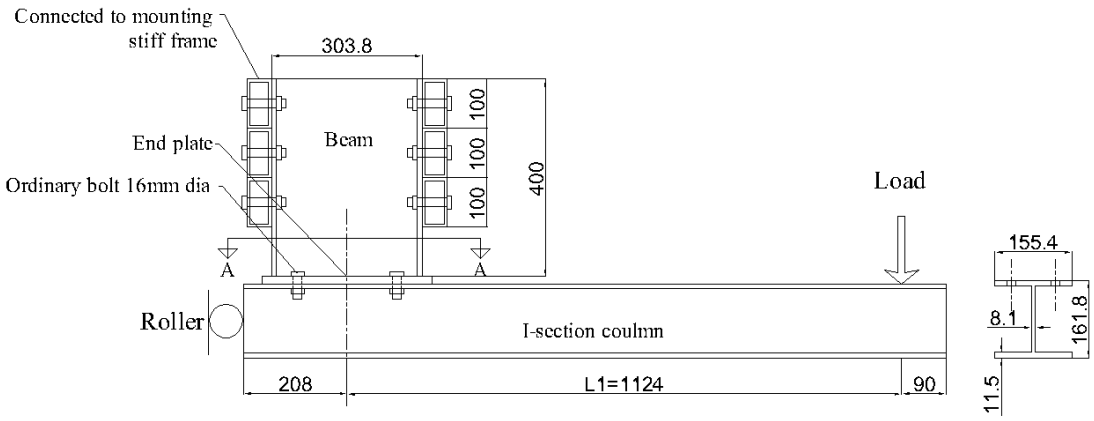

(a) Connection to I-section column with load applied at L_1 (dimensions in mm).

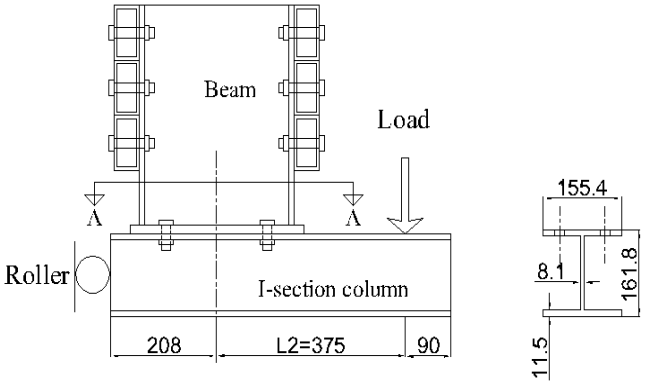

(b) Connection to I-section column with load applied at L_2 (dimensions in mm).

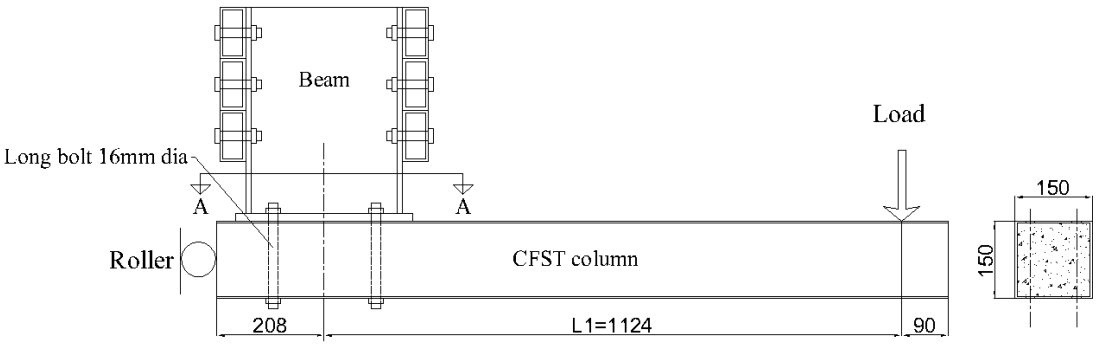

(c) Connection to CFST column with load applied at L_1 (dimensions in mm).

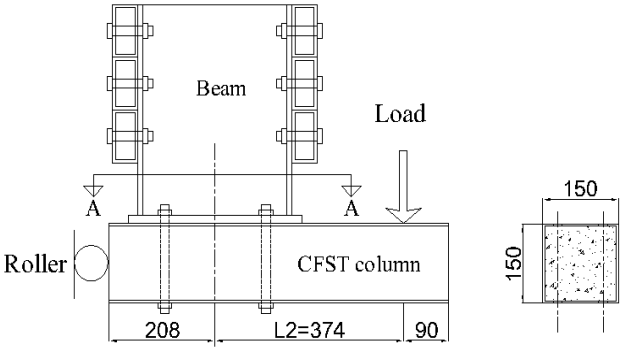

(d) Connection to CFST column with load applied at L_2 (dimensions in mm).

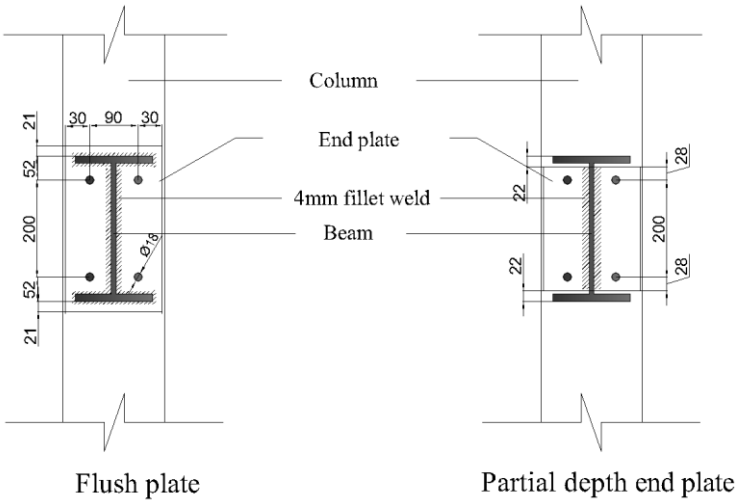

(e) Connection types to be investigated

Figure 3.10. Full details of specimens to be tested (dimensions in mm).

3.4 Test setup

3.4.1 Loading rigs

Figure 3.11 shows the overall assembly of the impact rig used to test the specimens under lateral impact load. The maximum height and maximum mass of the drop hammer are 2.9 m and 107.5 kg, respectively. The average theoretical velocity for the tests is 7.54 m/s corresponding to theoretical impact energy of 3058 J. The main component of the impact rig contains of a 150 x 90 x 23.9 channel column that served as a vertical guide for the mass and projectile. The lifting and drop mechanism is operated by a quick release pin connected to a

manually driven winch and a switch panel. Two steel plates of 20 mm x 10 mm were placed on each internal side of the channel in order to ensure the alignment of the mass of the drop hammer into position. Two steel equal angle sections of 75 x 75 x 7 mm were connected to the channel column to support the drop hammer laterally. A high strength steel flat projectile with a surface area of 100 x 100 mm was used in this study.

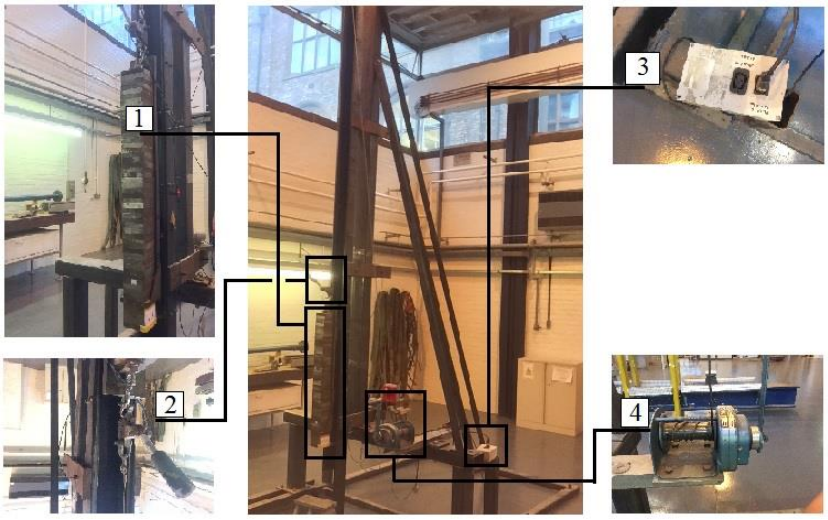

Figure 3.11. Impact rig components: (1) Drop hammer, (2) Quick release pin, (3) Switch panel (4) driven winch.

A hydraulic jack of 300 kN capacity was used to apply the quasi-static load on the specimen with a load increment of 1kN. The hydraulic jack was provided by a rigid beam to support the specimens. The quasi-static loading procedure is discussed with more details in section 3.4.3.2.

3.4.2 Mounting stiff frame

The specimens require a stiff reaction frame to support them under the applied loads. This frame should be stiff enough to minimize any movement during the test that may affect the results. The frame was designed and fabricated at the University of Liverpool and some trial tests were carried out to examine its suitability.

Figure 3.12 shows the details of the mounting stiff frame that used to support specimens. It can be seen that the frame contains three parts, i.e. floor mounted rails, moveable sub-

assembly and bracers. The rails provided a fixed location for the drop hammer operator. Also, holes in the rails were provided to allow the movable sub-assembly for variable lengths. Two vertically mounted supports fabricated were bolted to the rails to provide a rigid base. The cross members with a detachable clamping setup provided a method to rigidly clamp the samples. Three bracers were employed to connect the rails to both ends of the sub-assembly frame and the detachable clamping setup in order to minimize the rotational movement of the sub-assembly frame which supports the specimens. Roller support was attached to the end of column to prevent any horizontal sway of the column as in a practical situation and to enhance the rotational stiffness of the frame.

The rigidity of the reaction frame was examined prior to test the specimens. Hence, three additional trial specimens having a connection stronger than all of those to be investigated in this study were tested under impact load. The translational and rotational movements of the reaction frame at the detachable clamping where the specimen was connected to the stiff frame were recorded using a high speed camera. The maximum rotational angle and the maximum downward translation of the detachable clamp for all trials measured were 0.61° and 1.7 mm, respectively. However, it is expected that this error is to be minimized using weaker joints as proposed in this study.

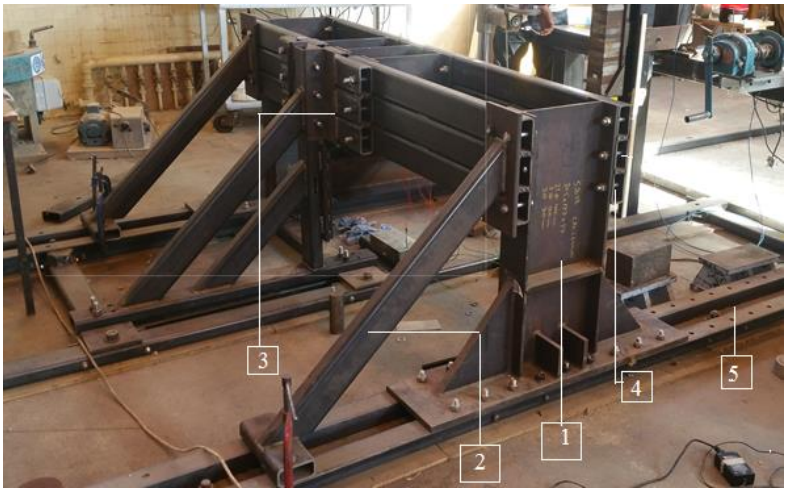

Figure 3.12. Mounting stiff frame: (1) Vertical mounted support (2) Bracer (3) Detachable clamp (4) Cross members (5) Floor mounted rail.

3.4.3 Final test setup

3.4.3.1 Impact test setup

The details of specimens, mounting stiff frame and impact rig used were discussed in the previous sections. In this section, the impact test setup is presented in details. Figure 3.13 shows a schematic diagram of the final impact test setup. Firstly, the assembled specimen was prepared as discussed in Section 3.3. At that time, the detachable clamping of the mounted stiff frame was removed. Then, the assembled specimen was moved using a crane with a capacity of 5 tons and the front beam web was connected with the cross members temporarily using six M16 high strength bolt. The detachable clamping was then connected to the back beam flange using another six M16 high strength bolts. Besides, the detachable clamping was connected from its ends by additional 6 M16 high strength bolts to the mounting stiff frame as shown in Figure 3.14. The specimen then aligned in order to ensure that the projectile and the column of the specimen have the similar centreline. After that, all the bolts by which the beam of the specimen was connected to the stiff frame were tightened up to a torque of 200 N.m using appropriate torque wrench. The middle bracer was then connected to the detachable clamp by three M16 high strength thread bars and to the floor mounted rails by four M16 high strength bolts.

3.4.3.2 Quasi-static test setup

The quasi-static tests were performed in this study for comparison purposes with specimens tested under impact load and to obtain good insight into the dynamic effect. The detachable clamp with its bracers was used to support the specimens, as shown in Figure 3.15. Two additional bracers were also provided for more support. The detachable clamp then connected to an existed rigid beam using four box sections of 100 x 50 x 6 mm and four M20 high strength thread bars. The rigidity of the frame used in quasi-static tests was examined prior to testing the specimens. Hence, one trial specimen having a connection stronger than all of those to be investigated was tested under quasi-static load.

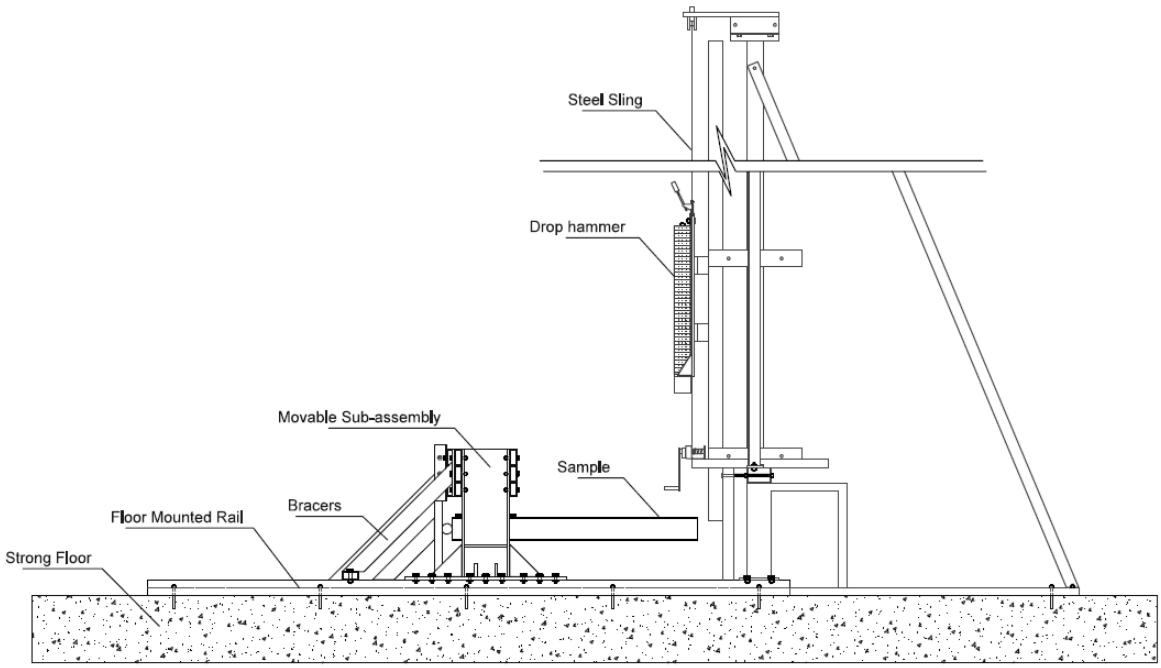

Figure 3.13. Schematic diagram of the test setup.

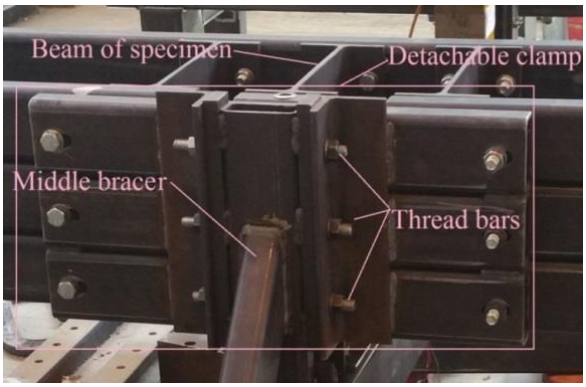

Figure 3.14. Details of detachable clamp.

The translational movements of the detachable clamp were recorded using two dial gauges. One of the dial gauges was placed horizontally on the top of detachable clamp whilst the other one was placed vertically at the bottom. The horizontal and vertical movements were recorded up to a considerable displacement, which were 0.9 mm and 0.8 mm, respectively. However, it is expected that this error is to be minimised using weaker connections as proposed in this study. In order to ensure the continuity of the contact between the loading

ram and the column, a steel sphere with a diameter of 56 mm was attached between the loading ram and a steel plate that was attached to the column as shown in Figure 3.16.

Figure 3.15. Quasi-static test setup: (1) Loading ram (2) Steel sphere (3) Loading frame (4) Detachable clamp (5) Bracer (6) M20 thread bars (7) Box sections (8) Rigid steel beam.

Figure 3.16. Quasi-static loading arrangement (1) Loading ram (2) steel sphere (3) column of specimen (4) LVDT.

3.1 Instrumentations

3.1.1 Instrumentation used in impact test

3.1.1.1 High speed video camera

In order to capture the maximum displacement at the free end of the struck column, a high speed camera (HSC, MotionPro X4, Model No. X4CU-U-4) with 10000 frames per second resolution, was used. A target is attached to the projectile and the HSC was placed in the same level when the projectile starts to hit the column. One high voltage light was also directed towards the target to increase clarity. As the mass of the impact rig was released using the switch panel, the HSC begins to record the video frames of impact event which takes not more than 50 ms. ProAnalyist motion analysis software was employed to convert the frames captured by the HSC to displacement time history curves. To obtain accurate results, a ruler was attached on the column channel of the impact rig near the target at which approximate displacement could be measured to compare with that measured by the HSC.

3.1.1.2 Laser Doppler Velocimeter (LDV)

A non-contact methodology using Laser Doppler Velocemeter (LDV) was employed to obtain the impact force-time history based on the velocity-time history. However, Dantec Flowlite LDV system was used in this study which includes a Burst spectrum Analyser (BSA) signal processor model 57N21. This technique was used by many researchers as an effective non-contact devise to acquire the force time history instead of the dynamic load cell [10, 14, 92] . Also, this technique was adopted here as no dynamic load cell is available in the laboratory. A computer was linked to the BSA via an interface card and setting of the BSA was performed prior to the impact test using BSA Flow software. As the projectile hits the column, the data is captured along the impact event. A special reflective tape was placed on a plate with 250 mm length and 50 mm width which was connected to the drop hammer by four 6 mm diameter screws. This tape reflects the laser beams which impinge the projectile and then the LDV processes the reflected beams to generate the velocity-time history. The details of the LDV system are shown in Figure 3.17 and the adopted BSA

settings, which are used in accordance to the recommendations of user's guide manual [93], is shown in

Table 3.3.

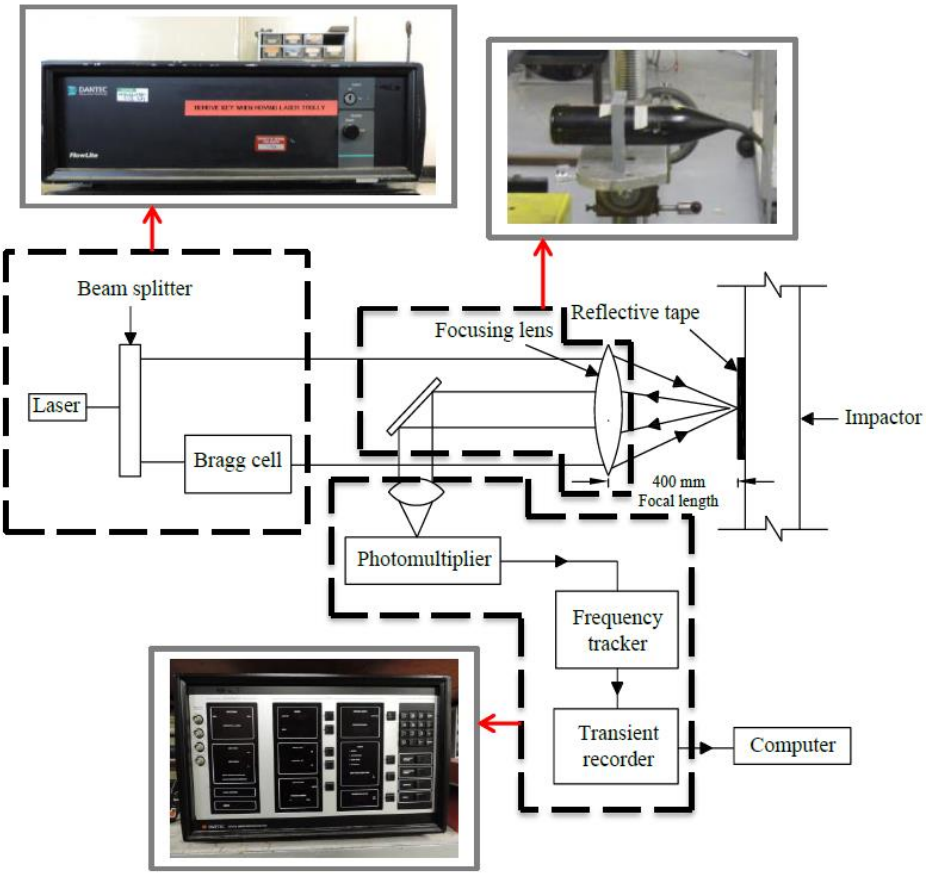

Figure 3.17. Schematic arrangement of the Laser Doppler Velocimeter [83].

Table 3.3. General settings of BSA.

	Parameter	Value
BSA data collection/buffering	Data collection mode	continuous
	Output buffer mode	Burst
	Number of burst	60000
	Measurement intervals	10
	Duty cycle	100%
BSA range/gain	Velocity centre (m/s)	3.31
	Velocity span (m/s)	13.2
	Record length	16
	High voltage (V)	848
	Signal gain (dB)	35
	Calibration (m/s)	6.61

Due to the noise included in the acquired velocity-time history obtained from LDV, a filtering process was performed to smoothen the data acquired. Hence, Low pass Butterworth filter with the fourth order was used. The acquired signals were processed using the digital filter software imPRESSion 6 (Nicolet Technology, 2002), as shown in Figure 3.18. Three stages in the velocity-time history curves could be specified in a typical velocity time history. The first stage occurred as the projectile hits the column with its maximum velocity which is about 7.5 m/s. In the second stage, the projectile and the column move downward together up to the maximum displacement of the column. In this stage, the velocity of the projectile decreases corresponding to an increase in the displacement of the column up to the maximum displacement. The third stage includes the bouncing back of both the column and the projectile due the elastic energy.

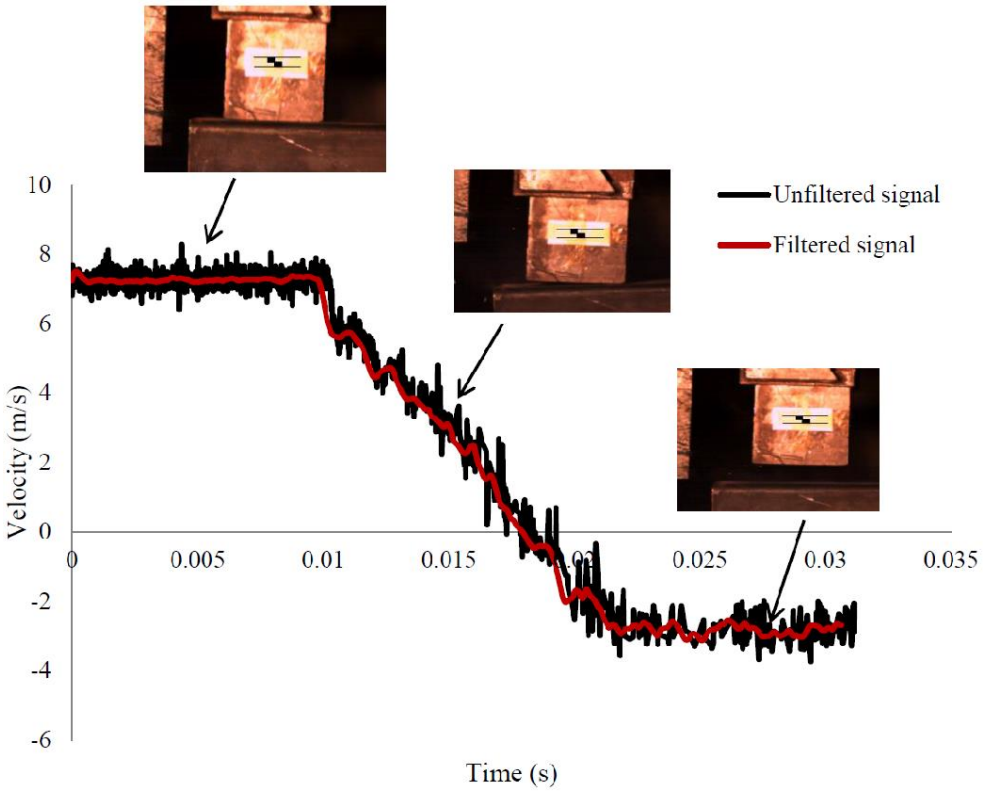

Figure 3.18. Typical filtered velocity-time histories of the impact test.

The raw data for each test was reduced to be within the period of the first contact between the projectile and column up to the rebound. The time increments are equalled using the

linear interpolation function available in the impression software and then, the data are filtered using the Low pass Butterworth filter. The impact force can be then obtained using Newton Second Law by multiplying the mass of the drop-hammer by the acceleration which was calculated from the differentiation of the impact velocity with respect to time.

3.1.1.3 Strain gauges

The measurements of strains under impact load require dynamic data logger able to acquire data within a short period of impact loading which is not available in the laboratory. Therefore, a plan was made to design a system at which the strain time history could be captured. Figure 3.19 shows a schematic drawing of the connection of the system developed in addition to the equipment used. In this system, a single 120 Ω strain gauge was attached on the specimen. A three wire connection was taken to an intermediate box where each gauge was then connected into a full Wheatstone bridge by adding three bridge completion resistors. Also, a calibrated resistor was added in this part of the circuit. The value of the calibration resistor, which was switched into the circuit in parallel to the gauge was 5880 Ω (equivalent to 10000 μƐ as indicated in the published table from the gauge manufacturer). A four wires connection was then taken from the intermediate box into a Fylde-359TA- Signal conditioner (amplifier). A bridge balance could be applied from here so that no load gives zero output. The gain of the amplifier was adjusted so that a 10000 μƐ change gives a 5 volt output. Hence, after 10000 με the system is saturated and unable to capture strain. The output of the amplifier is then taken to a digital storage oscilloscope (Tektronix TDS2024C oscilloscope of 2 Gs/s sampling rate) which can capture the transient signal as a volt time history. The strain time history could be then calculated using the calibration equation aforementioned as 5 volt=10000 μƐ.

The system developed was examined before testing using a small steel cantilever beam of 300 x 30 x 4 mm loaded at its end with different known masses. The cantilever beam was taken from the steel tube that was used for CFST column. Therefore, tensile test results of the cantilever beam were the same of the tube. A strain gauge was placed at the top extreme

fiber of the beam near the fixed end. The theoretical stress at the location of strain gauge was calculated using the following equation.

$$\sigma = M \cdot c / I \quad (3.2)$$

where,

M: bending moment at the strain gauge location.

c : distance from the centroid of the cross section to the top extreme fibre.

I: moment of inertia of the cross sectional area.

The strain was calculated using Hook's Law using a value of modulus of elasticity of 190 GPa which was taken from the results of tensile test of steel tube. Table 3.4 shows a comparison between the measured and calculated strain with different masses. Excellent agreement was obtained for all masses investigated, which indicates that the system is calibrated.

Table 3.4 Validation of measured strain using the strain measurement system developed and the theoretical strain.

Applied mass (kg)	Measured strain (μƐ)	Theoretical strain (μƐ)	% error
2	372.5	368	1.2
5	925.5	920	0.6
7	1302	1288	1.1
10	1856.5	1840	0.9

Due to the limitation of channels available in the oscilloscope, only four multipurpose strain gauges were used. Hence these gauges were attached to each specimen at different locations to capture the strain time history. Two of them were placed on the end plate, while the other two were located on the top flange of the column where the maximum moment was expected, and on the web of the beam as shown in Figure 3.20. Also, it should be mentioned that the procedure recommended by the manufacturer of the gauges was followed to attach

them on the specimens. However, the gauging area was cleaned and abraded first and then the centrelines of a gauge were marked by a pen. Then the gauge was covered by PCT2 tape to be transferred to the gauging area on the specimen. After that, the gauge was positioned using the marked centrelines into the specimen. The tape was then lifted in a shallow angle followed by applying a thin layer of catalyst liquid to increase bonding of the gauge to the surface. A drop of adhesive was placed underneath the lifted tape and the gauge-tape assembly was wiped down using gauze sponge. A thump pressure was applied on the gauge-tape assembly for one minute and additional two minutes was needed before removing the tape. However, after the gauge was bonded on the specimen wiring process should be started. The gauge was wired using appropriate wires which were connected to the gage using appropriate solder and thermal stripping. The resistance of the gauge was then checked using appropriate ohmmeter to ensure that the gauge has no damage after soldering. Finally, a protective coating was applied on the gauge to protect it from environmental changes.

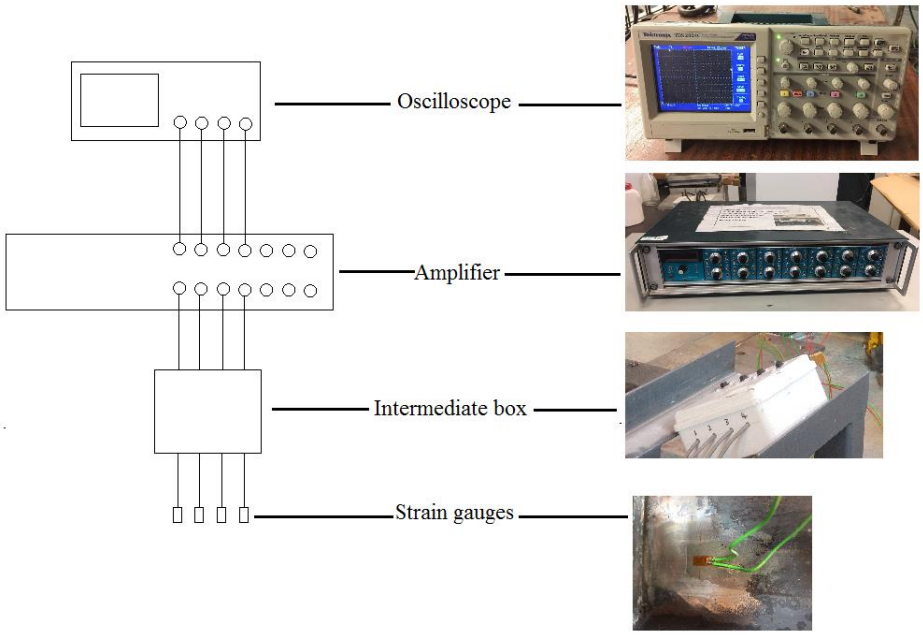

Figure 3.19. Strain measurement system.

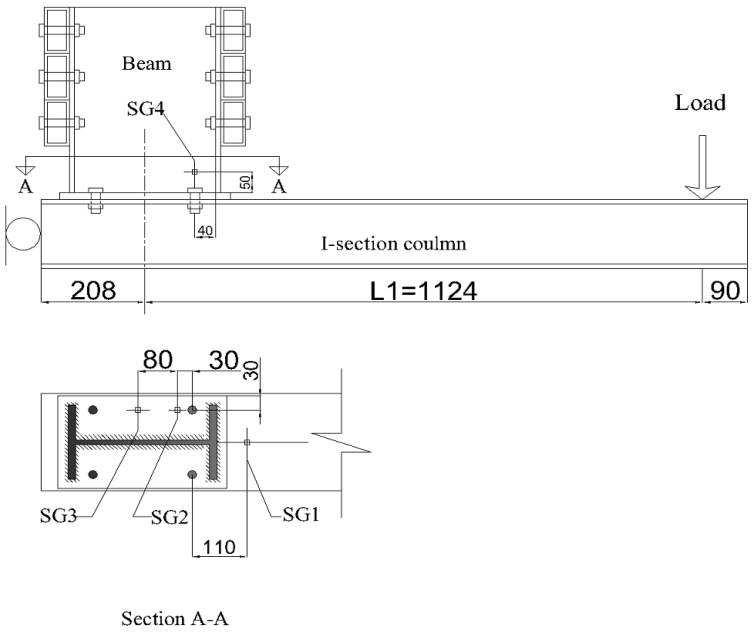

Figure 3.20. Locations of strain gauges on a specimen to be tested (Dimensions in mm).

3.1.2 Instrumentations used in quasi-static test

The data acquired in quasi-static tests were the load-displacement curves and the strains. Hence, with each load increment the displacement was recorded using one linear variable displacement transducer (LVDT) which was placed near the steel sphere to measure the displacement, as shown in Figure 3.16. Also, the strain was recorded with each load increment using the same system used in impact test but with longer time. The same type, number and locations of strain gauges that used in impact tests were used in quasi-static test for the comparison purpose.

3.2 Summary

The details of the impact and quasi-static tests carried out were presented in this chapter, including specimen preparation and test setup. The main tests to obtain mechanical properties of the materials were also described. Also, the parameters to be investigated experimentally were presented. Techniques and instrumentations to acquire the force-time history, displacement-time history in addition to strain time history under impact load were discussed. The instrumentations needed to acquire quasi-static test results were also described.

Chapter 4 : Experimental Results and Discussion

4.1 Introduction

This chapter presents the experimental results of all specimens tested under quasi-static and lateral impact loading. Here, the test results of all constituent steel materials and concrete used as an infill material in the CFST column are discussed first. Then the impact and quasi-static test results of specimens connected to a steel column using ordinary bolts are presented. Dynamic increase factors are then proposed based on the experimental force-displacement traces. Furthermore, the impact test results of specimens connected to a CFST column using long bolts technique are presented in this chapter. The performance of the latter connection is evaluated by comparing it with the former connection.

4.2 Material test results

The test procedure to obtain the properties of the materials that were used in the experimental programme of the current study was explained in Chapter three. However, the specifications to perform the compressive strength test of concrete and tensile strength test of steel were also presented in that chapter. In this chapter, the test results of these materials are presented and discussed. These test results are important to define the material properties used in the FE models and to ensure that the material strength lies in the range required by the specifications.

4.2.1 Concrete

As mentioned in Section 3.2.1 in the previous chapter that nine 100 mm concrete cubes were cast with each concrete batch to determine the concrete compressive strength at 7, 14, and 28 days. Hence uniaxial compressive force was applied on each cube using Tonipact loading machine. Based on the calculations explained in the aforementioned section, the compressive strengths of the concrete after 7, 14 and 28 days are shown in Table 4.1. The average compressive strength after 28 days was used to represent the compressive strength of concrete as explained in Section 3.2.1 in the previous chapter.

Table 4.1. The equivalent cylinder compressive strength of concrete used in CFST specimens.

Specimen	Average compressive strength after 7 days (MPa)	Average compressive strength after 14 days (MPa)	Average compressive strength after 28 days (MPa)
PFC8	15.1	18.9	24.3
FFC8	15.3	19.5	26.1
PNC8	15.1	19.2	25.9
FNC8	15.3	19.6	24.5
PFC15	14.4	18.6	25.3
FFC15	15.6	19.1	24.9

4.2.2 Steel

Mechanical properties of different steel components used in the current study were determined by performing quasi-static uniaxial tensile tests. Steel coupons were taken from each steel profile involved in the test specimens as explained in Section 3.2.2 in the previous chapter. The steel coupons were loaded up to fracture and the engineering stress-strain relationships for all profiles involved in the test specimen were obtained as shown in Figure 4.1. All the coupons exhibited an elastic behaviour until the yield point. After that, the plastic stage starts and the coupons experienced strain hardening up to failure. The modulus of elasticity (E) of each profile was determined as the slope of the elastic stage of the engineering stress-strain relationship. Nevertheless, the engineering stress-strain curves do not reflect the actual behaviour of steel under tension in the plastic stage because they do not account the reduction in area produced after necking of specimens. Therefore, these curves need be modified to obtain the true stress-strain curves before they are used in the FE modelling, which will be discussed in Section 5.2.4.1 in the next chapter. Table 4.2 shows the summary of the material properties obtained from the tensile tests. The failure modes of all coupons tested were characterized by necking followed by fracture, as shown in Figure 4.2 (a) and (b).

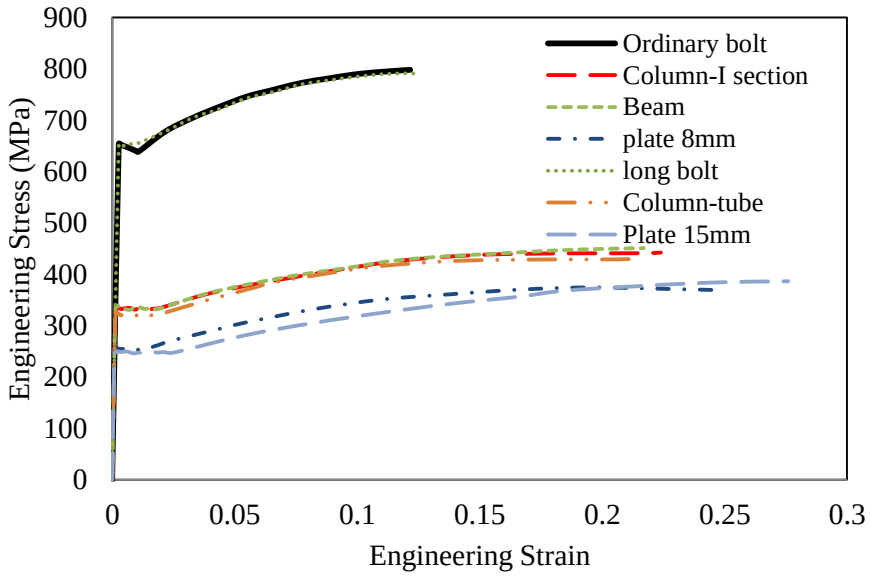

Figure 4.1. Engineering stress-strain relationships for steel components.

Table 4.2. Summary of material properties of steel profiles used in the experimental tests.

Profile	Modulus of Elasticity (E) (GPa)	Yield stress (fy) (MPa)	Ultimate stress (fu) (MPa)
Beam	191	337	448
Column (I-section)	192	336	442
Column (tube)	190	322	430
End plate-8mm	191	253	374
End plate-15 mm	190	247	386
Ordinary bolt	195	645	798
Long bolt	194	651	791

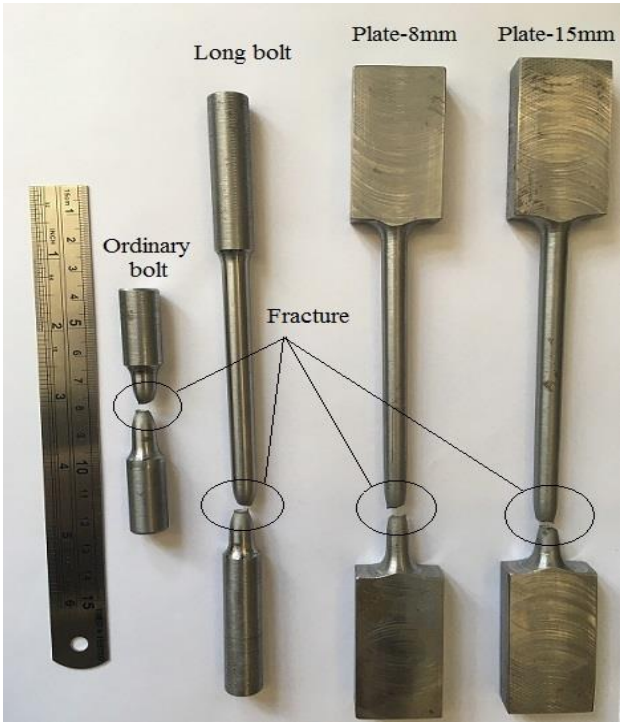

(a) Coupons with circular cross sections.

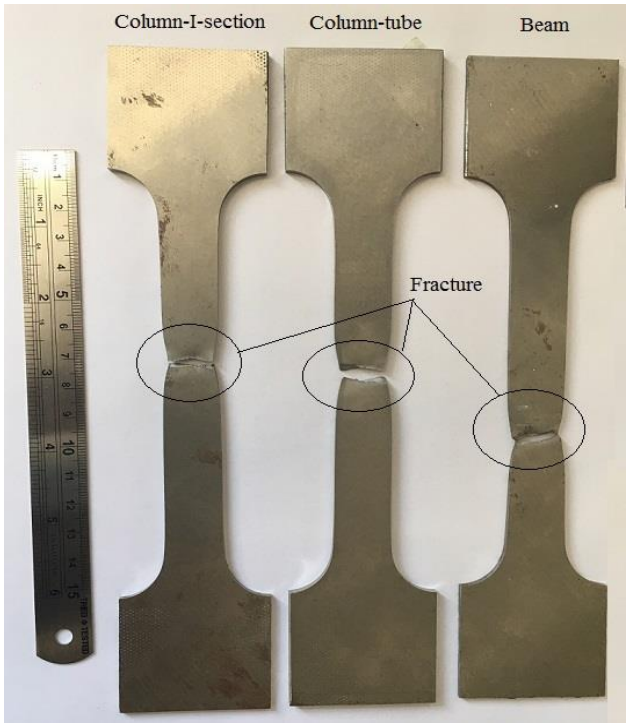

(b) Coupons with rectangular cross sections.

Figure 4.2. Failure mode of steel coupons under uniaxial tensile loading.

4.3 Impact test results of connections to steel columns

Seven full-scale specimens were tested under lateral impact load to investigate the effects of the connection type, impact loading location and plate thickness on the connection response of specimens connected to steel columns. The impact load was applied using a drop hammer with a mass of 107.5 kg hit the specimens from a height of 2.9 m. the corresponding initial impact energy was 3056 J. As the mass released, the projectile starts to move downward with the initial velocity, which starts to decelerate when the projectile starts to touch the column of the specimen. After that, the column starts to displace and the connection starts to deform. A target was placed on the projectile to be tracked by the high speed camera (HSC) to obtain the displacement time history during the impact event. Another target was also placed to obtain the velocity time history which is converted using Newton Second Law to obtain the impact force time history, as explained in Section 3.5.1.2 in Chapter three. Then both the time histories of displacement and impact force were combined to obtain the impact force-displacement relationships. It was adopted in this study to present the load displacement traces rather than the force and displacement time histories for the following reasons.

(1). the structural engineers are more interested in load-displacement traces than time histories. The energy dissipated and the recovered energy can only be derived from load-displacement traces. Also, the stiffness could only be obtained from load-displacement traces.

(2). the validation of load and displacement time histories could be combined by the validation of the load-displacement traces, since they have to be synchronised. As the result, the number of figures can be reduced in the current study. In fact, it is more challenge to validate the numerical models in the load-displacement trace.

(3). it is intended later to compare the impact results with quasi-static results. As known, the quasi-static results are time independent and presented as load-displacement traces. Therefore, it is better to present the impact results as load-displacement traces to be

compared with quasi-static results. It should be mentioned that for each test, only the data within the period from the first contact between the projectile and the column to the time of the rebound was adopted in the current study.

4.3.1 The Effect of impact loading locations

The effect of impact loading locations on both FPC and PDEPC was investigated by comparing the test results of specimen FNI8 with FFI8 and PNI8 with PFI8, respectively. The comparison is presented in terms of deformation modes and load-displacement traces.

4.3.1.1 Deformation modes

The impact test results for specimens selected to investigate the effect of impact loading locations demonstrated three different modes of failure, i.e. bending of end plate of PDEPC as shown in PDEPC

Figure 4.3, bending of first bolt pair as shown in Figure 4.4 and fracture of the end plate close to the weld toe (tearing failure) as shown in Figure 4.5. It can be seen that all specimens experienced large deformations at the end plate, while fracture of the weld toe occurred only in PDEPC. The bend of the first pair of bolts is noticed as well in all specimens, which is likely attributed to the bearing stresses between the end plate and the bolt shank. This may lead to another type of failure representing either by combined shear-bending of the bolt or bearing failure of the plate. Owens et al. [94] showed that the bearing failure of plate occurred under pure quasi static axial tensile load on the joint. The failure mode of FPC seems not to be influenced by changing the impact loading location. However, in PDEPC, it was observed that impacting the column near the connection demonstrated slightly higher tearing failure, as can be seen in Figure 4.5 (a) and (b).

(a) FPC (b) PDEPC

Figure 4.3. Bending of the end plate under lateral impact load in specimens connected to steel columns.

Figure 4.4. Bending of the first bolt pair.

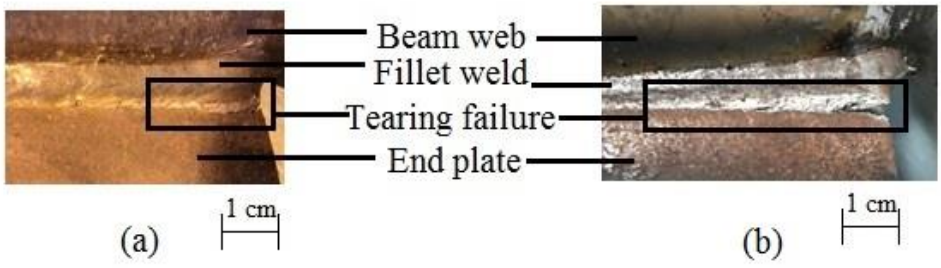

Figure 4.5. Fracture of the end plate close to the weld toe. (a) Specimen PFI8. (b) Specimen PNI8.

4.3.1.2 Force-displacement traces

The impact force-displacement curves were obtained by combining both the impact force time history acquired from the LDV and the displacement time history acquired from HSC. In general, three stages can be identified in the force-displacement relationships for all specimens tested that connected the steel to the CFST column, as shown in Figure 4.6. These three stages are as follows:

(1). the initial peak force stage: at which the impact force reaches its maximum value with less than 3 mm of displacement, which is approximately the same case in the results obtained by Aghadmy et al. [69] and Qu et al [63]. This peak force is produced due to the rapid change in the velocity before and after the first contact between the projectile and the struck column. A zero force was produced in some specimens with an increase in the displacement due to missing the contact of projectile to the struck column, where a clear gap was noticed between them by the HSC. The initial peak force may be followed by sequential lower peak forces before the onset of the second stage, especially in the specimens loaded far away from the connection;

(2). the plateau stage: in this stage, the connection begins to deform plastically with a relatively stable impact force after the initial peak or the final peak generated;

(3). the bounce stage: in this stage, the curve descends from the total displacement to a separation point as the projectile starts to separate from the struck column.

In other words, it can be said that the initial peak force stage and plateau stage represent a loading stage, while the bounce stage represents an unloading stage.

Figure 4.7 shows a comparison between the load-displacement traces of FPC that connected to a steel column in different impacting load locations (L_1=1.124 m and L_2=0.375 m). Changing the impact loading location from L_1 to L_2 leads to increasing the initial peak force by 24 %. After the initial peak force stage particularly when the load is far away from the joint (L_1), an obvious intermittent impact can be seen due to missing the contact between the projectile and the struck column as explained above. Besides, the peak forces followed the initial peak force, descending gradually until reaching the plateau stage as the difference in velocities between the projectile and column was smaller. Grimsmo et al. [78] also observed multiple hits leading to intermittent impact and gradual descending of peak forces in joints with a flexible end-plate under impact load. However, these peak forces were not followed by plateau force as the case in the load-displacements traces in the current study, as can be

seen in Figure 4.8 for two specimens selected. The first specimen (LS-RLD-6) refers to low speed in the reverse loading direction, while the second specimen (LS-DLD-7) refers to low speed in the design load direction. The plateau stage in the specimen loaded near the connection (L_2) starts from the displacement around 5 mm and ends with the maximum displacement, which is 22.35 mm, i.e. it represents around 78 % of the loading stages. However, the same stage represents not more than 40 % of the loading stages in specimen loaded far away from the connection (L_1). The multiple intermittent impact produced in specimen loaded far away from the connection delayed the onset of the plateau stage. In other word, a continuous force flow in the specimen loaded far away the connection starts after three sequential missing contact of projectile to struck column, while only one contact missing can be observed in specimen loaded near the connection. In order to compare the forces generated in plateau stage, the average of the upper and lower extremes in this stage is adopted and will be used in the current study. Based on this assumption, the average plateau force of specimens FNI8 and FFI8 is 139 kN and 51 kN, respectively, which means that the average plateau force of specimen with FPC loaded near the connection is 273% of that with PDEPC. In the third stage, the force starts to decrease to zero and the displacement retreated slightly to the permanent value when the projectile rebound back from the struck column.

Figure 4.9 shows a comparison between the load-displacement traces of PDEPC that connected to steel column in the selected impact loading locations. In general, similar trends can be seen to that of FPC but with more peaks prior to plateau stage. The initial peak force increases by 7% if the impact location is changed from L_1 to L_2, while it is 24% in FPC as mentioned before. Therefore, it can be said that the initial peak force of the stiffer connection is more affected by changing the impact loading location. Intermittent impact can be observed also in PDEPC as that in FPC. Moreover, the average plateau force of the specimen impacted near the connection is 233% of the one for the specimen impacted far away from the connection. Since the stiffness of PDEPC is lower than the stiffness of FPC, lower forces were produced in the former in all stages corresponding to lower displacements. Similar

conclusion was obtained by Al-Hussainy [14] in his numerical study to investigate the effect of using different boundary conditions on the lateral impact response of CFST. It was found that slight increase in the force corresponding to considerable decrease in the displacement was produced by changing the boundary conditions of CFST members from fix-fix to pin-pin.

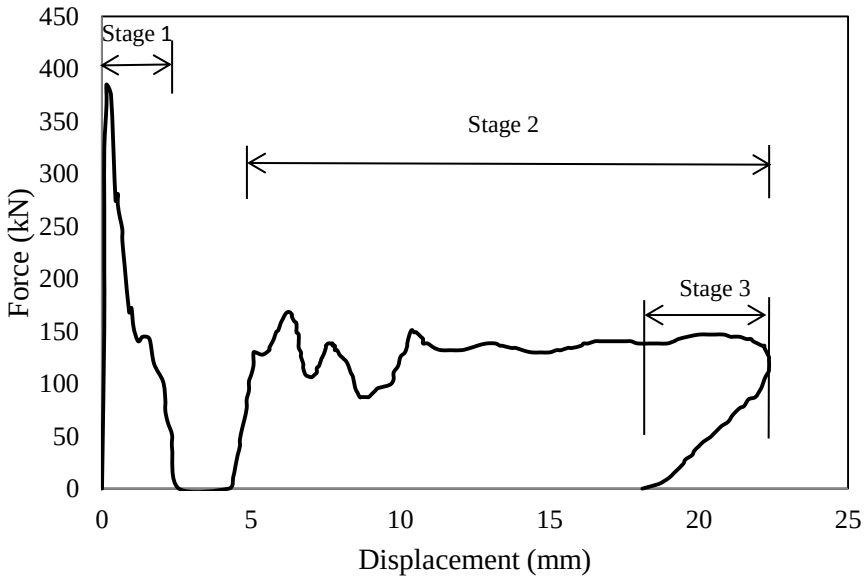

Figure 4.6. Typical stages of Load-displacement traces of selected specimen (FNI8).

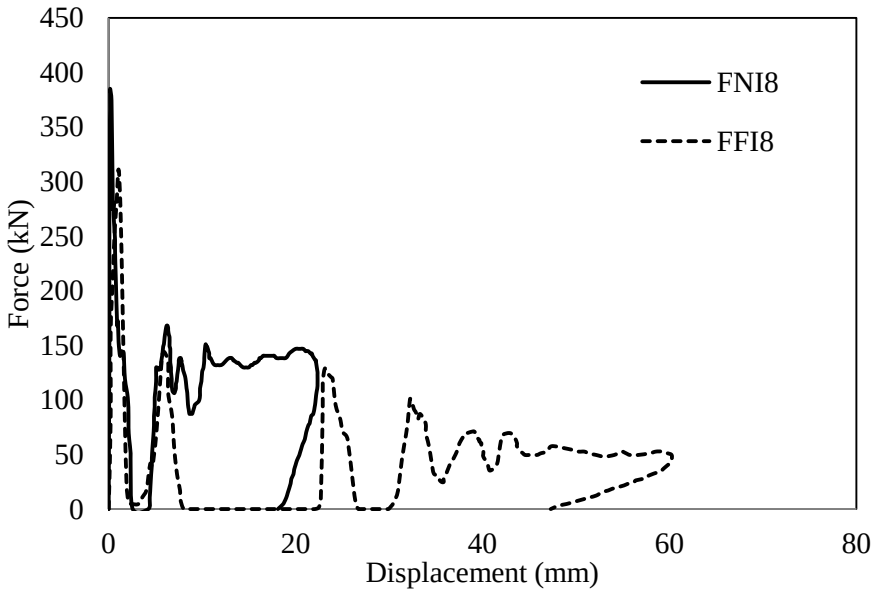

Figure 4.7. Effect of impact load location on load-displacement traces of FPC to steel column.

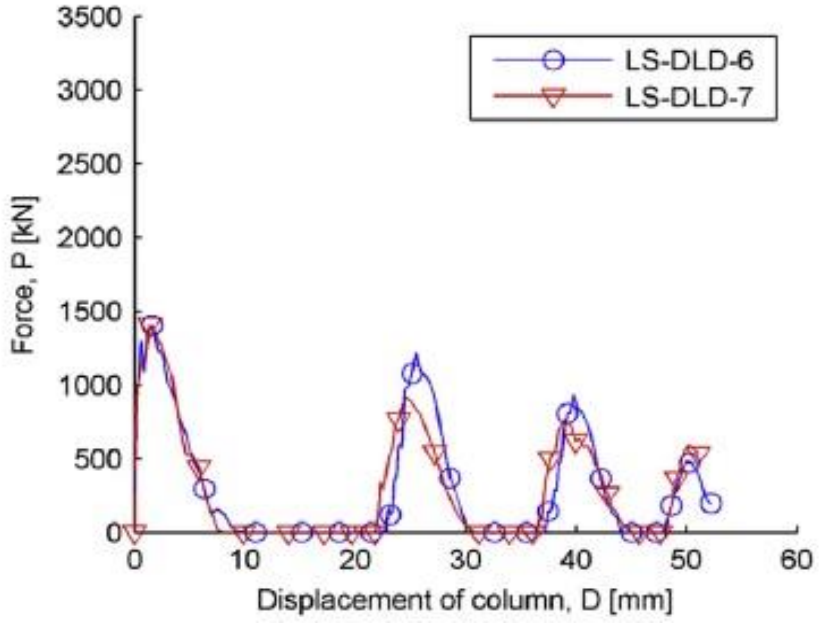

Figure 4.8. Force-displacement traces of selected test specimens under impact load obtained by Grimsmo et al. [78].

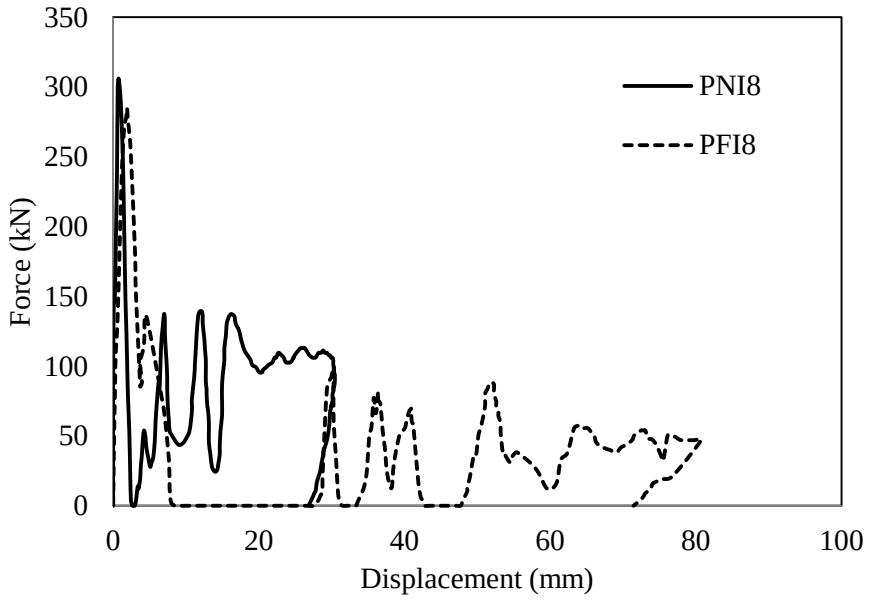

Figure 4.9. Effect of impact load location on load-displacement traces of PDEPC to steel column.

One of the important properties of a connection that can be obtained from the load-displacement traces is ductility. Providing ductile beam-to-column connections is required to help with preventing sudden failure of a connection [90]. The ductility of a beam-to-column connection can be defined as the maximum rotation that the connection demonstrated before fracture. This rotation can be calculated by dividing the maximum displacement at the free end of the column to the distance from the projectile to the connection. Thus, the rotation of specimen FNI8 can be calculated by dividing the maximum displacement (22.34 mm) to a distance of 375 mm, which gives a rotation of 3.41º, while specimen FFI8 gives a rotation of 3.07º using the same calculations. Then, a slight increase in ductility is produced in FPC if the specimen impacted near the connection. Similar trend can be noticed in PDEPC but with a higher rotation, i.e. rotations of 4.65º and 4.12º were determined in specimens PNI8 and PFI8. The effect of impact loading location on the connection behaviour was investigated numerically in a study performed by Wang et al. [9] to obtain the response of fin plate connection under falling floor impact load. The impact load in this study was applied on the beam, producing a combined dynamic shear-bending moment on the fin plate. The numerical results showed that the maximum rotation occurred at the impact point as in the results obtained in the current study. Also, it was found that the final deformation of the beam was significantly influenced by impact locations, while such the deformation was only slightly affected in the current study. This may be attributed to the different boundary conditions used by Wang et al. [9], if compared with the boundary conditions adopted in this study. More details will be presented in the next chapter using the validated model on the effect of using different boundary conditions on the connection response.

4.3.2 The effect of plate thickness

Specimens FFI8 and FFI15 were considered to investigate the effect of plate thickness on the structural behaviour of FPC while specimens PFI8 and PFI15 were chosen for PDEPC.

4.3.2.1 Deformation modes

To achieve the required ductility and flexibility of a connection, the SCI publication P212 [95] recommended to use a plate thickness between 8-12 mm. However, it is proposed, in this study, to investigate a thicker plate in addition to the recommended thicknesses to obtain more knowledge of their response under lateral impact, also to examine the validity of this recommendation under such loads. Hence, a specimen of the partial end plate connection with 15 mm thick (specimen PFC15-1) was fabricated and tested. Unfavourable connection failure was observed for this specimen, represented by the loosening of the nuts in the first bolt pair. Therefore, the test was repeated with the same details but with double nuts (specimen PFC15-2) to prevent this failure and to facilitate the comparison of the results later. A slight bending in the end plate was observed for both specimens, as shown in Figure 4.10, compared with that observed using a thin plate (specimen PFI8). No nut loosening was occurred in the repeated specimen. The absence of large deformation of the plate assisted to alleviate the bearing stresses between the plate and the first bolt pair. Thus, no bearing deformation on the first bolt was observed in PDEPC with a thick plate, instead of that observed in thin plate specimen. Moreover, the deformation was transferred from the plate to the column. And the crippling failure in the top flange of the column underneath the first bolt pair was observed, as shown in Figure 4.11. The intensity of crippling failure increased in FPC specimen with a thick plate as can be seen by comparing the crippling failure in Figure 4.11 with that in Figure 4.12. Also, it can be seen that FPC did not show any plastic deformation in the plate. Therefore, lower strain can be noticed in strain gauges located at thick plates than those in the thin plates, as shown in Figure 4.13 and Figure 4.14. Also, SG1 which is located in the column showed a higher strain in the specimen with thick plate than those with thin plate, as shown in Figure 4.15.

Figure 4.10. Slight bending of PDEPC with thick plate.

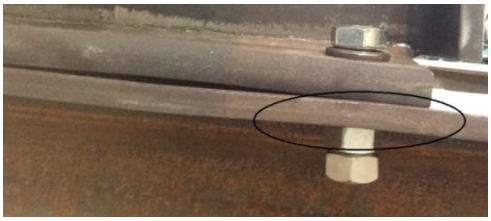

Figure 4.11. Flange crippling of steel column in PDEPC specimen with thick plate.

Figure 4.12. Flange crippling of steel column in FPC with thick plate.

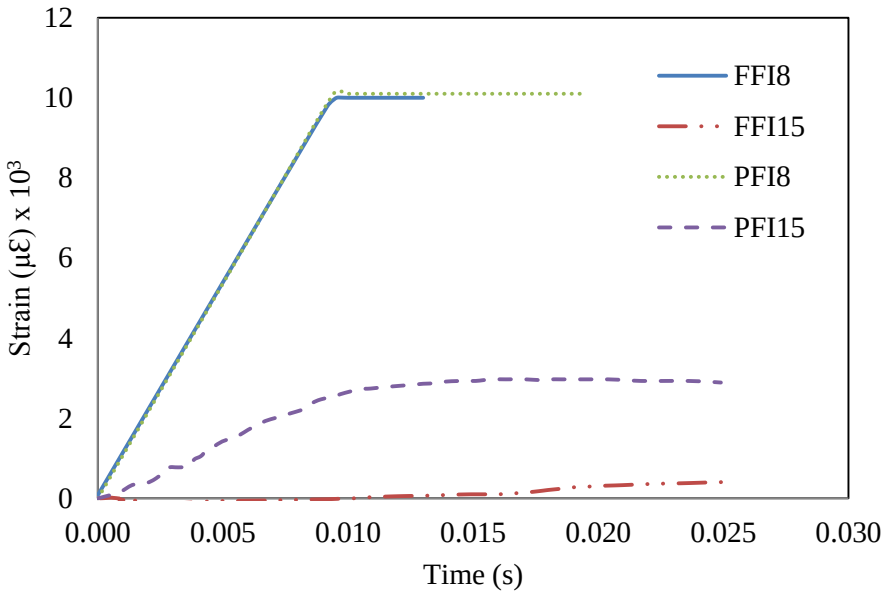

Figure 4.13. Strain time history of SG2 located at end plate.

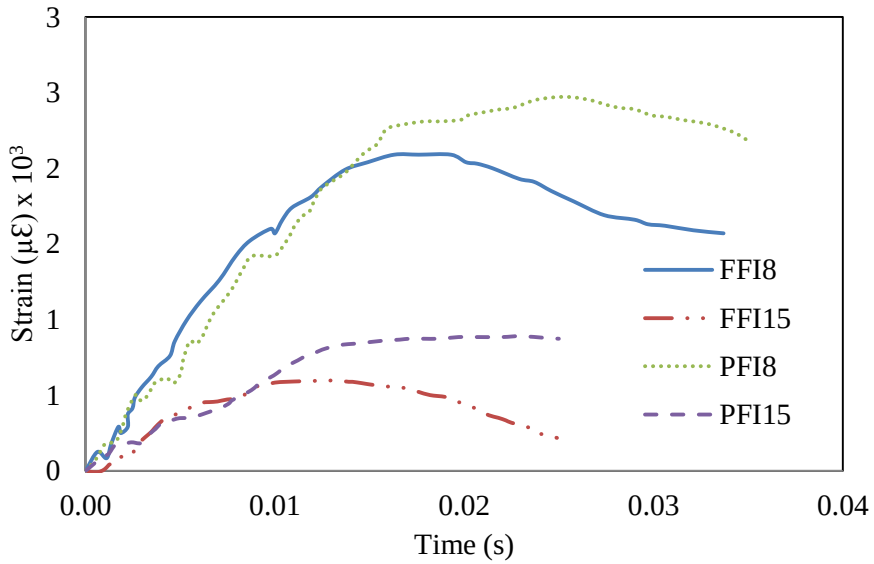

Figure 4.14. Strain time history of SG3 located at end plate.

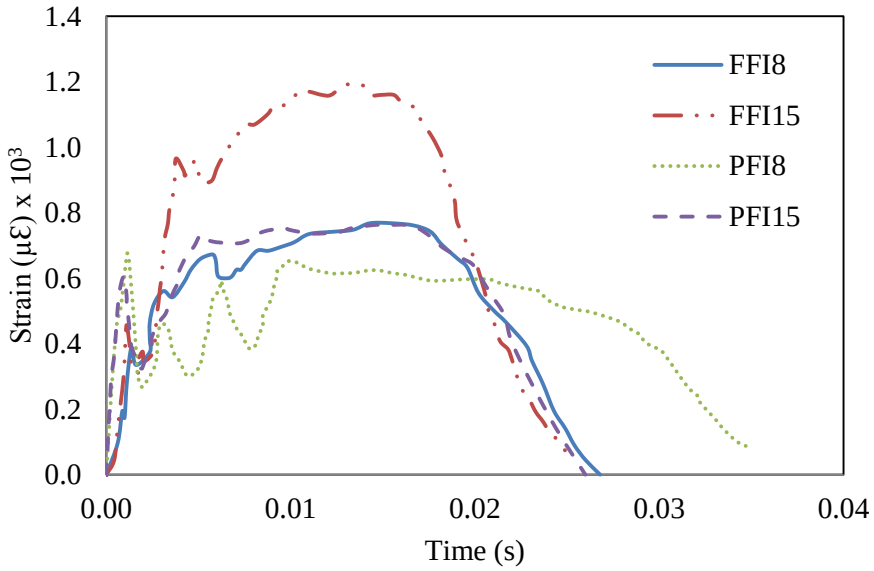

Figure 4.15. Strain time history of SG1 located at column.

4.3.2.2 Force-displacement relationships

The effect of changing end plate thickness on the impact response of both connections selected in the current study can be seen in Figure 4.16 and Figure 4.17. It is clear that using thicker plate for both connections leads to decrease the maximum displacement corresponding to a relative increase on the peak and plateau forces. Increasing plate thickness from 8 to 15 mm contributes to the increase of the initial peak force by 23% and 28% in PDEPC and FPC, respectively. These results were obtained assuming that there is no nut loosening failure. However, this would lead to increase the internal forces in the bolts, producing the sudden fracture of them and affecting the ductility of connection negatively. The maximum displacement can be used to examine the ductility of the connection for the similar impact location (i.e. similar distance from the impact load to the connection). The experimental results obtained in Figure 4.16 and Figure 4.17 indicate that both the connections become more ductile using a thinner end plate. However, the ductility of FPC and PDEPC increased by 13% and 36%, respectively, if the end plate thickness reduced from 15 mm to 8 mm.

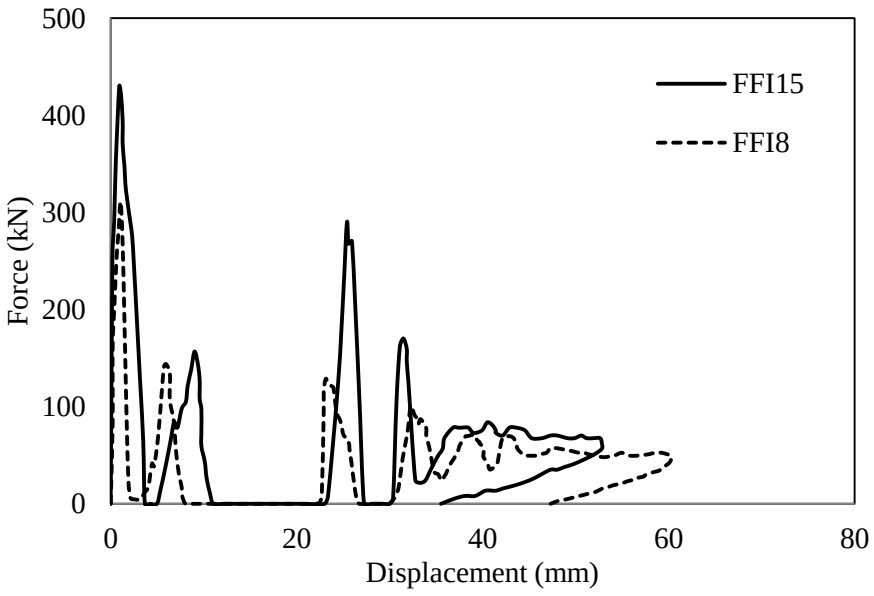

Figure 4.16. Effect of end plate thickness on load-displacement traces of FPC to steel column.

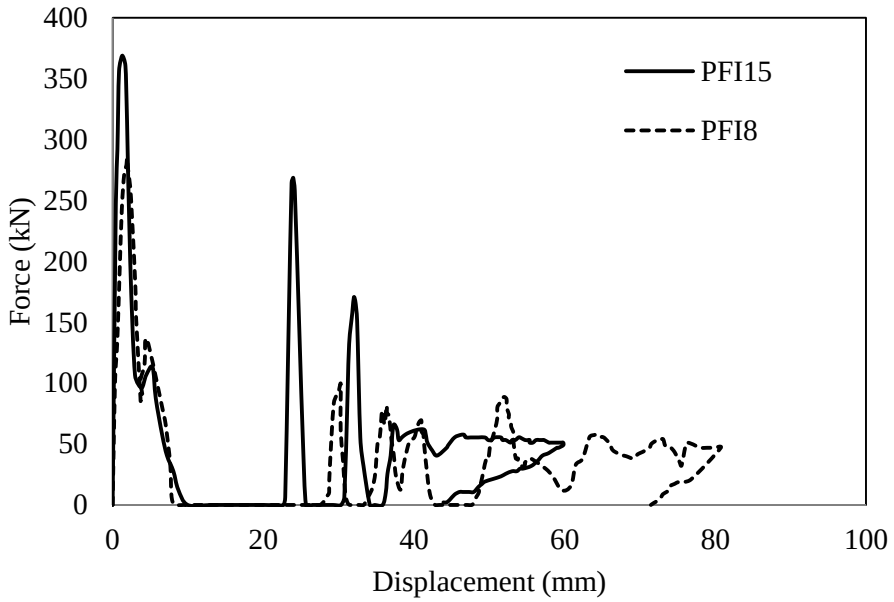

Figure 4.17. Effect of end plate thickness on load-displacement traces of PDEPC to steel column.

4.3.3 Comparison between response of FPC and PDEPC

In order to experimentally show the difference between the response of FPC and PDEPC under lateral impact, three groups were considered. Hence, FNI8 can be compared with PNI8, FFI8 with PFI8 and FFI15 with PFI15.

4.3.3.1 Deformation modes

Both types of connections investigated experienced a considerable bending at the end plate, particularly with using thin end plate. However, a lower bending on the end plate can be obtained with increasing its thickness. The main difference between the two types is the development of the fracture close to the weld toe in PDEPC, which was not observed in FPC. This failure resulted from the combination of the shear and tensile stresses developed in this region. These stresses were resisted by the weld between the beam web and the end plate only in PDEPC. Thus, welding the end plate to the flange in FPC type in addition to its web alleviates these stress effects and delays the development of this failure. More details

will be presented in the next chapter by using the validated models to examine the development of this failure along the impact event and to predict the location of this failure in FPC. Similar bolt deformation was observed in both connection types but with different intensity. Hence, PDEPC experienced a higher bolt deformation due to the higher bearing forces compared with FPC.

4.3.3.2 Force-displacement relationships

Figure 4.18 to Figure 4.20 show comparisons of load-displacement traces of FPC and PDEPC to steel column with different loading locations and end plate thickness. In general, higher forces can be seen in FPC traces compared with that of PDEPC. This is due to the relatively higher strength of the former type than the latter. Figure 4.18 shows the load-displacement traces of both connections with 8 mm thick end plate and loaded far away from the connection. The initial peak force of the specimen FFI8 is 8% higher than that of specimen PFI8. The other peak forces of specimen FFI8 also seem to be higher than that developed in specimen PFI8. These multiple peak forces, which resulted from the intermittent impact, delayed the appearance of plateau stage in addition to making it shorter and unrecognizable in comparison to other specimens tested.

Figure 4.19 shows a comparison between the force-displacement curves of FPC and PDEPC loaded near the connection. The specimen with FPC shows a higher initial peak force than PDEPC by 21% and the average plateau force of the former is determined to be 139 kN, which is considerably higher than the latter, by about 26%. Figure 4.20 shows a comparison between both connections, having a thick plate with an impact location far away from the connection. The initial peak force was decreased from 430 kN to 370 kN, i.e. by 14 % if FPC replaced by PDEPC. In addition to the higher forces produced in the impact event on specimens with FPC, lower displacements can be observed in these specimens compared with those with PDEPC. This is due to the higher stiffness of FPC compared with that of PDEPC.

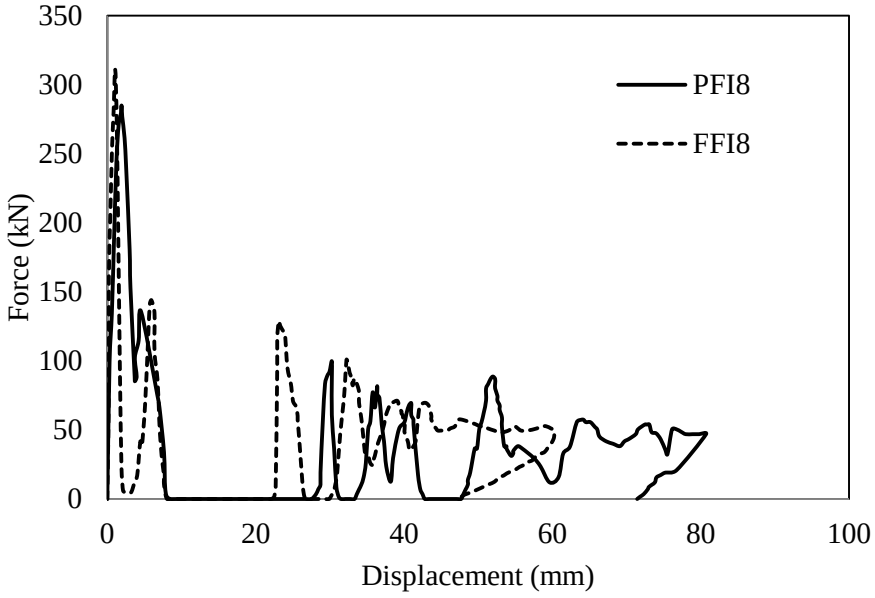

Figure 4.18. Comparison between the load-displacement traces of FPC and PDEPC to steel column loaded with lateral impact at L_1 with 8 mm end plate thickness.

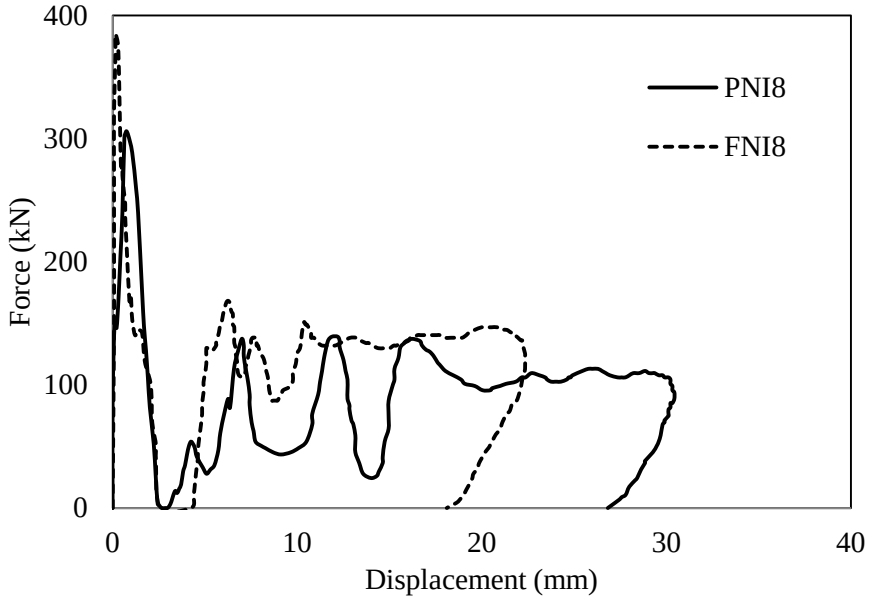

Figure 4.19. Comparison between the load-displacement traces of FPC and PDEPC to steel column loaded with lateral impact at L_2 with 8 mm end plate thickness.

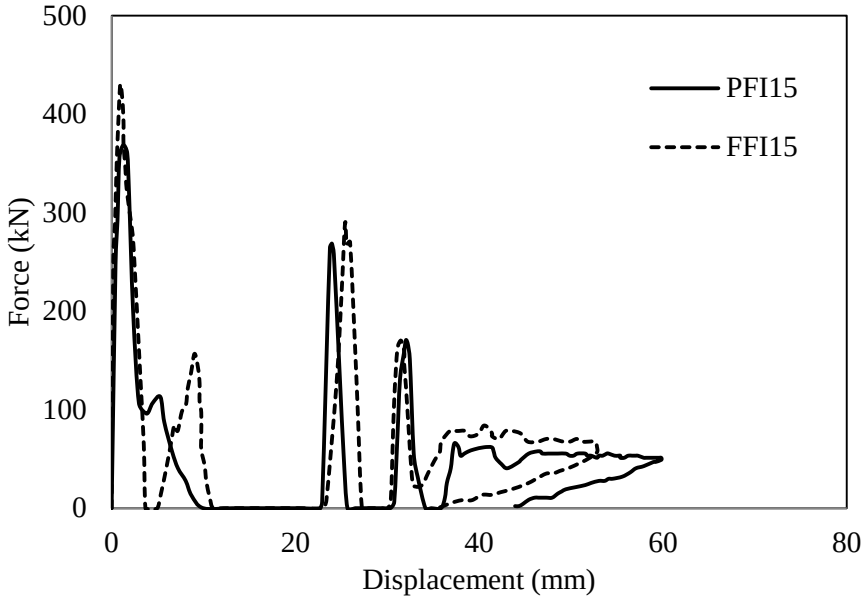

Figure 4.20. Comparison between the load-displacement traces of FPC and PDEPC to steel column loaded with lateral impact at L_1 with 15 mm end plate thickness.

4.4 Quasi-static test results of the connection to steel columns

Four quasi-static tests were carried out to show the difference between the behaviour of end plate connections under quasi-static loading and impact loading. Also, the dynamic effect that connections experienced under impact load can be predicted by comparing the impact test results with the quasi-static test rests. This dynamic effect is expressed in the literature as dynamic increase factor (DIF) or dynamic amplification factor (DAF), which will be discussed in more details in Section 4.5.

4.4.1 Deformation modes

Generally, the deformation modes of the four specimens that were tested under quasi-static load were similar to the corresponding specimens tested under impact load but with a slightly higher damage for PDEPC specimens close to the weld toe, as shown in Figure 4.21 which can be compared with Figure 4.5 (b) to see the difference between both deformation modes. The strain rate where the plate tearing occurred in specimens tested under impact load seems to be higher than the strain rates generated in other locations of the plate, which increases the stresses of the plate and then to delay the tearing failure in that location. Hence,

PDEPC responded relatively more ductile under impact load than quasi-static load. Also, this confirms the increase on the connection stiffness under impact load due to the strain rate effect at the crack tip. In other words, two major components contributed to produce this failure, i.e. excessive bending and shear on the plate and both of them were delayed due to the strain rate effect.

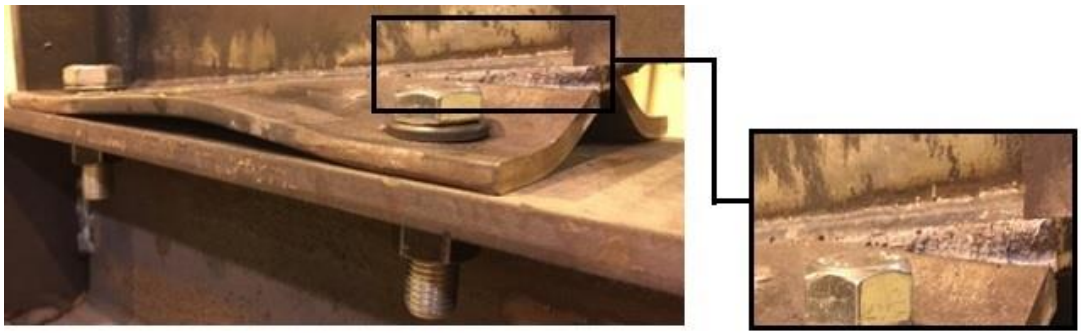

Figure 4.21. Tearing failure close to the weld toe of specimen PNI8S under quasi-static load.

4.4.2 Force-displacement relationships

Figure 4.22 and Figure 4.23 show the load-displacement curves of the four specimens tested under a quasi-static load. It can be seen that all the connections demonstrated bilinear behavior with noticeable degradation on the stiffness up to failure. FPC showed higher stiffness than PDEPC in both loading locations, as expected, since the former is a moment resistance connection. Also, PDEPC showed a considerable ductility up to failure though it is classified as a simple connection. Comparing the force displacement curves under a quasi-static load with that under an impact load, some observations can be made as follows.

a) More energy was dissipated in the first stage of specimens under an impact load than those under a quasi-static load as can be seen in Figure 4.24. This is due to the high initial peak force generated at the beginning of an impact event due to a large change in acceleration of the projectile,

b) As expected, continuous force flow can be observed in specimens loaded under quasi-

static load. However, the specimens tested under impact loading intermittent force due to the intermittent impact,

c) The forces in curves under quasi-static seem to be approximately equal to the plateau force that appeared on the specimens under impact load.

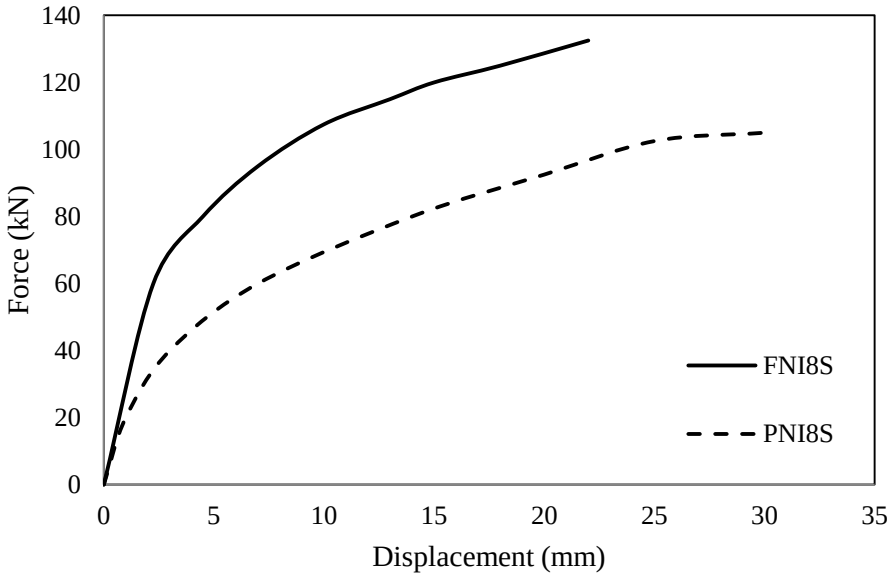

Figure 4.22. Force-displacement curves of the specimens loaded near the connection (FNI8S and PNI8S) under quasi-static load.

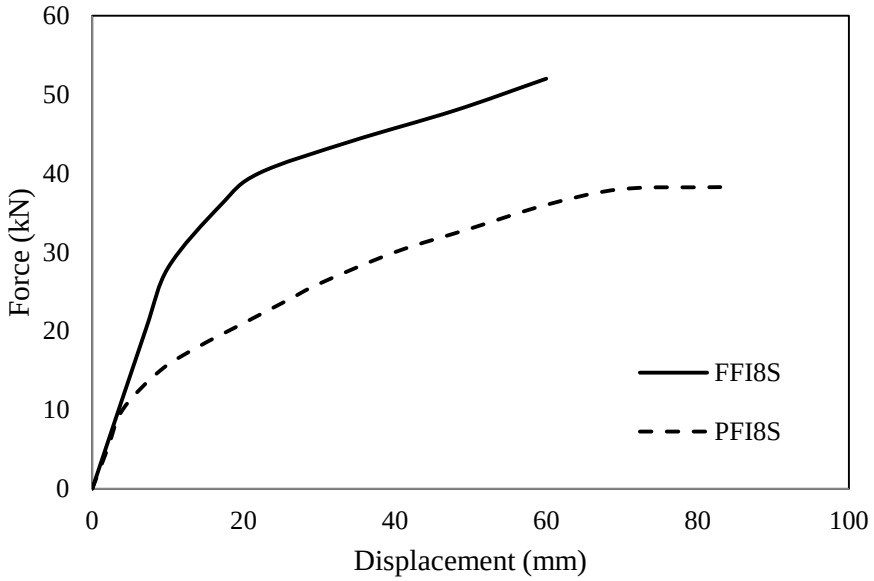

Figure 4.23. Force-displacement curves of the specimens loaded far away from the connection (FFI8S and PFI8S) under quasi-static load.

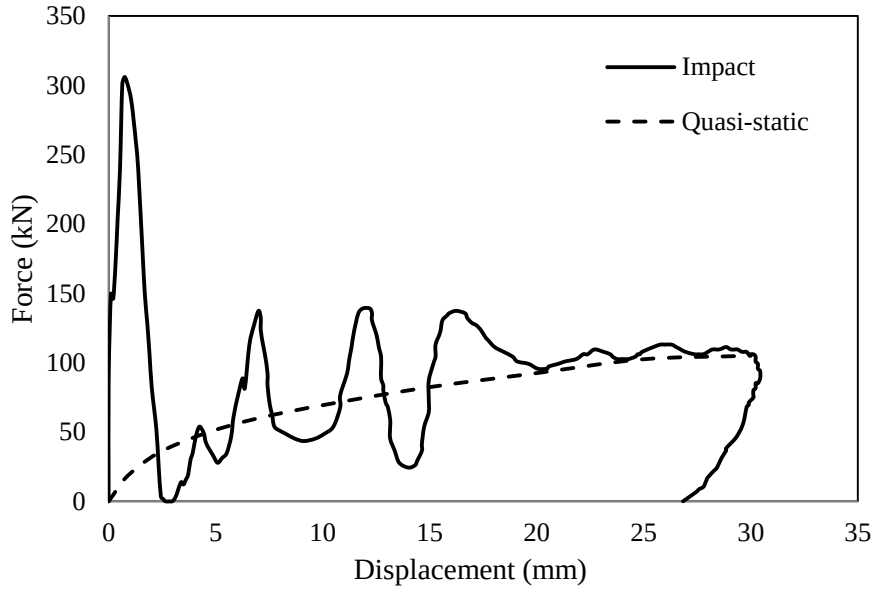

Figure 4.24. Force-displacement curve of specimen PNI8 under impact load and PNI8S under quasi-static load.

4.5 Dynamic increase factors

Dynamic increase factor (DIF) can be defined as the ratio of dynamic strength to its static counterpart of a material [96, 97] or structural member. Response of a structural member at high strain rate is more complicated than its static response. Therefore, one of the straight methods to predict the strength of a structural member under dynamic load is to enhance its static strength multiplying by an appropriate DIF. This approach was used by Wang et al. [88] to estimate the dynamic resistance capacity of concrete filled double steel tubular members under lateral impact. Also, it was used by Liu et al. [89] to address the appropriate DIF for the design of structures against progressive collapse. Generally, two types of DIF were commonly used: force-based DIF and displacement-based DIF [98]. The former is the ratio of the dynamic load to the static load of a structural system under the same displacement, whilst the latter is the ratio of the dynamic displacement to the static displacement under the same load. In the current study, the former was found to be more

appropriate so that the impact force-displacement relationships were recorded first. Then, the corresponding specimens were loaded under quasi-static loads up to the same maximum displacement acquired under impact load. Additionally, the DIFs were proposed in this chapter in terms of the energy principles. Also, the DIFs will be proposed in another way using the validated FE models in the next chapter based on the internal forces produced in the connection. The DIF proposed using energy principles can be determined by dividing the energy dissipated under an impact load to that dissipated under a quasi-static load. Hence, dissipated energy which represents the area under load-displacement traces was determined using digital filter software imPRESSion 6 [99] for specimens tested under both load regimes. Then the DIFs were calculated using the following equation.

$$\text{DIF} = \frac{E_i}{E_s} \tag{4.1}$$

where, E_i is the energy dissipated under impact load and E_s is the energy dissipated under quasi-static load. The static dissipated energy was calculated assuming that the specimen has the same initial stiffness after releasing the load as shown in Figure 4.25. Table 4.3 shows comparisons of the E_i and E_s obtained based on the experimental results for specimens tested in addition to the corresponding DIF.

Clearly, all the static results demonstrate the lower extremes of the energy dissipated than the impact results. Based on the experimental results, the DIF varies between 1.25 to 1.38 for all specimens tested. It could be said that the proposed DIFs based on the energy approach obtained a good insight into the dynamic effect that may produce on the end plate connections under lateral impact load.

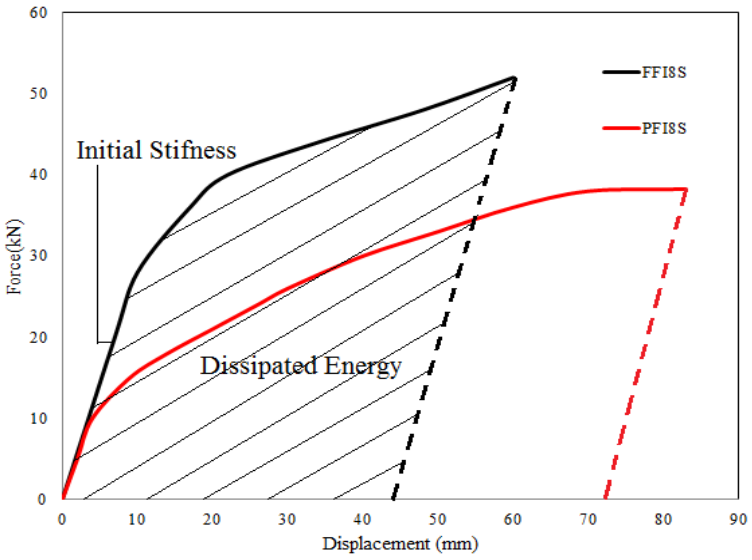

Figure 4.25. Dissipated energy of specimens tested under quasi-static load.

Table 4.3. Summary of dissipated energies under-quasi-static and impact load and proposed DIFs.

Specimen	Experimental results		DIF_{EP}
	E_s (J)	E_i (J)	
FNI8	1871	2575	1.38
FFI8	1862	2330	1.25
PNI8	2007	2760	1.38
PFI8	2030	2802	1.38

4.6 Impact test results of connections to CFST columns

It is intended in this part to present the lateral impact response of the end plate connections connected to CFST columns using the long bolt technique, which can then be compared with those using ordinary bolts. Hence, eight full-scale specimens were tested under lateral impact to investigate the effect of concrete infill, impact load location, plate thickness in addition to investigating the difference between the responses of the selected two types of connection. Again, the similar loading conditions that used to test the specimens connected to steel columns were used here, i.e. the impact load is applied using a drop hammer of a mass of 107.5 kg from a height of 2.9 m.

4.6.1 Deformation modes

The results from all tests demonstrate four different modes of failure in the connections, in addition to two modes occurred in the CFST column. The first mode that connection experienced was the bearing failure of the first bolt row due to the critical bearing stresses developed at the contact surface of the bolt and plate hole, as shown in Figure 4.26. This failure was observed in all specimens with a thin end plate. The corresponding specimens that connected to steel columns also demonstrated this type of failure in the first bolt row, but with relatively lower deformations. This is because the portion of long bolt that embedded in concrete is restrained by concrete in addition to the restriction by the bottom nut, while the ordinary bolts are restrained by the bottom nut only. This would make the lower portion of ordinary bolts free to move before the contact occurs, with the end plate hole leading to decreasing the bearing stresses between the ordinary bolt and end plate hole.

Figure 4.26. Bearing failure of first bolt row in specimen connected to CFST.

The second failure is the bending of plate due to prying action, as shown in Figure 4.27. With the increasing of the displacement due to the external impact load at the free end of the CFST column, the end plate starts to bend gradually due to prying action with developing a contact bearing force with the long bolt, leading to noticeable bearing in the bolt. The connection with the two failure modes aforementioned (bearing of bolt and bending of end plate) behaves in a preferable manner by ensuring the yield of end plate to occur prior to tensile fracture of bolt. Similar bending on the end plate was observed to both connection types in the corresponding specimens that connected to steel columns.

Also, similar to the specimens connected to steel columns, tearing fracture of PDEPC close to the weld toe was observed in specimens connected to CFST columns, as shown in Figure 4.28. This failure mode was captured in specimens contain thin end plate only and it occurred due to the combination of the high shear stresses and tensile stresses produced in the direction normal to the beam web as explained in Section 4.3.1.1. Moreover, the tearing failure became larger as the impact load location closer to the connection, which is the same case in specimens connected to steel columns.

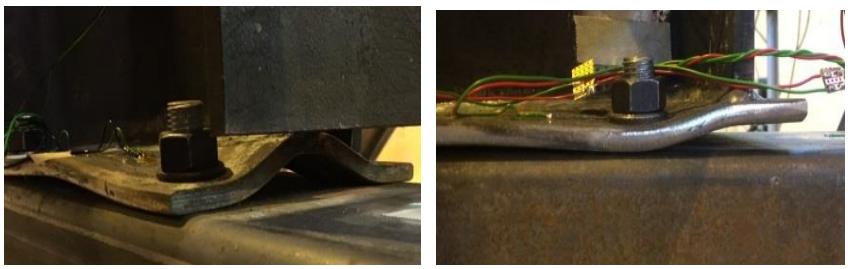

(a) PDEPC (b) FPC

Figure 4.27. Bending of the end plate failure in specimens connected to CFST columns.

Figure 4.28. Tearing failure of PDEPC

Similar procedure that adopted to test specimens with a thick plate connected to steel columns was used to test specimens with a thick plate connected to CFST columns. Hence, a specimen with PDEPC with 15 mm thick (PFC15-1) was fabricated and tested. Again, unfavourable connection failure was observed for this specimen, characterised by the loosening of the nuts provided for the first bolt rows, which is similar to the corresponding specimen that connected to steel columns. Therefore, the test was repeated in the same details but with double nuts (PFC15-2) to prevent this failure and to facilitate the comparison

of the results later. A small bending was observed on the plate of both specimens, as shown in Figure 4.29, and no nut loosening occurred in the repeated specimen.

Figure 4.29. Bending failure of PDEPC specimen with thick plate.

The efficiency of using long bolts as alternative method to connect end plate to CFST column is revealed by the similarity of the failure modes for the connection to CFST columns using long bolts technique to the connection to steel column using ordinary bolts, which is considered as the standard connection. However, this efficiency needs to be confirmed by comparing the load-displacement traces of specimens with long bolts to that with ordinary bolts as is discussed in Section 4.6.2.

In addition to the failure of the main components of connection (end plate and bolts), plastic deformations were observed also in CFST column. Punching shear failure was captured on the steel tube of CFST column around the bottom first holes provided as access for the long bolts to pass through CFST, as shown in

Figure 4.30. This failure mode occurred in specimens with thick plate only. As the thick plate experienced relatively small deformation, the impact energy was dissipated in the CFST column producing small plastic deformation on it. Hence, the portion of the CFST column underneath the end plate approximately keeps straight, while the other portion experienced a higher deformation. However, a high clamping force between the bolt and nut was produced as a result of bending deformation of the CFST column, leading to the punching shear failure. In the specimens connected to steel columns, no failure was observed in the bottom flange of the steel column as the ordinary bolts are connected to the top flange only, which in turn experienced a localised crippling failure as discussed in Section 4.3.2.1

(See Figure 4.11 and Figure 4.12). The other specimens with flush plate connection with a plate thickness of 15 mm (FFC15) were also tested with double nuts and no prying failure was observed on the end plate corresponding to a higher punching failure than that observed in PDEPC specimen, as shown in Figure 4.31.

Figure 4.30. Punching shear failure of CFST column around first bolt row.

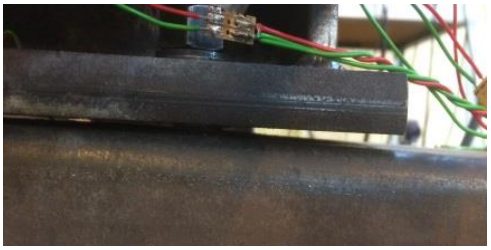

Figure 4.31. Failure mode of FPC with thick plate.

The change of the impact loading location did not affect the failure mode. Slight increase was noticed in the length and depth of the tearing cracks if the specimens loaded near the connection. The tearing crack was found to be larger in specimen with no concrete infill as the displacement in the free end of the CFST column was larger, as shown in Figure 4.32.

Figure 4.32. Tearing failure of end plate of PDEPC connected to hollow tube.

Considerable attention was paid to monitor thread stripping of the bolt after the tests. This failure was captured by Grimsmo et al. [78] by applying a combined impact shear and tensile stresses on bolt to investigate impact response of extended end plate connection. Also, Mourtiz [100] showed that failure load of a mild steel bolt thread under impact tension load decreased with increasing strain rate. However, this type of failure was not observed in all specimens tested in the current study including the specimens that connected to steel columns.

In order to observe the failure modes of the concrete filling, the outer steel of the CFST specimens were removed after the tests. Concrete cracks were observed around all the long bolts in specimens connected to thin plate, as shown in .

Figure 4.33 (a) for a selected specimen. These cracks were observed only around the first bolt row for specimens with thick plate, as can be seen in .

Figure 4.33 (b). Also, cracks were clearly observed in the location of impact, particularly for specimens loaded far away the connection. Other areas of the concrete filling have no obvious cracks.

(a) Side view of concrete cracks in a CFST specimen connected to thin end plate.

(b) Top view of concrete cracks in a CFST specimen connected to thick end plate.

Figure 4.33. Concrete cracks in CFST column.

Table 4.4 summarised the failure modes of specimens connected to CFST columns. In general, it can be said that all aforementioned individual failure modes were noticed in specimens having partial end plate connection with a thin plate, except for nut loosening. Also, the same case was applied to specimens with thin flush plate but without visible tearing of plate. On the other hand, thick plate seems to be unfavourable choice under lateral impact even with preventing the nut loosening failure. This is attributed to the possibility of the tensile failure of the bolts prior to the yielding of the end plate.

Table 4.4. Failure modes of test specimens connected to CFST columns.

specimen	connection				CFST column	
	Bearing failure of bolt	Prying failure of end plate	Tearing of end plate	Nut loosening	Concrete cracking	Punching shear
PFC8	Yes	Yes	Yes-slight	No	Yes	No
PFC15-1	No	Yes-slight	No	Yes	Yes	Yes-slight
PFC15-2	No	Yes-slight	No	No	Yes	Yes-slight
PF68	Yes	Yes	Yes	No	Hollow	Yes
PNC8	Yes	Yes	Yes	No	Yes	No
FFC8	Yes	Yes	No	No	Yes	No
FFC15	No	No	No	No	Yes	Yes
FNC8	Yes	Yes	No	No	Yes	No

4.6.2 Force-displacement relationships

In the previous section, it was showed that the failure modes of the connections to CFST columns are similar to those modes of connections that connected to steel columns. Basically, this gives a good indication that behaviour of connections with long bolts may approach to the behaviour of connection with ordinary bolts (standard). The only disadvantage that identified for specimens connected to CFST column using long bolts was the excessive cracking of concrete surrounding the long bolts and on the impact point. These cracks may lead to reduce the axial capacity of the CFST column. Moreover, it is expected that these cracks may be formed during the construction of a structure. However, this issue needs to be covered by the researchers and the assumption of cracked concrete in the connection zone may be appropriate to account the reduction in the axial capacity of the CFST column due to concrete cracking.

In the following sections, the effects of concrete infill, impact load location and end plate thickness on the force-displacement relationships are presented. Also, a comparison between the load-displacement traces of FPC and PDEPC to CFST columns using long bolts is discussed. Comparison between the force-displacement traces of specimens connected to the CFST columns and steel columns are also included.

4.6.2.1 Effect of concrete infill

Specimens PFC8 and PF68 are selected to compare the impact response of the connection to hollow tube and CFST tube. The tube of the specimen PFC8 was filled with concrete, while the tube of the specimen PF68 was empty. Both specimens have PDEPC with 8 mm end plate thickness. To avoid the local deformation that the empty tube may experience, a 6 mm tube thickness was used, while 4 mm tube thickness was kept for the concrete filled specimen. Figure 4.34 displays the force-displacement curves for both specimens. It is clear that the concrete infill enhanced the connection strength by reducing the maximum displacement from 101.9 mm to 81.5 mm, i.e. by 20%. This reduction in the maximum displacement is likely attributed to the higher flexural strength of the CFST column compared with hollow specimen. It was also found that the concrete infill increases the initial peak force from 182.3 kN to 274.5 kN. Besides, the energy absorbed in the initial peak force of the filled specimen before the first separation of contact between the projectile and the struck column is about 37% higher than that absorbed in the hollow specimen.

4.6.2.2 Effect of impact load location

Figure 4.35 shows a comparison between the load-displacement traces of FPC specimens that were connected to CFST column in the selected impact loading locations. Changing the location of impact load from L_1 to L_2 leads to increasing the peak force by 12%. After the initial peak force stage particularly when the load is far away from the joint (L_1), a clear

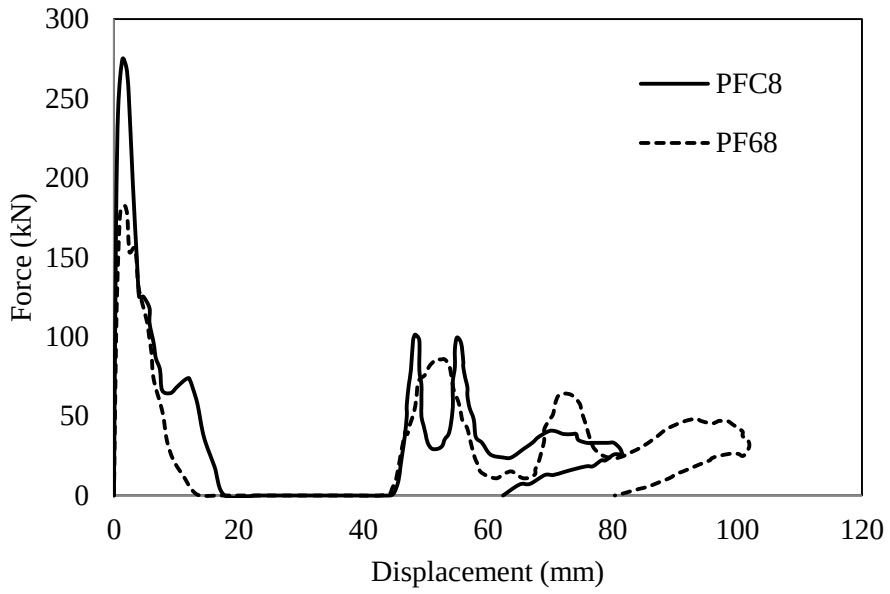

Figure 4.34. Force-displacement relationships of specimen with hollow column (PF68) and CFST column (PFC8).

intermittent impact can be seen as was noticed in the corresponding specimen that connected to steel column. The plateau stage in specimen loaded near the connection (L_2) starts from the displacement around 10 mm and ends with the maximum displacement, which is 24 mm, i.e. it represents around 58 % of the loading stages. However, the same stage represents not more than 42 % of the loading stages in the specimen loaded far away from the connection (L_1). The multiple intermittent impact produced in the specimen loaded far away from the connection delayed the onset of the plateau stage. In other words, a continuous force flow of the specimen loaded far away from the connection starts after three sequential contacts missing of projectile to struck column, while no contact missing was produced in specimen loaded near the connection. Moreover, the specimen impacted near the connection shows a significantly higher average plateau force than the specimen impacted far away from the connection by about 225 %. In the unloading stage, the projectile rebounds and the force starts to decrease to zero with the displacement approaching to the permanent value as usual.

Figure 4.36 shows a comparison between the load-displacement traces of PDEPC that were

connected to CFST column in the selected impact loading locations. In general, similar trends can be seen to that of FPC, but with more peaks prior to plateau stage. The initial peak force decreases slightly by 2% if the impact location is changed from L_2 to L_1. Intermittent impact can be observed only in PDEPC, while it was not noticed in FPC.

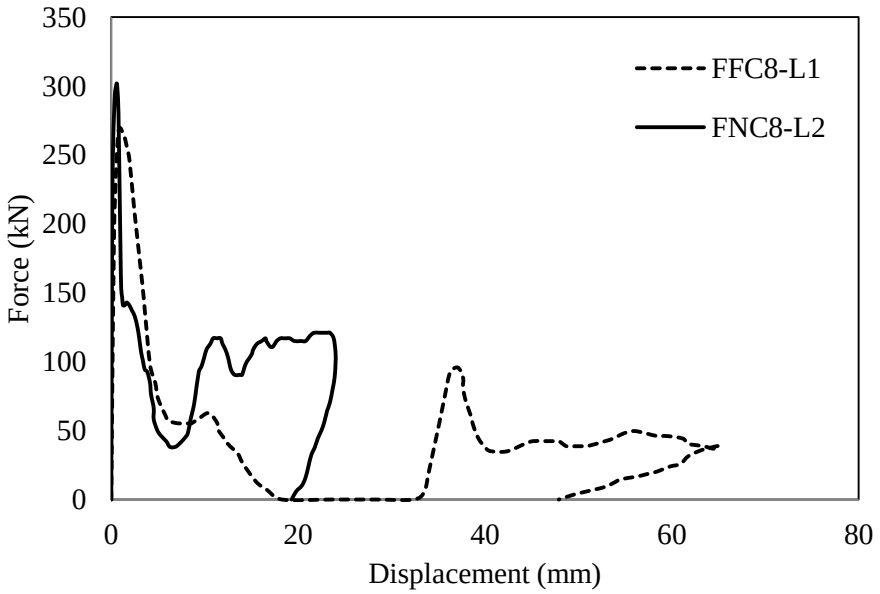

Figure 4.35. Effect of impact loading location on load-displacement traces of FPC to CFST column.

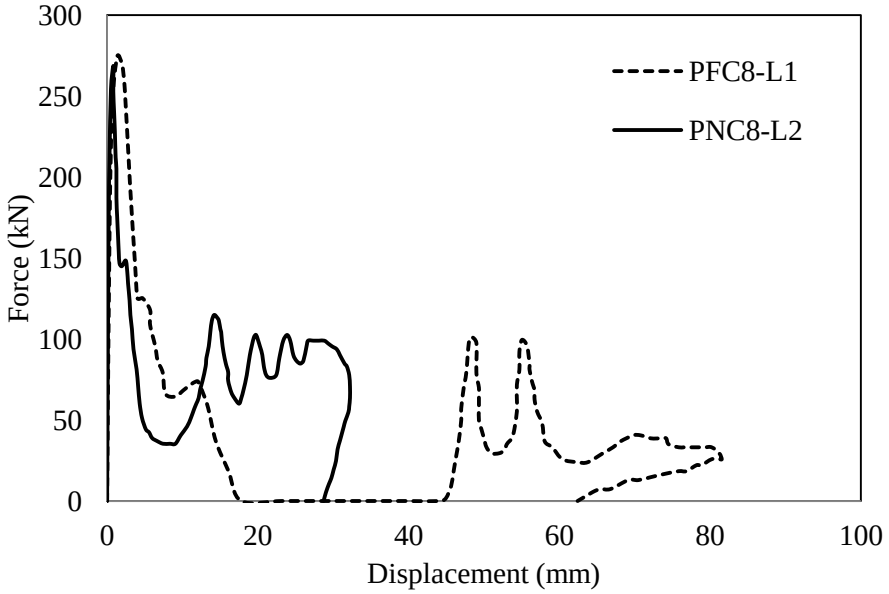

Figure 4.36. Effect of impact loading location on load-displacement traces of PDEPC to CFST column.

4.6.2.3 Effect of plate thickness

The effect of changing end plate thickness on the impact response of both connections selected in the current study can be seen in Figure 4.37 and Figure 4.38. It is clear that using thicker plate for both connections leads to decrease the maximum displacement corresponding to relative increase in the initial peak and plateau forces. Increasing plate thickness from 8 to 15 mm contributes to increase the initial peak force by 25% and 34% in PDEPC and FPC, respectively. These results were obtained by assuming there is no the nut loosening failure. However, this would lead to increase the internal force in the bolts, producing a sudden fracture of them and having a negative impact on the ductility of connection. The maximum displacement can be used to examine the ductility of the connection for the similar impact location. Observation of the experimental results shown in Figure 4.37 and Figure 4.38, indicates that both connections become more ductile using thinner end plate. Yet, the ductility of FPC and PDEPC increased by 24% and 31%, respectively, if the end plate thickness reduced from 15 mm to 8 mm.

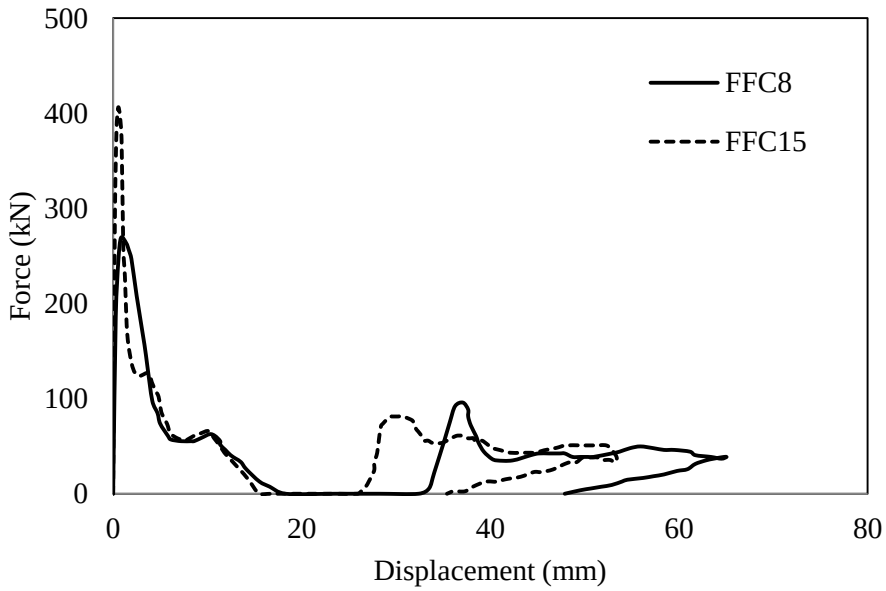

Figure 4.37. Effect of end plate thickness on load-displacement traces of PDEPC to CFST column.

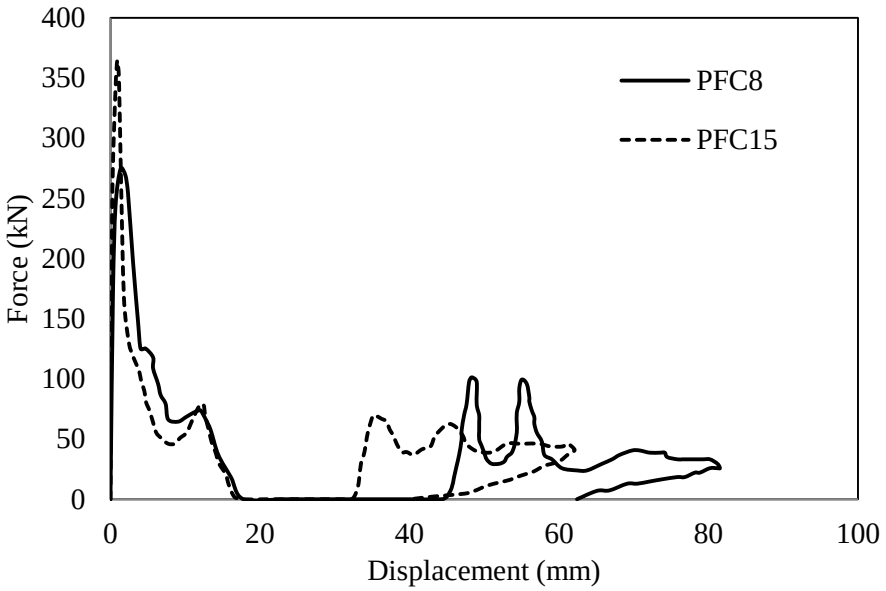

Figure 4.38. Effect of end plate thickness on load-displacement traces of PDEPC to CFST column.

4.6.2.4 Comparison between the responses of FPC and PDEPC to CFST columns

Figure 4.39 to Figure 4.41show comparisons of load-displacement traces of FPC and PDEPC to CFST column with different loading locations and end plate thickness. Figure 4.39 presents the load-displacement traces of both connections with 8 mm thick end plate and loaded far away from the connection. The initial peak force of the specimen FFI8 is slightly lower than that of the specimen PFI8 by 2%. Moreover, the plateau force of the former specimen is 44.2 kN, which is higher than the plateau force of the latter by 25%. This difference in forces increases when the specimens loaded near the connection as can be seen in Figure 4.40, i.e. the specimen with FPC shows a higher initial peak force than PDEPC by 11% and the average plateau force of the former specimen is higher than the latter by about 25%. For specimens with a thick plate, the initial peak force was decreased from 430 kN to 370 kN, i.e. by 14 % if FPC replaced by PDEPC as shown in Figure 4.41.

In addition to the higher forces that were produced in the impact event in specimens with FPC if compared with those specimens with PDEPC, lower displacements can be observed due to the higher stiffness of FPC. Replacing PDEPC with FPC leads to reduce the

maximum displacement by 20% and 14% in specimens impacted far away from the connection with thin and thick end plate, respectively. Similar trend can be seen for specimens impacted near the connection with a thin plate, but with a reduction of 25% in the maximum displacement which is attributed to a higher tearing failure on the end plate due to the impact load being located near the connection. Besides, it can be said that both connections show a good ductility under lateral impact prior to failure by allowing the yielding of the end plate before the fracture of the bolts.

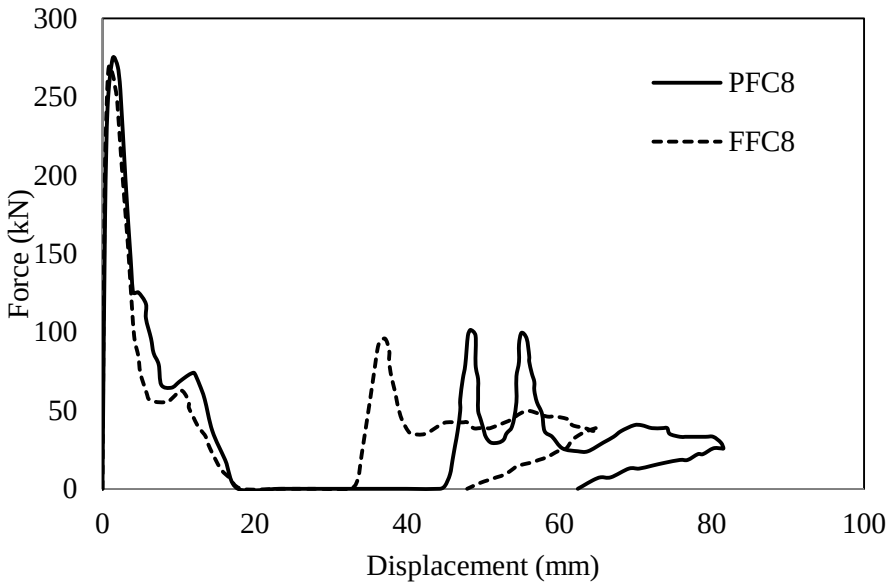

Figure 4.39. Comparison between the load-displacement traces of FPC and PDEPC to CFST column loaded with lateral impact at L_1 with 8 mm end plate thickness.

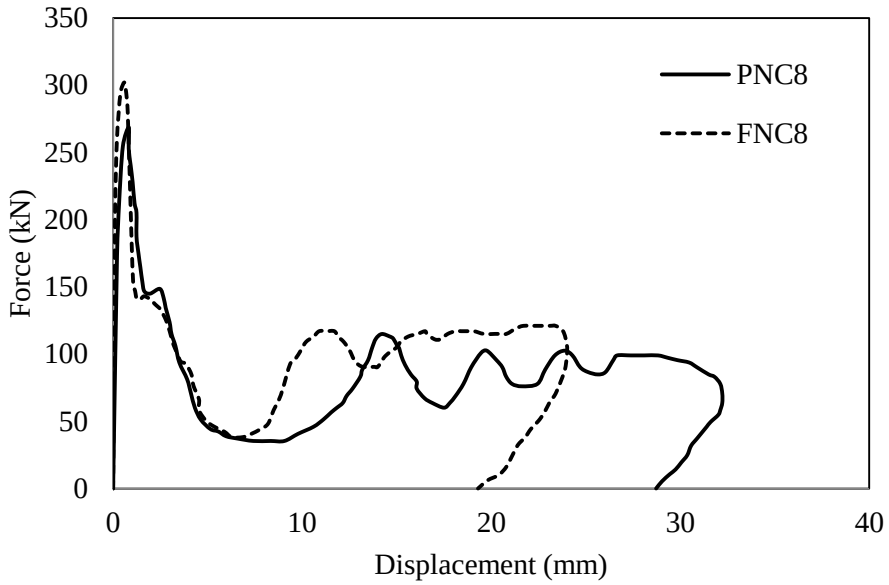

Figure 4.40. Comparison between the load-displacement traces of FPC and PDEPC to CFST column loaded with lateral impact at L_2 with 8 mm end plate thickness.

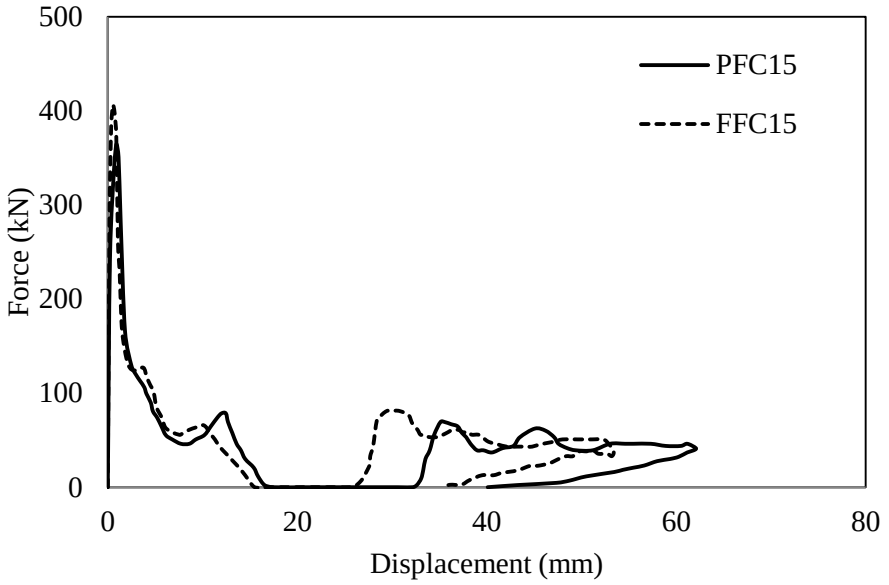

Figure 4.41. Comparison between the load-displacement traces of FPC and PDEPC to CFST column loaded with lateral impact at L_1 with 15 mm end plate thickness.

4.7 Summary

In this chapter, material testing results including steel profiles and concrete were presented. Also, the experimental results of structural testing of all specimens under quasi static and lateral impact loading were introduced, including the force-displacement traces, strain time histories and deformation modes. Moreover, dynamic increase factors were proposed based on the energy principle using the experimental force-displacement traces. Furthermore, an evaluation of the using of the long bolt technique to connect CFST column with steel beams using end plate connection was discussed. The results show that the end plate connection with long bolts almost showed similar behaviour of that with ordinary bolts. Also, slightly higher maximum displacement and lower initial peak force were obtained in specimens with long bolts compared with those with ordinary bolts.

.

Chapter 5: Numerical Procedure

5.1 Introduction

This chapter presents the numerical procedures and techniques that are employed to simulate the behaviour of the end plate beam-to-column connections under both impact and quasi-static loadings. Here, the commercial finite element analysis software, ABAQUS, is used to develop numerical models to help understand the performance and the structural behaviour of the end plate beam-to-column connections under lateral impact and quasi-static loadings. Two analysis procedures are available in ABAQUS to be used in simulation, i.e. Implicit and Explicit solution. However, the explicit solution is adopted in this study for the following reasons.

1. The explicit procedure is more appropriate to analyzing high-speed dynamic events such as impact and blast problems as in the present study [101];

2. Beam-to-column connection includes various contact interactions between the contacted bodies. The contact interaction can be formulated more easily in ABAQUS/Explicit rather than an implicit procedure [101];

3. Convergence problems could be mitigated considerably in ABAQUS/Explicit if compared with implicit procedure especially in quasi-static modelling;

In this chapter, the geometrical modelling including element types and mesh size is presented in details for all parts of the connection. Also, the modelling of loading and boundary conditions are described. The techniques of modelling steel and concrete materials in the elastic, plastic and damage stage is also presented. In addition, the interaction type and the interaction properties between the steel parts and between the steel and the infilled concrete are also discussed.

5.1 Modelling of the end plate connection under lateral impact loading

5.1.1 Geometries and boundary conditions

Figure 5.1 shows the geometrical details of a model and boundary conditions used. Due to

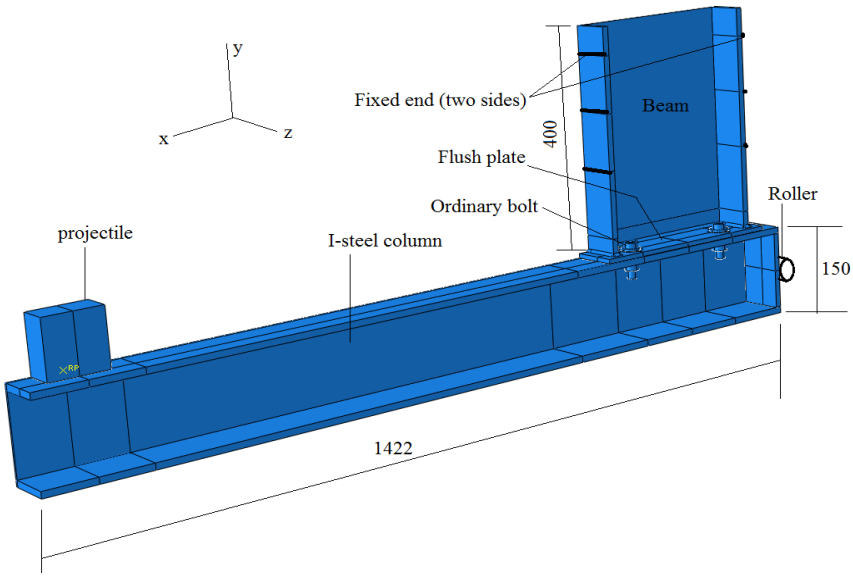

a) The half geometry and boundary conditions of the specimen FFI8.

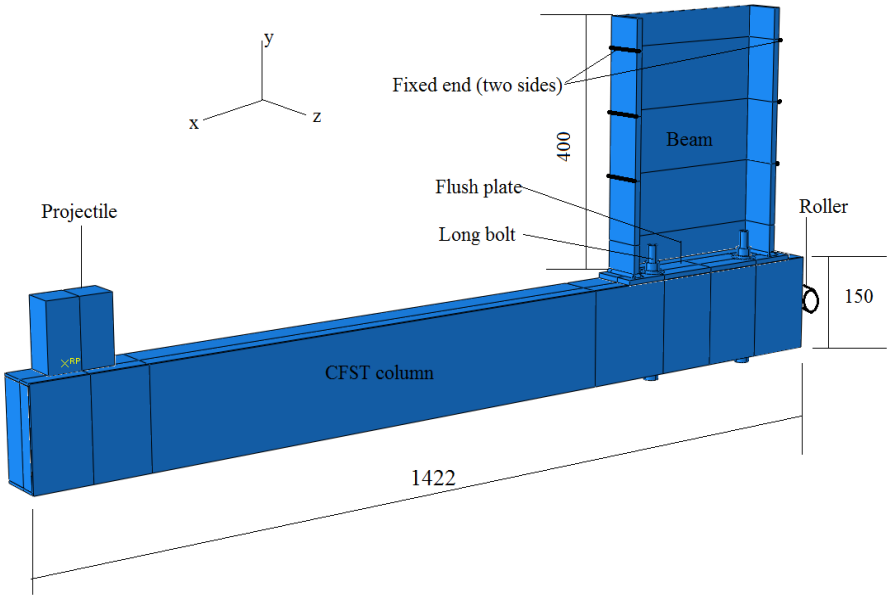

b) The half geometry and boundary conditions of the specimen FFC8.

Figure 5.1. Geometries and boundary conditions of beam-to-column connection (dimensions in mm).

symmetry about x-axis, half model was used for all models to save the computational time of analysis. As the rotational and translational movements of the mounting stiff frame were neglected as discussed in Chapter three, the twelve bolts that connect the beam of the specimen to the mounting stiff frame were modelled as fixed end as shown in Figure 5.1.Roller support was modelled using displacement/rotation boundary conditions at which the column was restrained in x-direction only. The projectile was restrained against all degrees of freedom, except for the vertical displacement (y-axis). The projectile was modelled with a mass of 107.5 kg for all specimens. The experimental tests showed that the initial velocity of all specimens tested was 7.5 ± 0.05 m/s. Therefore, a constant initial velocity of 7.5 m/s was used for all specimens. All individual parts were modelled to have their real dimensions with some modifications to simplify the geometry. However, fillet radii of the beam, column, washers and nuts were not considered here. The bolt was modelled without threads but their effect was considered by a reduction of the area of the threaded region. Hence, a hole is centrally located through the threaded region only with an area equal to the gross area of the bolt minus the net tensile area as shown in Figure 5.2. A representative hole with a diameter of 7.9 mm was applied to make the equivalent area where the hole is located equal to 152 mm^2. The same procedure was applied to model the long bolts as they have the similar diameter.

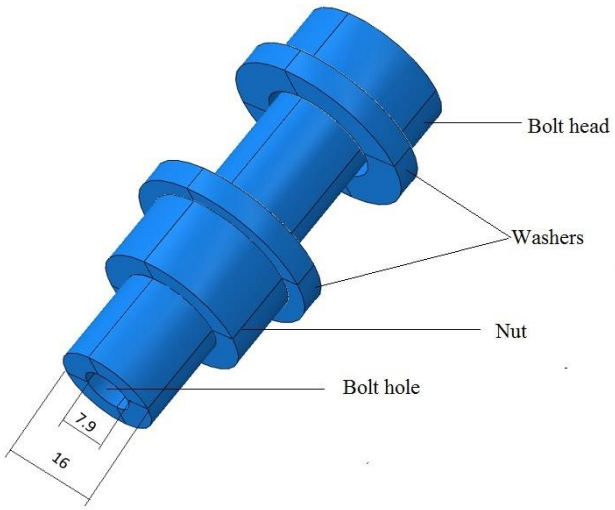

Figure 5.2. Modelling of the bolt (dimensions in mm).

5.1.2 Element type and mesh size

The previous studies showed that using the 8-noded element with reduced integration (C3D8R) was efficient to model the impact problems [13, 14, 57]. The reduced integration refers to using lower order integration to form the element stiffness. Hence, the computational time will be reduced in comparison to other solid elements with full integration. Also, with the reduced integration elements, the strains and stresses are calculated at the locations that provide optimal accuracy. One of the common problems that element C3D8R may experience is hourglass phenomenon. Hourglass is nonphysical mode of deformation that occurs in elements and produces no stress. Since such elements have only one integration point, it is possible for them to deform in such a way that strains calculated at the integration point is zero. This will lead to uncontrolled distortion of the mesh. To overcome the hourglass problem, ABAQUS/Explicit provides a small value of artificial stiffness called "hourglass stiffness" to an element. Also, at least four elements should be used over the wall thickness of a part that may experience large deformations.

The strategy to select the mesh size in this study depends upon the deformation that a part of specimen experienced. Figure 5.3 shows the numerical models with selected element sizes of specimens connected to steel I-section. It can be seen that smaller mesh sizes were used for the plate and bolt as they experience larger deformations than other parts, i.e. column and beam. Mesh sensitivity study was performed in a selected specimen (FNI8) to identify the proper mesh size. Rebeiro et al. [81] proposed using element size of plate and bolt of 1.5 and 1 mm, respectively to model T-stub connection under impact load, which is also related to this study. The use of these mesh sizes was validated in different situations up to failure of the T-stub connection. Thus, these elements sizes were added to the mesh sizes to be investigated in the mesh sensitivity study. Hence, four mesh sizes for plate and bolt, including that adopted by Rebeiro et al. [81], were examined on specimen FNI8, as shown in Table 5.1. Finer mesh was used for the column region underneath the end plate to avoid contact penetration [101], as is discussed in Section 5.2.3.

Table 5.1 Mesh sizes selected to be investigated in mesh sensitivity study.

Part	Mesh 1 (mm)	Mesh 2 (mm)	Rebiero et al. (mm)	Mesh 3 (mm)
Plate	4	3	1.5	0.5
Bolt	2	1.5	1	0.5
Time of analysis (minutes)	262	301	358	441

The projectile was modelled as a rigid body as it is made from high strength steel and its deformations are negligible. The motion of all nodes and elements of the rigid body is governed by the motion of a single reference point that has both translation and rotational degrees of freedom. The 4-noded 3D bilinear rigid quadrilateral element (R3D4) was used to simulate the projectile. Moreover, the mesh size of the projectile was selected to be finer than the struck column as shown in Figure 5.3 to avoid contact penetration of the projectile into the struck column [101]. The mesh of plate and bolt with element size of 1.5 mm and 1 mm, respectively, showed a reasonably good agreement with the experimental data, as shown in Figure 5.4. However, reducing the element sizes as adopted in mesh 4 did not effectively improve the accuracy of the FE results. Consequently, a mesh size of 1.5 mm and 1 mm for plate and bolts is selected.

Similar mesh sizes were used for specimens connected to CFST columns for all parts, except for concrete, which is not included in specimens that connected to steel I-sections. Three mesh sizes were investigated for concrete infill, i.e. 15, 10 and 7 mm with a constant finer mesh of 2.5 mm around the region of long bolts as shown in Figure 5.5. The results showed that decreasing the mesh size enhances the accuracy of the model in terms of load-displacement relationship and failure mode. Nevertheless, mesh size of 10 mm was selected as it has a balance between the computational time and the necessary accuracy.

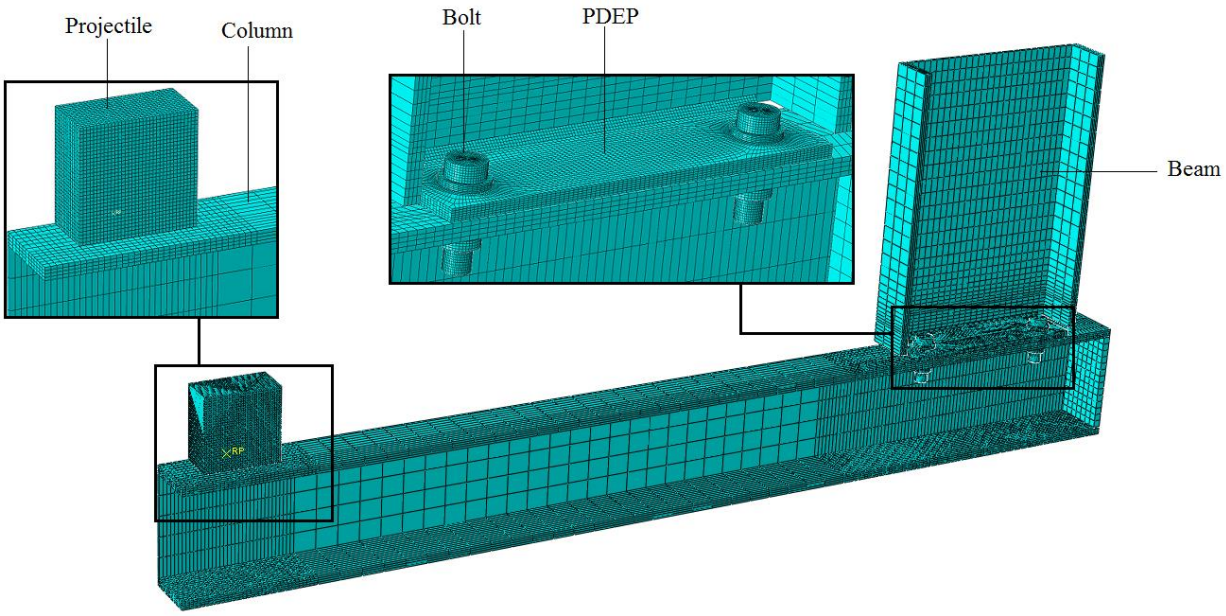

Figure 5.3. The mesh of specimens connected to I-section steel columns.

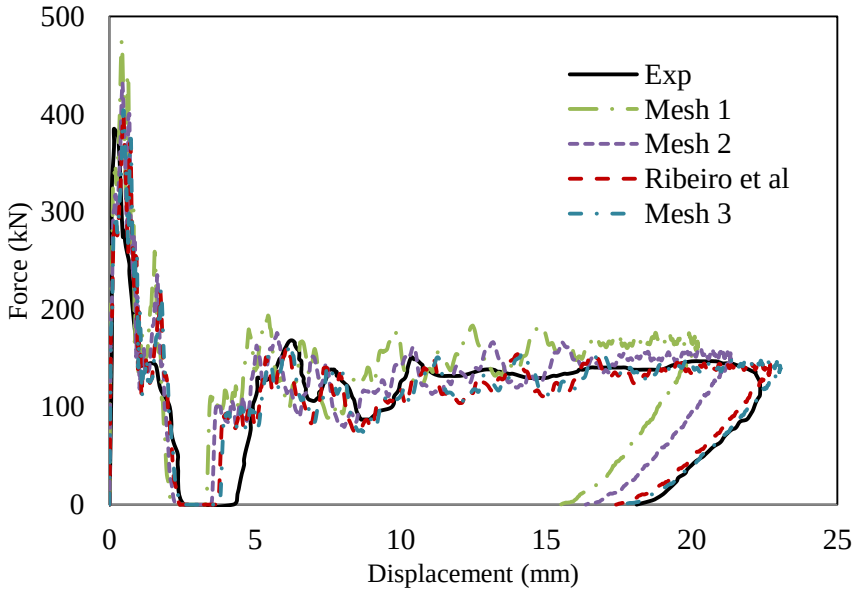

Figure 5.4. The element size effect on the accuracy of the FE model under impact loading.

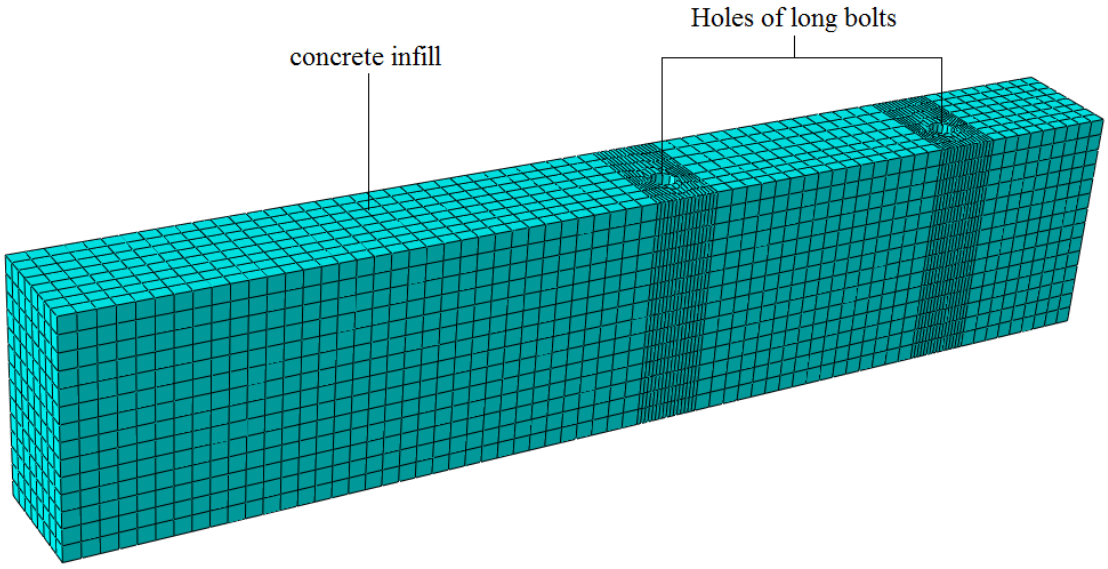

Figure 5.5. The mesh of concrete infill.

5.1.3 Contact interactions

Modelling of contact between various surfaces is one of the most critical processes. Hence, considerable attention was made to select the proper master and slave surfaces and to assign appropriate interaction properties to model the interaction. Tie constrains and surface to surface contact formulations were used to model contact surfaces. The former was employed to connect weld to the beam and plate, nuts to bottom washers, and nuts to bolts as no visible deformation was observed on these parts during the experimental tests. However, the surface to surface contact was employed between bolt heads (or top nut of the long bolt) and top washers, washers and end plate, bolt shank and clearance holes of plate and column, plate and column, in addition to projectile and column. Penalty friction formulation with a coefficient of friction of 0.2 between contact surfaces was selected to simulate the tangential behaviour of the contact, whilst the normal hard contact allowing separation was assumed for all interaction surfaces. The surface to surface contact algorithm was also used to define the contact between concrete infill and both the steel tube and long bolts. Penalty friction formulation with a coefficient of friction of 0.25 was used between the steel tube and the concrete infill, whilst a value of 0.4 was used between the long bolt and the concrete infill as

the long bolt includes threads and more frictional forces are expected. It is recommended to set the surface of the stiffer body as a master surface and the other one as the slave surface [101]. Hence, the internal steel tube surface was selected as the master one when it is in contact with concrete infill (slave surface), while the projectile was selected as a master surface when it is in contact with steel column (slave surface), as shown in Figure 5.6. In order to avoid the penetration of the master surfaces into the slave surfaces, the contact surfaces that are defined using pure master-slave approach should be refined as shown in Figure 5.7. This problem is likely to occur as there is contact between a relatively rigid body and a deformable body.

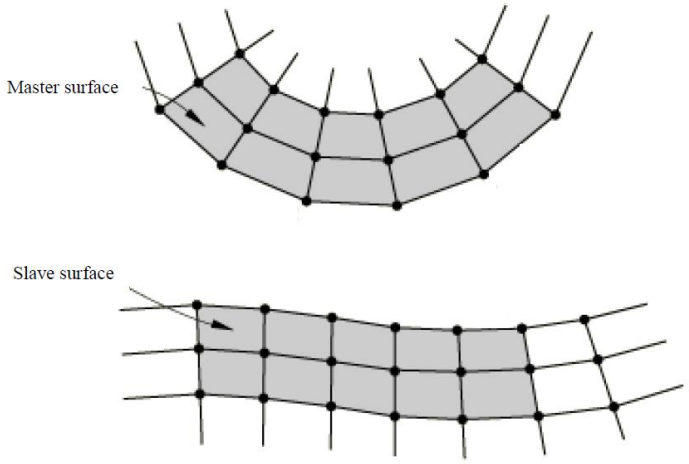

Figure 5.6. Master and slave configuration in surface to surface contact [93].

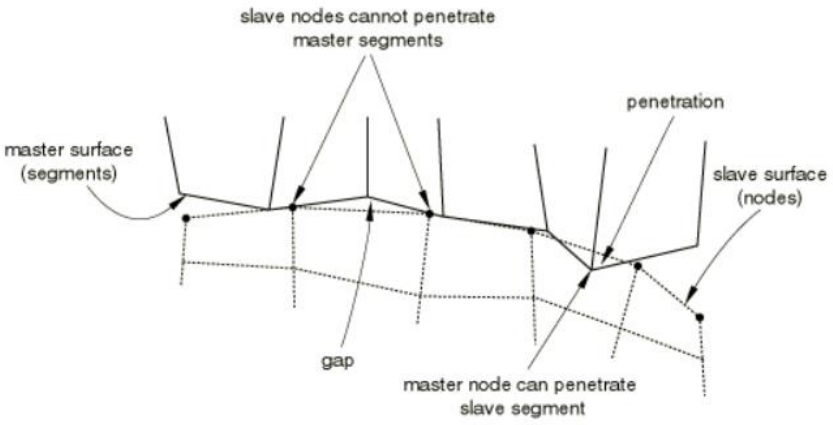

Figure 5.7. The contact penetration of the master surface into the slave surface [93].

5.1.3.1 Contact force calculations

The development of impact force between the projectile and the struck column due to impact loading takes a very short time, which depends on the velocity of the projectile at the contact time, the type and the mechanical characteristics of the contact between the projectile and the struck column and the material properties at the time of the impact. Once the two bodies, i.e. projectile and steel or CFST column, separate, the contact force disappears. Hence, it is very important to define an accurate simulation for the interaction between the bodies in contact to produce realistic true contact forces. The penalty method, which is available in ABAQUS to solve the contact problems, can be employed to determine the contact force between the impactor and the struck column by placing normal interface springs to prevent the penetration between the elements of the master and slave surfaces as shown in Figure 5.8. As soon as a penetration is detected in a time step, an internal force that is given by the spring will be applied to prevent the aforementioned penetration. This force is a function of the contact stiffness and the penetrated distance which can be written as [102]:

$$F = k \cdot x \qquad (5.1)$$

where x is the penetrated distance and k is the contact stiffness which can be calculated from

$$k = P_f A_e^2 K_B / V_e \qquad (5.2)$$

where P_f is the penalty stiffness factor, A_e is the area of the contact element, K_B is the bulk modulus and the V_e is the volume of contact element.

5.1.4 Material modelling

5.1.4.1 Steel

The tensile test procedure of the steel materials was presented in Section 3.2.2 in Chapter three followed by presenting the engineering stress-strain curves in Section 4.2.2 in Chapter four. The Elasto-plastic behaviour of steel materials was modelled using ABAQUS/Explicit based on the experimental engineering stress-strain curves. Hence, Modulus of elasticity (E) and yield stress (σ_y) were taken from the curves for each material used as input data to

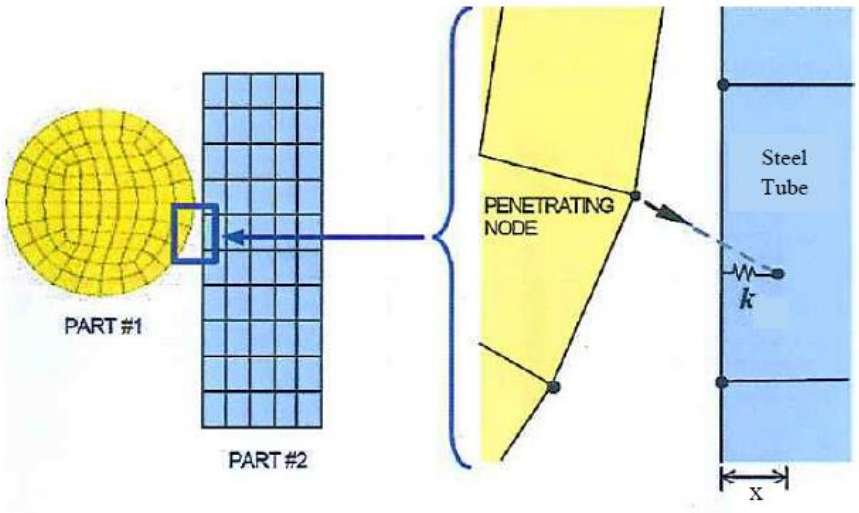

Figure 5.8. The formulation of the contact using Penalty method [94].

define the elastic stage up to the yielding point. In order to obtain reasonable material properties in the plastic stage, the engineering stress-strain curves were modified to obtain the true stress-strain curves using the following equations.

$$\sigma_{true} = \sigma_{eng} (1 + \varepsilon_{eng}) \quad (5.3)$$

$$\varepsilon_{true} = \ln (1 + \varepsilon_{eng}) \quad (5.4)$$

where, σ_{eng} and ε_{eng} are the engineering stress and the corresponding engineering strain, respectively. These equations were used up to the onset of necking (at the point of ultimate stress (Fu)). Beyond necking, a tri-axial strain starts to develop which makes the behaviour more complicated and the equations above are not valid. Therefore, a simplified methodology was used to draw the true stress strain curve beyond necking by assuming that the material experiences considerable strain corresponding to a constant stress level. The ultimate stress (Fu) was used as the constant stress value, whilst the fracture strain was calculated using Bridgman strain equation [87].

$$\varepsilon_{true_f} = \ln \frac{A_\circ}{A_f} \quad (5.5)$$

where $A_\circ$ is the original cross sectional area of the tensile specimen tested and A_f is the cross sectional area after fracture. Plastic strain hardening behaviour up to the peak stress was modelled based on the stress-strain relationships after the yielding point. These curves then were modified using the dynamic increase factor included in Johnson-Cook (DIF_{JC}) model to account strain rate effect as follows.

$$DIF_{JC} = 1 + C \ln \dot{\varepsilon}^* \quad (5.6)$$

Here, C is the strain rate constant; $\dot{\varepsilon}^* = \dot{\varepsilon}/\dot{\varepsilon}_0$ is the strain rate ratio, where $\dot{\varepsilon}$ and $\dot{\varepsilon}_0$ are the current strain rate and the reference quasi static strain rate ($\dot{\varepsilon}_0$= 0.001 s^{-1}), respectively. The constant C was assumed to be 0.039 for the end plate and weld, and 0.0072 for high strength bolt, washers and nuts as adopted by Ribiero et al. [81]. The beam and column were not considered as strain-rate sensitive materials in the modelling of the low velocity impact.

After the strain hardening stage, onset of damage and damage evolution need to be modelled. Figure 5.9 shows a typical stress strain curve with progressive damage degradation of an isotropic material. The solid line after onset of damage (Damage parameter (D) =0) represents the initiation of damage, whilst the dashed curve refers to the material response without damage. Hooputra et al. [103] proposed a procedure at which ductile damage and shear damage could be predicted for aluminium alloys. This approach was adopted to predict damage for isotropic ductile material. In this paper, ductile damage under impact load was modelled using the equivalent plastic strain-triaxial stress state envelope developed by Ribeiro et al. [81] as shown in Figure 5.10. It was used to estimate the damage initiation of T-stub connection under impact load which was related to this study. Also, it was developed for both of bolts and plate which have more or less the same material properties of those used in this study. Shear damage initiation modelling in ABAQUS is described as a function of shear stress ratio, strain rate and the equivalent plastic strain ($\bar{\varepsilon}_o^{pl}$). In order to define these parameters, the same model was employed using isotropic metal plasticity constitutive model and both of shear stress ratio and strain rate were requested as output in a group of

elements where the shear failure occurred close the weld toe on the plate. Then, the fracture strain is obtained from true stress-strain relationship under uniaxial tension. Once damage initiation is detected at any element, the damage evolution stage starts to lead to the progressive degradation of the element stiffness until the ultimate failure. In this study, an effective plastic displacement assuming a linear relationship between effective plastic displacement (u^{pl}) and the damage variable (D) was adopted to model the damage evolution. It is considered also that the effective plastic displacement to be an input to the model is a function of the mesh size and the equivalent plastic strain as follows.

$$u^{pl} = L_c \, \bar{\varepsilon}_o^{pl} \tag{5.7}$$

where L_c is the element size. ($\bar{\varepsilon}_o^{pl}$) can be determined in Figure 5.9, depending on the stress-strain curve of the materials tested.

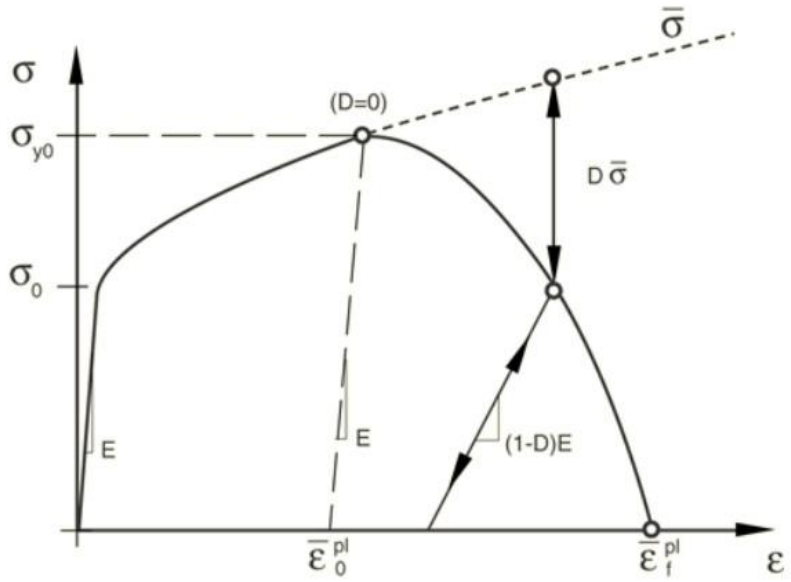

Figure 5.9. Stress-strain curve with progressive damage degradation [93].

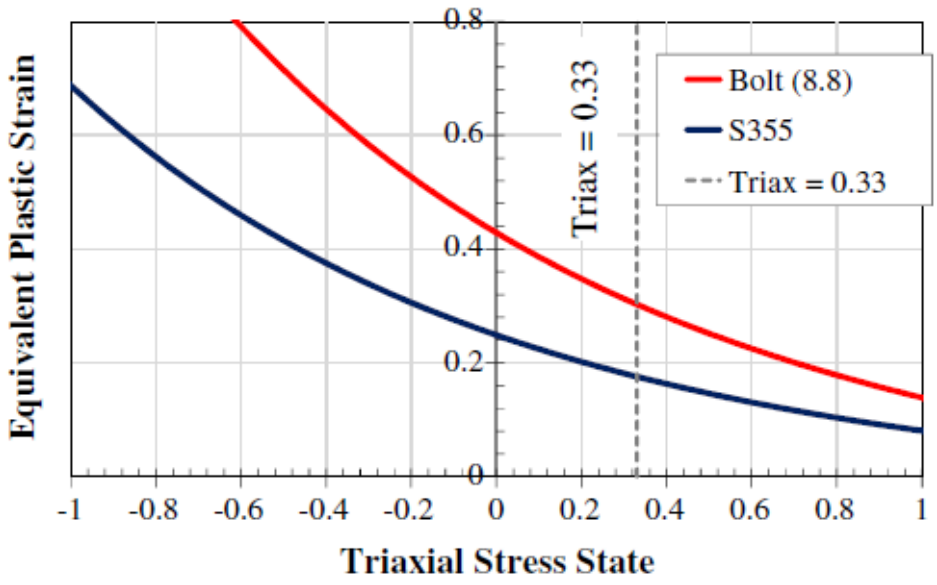

Figure 5.10. Equivalent plastic strain-tri-axial stress state envelope developed by Ribeiro et al. [71].

5.1.4.2 Concrete infill

The elasto-plastic tension and compression behaviour of the concrete infill was modelled as confined concrete, as is discussed in this section later. The concrete damage plasticity (CDP) constitutive model available in ABAQUS was used for this task. In this model, it is assumed that the damage plasticity characterises the failure of concrete in both tensile cracking and compressive crushing, as can be seen in Figure 5.11. Plastic behaviour of concrete is represented by CDP using the concept of the isotropic damage evolution in combination with isotropic plasticity. Both strain hardening in compression and strain softening in tension in addition to the damage initiation can be defined in this model. In Figure 5.11 (a), it can be seen that under uniaxial tension, the stress-strain is linear up to the ultimate (failure) stress (σ_{t0}). The failure stress begins with the initiation of the micro-cracking in the concrete, while the post failure stress is characterised by softening stress-strain behaviour. Under uniaxial compression, the stress-strain behaviour follows a linear elastic relationship up to failure stress (σ_{c0}) initially. The strain hardening followed by strain softening represents the concrete response after the ultimate stress (σ_{cu}), as shown in Figure 5.11 (b) [101].

The elastic stiffness of the material may be damaged due to unloading the concrete specimen within the stress softening part of the stress-strain relationship. This degradation is characterized by two damage variables (*dt* and *dc*), which are functions of the equivalent plastic strains in tension and compression (ε_{tpl},), temperature (Θ), and field variables (*fi*), i.e.

$$d_t = d_t(\varepsilon_t^{pl}, \theta, f_i) \qquad 0 \le d_t \le 1 \tag{5.8}$$

$$d_c = d_c(\varepsilon_c^{pl}, \theta, f_i) \qquad 0 \le d_c \le 1 \tag{5.9}$$

The tensile and compressive damage d_t and $d_{c\,can}$ be calculated as followed.

$$d_t = 1 - \frac{\sigma}{f_t} \tag{5.10}$$

$$d_c = 1 - \frac{\sigma}{fc'} \tag{5.11}$$

where σ is the corresponding stress to the specific crack width displacement. f_t and fc' are the tensile and compressive strengths of concrete, respectively. Under uniaxial tension and compression loading, the stress-strain relationship for the concrete having an initial elastic stiffness of E_o, can be expressed as, respectively.

$$\sigma_t = (1 - d_t)\, E_o(\varepsilon_t - \varepsilon_t^{pl}) \tag{5.12}$$

$$\sigma_c = (1 - d_c)\, E_o(\varepsilon_t - \varepsilon_c^{pl}) \tag{5.13}$$

Hu et al [104] presented a study to simulate the confined concrete in circular and square CFST. Ellobody et al [105], Dai and Lam [106] and Al-Husainy [14] adopted this model in their finite element analyses, where the numerical results showed a good agreement with the corresponding experimental data. Figure 5.12 shows a comparison between the behaviour of the confined and the unconfined concrete.

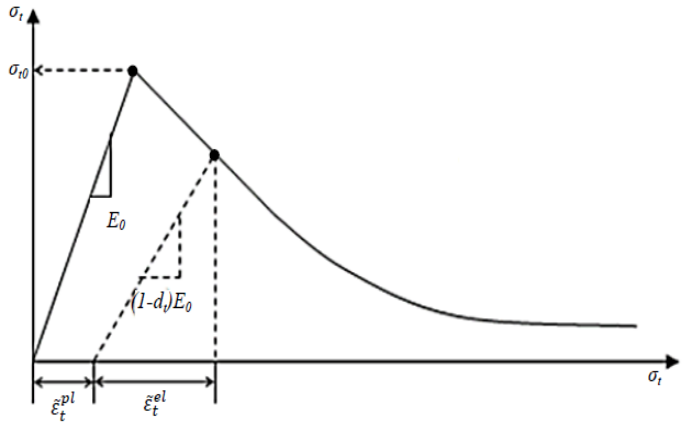

(a)

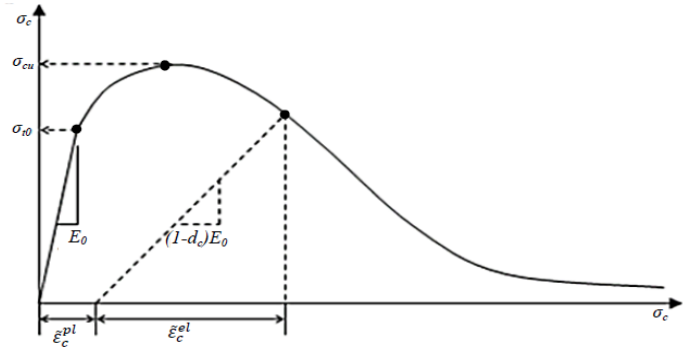

(b)

Figure 5.11. Concrete response under uniaxial loading in tension (a) and compression (b) [93].

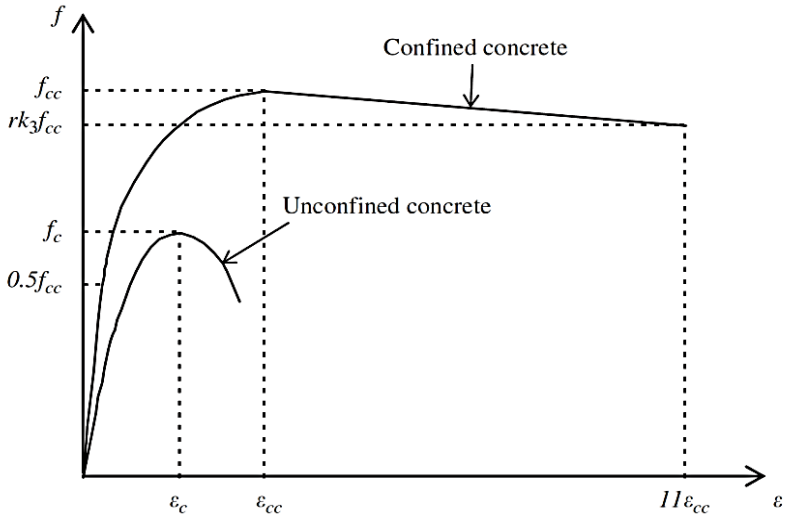

Figure 5.12. Stress-strain relationship of confined and unconfined concrete [98].

The f_c is the cylinder compressive strength of the unconfined concrete which is equal approximately to 83% of the unconfined cube strength ($f_{c,\,cube}$) as discussed in Section 3.2.1, whilst f_{cc} represents the cylinder compressive strength of the confined concrete. ε_{cc} and ε_{ck} are the corresponding strain for f_{cc} and f_c, respectively. The compressive strength for the confined concrete can be predicted by the proposed empirical relationship between f_{cc} and f_c [107]

$$f_{cc} = f_c + k_1 f_l \tag{5.14}$$

$$\varepsilon_{cc} = \varepsilon_{ck}\,(1 + k_2\, f_l / f_c) \tag{5.15}$$

k_1 and k_2 are assumed to be 4.1 and 20.5, respectively, as suggested by Richart et al. [108] and the common failure strain value of unconfined concrete ε_{ck} can be taken as 0.003. Based on the formulae proposed by Hu et al. [104], the lateral stress f_l can be predicted as:

$$f_l / f_y = 0.055048 - 0.001885\,(\mathrm{B/t}) \qquad for\ 17 \le \mathrm{B/t} \le 29.2 \tag{5.16}$$

$$f_l / f_y = 0 \qquad for\ 29.2 \le \mathrm{B/t} \le 150 \tag{5.17}$$

where B is the external dimension of the square steel tube, t and f_y are the wall thickness and the yield strength of the steel tube, respectively. In this study, B/t equals to 37.5, which means that $f_{cc} = f_c$ as in equation (5.13). Hu et al. [104] and Ellobody et al. [105] suggested the linear elastic portion of the stress in the confined concrete stress-strain curve to be 0.5 f_{cc}. ACI (1999) empirical formula can be used to predict the modulus of elasticity for the confined concrete E_{cc}, which is expressed as $E_{cc} = 4700\sqrt{f_{cc}}$ MPa [106]. The following formula suggested by Saenz [109] was used to predict the compressive strength f between the elastic limit 0.5 f_{cc} and the maximum compressive f_{cc}.

$$f = \frac{E_{cc}\varepsilon}{1 + (R + R_E - 2)\left(\frac{\varepsilon}{\varepsilon_{cc}}\right) - (2R - 1)\left(\frac{\varepsilon}{\varepsilon_{cc}}\right)^2 + R\left(\frac{\varepsilon}{\varepsilon_{cc}}\right)^3} \tag{5.18}$$

where

$$R_E = \frac{E_{cc}\ \varepsilon_{cc}}{f_{cc}}\ , R = \frac{R_E\ (R_\sigma\ - 1)}{(R_\varepsilon - 1)^2} - \frac{1}{R_\varepsilon}\ , \qquad R_\sigma\ =\ R_\varepsilon = 4$$

The third portion of the strain-stress curve starts with f_{cc}, and end with $f_u = rk_3f_{cc}$. The value of the parameter r can be taken as 1.0 for normal strength concrete and the correspondence strain for f_u is '$\varepsilon_u = 11\varepsilon_{cc}$' [104-106]. For the square steel tube section with $17 \leq B/t \leq 70$, the value of the parameter k_3 can be obtained from Eq. (5.18) or (5.19) proposed by Hu et al. [104]

$$k_3 = 0.000178\,(B/t)^2 - 0.02492\,(B/t) + 1.2722 \qquad (5.19)$$

The final stress-strain curve for confined concrete used in this study is shown in Figure 5.13. Regarding the modelling of tensile behaviour of concrete, the model proposed by Li et al. [110] is used in this study, which was adopted by Liu [111] and Al-Husainy [14].

$$\sigma = f_t\,\{1 - [-(\frac{0.05}{w_c/w_{ccr}})^{1.3}]\} \qquad (5.20)$$

where ft is the tensile strength of concrete and it could be predicted from the equation proposed by Li et al. [110] as a function of compressive strength of concrete (fc') as

$$f_t = 0.34\,\sqrt{fc'} \qquad (5.21)$$

The final stress-crack width curve of the concrete in tension was drawn for different crack widths (w_c) up to a critical crack width (w_{ccr}) of 1.5 mm as recommended by Begum et al [112] and Liu [111]. Figure 5.14 shows the relationship between the stress and crack width of concrete that used in the modelling. The Poisson's ratio for the concrete under uniaxial tension and compression was assumed to be 0.2 in this study.

The other parameters needed to be defined in the CDP model are shown in Table 5.2. These parameters were assumed as recommended by Al-Husainy [14]

Table 5.2. Plasticity parameters for CDP model.

Dilation Angle, φ	Eccentricity	f_{b0}/f_{c0}	K	Viscosity Parameter
20°	0.0	1.16	0.667	0

where,

f_{b0} is the initial equi-biaxial compressive yield stress, f_{c0} initial uniaxial compressive yield stress, K is the ratio of the second stress invariant on the tensile meridian to that on the compressive meridian.

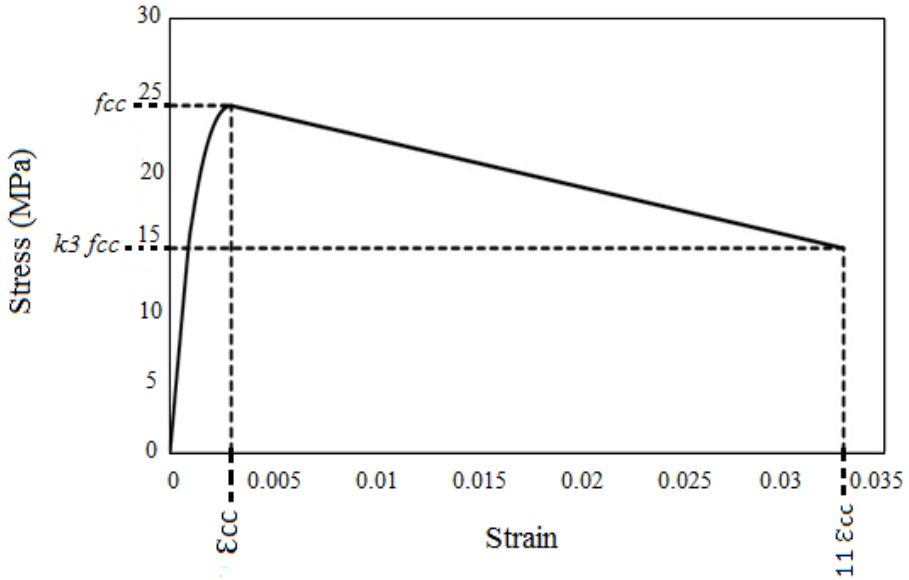

Figure 5.13. Stress-strain relationship of confined concrete used in the modelling.

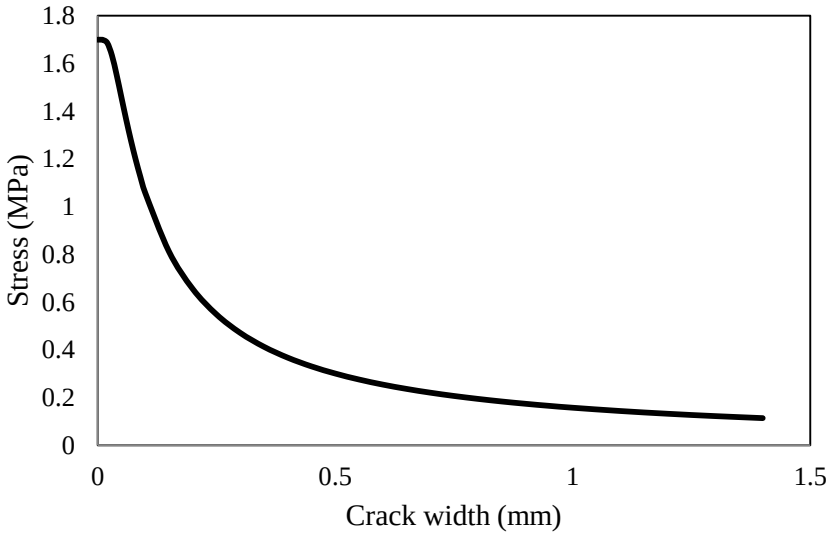

Figure 5.14. Concrete material behaviour in tension.

It should be mentioned that no studies available on the effect of strain rate on fully confined concrete as in the case of concrete filled steel tube. Nevertheless, a study was conducted on concrete partially confined using spiral reinforcement by Kono et al [113]. The results showed that an increase in the peak stress of less than 7% could be produced if the concrete partially confined with spirals of a yield strength of 300 MPa. Therefore, it could be concluded that the effect of strain rate will be decreased if the concrete fully confined as in concrete filled steel tube. The effect of strain rate on the dynamic behaviour of concrete was considered in some researches [63, 69, 114], whilst it was not considered in other studies [12, 14, 115, 116]. The numerical results of these studies still showed a very good agreement with the experimental ones. In the current study, the confined concrete was modelled without considering the effect of strain rate.

5.1.5 Simulation of impact loading

The impact load can be simulated using ABAQUS/ Explicit by defining the mass of the impactor and pre-defining the initial impact velocity which is obtained from the experimental results. The impact time can be set in the dynamic explicit step. Here, the impact time selected in the models was slightly longer than that obtained from the experimental results to ensure the simulation of the complete failure of the connection. The contact interaction defined between the projectile and the struck column was utilized to obtain the impact force time history. However, the displacement time history was obtained by requesting the displacement in a specific location on the projectile.

5.2 Modelling of end plate connection under quasi-static loading

Non-linear static analysis was used by many researchers to model the bolted connections under quasi-static loading. Due to the limitations of computational capabilities, the attempts were firstly developed using two-dimensional (2D) models [117-119]. It was found that the 2D models are unable to accurately predict the connection behaviour. Later and with the development of computers, many studies were carried out using three dimensional (3D)-

implicit models with considering various geometries [120-122]. However, this concept may result in convergence difficulties at which the model is aborted. This is due to the complex geometry and contact surfaces that such connections contain. The state-of-the-art- finite elements modelling adopted uses dynamic analysis for modelling the quasi-static behaviour to avoid convergence difficulties and geometric complexities. Also, explicit procedure is more convenient than implicit procedure for problems involving post-buckling behaviour, highly nonlinear quasi-static problems and damage problems [123] . Abdullah et al. [124] presented a method for modelling steel deck-concrete slabs under quasi-static load using non-linear dynamic finite element analysis. The numerical load-displacement curve results showed good correlation with the experimental results but with some oscillation in the plastic stage. Natario et al. [125] also used the explicit integration to evaluate the web crippling behaviour of cold-formed steel beams under quasi-static load. It was concluded that this type of analysis is effective to model web crippling failure in terms of load-displacement curves and failure modes.

In this study, the dynamic analysis using ABAQUS/Explicit is employed to model the end plate connections under quasi-static loading. This concept was adopted in this study for the aforementioned reasons. Also, it is a good opportunity to investigate the validity of this concept to model bolted connections after confirming its validity for other structural members as mentioned in references [123-125]

5.2.1 Geometries and boundary conditions

All the geometries and boundary conditions used in the modelling of the structural impact response are similar to those used for quasi-static load case, except for the projectile and load configuration. The projectile in impact modelling was replaced by a rigid body of 50 x 50 x 15 mm. Load application will be discussed in Section 5.3.5.

5.2.2 Element type and mesh size

The FE model developed for modelling the impact response was modified for quasi-static

models. The element C3D8R used in impact analysis is adopted here in the quasi-static analysis. It was initially started to model the quasi-static response of the connections using the similar mesh size to that used in the impact analysis (M_i). However, the numerical results showed very good correlation with the experimental one but the CPU time was uneconomical. Therefore, mesh sensitivity study was conducted to select the optimum mesh size at which the time of analysis is reduced without noticeable difference comparing with the experimental results. It was found that the coarser mesh could be used for quasi-static analysis comparing with that for the impact one. Table 5.3 shows a comparison for mesh sizes used in quasi-static analysis on a selected specimen (FNI8). The first group of the mesh sizes were similar to that used in the impact analysis for all individual parts and was named as (M_i). Three additional mesh configurations were examined, named Mesh1S, Mesh2S and Mesh3S, as shown in Table 5.3. Figure 5.15 shows the effect of mesh size on the accuracy of the model. It can be seen that adopting M_i, Mesh1S and Mesh2S has very small effect on the accuracy of the load-displacement curves but with considerable difference in analysis. Also, using Mesh3S makes the model stiffer than the other mesh sizes proposed. Before adopting these mesh sizes in the analysis, the tensile test of steel plate was modelled using the same mesh size as suggested by Ribeiro et al. [21], which is 1.5 mm. The calculated true stress-strain relationship was used as input data to define the material behaviour up to failure.

Table 5.3. Proposed mesh configurations for quasi-static analysis.

Location	Element size (mm)			
	M_i	Mesh1S	Mesh2S	Mesh3S
Bolt, washer and nut	1	1.75	2.5	3.5
End plate	1.5	2	3	4
Time of analysis (minutes)	913	726	522	316

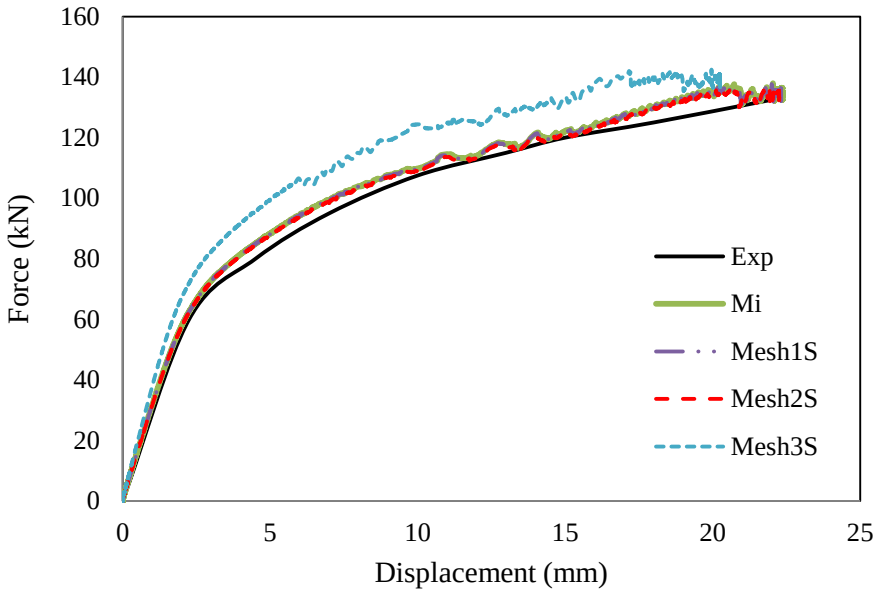

Figure 5.15. The element size effect on the accuracy of the FEA model under quasi-static loading.

The modelling output showed a very good agreement with the test results in terms of the deformation and failure modes. The experimental results showed that the fracture occurred at the deformation of 18.1 mm, whilst the numerical modelling showed that element deletion initiated at 17.9 mm as shown in the Figure 5.16. Also, the location of fracture and the failure mode in the numerical model were similar to that in the experiment. It should be also mentioned that the gauge length of the tensile test coupon was 90 mm, as indicated in Chapter three in Section 3.2.2, and the experimental engineering stress-strain curve started to degrade at a strain of 0.176, which is corresponding to the true strain of 0.162. This means the gauge length being extended to 104.6 mm. Since the ultimate gauge length of the specimen was recorded as 108.1 mm, then it could be said that the sample was displaced 3.5 mm after the initiation of necking up to the final fracture. However, the element sizes of Mesh2S can be considered as the optimum sizes at which high accuracy can be obtained in a shortest time of analysis. Therefore, element sizes proposed in Mesh2S were adopted in this study for quasi-static analysis as shown in Figure 5.17.

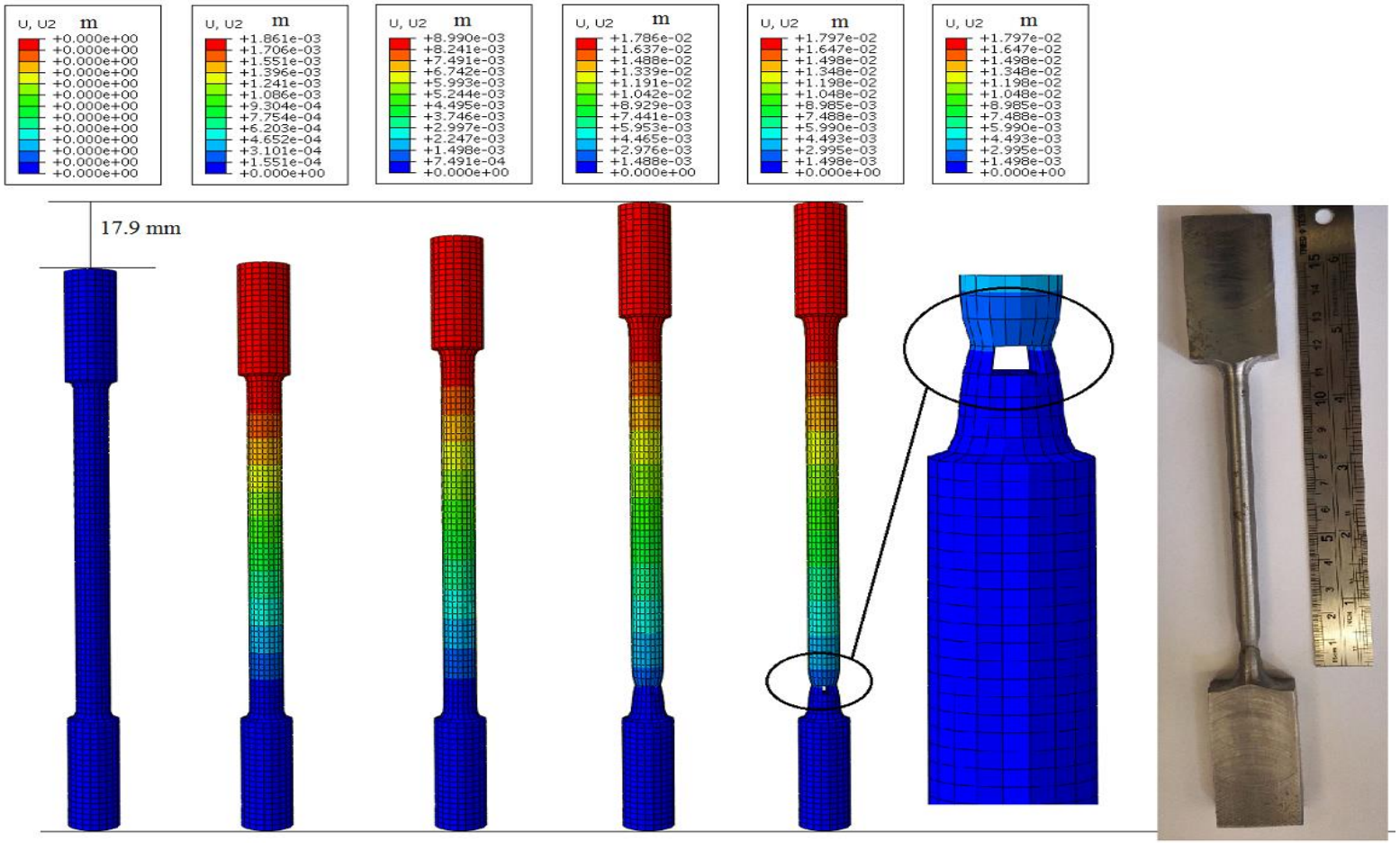

Figure 5.16. The modelling of tensile test of 8 mm steel plate and the validation of using the adopted mesh size.

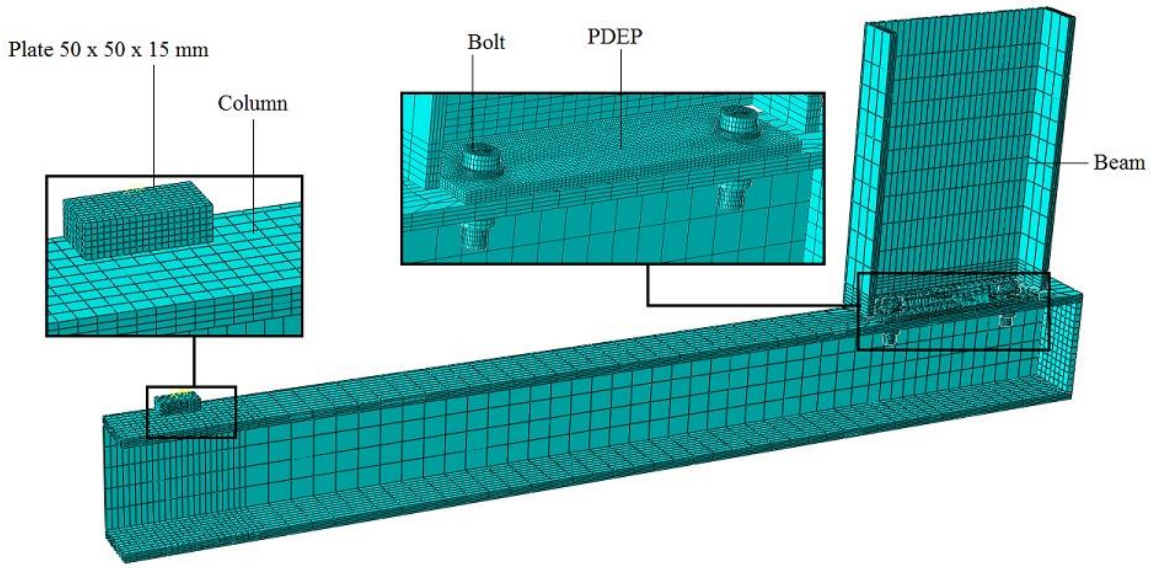

Figure 5.17. The mesh of specimen PFI8C connected to I-section steel columns under quasi-static loading.

5.2.3 Contact interactions

Similar contact formulation was used in quasi-static analysis to that in impact analysis. Hence, all the master and slave surfaces that defined in quasi-static analysis were similar to that in impact analysis. The projectile was replaced with a rigid body of 50 x 50 x15 mm as discussed in Section 5.3.1 and the normal contact interaction between the rigid body and the column was used to calculate the applied static force. Tie constrains were also defined as in impact analysis because similar geometry was used under both loading regimes.

5.2.4 Material modelling

5.2.4.1 Steel

The elasto-plastic behaviour of steel under quasi-static loading was modelled as that adopted in the impact analysis but without considering the strain rate effect. Hence, the true stress-strain curves that generated based on the experimental engineering stress-strain curves were used. The modelling of ductile and shear failure under quasi-static was performed using ABAQUS keyword option. Hence, the ultimate tensile stress of the plate and bolt were used

as input data to model the ductile damage. Also, shear damage of the end plate was modelled in the same way of ductile damage and a value of the equivalent plastic strain at the onset of shear damage ($\bar{\varepsilon}_s^{pl}$) of 0.2 was complied with the experimental results for all models.

5.2.4.2 Concrete

As no effect of strain rate was taken into account for the concrete infill under impact loading, as mentioned in Section 5.2.4.2, similar Elsto-plastic behaviour and damage behaviour adopted in impact analysis was adopted here under quasi-static loading.

5.2.5 Simulation of quasi-static loading

The explicit solution is a true dynamic procedure originally developed for simulating impact events, in which inertia plays a dominant role in the solution. Some special considerations requires when applying the explicit dynamic procedure to quasi-static problems. It is often computationally impractical to simulate quasi-static event in its natural time scale. Thus, the event must be accelerated in some way to obtain an economical solution. As the event is accelerated, the static equilibrium evolves into the dynamic equilibrium, in which inertial forces become more dominant. The goal is to model the event in the shortest time period in which dynamic effect remains insignificant [101]. Two solutions are available to eliminate the dynamic effect to model quasi-static loading using ABQUS/Explicit. The first one is to select lower loading rate (LR) and the second one is to apply a mass scaling factor to the analysis. Loading rate can be defined as the ratio of the maximum displacement at the free end of the loaded column to the assumed step time. However, lower loading rate could be obtained by increasing the step time which in turn increase the time of analysis. Therefore, mass scaling factor (MSF) could be employed in combination with using lower loading rate to reduce the time of analysis. Two indications can be used to ensure that the dynamic effect is insignificant. The first one is to ensure that no highly localized deformation is produced on the column where the quasi-static load is applied. The second indication is to examine the ratio between the kinetic energy (Ek) to internal energy (Ei) which should not exceed 5% [101].

Figure 5.18 shows a procedure that was used to select the optimum loading rate and mass scaling factor to model the quasi-static loading using ABAQUS/Explicit. The procedure begins with selecting a random step time to specify the loading rate used in the analysis by dividing the maximum displacement to the step time. This loading rate was tested then with different mass scaling factors to ensure that the ratio of kinetic energy to internal energy of the whole model (Ek/Ei) does not exceed 5%. With this condition, the dynamic effect produced from the explicit procedure can be eliminated and the CPU time is reduced. Hence, the first trial was carried out using a mass scaling factor of 108 with three loading rates of 10, 2 and 0.67 mm/s. It is concluded that using high loading rate leads to increase the energy ratio corresponding to a highly localized deformation mode in the loaded column, which is not the case in experimental deformed shape, as shown in Figure 5.19 (a). Yes, the localised deformations are significantly reduced using a lower loading rate, as shown in Figure 5.19 (b). In spite of the matching between the experimental and numerical deformed modes using a lower loading rate, the dynamic effect seemed to be unacceptable because the energy ratio (Ek/Ei) exceeds the limit aforementioned, as shown in Figure 5.20 (a). This may be attributed to the use of a high mass scaling factor. Therefore, three additional mass scaling factors less than 108 were investigated with a loading rate of 0.5 m/s, as shown in Figure 5.20 (b) to (d). In these figures, it can be seen that the dynamic effect is reduced with a lower mass scaling factor. Consequently, an initial loading rate of 0.67 mm/s and a mass scaling factor of less than 106 were used to in the FE modelling with reasonable CPU time.

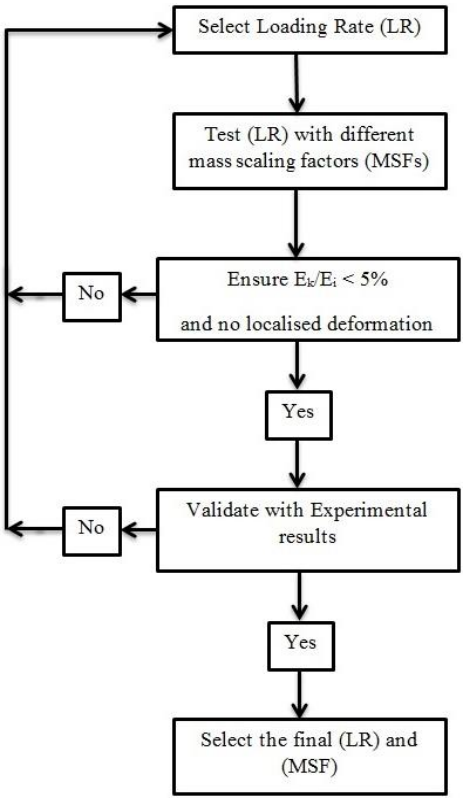

Figure 5.18. The adopted procedure to select the optimum loading rate and mass scaling factor in quasi-static modelling using Abaqus/Explicit.

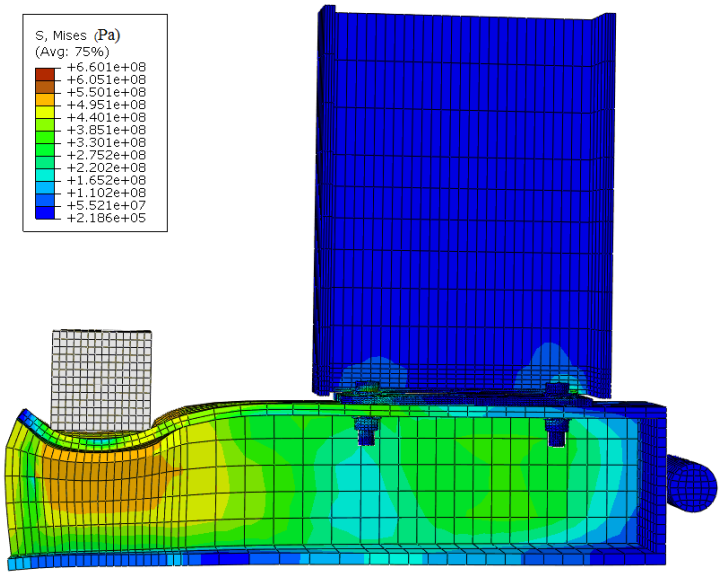

(a) Loading rate = 10 mm/s

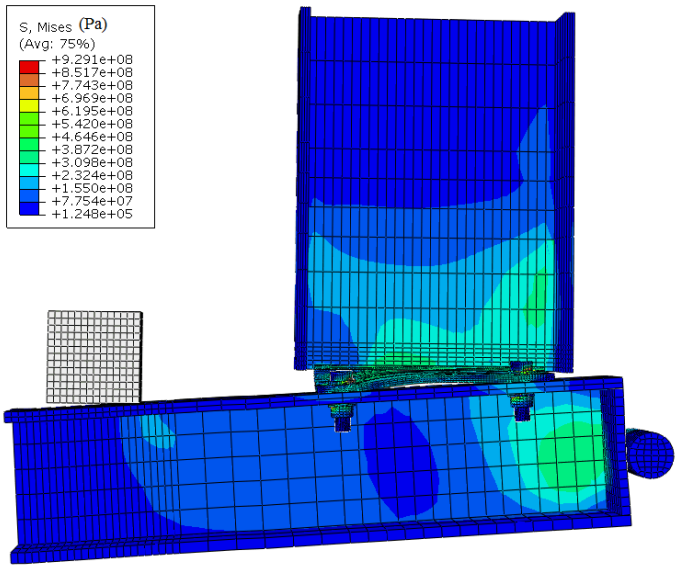

(b) Loading rate = 0.5 mm/s

Figure 5.19. Deformation mode with a mass scaling factor of 10^8 and different loading rates.

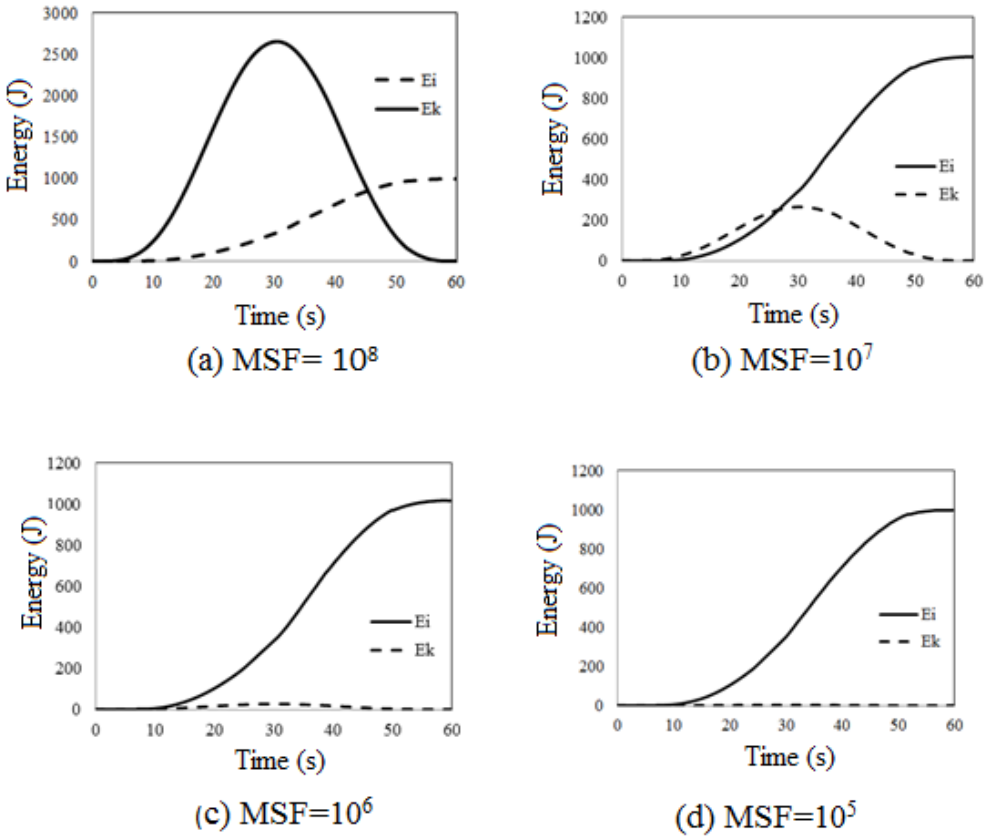

Figure 5.20. The dynamic effect with a loading rate of 0.5 mm/s and different mass scaling factors.

As mentioned in Section 5.2.5 that the impact load was applied by defining a mass and velocity. However, in quasi-static analysis, another procedure was adopted. The load application in quasi-static analysis is made using a reference point created at the rigid body with dimensions of 50 x 50 x15 mm used in the test to transfer the load from the loading ram to the column. One face of the rigid body was in contact with the free end of the column to apply the load. The load is applied through a displacement using smooth step amplitude, which is particularly recommended due to its efficiency to reduce noise generated from the initial kinetic energy [101]. Figure 5.21 shows typical smooth amplitude that used for quasi-static analysis.

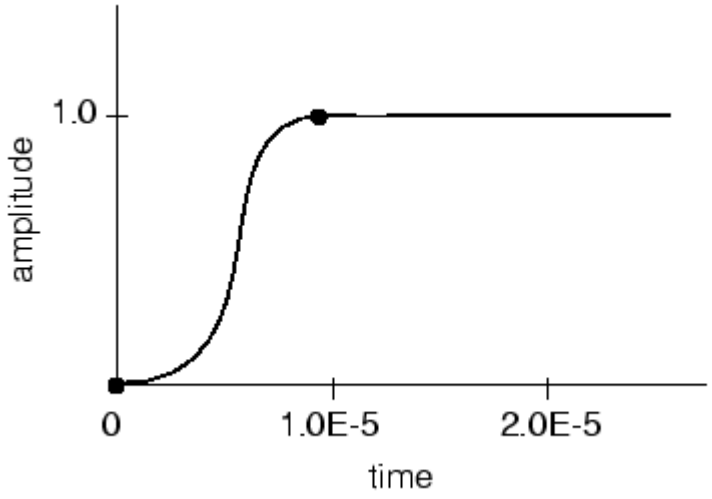

Figure 5.21. Typical smooth step amplitude used in quasi-static analysis.

5.3 Summary

This chapter has presented the theories and numerical simulation procedures that used to predict the response of the end plate connections under lateral impact and quasi-static loadings. The commercial software ABAQUS was used for developing the FE models. The geometry, material properties, contact interactions and properties, boundary conditions and loading conditions for the different models were discussed. The selection of the element sizes for all individual parts involving in the test specimens were discussed. The modelling of steel and concrete material up to failure was presented in details. Also, the load applications under impact load and quasi-static load were presented.

Chapter 6: Numerical Results and Discussion

6.1 Introduction

In the previous chapter, the finite element theory and the related modelling procedures in this study programme were introduced. In this chapter, the modelling results are presented, which are compared with the experimental results to validate the finite element models. Dynamic increase factors (DIFs) are also proposed based on the internal forces produced in the connections. Finally, using the validated models, full range analyses and parametric study are then performed to investigate the internal forces generated in the connections subjected to lateral impact loading in order to obtain insight into the response of such connections under different circumstances.

6.2 Modelling outcomes of end plate connections to steel columns

Finite element models using ABAQUS/Explicit were developed to simulate the response of beam-to-column connections under both lateral impact and quasi-static loading. The geometric, loading and boundary conditions adopted in the simulation were similar to those used experimentally.

6.2.1 Validation of the modelling of impact results

The six tested specimens are divided into three groups to facilitate the validation process. Each group contains two specimens. The first group contains specimens FNI8 and PNI8, which represent the specimens with both the types of connections selected in this study with a thin plate (8 mm) impacted near the connection (L_2). The second group includes the similar specimens to that of the first group but impacted far away the connection (L_1), which are specimens FFI8 and PFI8. Specimens FFI15 and PFI15, with a thick plate (15 mm) impacted at L_1, represent the third group.

6.2.1.1 Validation of the modelling of specimens FNI8 and PNI8

Figure 6.1 and Figure 6.2 show the predicted and the associated experimental force-displacement traces for specimens FNI8 and PNI8, which were impacted near the connection. The overall features of the experimental force-displacement traces were

predicted reasonably well. The predicted initial peak force for the above specimens were 399.5 and 323.6 kN, respectively, which are 3.7 and 3.9% higher than the experimental results, respectively. The predicted plateau forces for both specimens are in a good agreement with the corresponding experimental results. Moreover, very good correlation was obtained between the predicted and experimental maximum displacement. The predicted maximum displacements for both specimens were 22.7 and 32.7 mm, which were 1.6 an 7.3% higher than the experimental results, respectively. The model also shows the ability to capture the zero forces due to intermittent impact between the projectile and the struck column, as can be seen in Figure 6.1 for specimen FNI8 before a displacement of 5 mm.

Figure 6.3 and Figure 6.4 show the numerical and experimental deformation modes of both the connection types under lateral impact load. The predicted deformation modes correlated reasonably well with the experimental observations. Also, the model is capable of capturing the tearing failure of PDEPC close to the weld toe as shown in the close up in Figure 6.4.

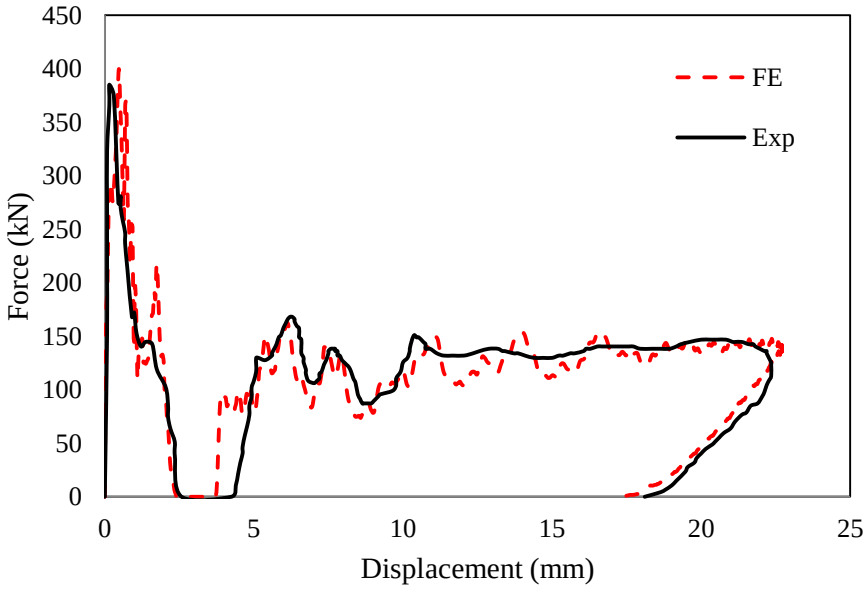

Figure 6.1. Force-displacement traces of specimen FNI8 subjected to lateral impact load: comparison of experimental data with FE simulation.

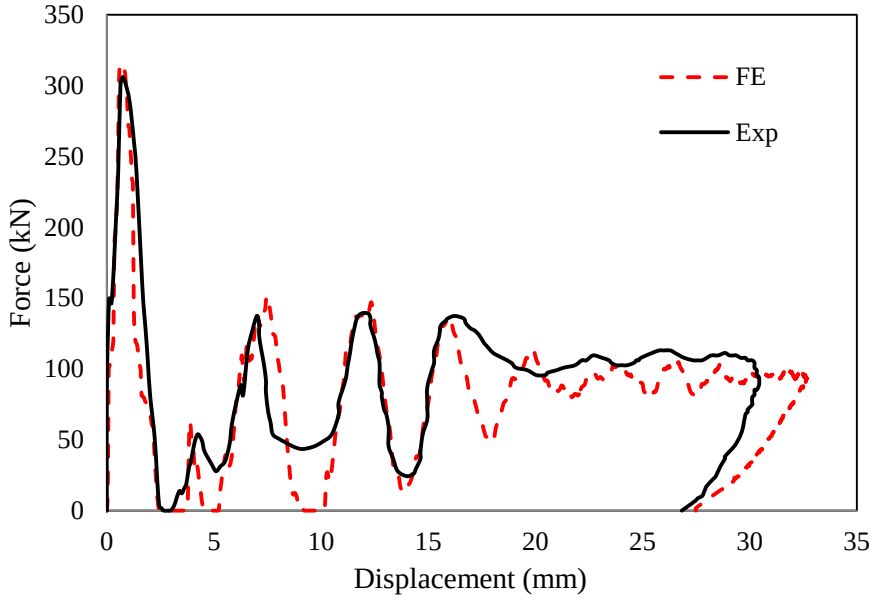

Figure 6.2. Force-displacement traces of specimen PNI8 subjected to lateral impact load: comparison of experimental data with FE simulation.

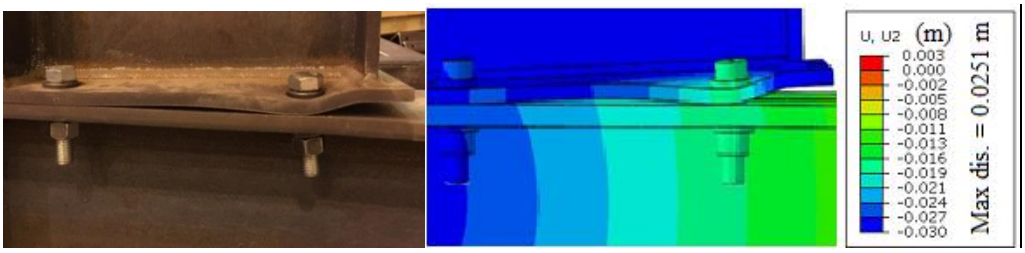

Figure 6.3. Deformation mode of the specimen FNI8 under lateral impact load.

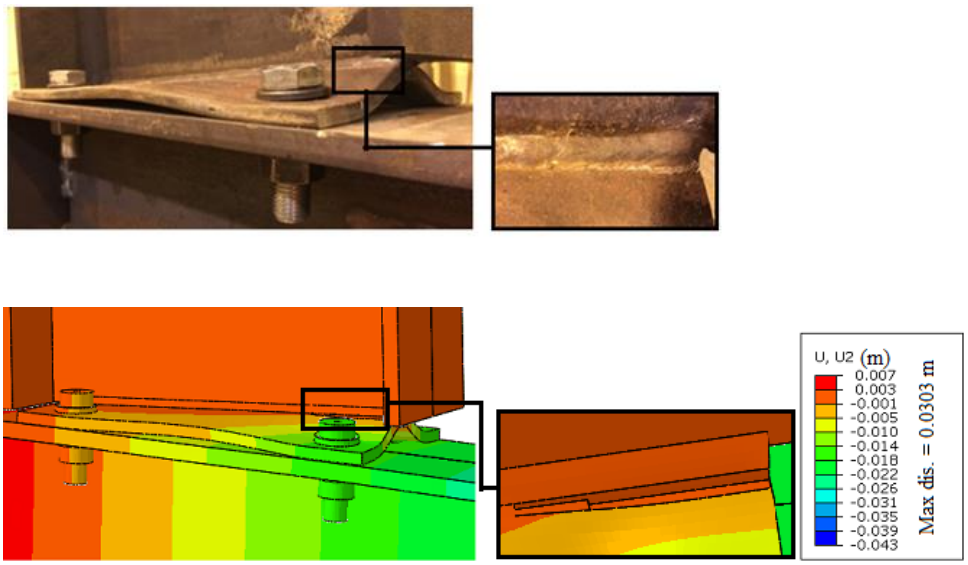

Figure 6.4. Validation of prying deformation of end plate in specimen PNI8.

In order to investigate the locations of the initial crack tips in specimen FNI8, the scaler variable (SDEG) available in ABAQUS is used. This option is used to evaluate the damage state of each element, indicating a level of the softening phase in the stress-strain curve of the material. As an element reaches a determined level of damage, it is deleted from the mesh producing simulation of the fracture. Contour plots of the scaler variable (SDEG) of specimen FNI8 is shown in Figure 6.5. It can be seen that the locations of the crack tip is developed up to SDEG value of about 20% near the weld to beam web and flange opposite to the first bolt pair.

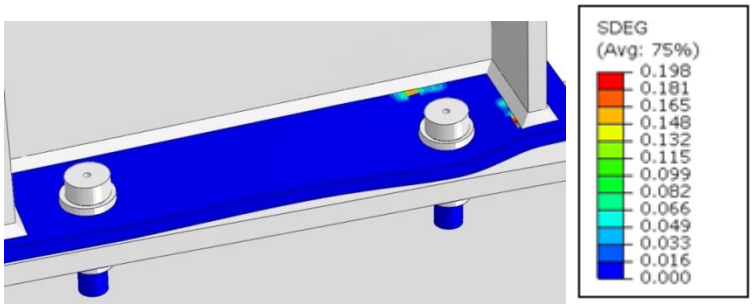

Figure 6.5. Predicted the first crack location of the specimen FNI8 under lateral impact load.

As mentioned in the previous chapter, the large deformation of an end plate led to developing bearing forces between the bolts and the end plate clearance hole. The models show a reasonable ability to capture this deformation mode, as can be seen in Figure 6.6.

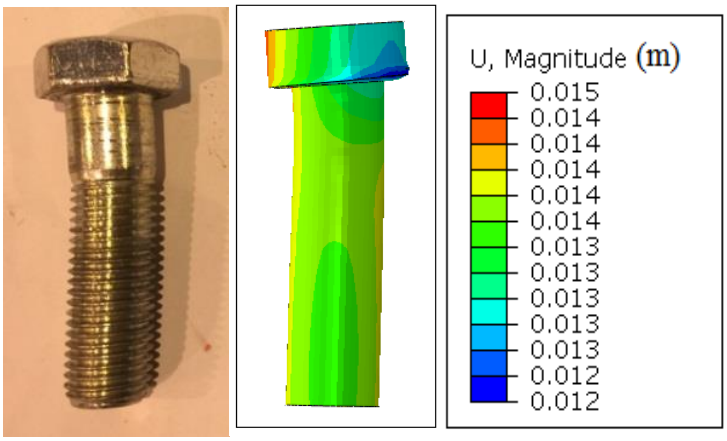

Figure 6.6. Bearing deformation of first bolt under lateral impact load.

In addition to the failed shape, the strain time histories in the four critical locations of each specimen were also examined and verified against the measurements, which confirms the validity of the FE models developed. Figure 6.7 and 6.8 show the validation of strain time histories in these locations for the specimen FNI8 and PNI8, respectively. A good agreement is obtained for all the gauges except SG2 which saturated at 10000 με that is the maximum strain to be captured the system employed to measure the strain as mentioned in section 2.4. Also, the model seems to be more sensitive than the strain gauges to the vibration especially in the initial peak stage.

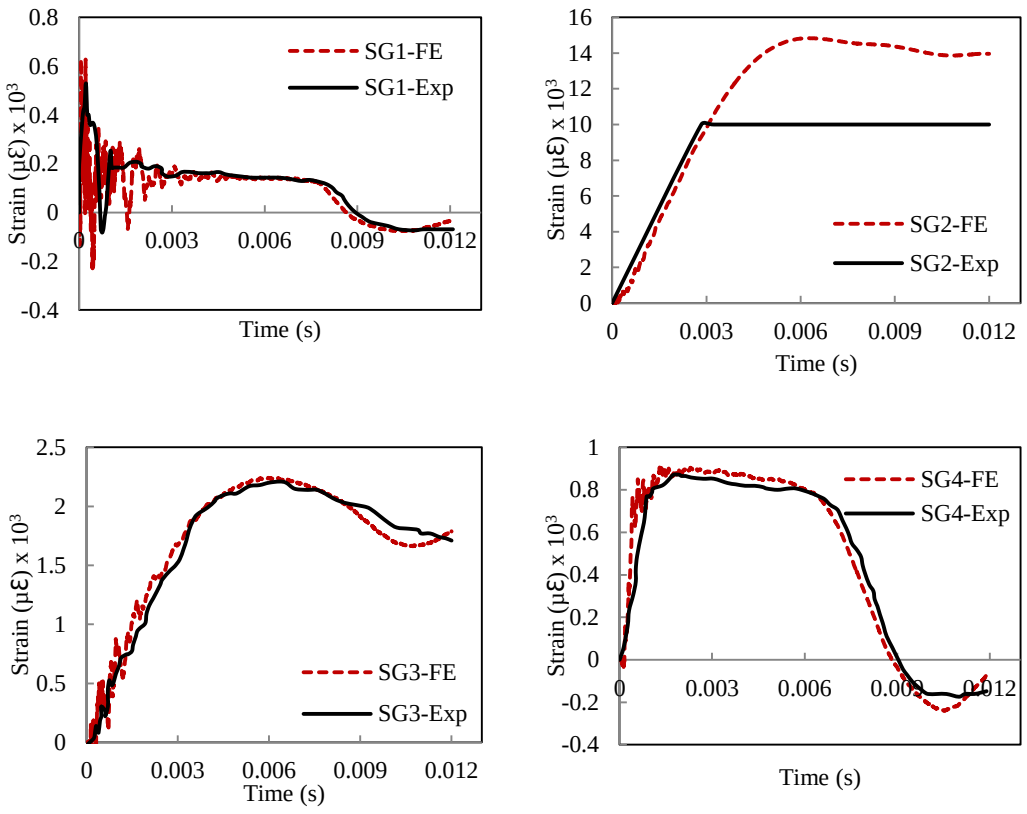

Figure 6.7. Comparison between the experimental and FE results of strain time histories of specimen FNI8.

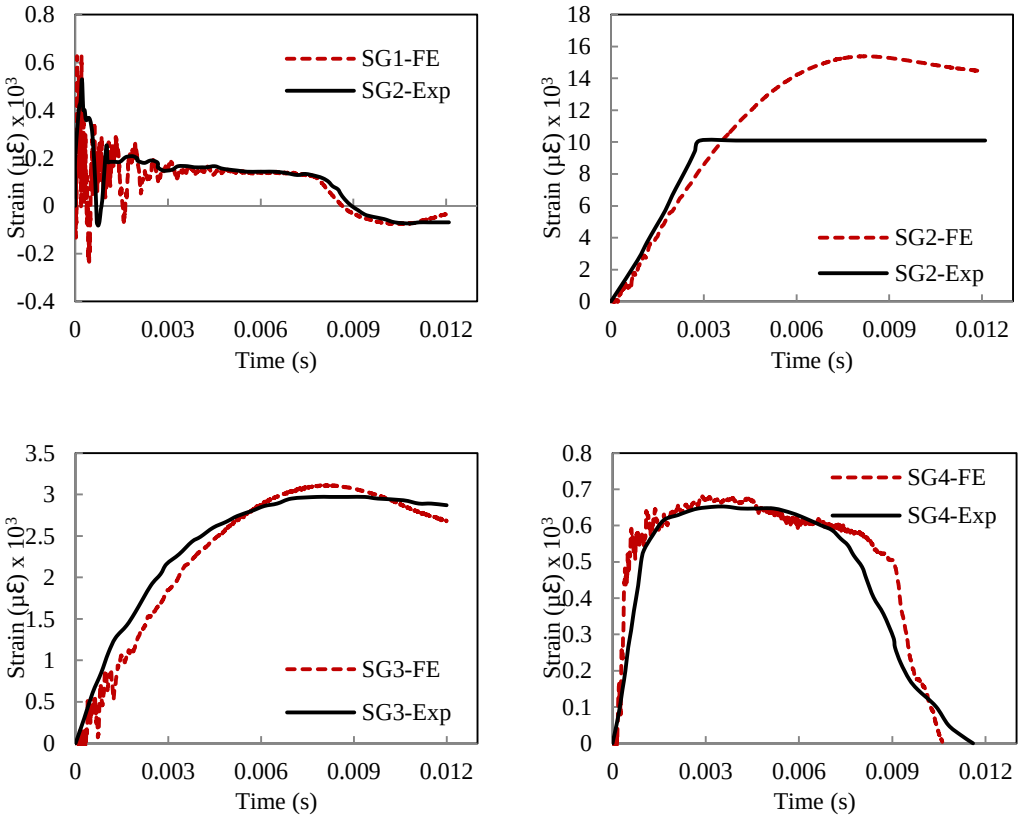

Figure 6.8. Comparison between the experimental and FE results of strain time histories of specimen PNI8.

6.2.1.2 Validation of the modelling of specimens FFI8 and PFI8

Finite element models were also developed to simulate the response of the specimens FFI8 and PFI8, which were impacted far away from the connection (L_1). Figure 6.9 and Figure 6.10 show the predicted force-displacement traces. For a clearer comparison, the corresponding experimental results are also indicated in the figures. A good agreement is obtained between the numerical simulations and the experimental results in terms of the initial peak forces, average plateau force and maximum displacement. The predicted initial peak force for specimen FFI8 and PFI8 were 323.6 and 320.2 kN, respectively. Compared to the corresponding experimental values of 311.2 and 285.0 kN, the predicted initial peak forces were 4 and 12% higher, respectively. The higher forces produced may be attributed to the assumption that the rigid projectile has a much higher contact stiffness than the deformable one used in the test. Also, the assumption of perfect support may contribute to

obtain the higher initial peak forces. Both the predicted forces that followed the initial peak force and those in the plateau stage correlate well with the experimental data. Also, the predicted maximum displacements were in a good agreement with the corresponding experimental results, with a discrepancy of only 2%.

The FE models also demonstrated good correlation with the observed failure modes in specimens impacted far away the connection which were almost similar to that for specimens impacted near the connections as was explained in Section 4.3.1.1. As before, the validity of the FE model was also examined by comparing the experimental and the numerical strain time history in the four locations selected. The comparison showed a good agreement between them as can be seen in Figure 6.11 and Figure 6.12. Again, the measured strain in SG2 exceeded 10000 με, which cannot be captured by the system employed to measure the strain as explained in Section 2.4.

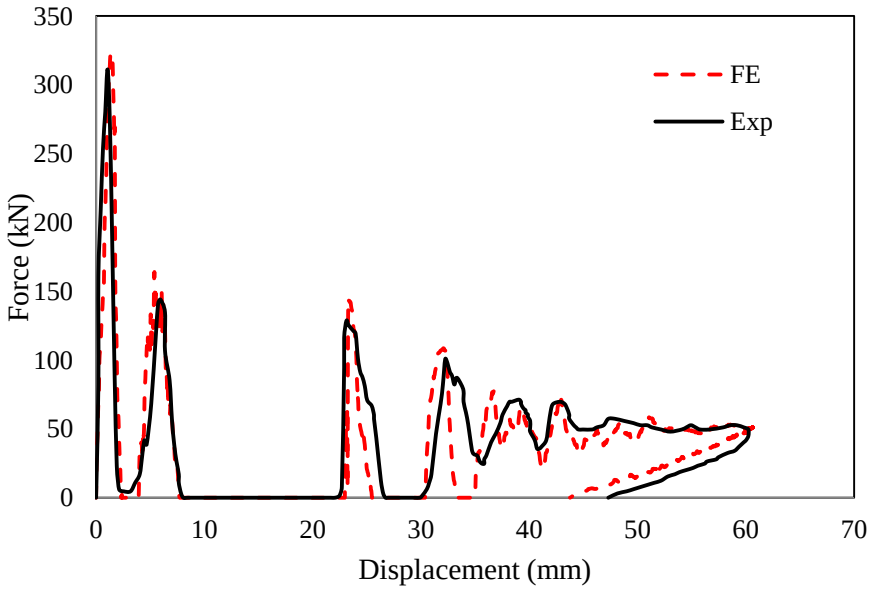

Figure 6.9. Force-displacement traces of specimen FFI8 subjected to lateral impact load: comparison of experimental data with FE simulation.

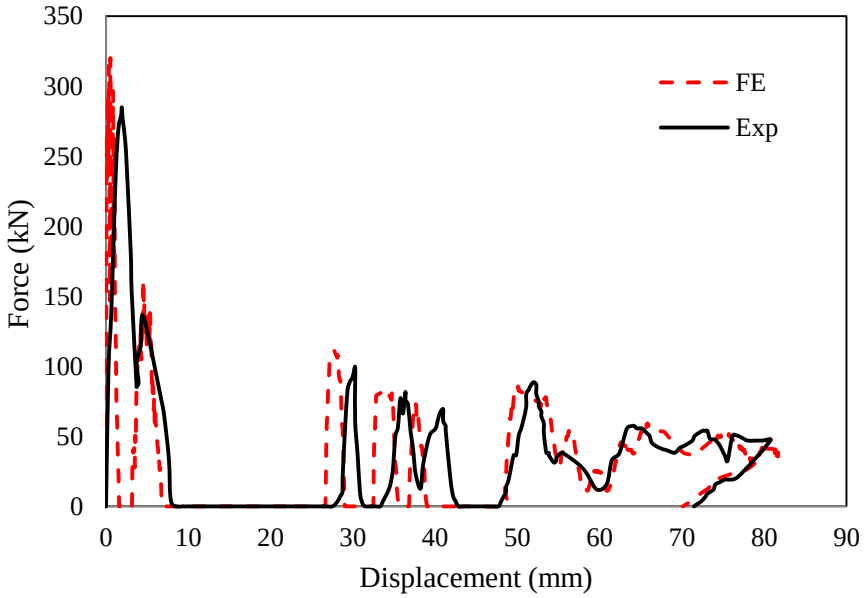

Figure 6.10. Force-displacement traces of specimen PFI8 subjected to lateral impact load: comparison of experimental data with FE simulation.

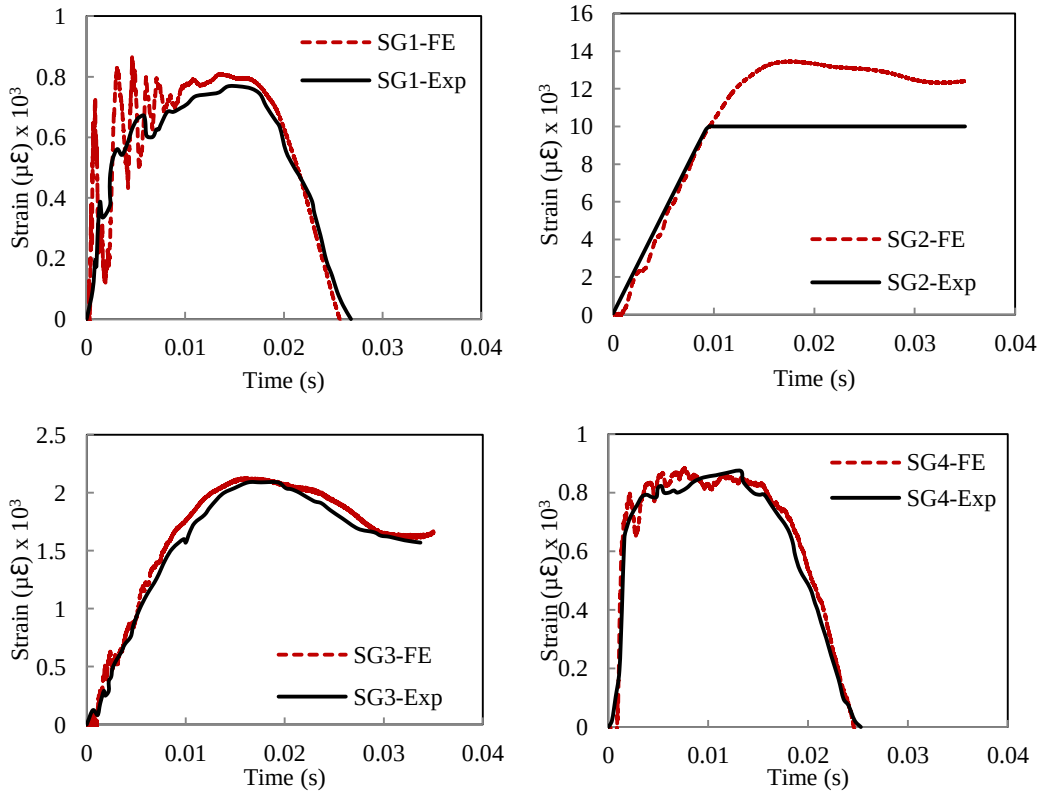

Figure 6.11. Comparison between the experimental and FE results of strain time histories of specimen FFI8.

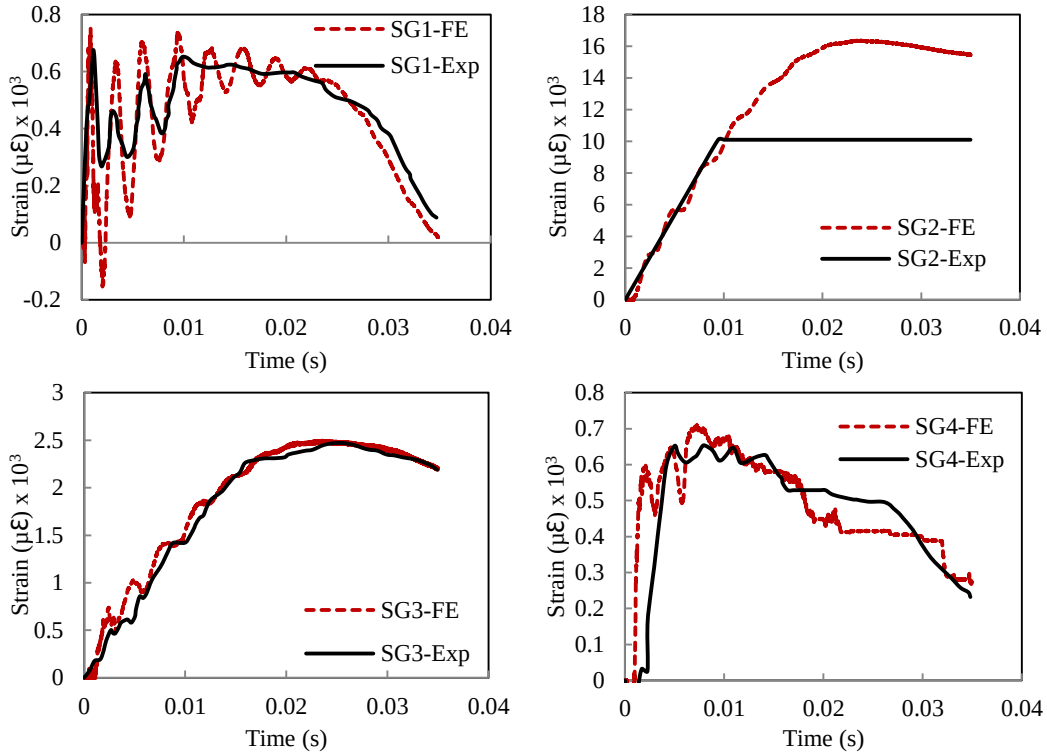

Figure 6.12. Comparison between the experimental and FE results of strain time histories of specimen PFI8.

6.2.1.3 Validation of specimen (FFI15 and PFI15)

Figure 6.13 and Figure 6.14 show the simulated and associated experimental force-displacement traces of specimens FFI15 and PFI15. The predicted initial force and the maximum displacement were in a reasonably good agreement with the corresponding experimental results. Also, the models show a good ability to capture the zero forces produced due to the contact missing between the projectile and the struck column. Again, the higher initial forces were obtained in the FE models than those obtained experimentally by less than 14%. The predicted maximum displacements of both specimens did not exceed 2.5% of the measured ones.

Figure 6.15 to Figure 6.17 show comparisons of the simulated and experimental deformation modes of these specimens. It can be seen that the numerical models are capable of capturing both the crippling of column flange as shown in Figure 6.15 and Figure 5.16 and the slight prying of PDEPC as shown in Figure 6.17.The strain time histories in the

selected four points were also examined numerically and the result showed good correlation with the experimental data as can be seen in Figure 6.18 and Figure 6.19.

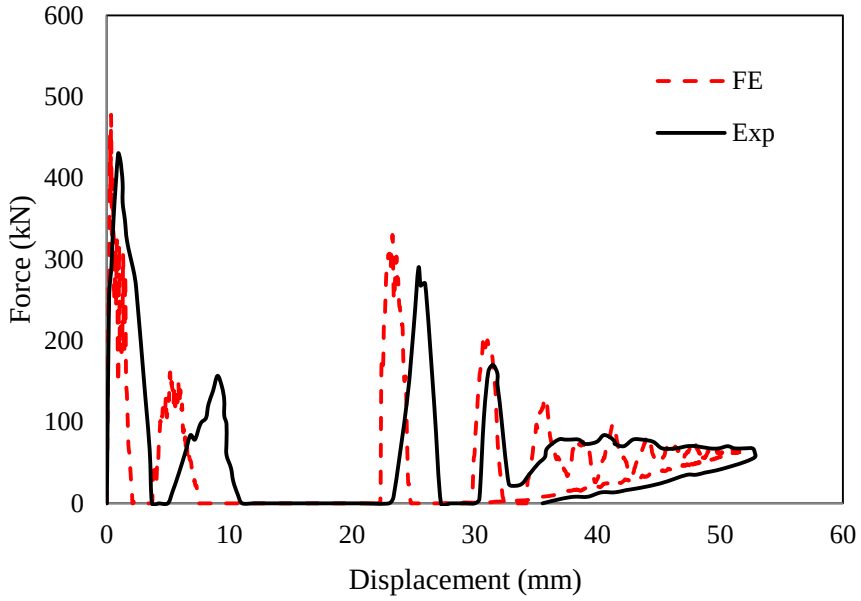

Figure 6.13. Force-displacement traces of specimen FFI15 subjected to lateral impact load: comparison of experimental data with FE simulation.

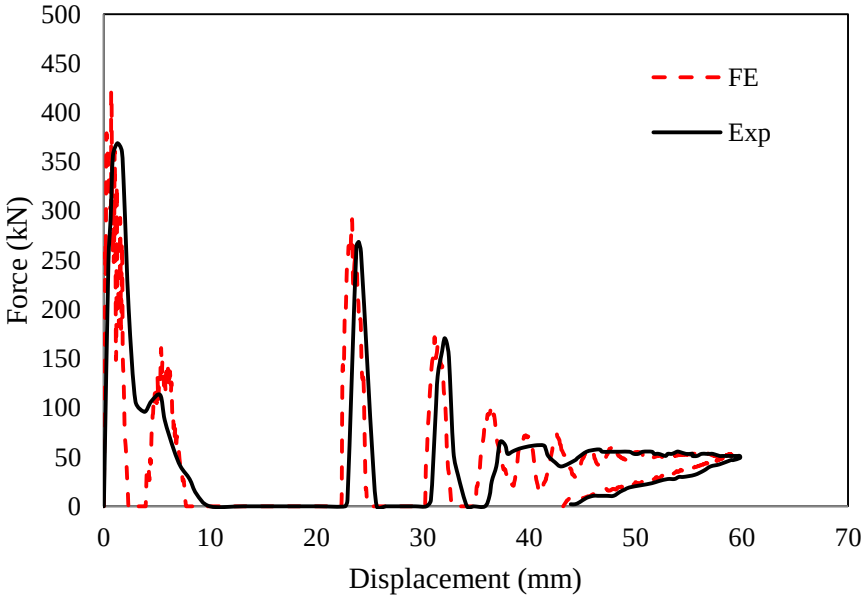

Figure 6.14. Force-displacement traces of specimen PFI15 subjected to lateral impact load: comparison of experimental data with FE simulation.

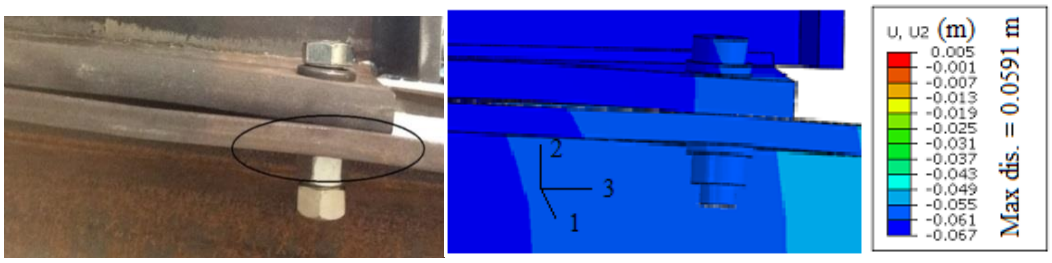

Figure 6.15. Validation of crippling of column flange in specimen PFI15.

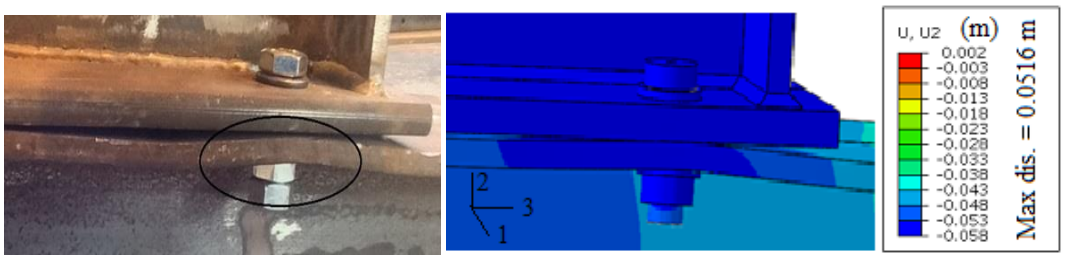

Figure 6.16. Validation of crippling of column flange in specimen FFI15.

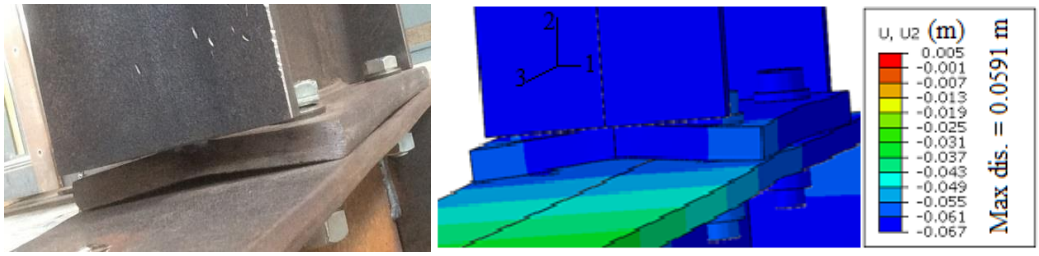

Figure 6.17. Validation of prying deformation of end plate in specimen PFI15.

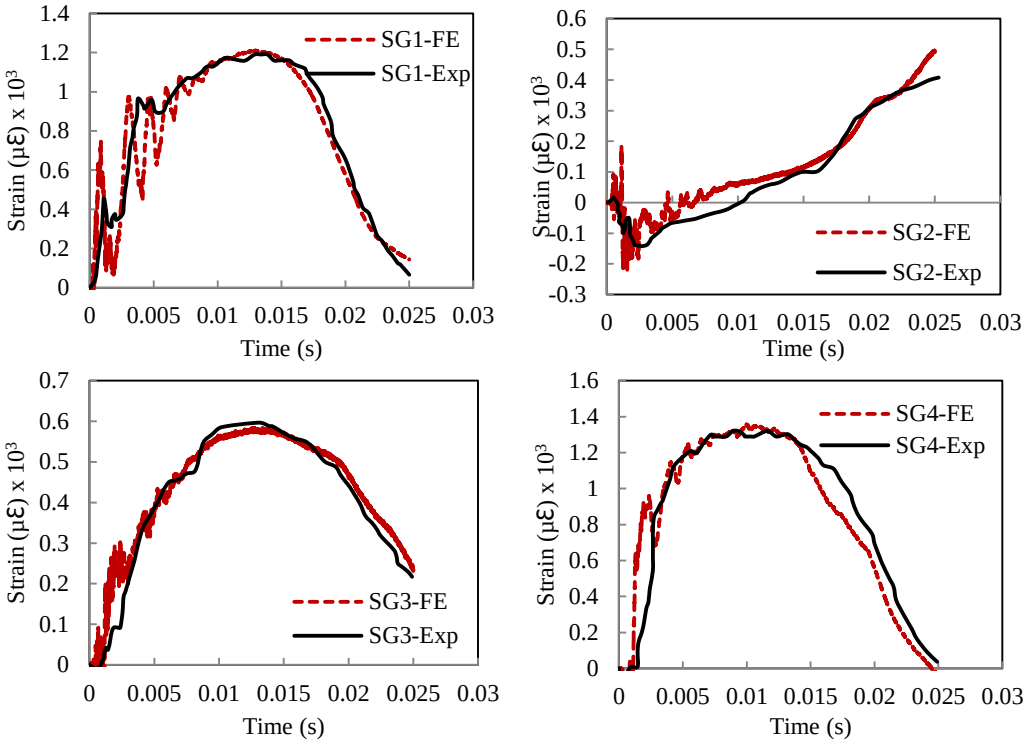

Figure 6.18. Comparison between the experimental and FE results of strain time histories of specimen FFI15.

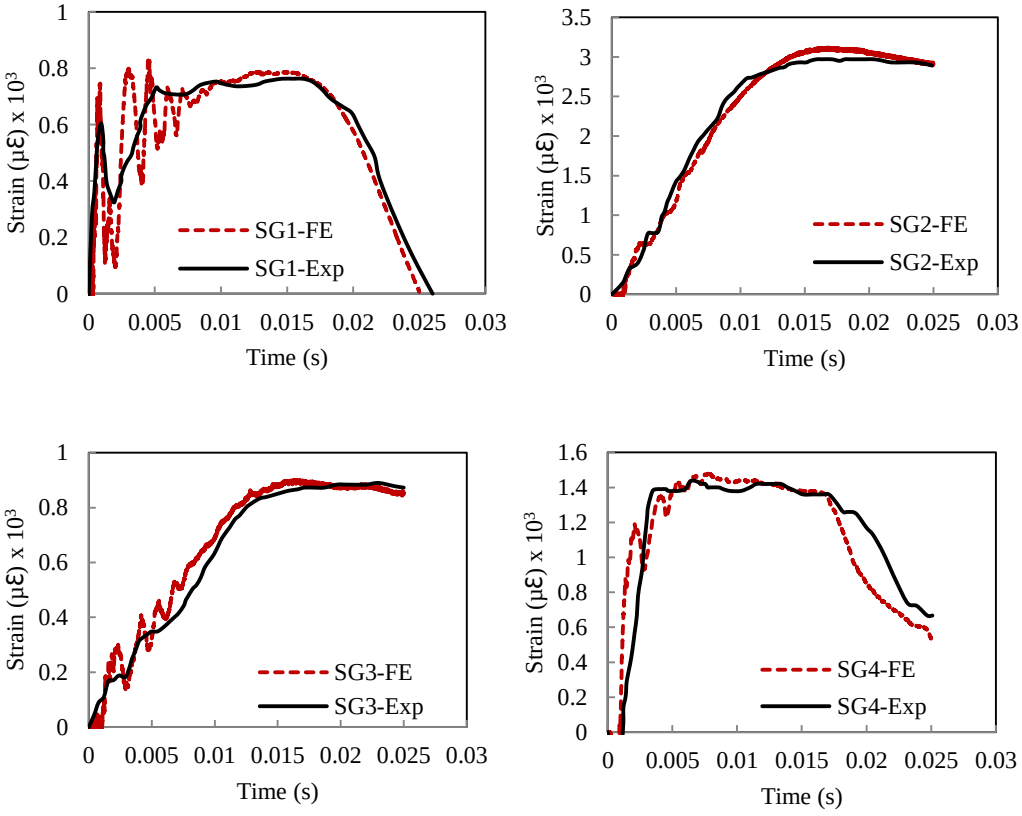

Figure 6.19. Comparison between the experimental and FE results of strain time histories of specimen PFI15.

6.2.2 Validation of the modelling of quasi-static results

Four specimens (FNI8S, PNI8S, FFI8S and PFI8S) were tested under quasi-static loading conditions to investigate the dynamic effect on the connection by comparing the static results with the impact results as explained in Section 4.4. Hence, the corresponding specimens were loaded under quasi-static loads up to the same maximum displacement acquired under impact load as discussed in Section 4.5. The DIFs were proposed based on the energy principles in Chapter four. Another method will be employed to propose DIFs based on the internal forces on the connection using the validated models. However, in the next section, the validation of FE quasi-static results is presented to help with proposing such DIFs then.

6.2.2.1 Validation of force-displacement traces

Figure 6.20 and Figure 6.21 show comparisons between the numerical and experimental force-displacement traces of specimens tested under quasi-static load. As mentioned in Section 5.3, ABAQUS/explicit was found to be the appropriate approach for simulating a connection with complex contact conditions under quasi-static loading. Good agreements are obtained for the bilinear force-displacement traces in spite of the slight oscillations produced in theses curves particularly after the onset of fracture. These oscillations can be controlled using low loading rate which in turn leads to increase the time of analysis. Hence, this was avoided in this study because very slight effect was found on the internal forces using the low loading rate.

6.2.2.2 Validation of deformation modes

As mentioned in Section 4.4.1, the deformation modes under quasi-static load were similar to that under impact load for all specimens but with a higher damage for PDEPC specimens close to the weld toe. Figure 6.22 shows the experimental and predicted failure mode of specimen PNI8S. It is clear that the model is capable of capturing the prying failure of the end plate, in addition to the tearing failure closed to the weld toe.

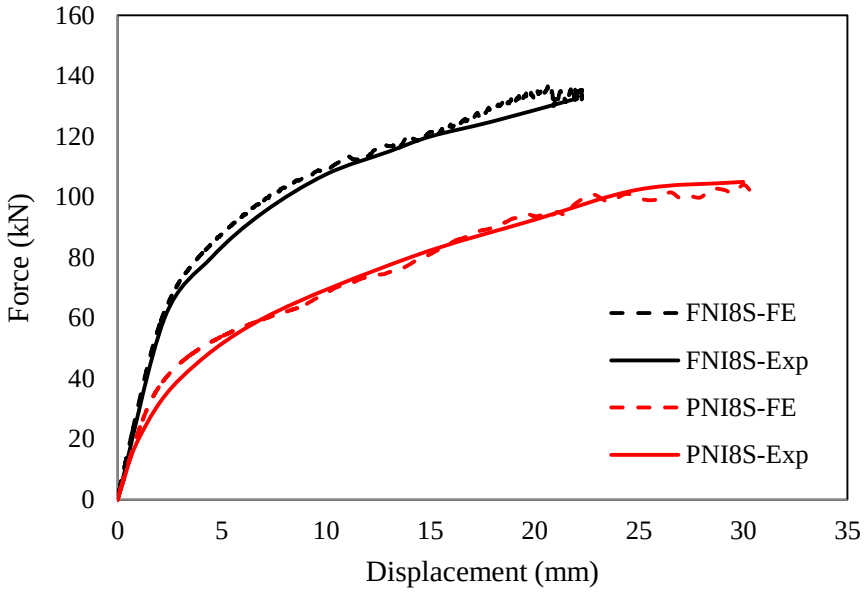

Figure 6.20. Force-displacement traces of specimen FNI8S and PNI8S subjected to quasi-static load: comparison of experimental data with FE simulation.

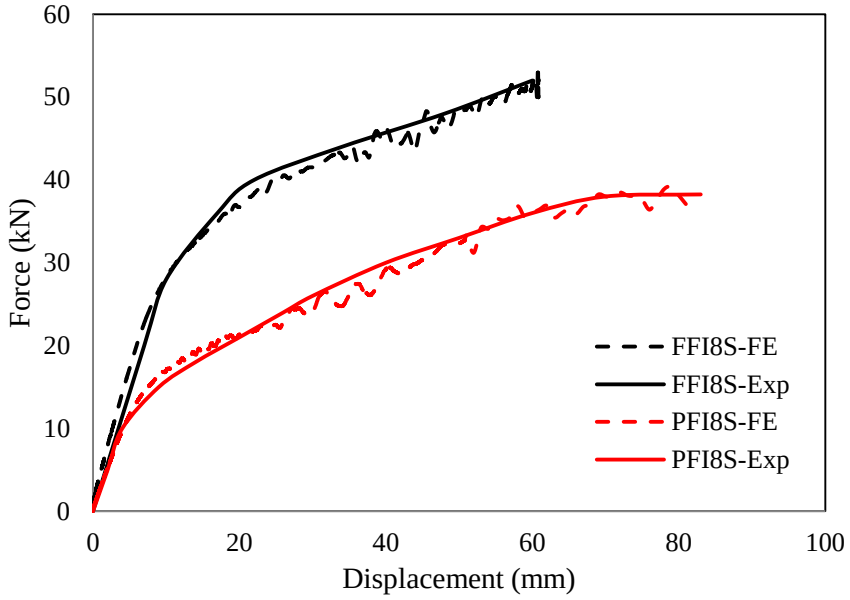

Figure 6.21. Force-displacement traces of specimen FFI8S and PFI8S subjected to quasi-static load: comparison of experimental data with FE simulation.

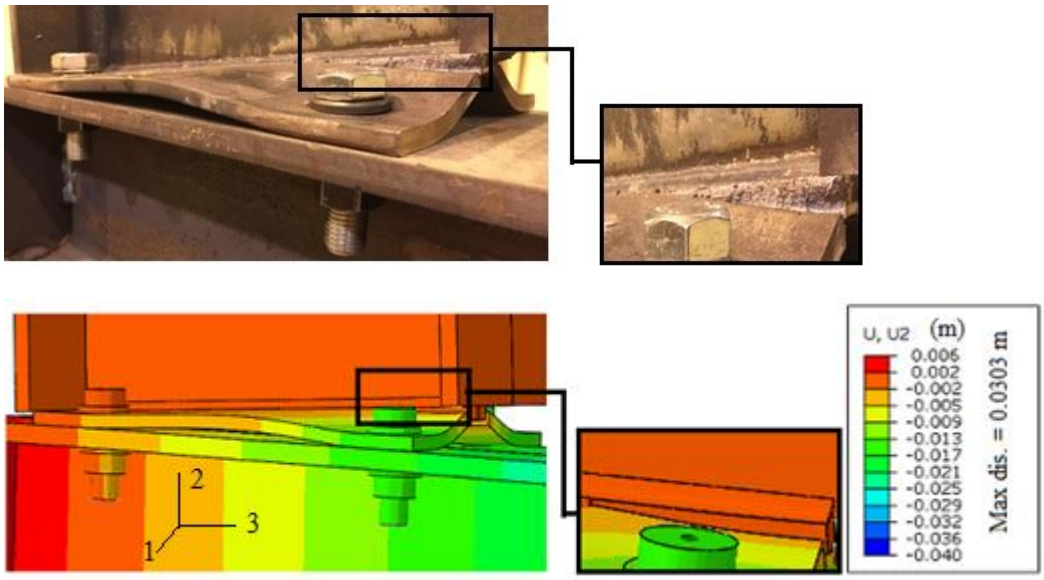

Figure 6.22. Deformation mode of specimen PNI8S under quasi-static load: comparison between experimental observations and numerical results.

6.2.2.3 Validation of strain gauges results

The strains were measured using the same system employed to measure the strain under impact load but with setting longer time as more time is required to perform quasi-static test compared with impact test. The strain and the displacement in the free end of the column were recorded with each load increment. Then, the displacement-strain curves were tabulated for each strain gauge to be compared with the numerical results. Figure 6.23 to Figure 6.26 show comparisons between the predicted and the experimental displacement-strain traces under quasi-static loading. In general, a good degree of the correlation was obtained between the experimental results and the numerical simulations. Some oscillations can be seen in the simulation results due to the dynamic effect produced particularly within the plastic deformation of the connection as shown in results of SG1 and SG4. Also, a short delay is produced in all experimental strain readings compared with the simulation results which may be attributed to the assumption of the perfect supports. Moreover, the strains measured in SG2 in all specimens showed good correlation with the numerical results up to 10000μƐ. After that, the system is saturated and unable to capture strain due to the limitations explained in Section 3.4.2.3.

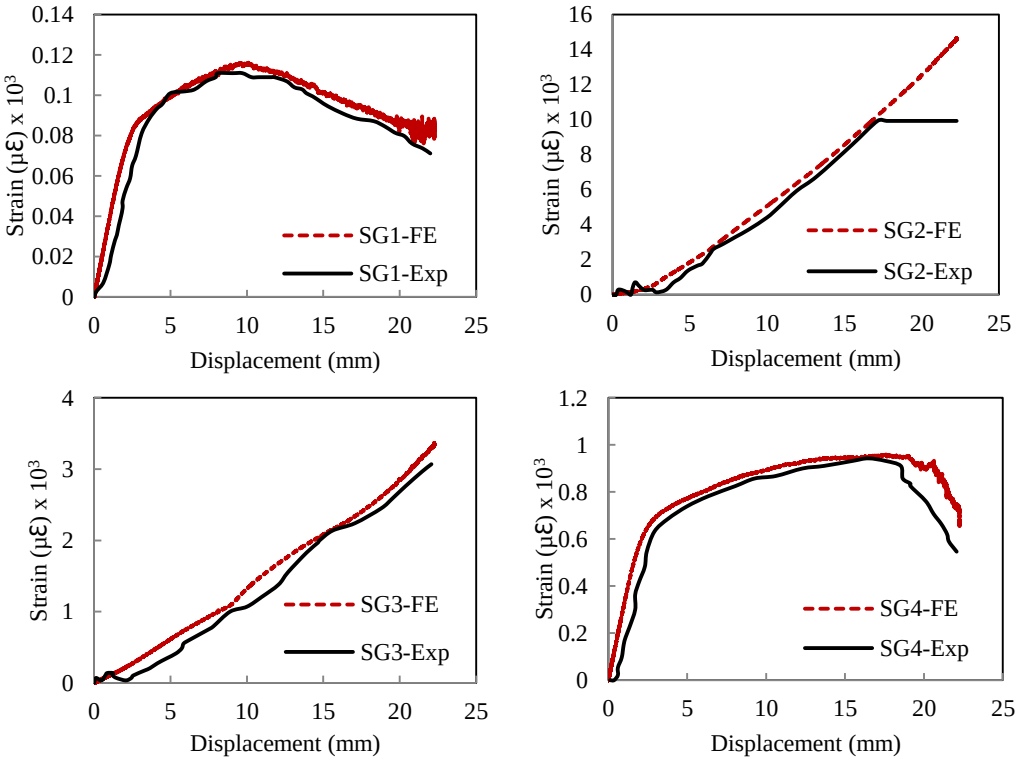

Figure 6.23. Comparison between the experimental and FE results of strain time histories of specimen FNI8S.

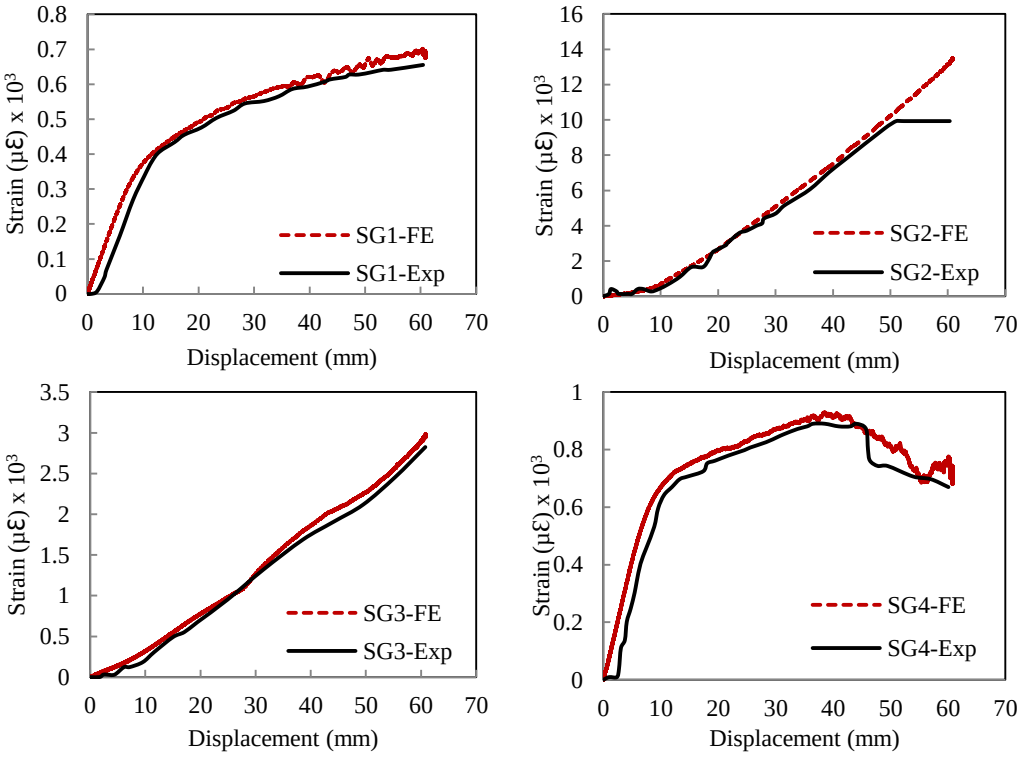

Figure 6.24. Comparison between the experimental and FE results of strain time histories of specimen FFI8S.

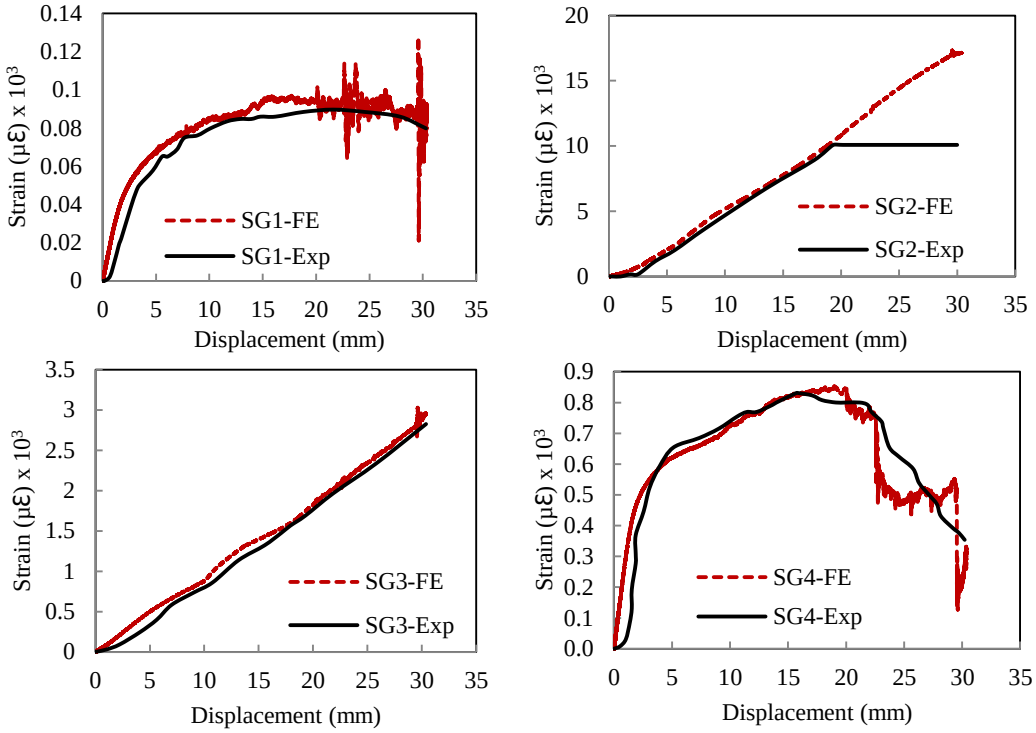

Figure 6.25. Comparison between the experimental and FE results of strain time histories of specimen PNI8S.

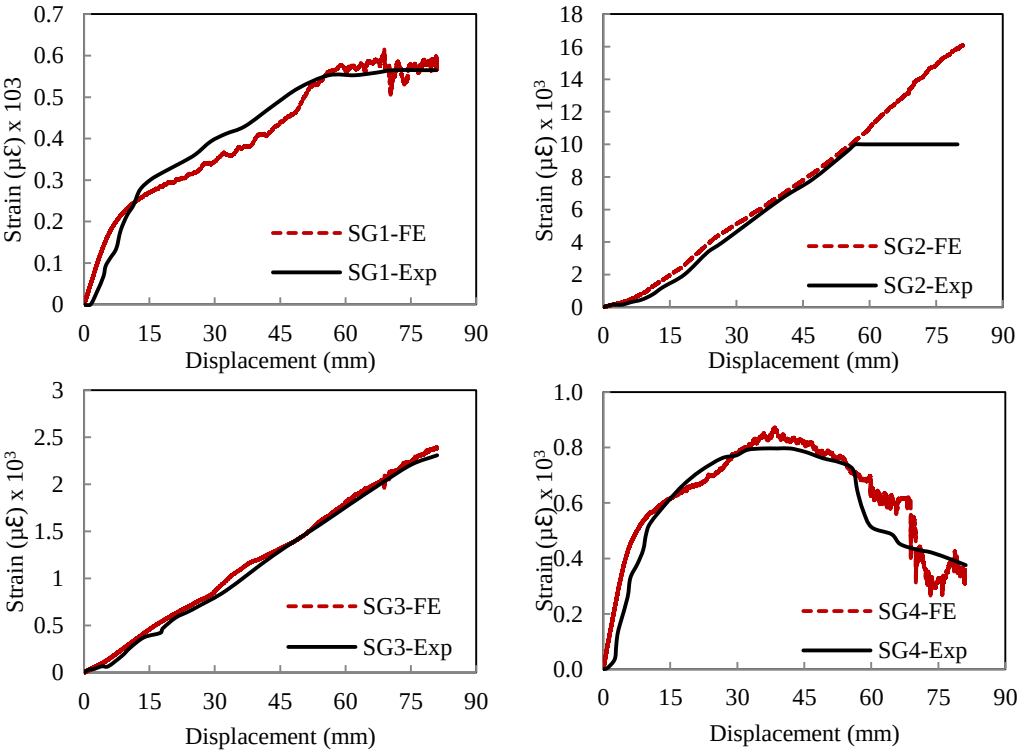

Figure 6.26. Comparison between the experimental and FE results of strain time histories of specimen PFI8S.

6.2.3 The full range analyses of the structural response

The experimental results were used to predict DIFs based on energy principles as explained in Section 4.5. In this chapter, the validated FE models are used to analyze the full-range response of end plate connections under quasi-static and impact load, including the internal forces in bolts, the axial and moment resistances of the connections investigated. These outputs represent the key factors that affect the joint response under lateral loads. Also, this analysis helps with proposing a DIF for each key factor separately and then to propose a preliminary DIF at which the impact response can be predicted using static analysis that is a preferable procedure for structural engineers. The validated model is also employed to estimate the strain-rate distribution in the critical parts of the connection.

6.2.3.1 Internal forces on bolts

The tensile forces on the bolt were requested in the FE model as the contact force between the bolt head and the top washer. Figure 6.27 and Figure 6.28 show the force time histories of the first and second bolt under impact load for specimens tested with a thin end plate. Generally, continuous force flow with a few spikes can be seen for all specimens in spite of intermittent impact observed in the impact force-displacement relationships. This is because the struck column was kept accelerated and displaced despite of the contact separation of the impactor. The numerical results showed that the first bolt for all specimens experienced a faster change in force than the second bolt after the onset of loading (for example in specimen FFI8, the first bolt needs less than 1.5 ms to reach 60 kN, while the second bolt reaches the same load by more than 6 ms). Also, it can be seen that after the maximum displacement of the free end of the column, the forces on both bolts begin to degrade rapidly due to the fast deceleration of the applied force in the bounce stage. Moreover, specimens loaded at L_2 from the joint centre experienced a faster bolt force degradation to reach the separation point. Besides, it can be seen that the first bolt for all specimens loaded dynamically gains a considerable amount of its peak force in a short period, which indicates that the bolt experienced a high strain rate. This may lead to bolt thread stripping failure

which is a type of failure to be avoided in connection. This type of failure was not observed in all specimens tested as mentioned in Section 4.6.1, which may need to be examined under higher impact energies.

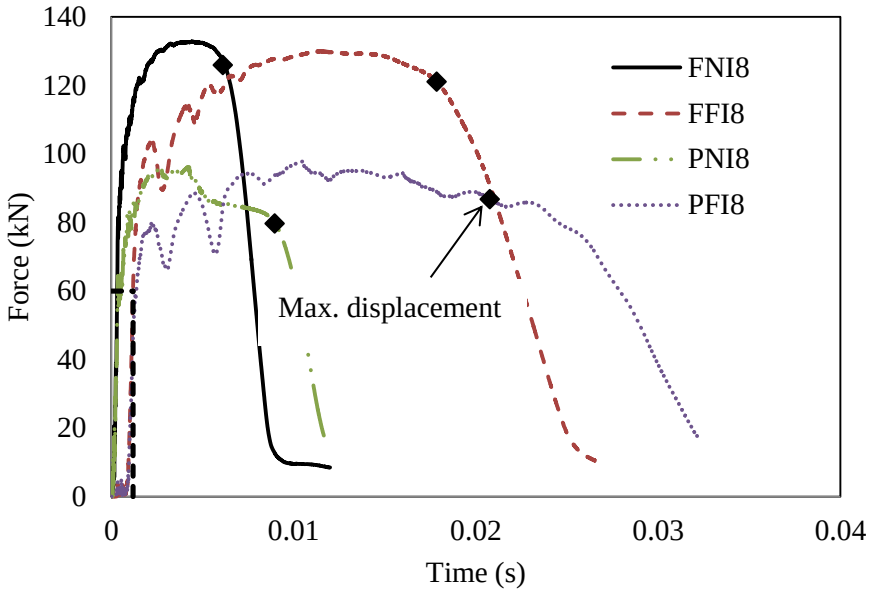

Figure 6.27 Internal tensile force time histories of the first bolt row of specimens with thin plate connected to steel columns under impact load.

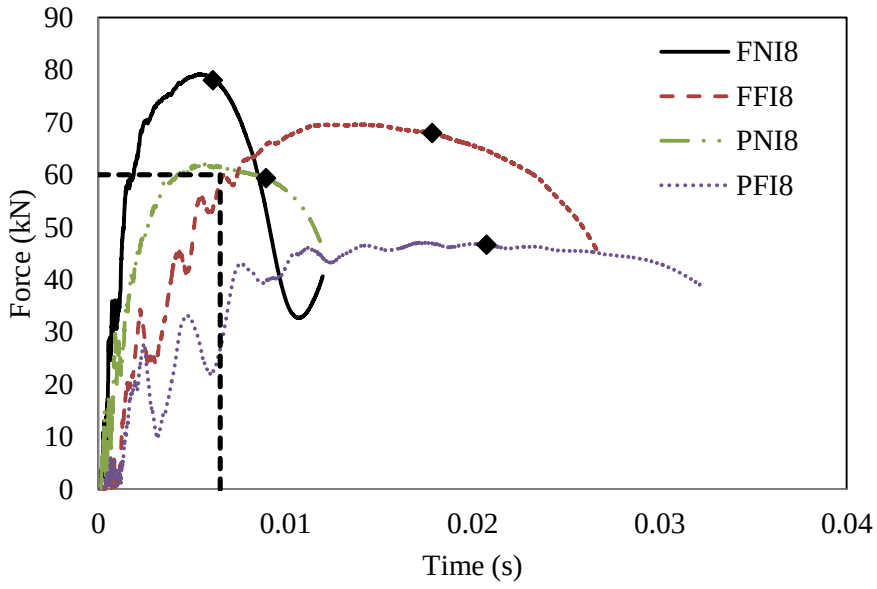

Figure 6.28. Internal tensile force time histories of the second bolt row of specimens with thin plate connected to steel columns under impact load.

Figure 6.29 and Figure 6.30 show the force time histories of the first and second bolt under impact load for specimens tested with thick end plate. It is clear that the maximum force generated in the first bolt in both connection types did not affect, as shown in Figure 6.29. However, the maximum force generated in the second bolt in FPC is 10% higher than that in PDEPC, as shown in Figure 6.30. Moreover, as in specimens with a thin plate, the strain rate effect seems to be more effective in the first bot row than the second one.

In addition to the dynamic tensile force that the bolt experienced, a bearing force was developed between the bolt and the clearance hole of the end plate leading to bearing deformation of the bolts as explained before in Section 4.6.1. Figure 6.31 shows the bearing forces produced on the first bolt row. As the prying failure is developed in the end plate, the clearance hole starts to move from its position until the contact occurs between the exterior surface of the bolt and the clearance hole, which develops a bearing stresses. Hence the bearing force time histories indicated in Figure 6.31 show zero forces in the onset of impact loading as the aforementioned contact has not occur yet. The higher prying failure of the end plate, the higher bearing force produced. Therefore, the bearing force developed on specimens with a thick plate was lower than those of a thin plate, as the former specimens did not show a large prying failure as the latter. The numerical results showed that the maximum bearing force was 60.05 kN in the specimen with thin PDEP impacted far away from the connection (PFI8), while the minimum force was zero, which was identified in specimen FFI15. The bearing resistance of bolts grade 8.8 in contact with a 8 mm thick plate is 54.4 kN, according to BS EN 1993-1-8 [7]. In spite of the high deformation that the some specimens tested experienced, specimen PFI8 only exceeded this limit, which interprets the higher bearing failure experienced by this specimen in comparison to other specimens tested. The bearing resistance of bolts could be added to the prying resistance of the end plate and tensile resistance of bolts as factors to enhance the ductility and energy dissipation of the connection.

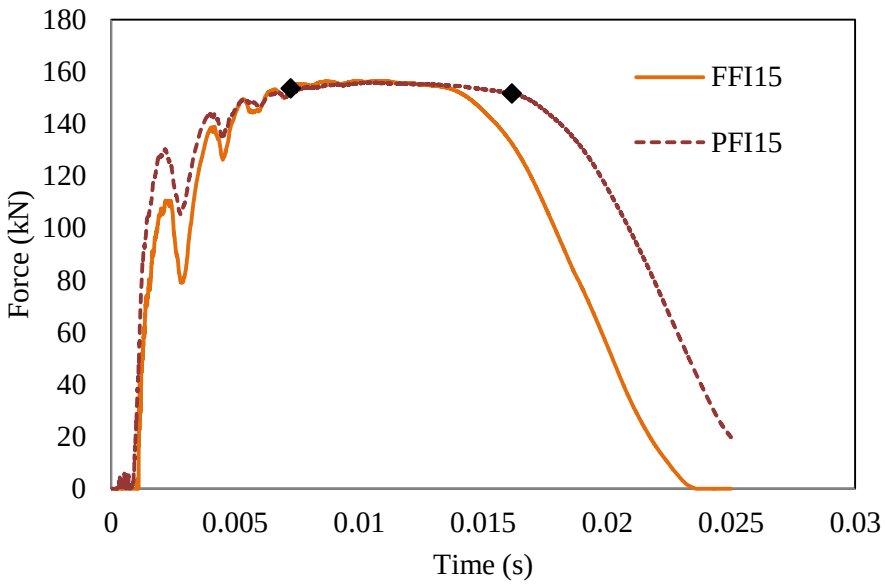

Figure 6.29. Internal tensile force time histories of the first bolt row of specimens with thick plate connected to steel columns under impact load.

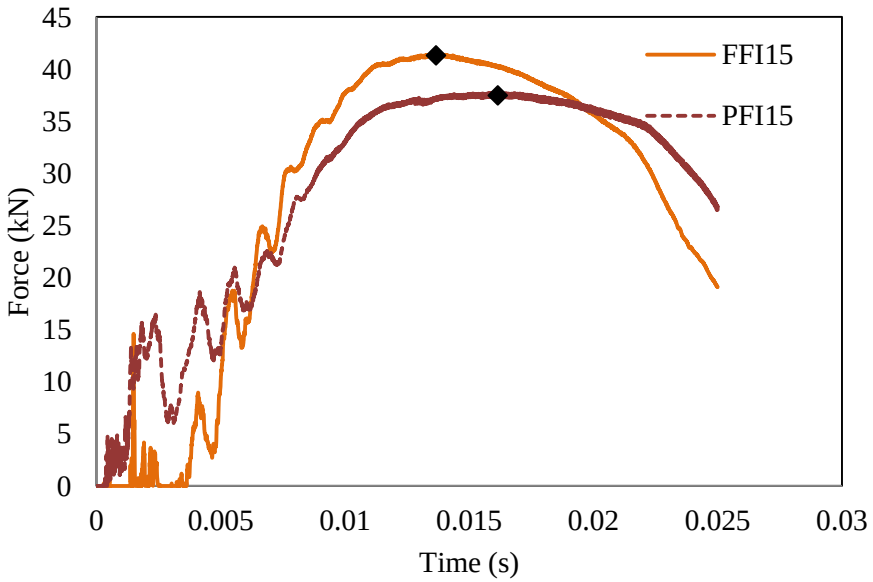

Figure 6.30. Internal tensile force time histories of the second bolt row of specimens with thick plate connected to steel columns under impact load.

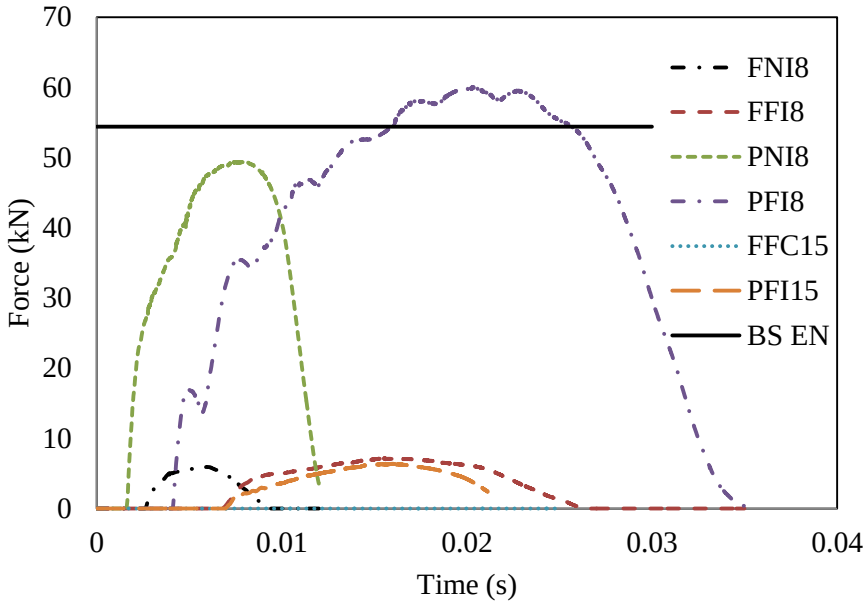

Figure 6.31. Internal bearing force time histories of the first bolt row of specimens connected to steel column using ordinary bolts under impact load.

6.2.3.2 Internal axial resistance of connections

The axial capacity of the joint plays a very important role in the progressive collapse failure, which is referred in Eurocode as a tying force [7]. Hence, a section was made in the beam near the joint using "free body cut" command available in ABAQUS, as shown in Figure 6.32, and axial force versus time was requested to represent the axial resistance of the connection. Figure 6.33 shows the axial resistance versus time curves for specimens with a thin plate tested under impact load. It can be seen that the connection axial force loaded at L_1 started with a considerable negative value of about 50 kN. In this short period of time, the column tried to push the beam upward, creating downward (negative) reaction which is opposite to the situation under quasi-static load. In order to prove this, a beam translation was tracked in y-axis using FE model with a large deformation scale factor of 10, to that the upward translation of the beam was observed during that period. Moreover, disregarding the negative peaks of those specimens it shows that FPC specimens need a shorter time to reach their peak force than PDEPC specimens. The specimens loaded far away from the joint seem having more vibration than other ones loaded near the joint (L_2), as can be seen in

Figure 6.33, which may be considered as a precaution of the nut loosening that is an unfavourable connection failure.

Again, the numerical results show the similar axial behaviour of FPC connection to that of PDEPC with a thick plate as shown in Figure 6.34. Both types experienced considerable vibration in the onset of the impact event followed by a stable force to the end of the impact event. This may indicate the possibility of occurrence of nut loosening failure during the development of the initial peak force.

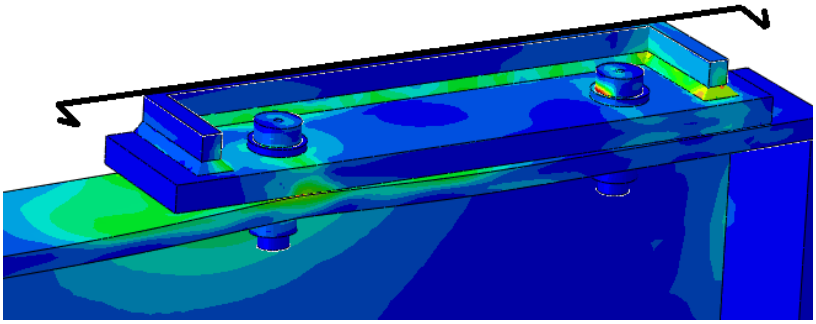

Figure 6.32. Free body cut section

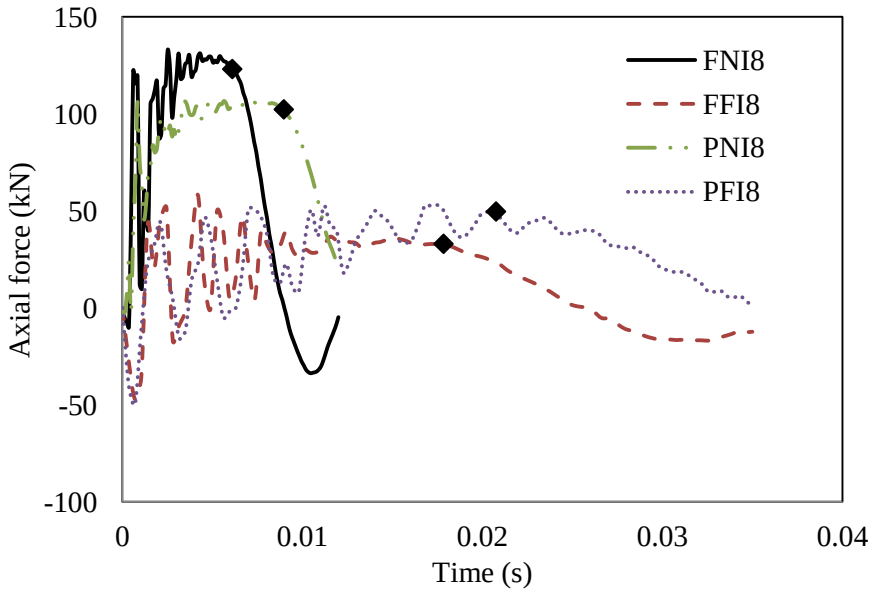

Figure 6.33. Internal axial resistance time histories of the specimens with thin plate connected to steel columns under impact load.

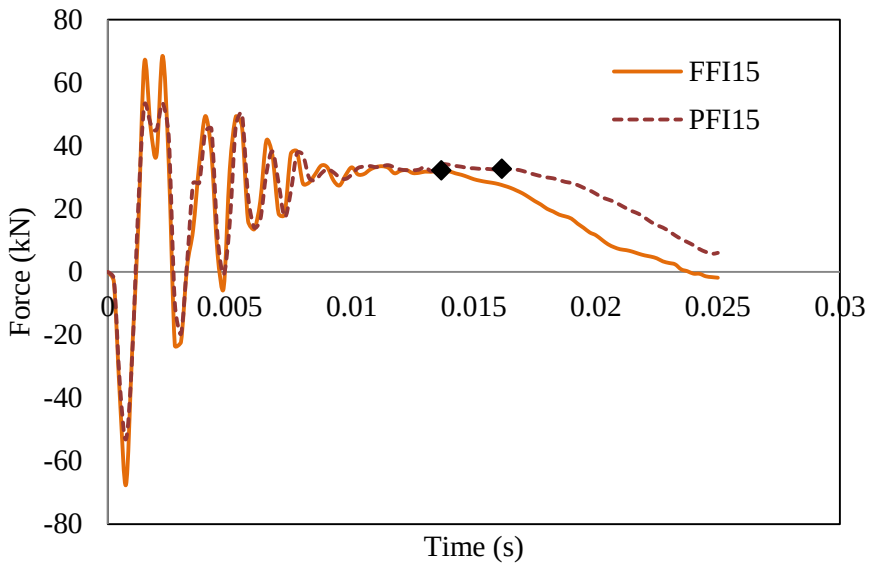

Figure 6.34. Internal axial resistance time histories of the specimens with thick plate connected to steel columns under impact load.

6.2.3.3 Bending moment capacity of connections

Perhaps, there is no concern about the integrity and robustness of a structural frame having connections with full strength moment resistance. Hence, it was suggested to use them to improve the structural robustness of building frames subjected to terrorist explosion attack in the US [126]. However, using simple connections may raise the possibility of local failure followed by progressive collapse. Therefore, it would be beneficial to investigate the internal moment capacity under impact and static loads to have a deep insight into the structural behaviour. The "Free body cut" command was used again in the same section that was used to investigate the internal axial force to examine the internal moment resistance of the connection under both load regimes. Figure 6.35 shows the internal moment versus time curves of the specimens with a thin plate tested under lateral impact load. As expected, PDEPC demonstrated a lower moment resistance than FPC in both loading points. For a fair comparison between the moment resistances of the connections, the maximum displacement at the free end of FPC was used here as a bench mark. The comparison showed that specimens FFI8 and PFI8 have an internal moment resistance of 39.27 kN.m and 15.79 kN.m, respectively at a displacement of 60.2 mm (at time = 0.0179 s). In other words, the

internal moment resistance of PDEPC was about 40% of that of FPC when loaded at L_1, while this ratio decreased to 25% for specimens loaded at L_2. Moreover, it can be seen that both the connection types reach the peak moment faster as the loading point is moving towards joint. Therefore, the specimens loaded close to the joint required less than 1 ms to reach its peak moment resistance, while more than 5 ms was needed for others loaded far away from the connection.

The internal moment resistance of specimens with a thick plate under lateral impact load were also examined as can be seen in Figure 6.36. Both connection types demonstrated similar moment time history trend but with higher moment resistance for FPC. At the maximum displacement, the moment resistance of the FPC and PDEPC were 31.97 and 19.95 kN.m, respectively.

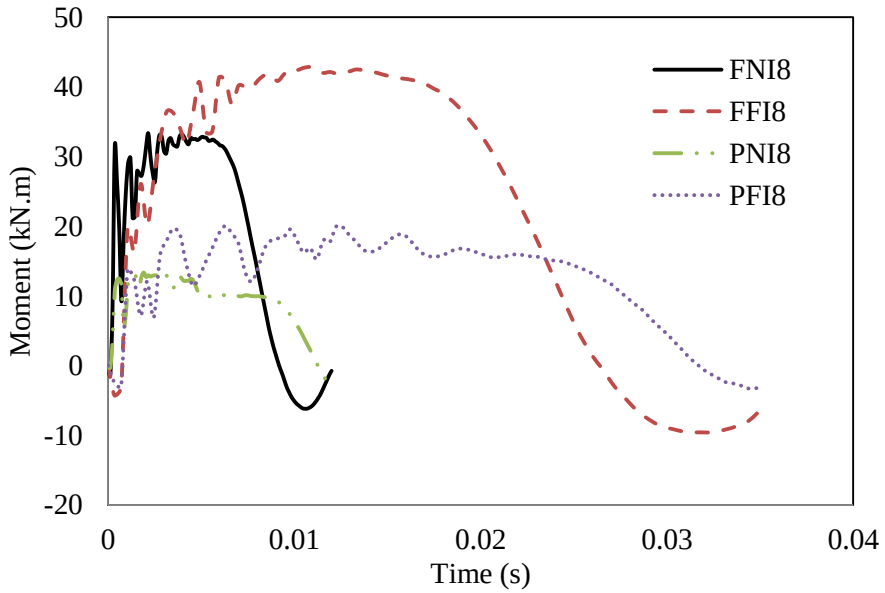

Figure 6.35. Internal moment resistance time histories of the specimens with thin plate connected to steel columns under impact load

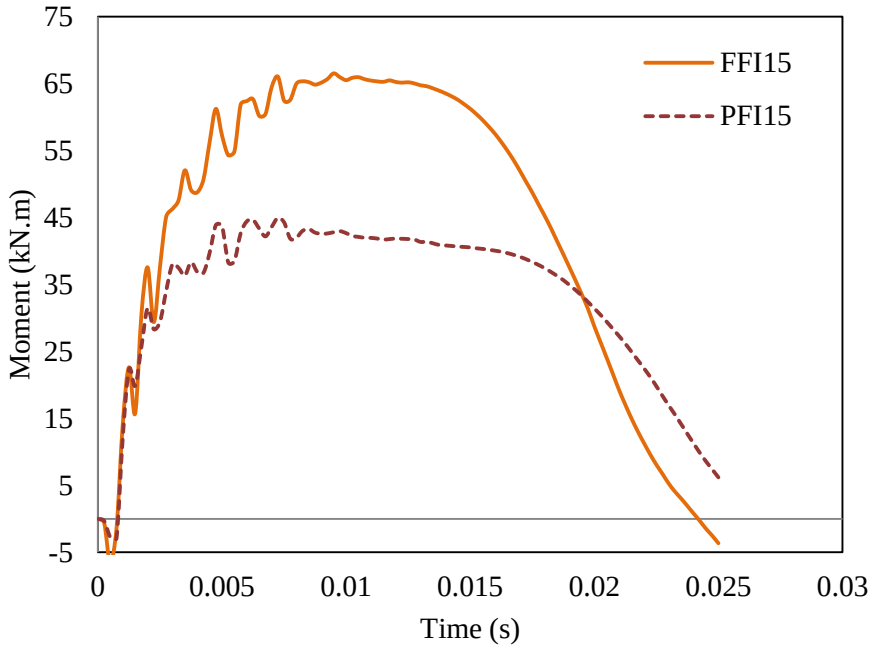

Figure 6.36. Internal moment resistance time histories of the specimens with thick plate connected to steel columns under impact load.

6.2.4 Dynamic increase factors (DIFs) based on internal forces

In chapter four, the experimental force-displacement traces were used to propose dynamic increase factor (DIF) based on the energy principles. The results showed that the DIF varies between 1.25 to 1.38 for all specimens tested. In this section, the validated FE models were used to propose DIFs based on the internal forces. This can be achieved by comparing the internal forces obtained under quasi-static and impact loading. The internal forces under impact loading were presented and discussed before in Section 6.2.1.3. Similar procedure to that used to obtain these internal forces under an impact load was used to obtain the internal forces under a quasi-static load. Table 2 shows comparisons of the extreme values of the main components in the connection that affect the connection response under quasi static and impact loads. Clearly, all the static results demonstrate the lower extremes than the impact results in different levels. The first bolt row in all specimens shows a small difference in DIF, with a range of 1.17 to 1.21 being recorded. On the other hand, the second bolt row demonstrates the lower dynamic effect than the first row in a range of 1.02 to 1.16. The DIFs predicted for the axial connection resistance were identified for FPC to be 1.03 and 1.12 for

specimens loaded at L_2 and L_1, respectively. However, these factors increased from 1.15 to 1.36 in PDEPC specimens. Hence, the axial capacity of moment resistance connections loaded close to the connection seems to be less affected dynamically than those loaded far away. PDEPCs exhibited the similar trend of the DIF for both loading locations but 20 % higher than those of the moment resisting connection. Regarding the internal moment resistance, PDEPC demonstrated higher DIFs than those of FPC, particularly if the load applied far away from the connection. Then a considerable reduction from 1.45 to 1.22 (about 16 %) was produced if FPC replaced by PDEPC for specimen loaded far away the connection. Here, a difference of about 2% could be noticed if the load applied near the connection for both types of connection. This could be attributed to the higher moment resistance of FPCs than those of PDENCs, which are not designed to resist bending moment. However, it could be said that PDEPCs showed a good impact moment resistance, although they are not designed to resist bending moment.

Table 6.1. Summary of extreme internal forces under impact and quasi-static loads of connections and proposed DIFs.

Specimen	Static tensile force in first bolt row (kN)	Impact tensile force in first bolt row (kN)	DIF- 1st bolt row	Static tensile force in second bolt row (kN)	Impact tensile force in second bolt row (kN)	DIF - 2nd bolt row	Static axial resistance (kN)	Impact axial resistance (kN)	DIF-axial resistance	Static moment resistance (kN.m)	Impact moment resistance (kN.m)	DIF – moment resistance
FNI8	109.40	132.84	1.21	68.05	79.21	1.16	128.76	133.08	1.03	23.94	33.35	1.39
FFI8	109.10	130.03	1.19	63.32	69.65	1.10	50.26	58.03	1.15	34.87	42.86	1.22
PNI8	82.47	96.64	1.17	56.60	62.12	1.10	95.27	107.50	1.12	9.49	13.51	1.42
PFI8	81.03	97.85	1.21	46.12	47.13	1.02	39.12	53.01	1.36	13.79	20.05	1.45

6.2.5 Strain-rate distribution

Strain rate is defined as the change in strain of a material with respect a time. To obtain more knowledge on the strain rate distribution, the strain time histories were requested at the elements in the connection that experienced large deformations such as the end plate and the first bolt. The scalar variable SDEG available in ABAQUS was used to specify the elements that initiate the damage degradation earlier. The places selected to investigate the strain rate distribution in this study are shown in

Figure 6.37 as P1, P2, P3 and P4. Figure 6.38 shows the average strain rate in these points. To compare strain rate on the plate of both types of connections, P1 could be compared with P2 and P3. Hence, it could be noticed that the strain rate of the specimen PNI8 was 32.39 s^{-1}, while it was 15.31 s^{-1} in P2 and 18.15 s^{-1} in P3 in the specimen FNI8. In other words, PDEPC experienced a higher strain rate of about two times of FPC if the load was located near the connection. Also, the similar trend could be identified if the specimens loaded far away from the connection. This could be attributed to the higher deformation that PDEPC exhibited at a specific time if compared with FPC as the latter is stiffer than the former. The specimens with a thick plate demonstrated a lower strain rate than those with a thin plate in P1, P2 and P3. However, the thin plate would gain higher strength magnification due to the effect of strain rate than the thick plate.

P4 could be used to compare the strain rate at the critical point on the first bolt. It is clear that specimens loaded near the connection experienced a higher strain rate than those loaded far away from the connection. For instance, the first bolt of the specimen FNI8 experienced a strain rate of 12.54 s^{-1}, while it was 3.92 s^{-1} in specimen FFI8. This is because the first bolt of the specimens loaded near the connection needs less time than those loaded far away to reach its maximum force, as shown in. Again, lower strain rate is produced in thick plate specimens in P4 than those with thin plate, which makes the bolts with the less enhanced strength due to strain rate effect, then to accelerate the fracture of the bolt prior to the yielding of the end plate.

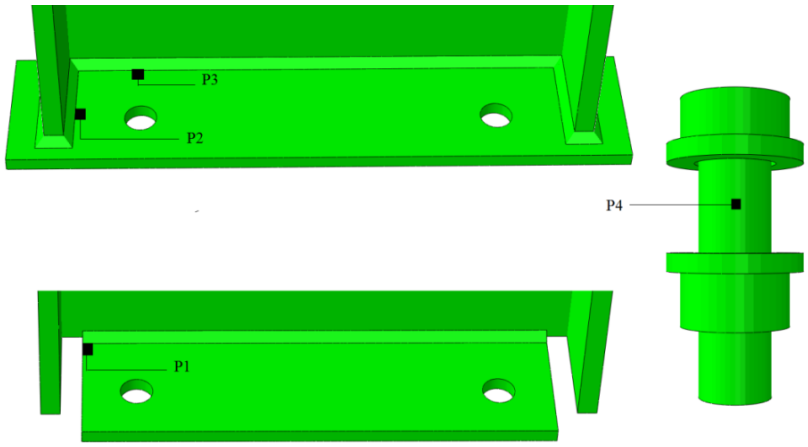

Figure 6.37. The locations of critical places selected to investigate the effect of strain rate.

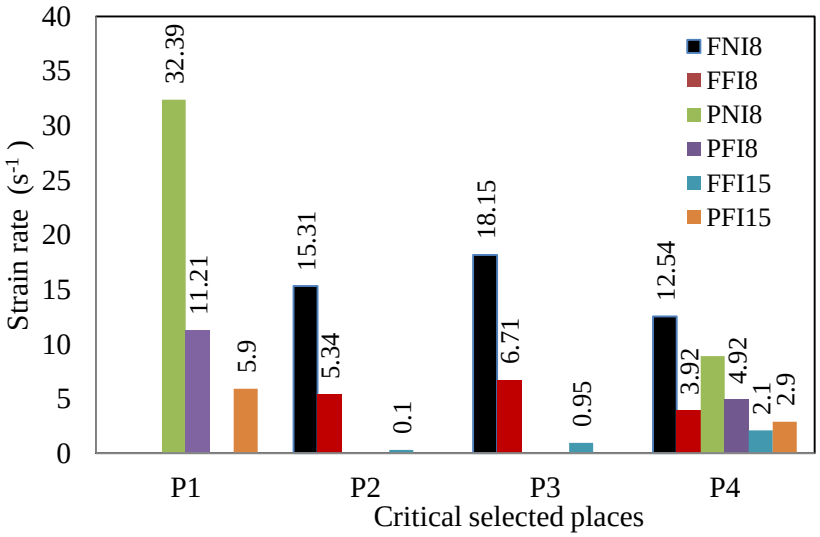

Figure 6.38. Average strain rate distribution at the selected critical places

6.2.6 Energy dissipation

One of the important properties of a structure subjected to dynamic load is the ability to absorb energy. In order to investigate the energy absorption, the validated FE models were employed to request the time history of plastic dissipated energy for each component involved in the connection. It was found that most of the energy (about more than 90% of the total plastic dissipated energy) was dissipated in the end plate and steel column. Hence, the energy dissipation of these components is discussed here only. Figure 6.39 shows the dissipated energy by the steel column and the end plate separately for all specimens tested. It

can be seen that specimens with a thin end plate demonstrates a higher dissipated energy than those with a thick plate. In PDEPCs, reducing the end plate thickness from 15 to 8 mm increased the energy dissipation by 88%, while the energy dissipated in FPCs with 15 mm end plate thickness is almost non-existed if compared with that with 8 mm. This is attributed to the lower plastic deformation that the thick plate experienced, compared with the thin plate for both connection types as discussed in Section 2.4.1. The lower amount of energy dissipated by the thick plate was transferred to be dissipated by the steel column. Hence, more energy was dissipated by the steel column of the specimens with thick plate than those with thin plate. In FPCs the energy dissipation in the steel column was increased by 314% if the plate thickness was increased from 8mm to 15mm while the energy dissipation increased by 40% in PDEPC. Therefore, using a thick plate enhances the connection capacity by dissipating more energy in the steel column. This, in turn, will reduce the capacity of the steel column, which may raise the possibility of the column failure due to prevention of the connection from deforming in a ductile manner, and therefore, increasing the possibility of column removal scenario, which will lead to the progressive collapse.

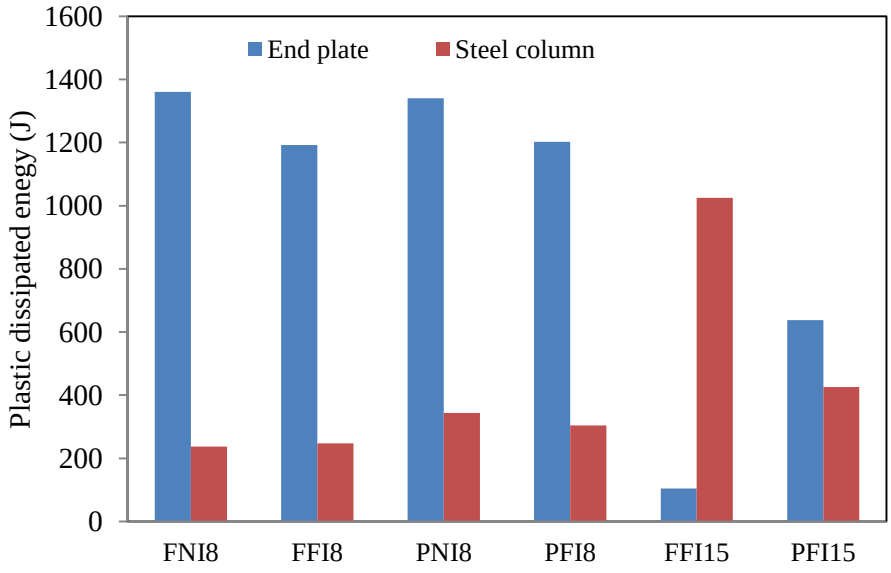

Figure 6.39. Plastic energy dissipation of connection components.

6.2.7 Parametric study

After verifying the reliability of the proposed ABAQUS models in predicting the response of beam-to-column connections under lateral impact load, a series of parametric studies was carried out to explore the structural behaviour of such connections with extended parameter variations, both within and outside the range of experiments. Despite the fact that experimental investigations are more reliable and very important for engineering research, they are expensive, time consuming and sometimes difficult to carry out. Comparatively, the numerical analysis is more affordable and allows the experimental investigation to include a wide range of parameters. In the previous sections of this chapter, the validity of the proposed FE models was verified through comparisons with experimental results. The models were found to be able to accurately predict the force-displacement traces and the failure modes as observed in the experiments. In this section, a series of extensive parametric studies is carried out to investigate the effect of several geometrical and material parameters on the lateral impact response of end plate beam-to-column connections and produce a comprehensive database in addition to that obtained from the experiments.

6.2.7.1 Effect of mass and velocity

A drop hammer of a mass of 107.5 kg with an initial velocity of 7.5 m/s was used to apply constant impact energy of 3023 J on the specimens tested. Under this impact energy, the connections showed good level of plastic deformation particularly specimens tested with thin plate. The impact energy is directly related to the impact velocity and the mass of drop weight and can be computed as follows:

$$E = \frac{1}{2} mv^2 \qquad (6.1)$$

where, m and v are the mass of the drop weight and the impact velocity, respectively. Three numerical tests with similar impact energy but with different masses and velocities for each connection type were examined. Table 6.2 shows the details of these numerical tests with a summary of their numerical results, which were obtained from their force-displacement traces in Figure 6.40 and Figure 6.41. The numerical results show that increasing the mass

with decreasing the impact velocity lead to decrease the initial peak force and increase the maximum displacement and corresponding time. This indicates that the connection has a better capacity to resist an impact with a higher velocity and a heavier mass as a lower maximum displacement is corresponded. The reason may be attributed to strain rate effect, that is, a higher impact velocity causes higher strain rate, which increases the material strength. The plateau stage seems to be longer and more stable in specimens impacted with lower mass and higher velocity, as can be seen in Figure 6.40 and Figure 6.41.

Table 6.2. Summary of details and results of both connections with different masses and impact velocities.

Designation	Connection type	Mass (kg)	Velocity (m/s)	Impact energy (J)	Initial peak force (kN)	Maximum displacement (mm)	Time at maximum displacement (ms)
A1	FPC	60.5	10	3025	388	57.16	13.0
A2	FPC	107.5	7.5	3023	317	59.96	16.2
A3	FPC	672	3	3024	251	65.01	36.7
A4	PDEPC	60.5	10	3025	349	79.65	18.5
A5	PDEPC	107.5	7.5	3023	360	79.20	21.2
A6	PDEPC	672	3	3024	235	90.50	52.5

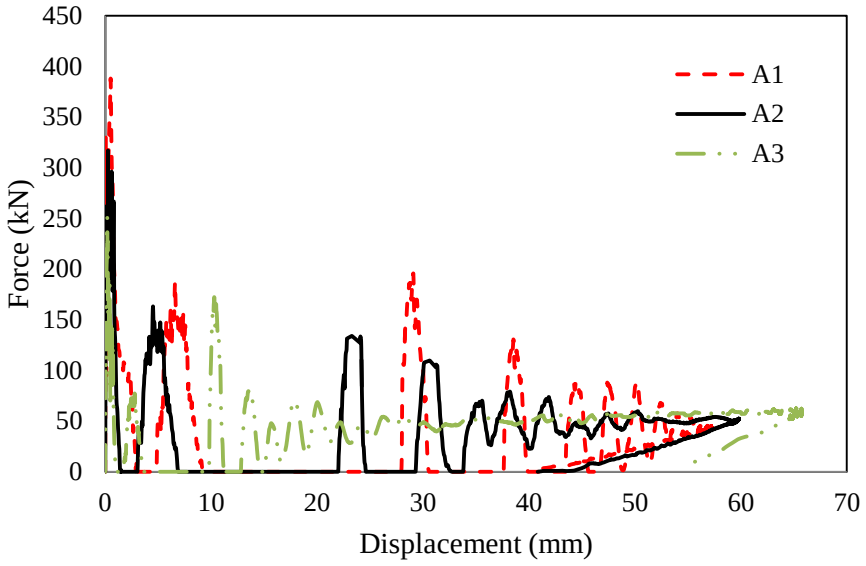

Figure 6.40. Force-displacement traces of FPC with different masses and impact velocities.

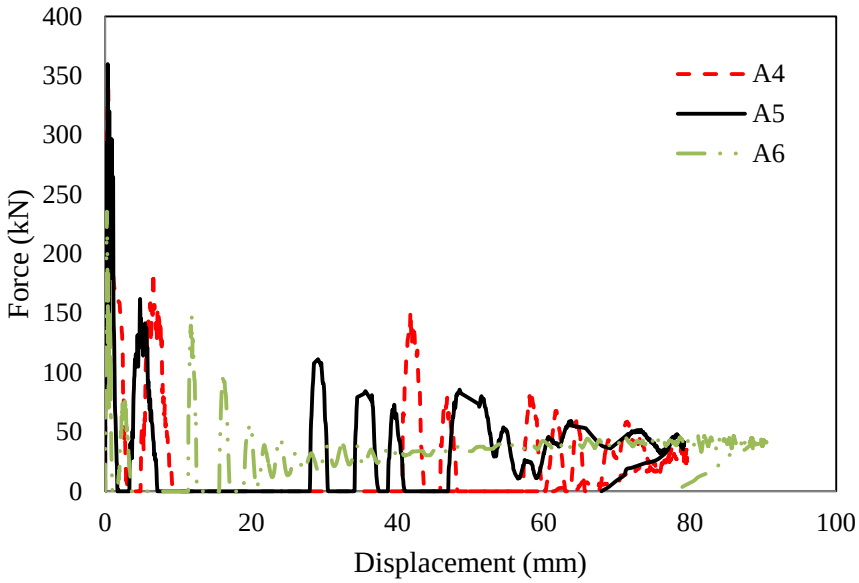

Figure 6.41. Force-displacement traces of PDEPC with different masses and impact velocities.

6.2.7.2 Effect of Projectile shapes

Limited research work has been conducted to investigate the response of composite structures under low velocity impact considering the effect of projectile shapes [127, 128]. They reported that the different projectile shapes have great effects on damage mechanisms. Also, it was concluded that the projectile with a larger contact surface produced higher stresses and a shorter contact time duration. The recommendation practice DNV-RP-C204 [129] also mentioned that both the impact force and deformation increase with increasing the contact area. To date, no literature review is available on the effect of the projectile configuration on the impact response of beam-to-column connections. Hence, it will be beneficial to exploit the validated models to predict the effect of different projectile shapes on the dynamic response of connections. In addition to the flat projectile that used in the experiments, spherical and cylindrical projectiles were also examined for a selected specimen (PFI8), as can be seen in Figure 6.42. Figure 6.43 shows the force-displacement traces related to different projectile configurations. It can be seen that the flat projectile produces higher contact forces in all three stages of the impact event and lower maximum displacement than the other configurations. However, the maximum displacement was

measured at the centre of the contact area of the projectile. Therefore, the maximum displacements of both spherical and cylindrical projectile are equal to the corresponding maximum displacement of the struck column. Also, a gap was generated between the centre of contact surface of the flat projectile and the struck column at which a difference in the maximum displacement of the projectile and the struck column was produced. Therefore, the maximum displacement of the struck column underneath the centre of the projectile contact surface can be used to ensure a fair comparison amongst the three projectile configurations. The results show that the projectile shape has a negligible effect on the maximum displacement as can be seen in Figure 6.44. The numerical results show also that the internal forces in the bolts were not influenced by changing the projectile shape as shown in Figure 6.45. Besides, similar deformation modes were obtained in the connection for different projectile configurations corresponding to higher localised deformation in the struck column underneath the spherical projectile if compared with flat and cylindrical projectile. Therefore, the model shows that the energy dissipated in the column impacted with the spherical projectile is 23% and 41% higher than those impacted with cylindrical and flat, respectively.

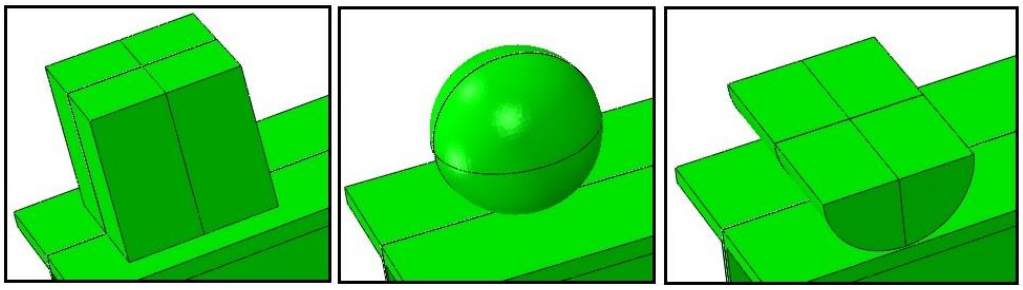

(a) Flat projectile (b) Spherical projectile (c) Cylindrical projectile

Figure 6.42. Projectile configurations used in the parametric study.

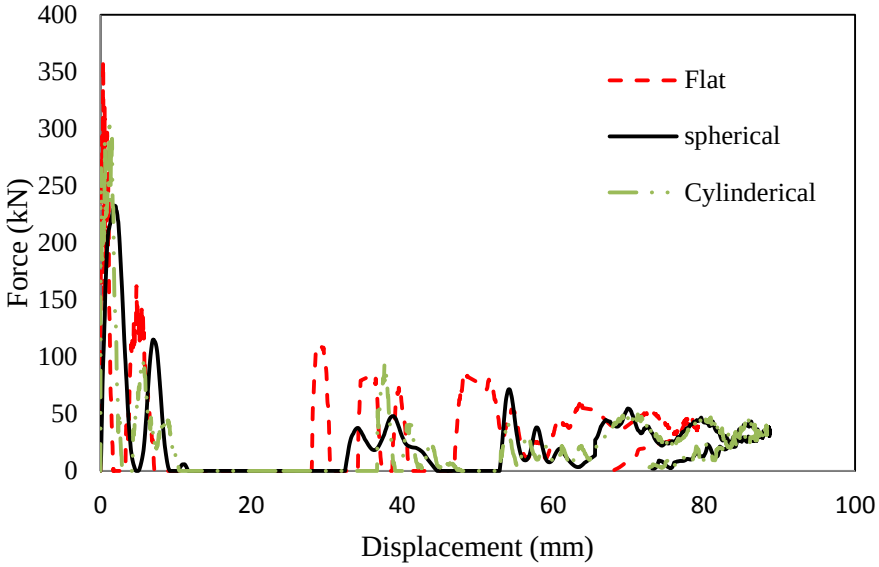

Figure 6.43. Effect of projectile shape on force-displacement traces.

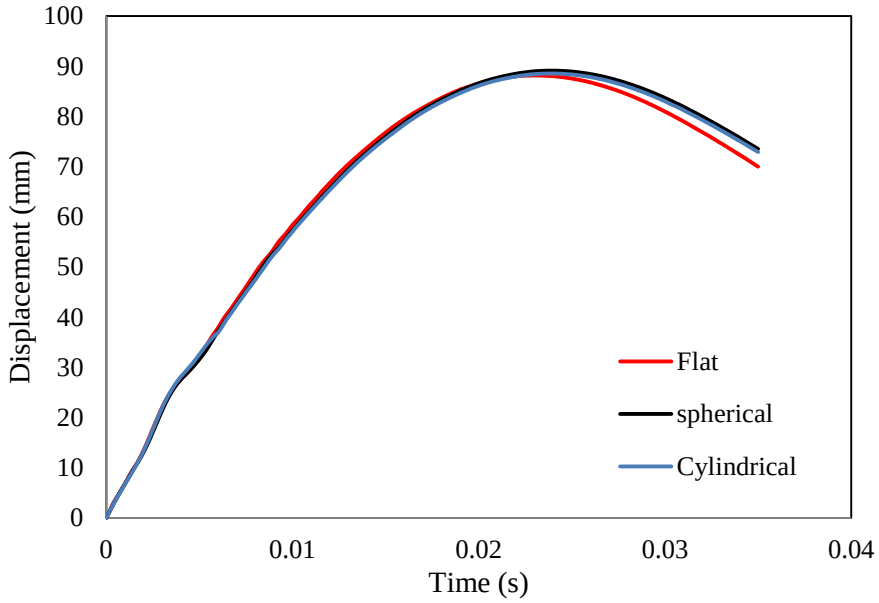

Figure 6.44. Displacement time histories for a selected specimen (PFI8) with different projectile configurations.

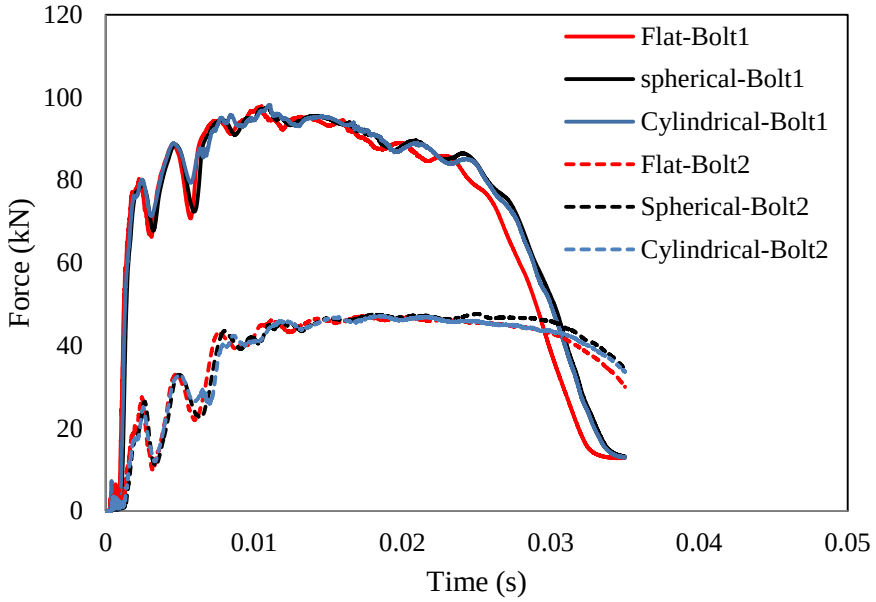

Figure 6.45. Effects of projectile shape on the internal forces of bolts.

6.2.7.3 Effect of number of bolts

The number of bolts may be increased to enhance the shear, bending and tying capacity of a beam-to-column connection in structural frames. All experiments were carried out using four bolts with two rows. The validated models are employed here to investigate the connection response with six bolts to be compared then with that with four bolts. Hence, two clearance holes were generated in the end plate and top flange of column for both types of connection in the centre of the distance between the existed two bolt rows and a centre bolt row is added, as shown in Figure 6.46. The simulation results showed that the maximum displacement decreased by 9.3 and 13.4 % for PDEPC and FPC, respectively, if the bolts number increased from four to six. Conversely, the time corresponding to the maximum displacement decreased by 6.2 and 14.9 % in PDEPC and FPC, respectively. The numerical results showed that the maximum damage parameter in the tearing area closed to the weld toe did not exceed 20% of that for PDEPC with three bolt rows. Meanwhile, the elements in this area were totally removed from the model as the damage parameter reach to its maximum value of 1, which indicates the propagating of the tearing failure, as can be seen in Figure 6.47. Hence, the deformation mode was not influenced significantly by increasing the number of bolts but it helps with delay the tearing failure close to the weld toe. The centre

bolt row that added between the existed two bolt pairs restricted the bending of the end plate leading to minimize the prying failure of the plate. The internal bolt forces were also examined and the numerical results showed that adding the centre bolt row did not contribute to decrease the maximum tensile force produced in the first bolt by more than 2.2 % for both connection types. However, the maximum impact force produced in the second bolt decreased by about 26 and 50 % in FPC and PDEPC, respectively. In other words, the first bolt might still exhibit a fracture even with increasing the number of bolts.

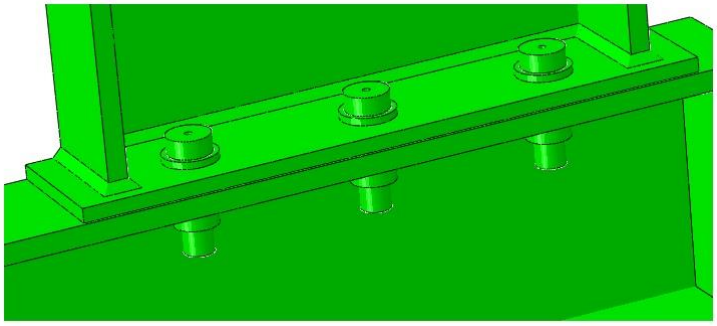

Figure 6.46. Three bolts configurations adopted to predict the effect of increasing number of bolts on the lateral impact response of connection.

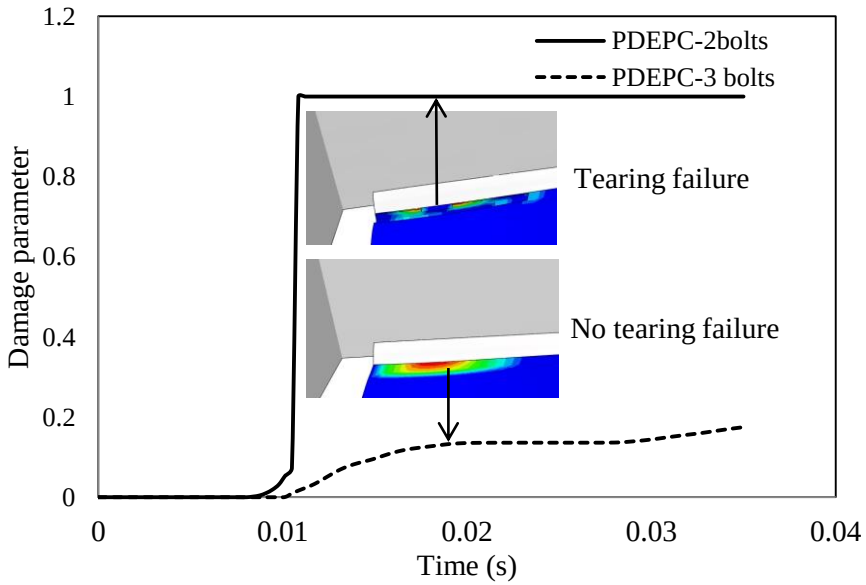

Figure 6.47. Effect of increasing number of bolts on tearing failure in PDEPC.

6.2.7.4 Prediction of lateral impact response of the extended end plate connections

The flush plate can be extended from one or two of its edges to form a connection called the extended end plate connection (EEPC), which has a higher moment resistance than the flush plate connection. However, the modelling of the extended end plate can be performed using the same procedure (including material properties and geometry) used to model flush plate connections but with extend the length of flush plate and adding a bolt row in the extension zone, as can be seen in Figure 6.48. Similar loading and boundary conditions that used in the flush plate modelling are used here, i.e. 107.5 kg dropped mass, 7.5 m/s impact velocity, fixed support on beam and roller supports on the column. The predicted failure demonstrated plastic prying deformations on the extended end plate, as can be seen in Figure 6.49 (a). Also, the failure mode did not change if the impact velocity raised from 7.5 to 9 m/s, as can be seen in Figure 6.49 (b).

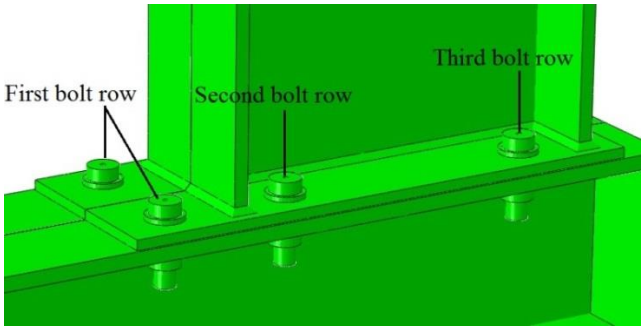

Figure 6.48. Extended end plate connection geometry with three bolt rows.

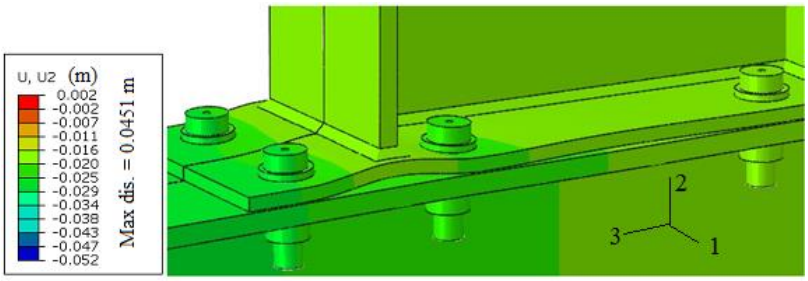

(a) Impact velocity = 7.5 m/s

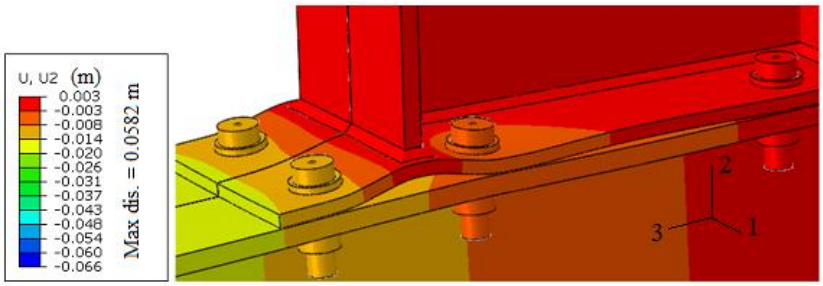

(b) Impact velocity = 9 m/s

Figure 6.49. Predicted failure mode of extended end plate under lateral impact load.

Figure 6.50 shows the force-displacement traces obtained from the numerical models for EEPC with 7.5 and 9 m/s impact velocity. Increasing the impact velocity from 7.5 to 9 m/s leads to slightly increase the initial peak force by 3.4%, but corresponding to significant increase in the maximum displacement by 28.3%. The similar trend of the force-displacement traces was obtained here, compared with that obtained in FPC, as all the three loading stages and intermittent impact can be seen. Full range analysis was performed to predict the internal tensile forces produced in the three bolts rows of EEPC. As can be seen in Figure 6.51, the similar trend of the force-time history was obtained for the three bolt rows if the impact velocity raised from 7.5 to 9 m/s. With the selected end plate thickness (8 mm), the maximum tensile force occurred in the second bolt row after significant yielding of the end plate. Hence, the fracture is expected to occur in the second bolt row first. This behaviour seems to be reasonable as the calculation procedure following Eurocode 3 [130] provides the prediction that the combined end plate yielding and bolt fracture gives the lowest resistance for the second bolt row when using 8 mm end plates.

Figure 6.52 shows the predicted internal moment resistance time histories of different connection configurations including PDEPC, FPC and EEPC. As EEPC is classified as a full strength moment resistance connection, it demonstrates the higher moment resistance compared with PDEPC and FPC.

The internal moment resistance of EEPC exceeded that of FPC with three bolts by 32.5 %. In spite of this considerable increase in the moment resistance, a small difference in the energy

dissipation of end plate was obtained in the numerical results amongst connection types examined as can be seen in Figure 6.53.

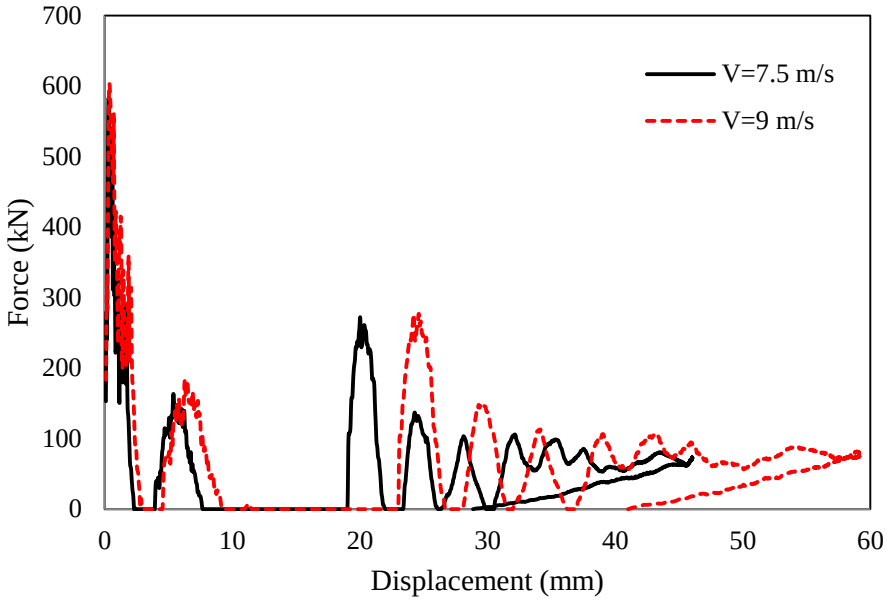

Figure 6.50. Predicted force-displacement traces of EEPC with different impact velocities.

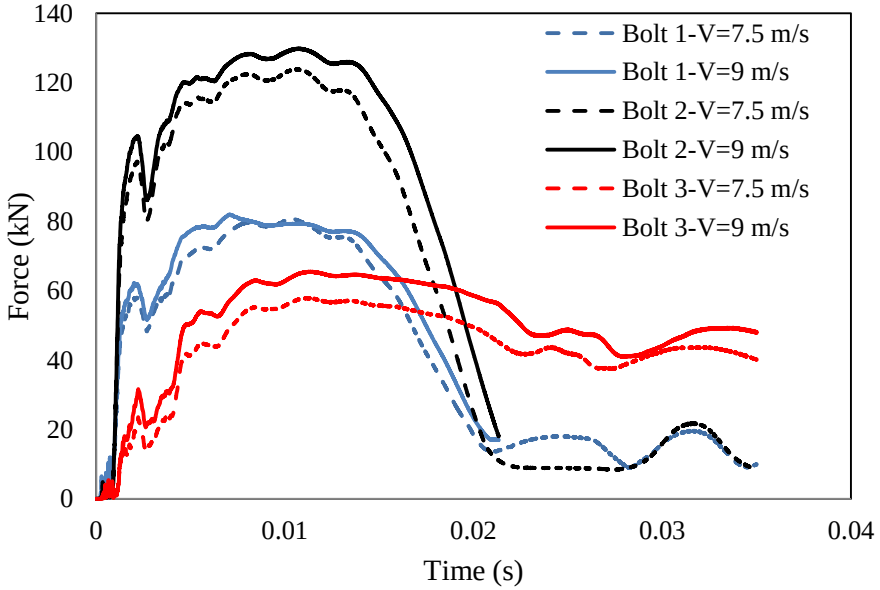

Figure 6.51. Predicted internal forces produced in the bolts of EEPC under lateral impact load.

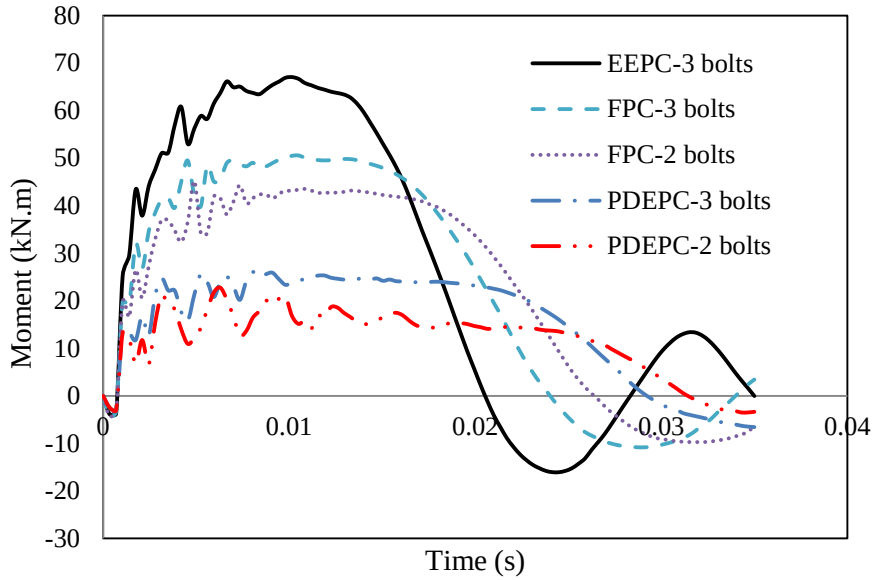

Figure 6.52. Predicted internal moment resistance time histories of different connection configurations.

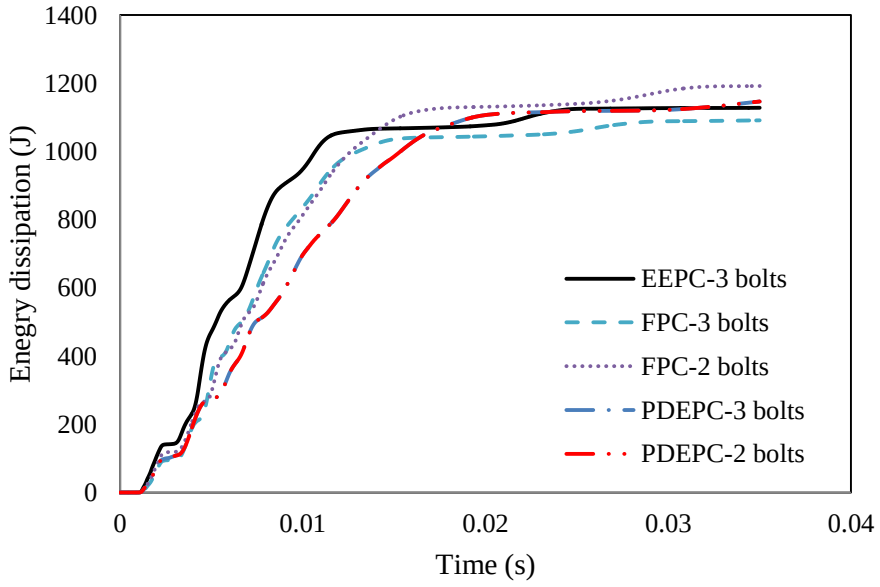

Figure 6.53. Energy dissipation of end plate in different connection configurations.

The extended end plate connection may be stiffened to increase its stiffness and strength and therefore the thinner end plate may be required for the unstiffened one [131]. To investigate the lateral impact response of the stiffened EEPC, a 10 mm thick triangular stiffener having

the similar material properties of the extended end plate is created. It was then connected to both beam flange and the extended end plate using tie constrain, as shown in Figure 6.54. The numerical results showed that the maximum displacement decreased by 13.6 % if EEPC stiffened. Also, the similar failure mode was obtained to that of the unstiffened EEPC but with prying deformations developed underneath the stiffener. This can be seen by comparing failure modes in Figure 6.55 with that of Figure 6.49 (a). The prying deformations developed increase the maximum internal bolt force in the first bolt row by 26.3 %, compared with the unstiffened connection as can be seen in Figure 6.56. In addition, the maximum internal force in the second and third bolt row decreased by 5.2 and 17 %, respectively, if the stiffener is added to the connection.

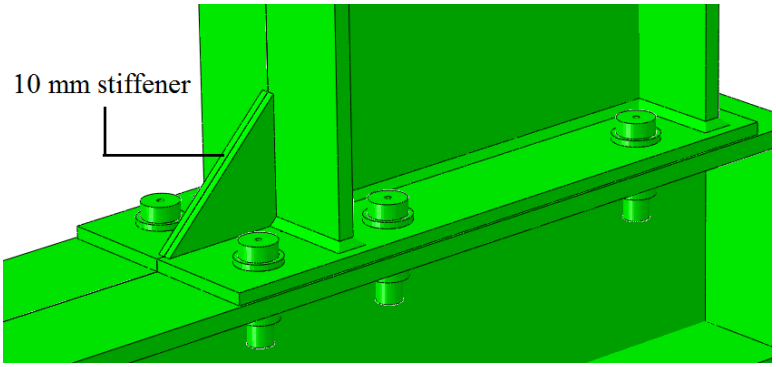

Figure 6.54. Stiffened EEPC configuration.

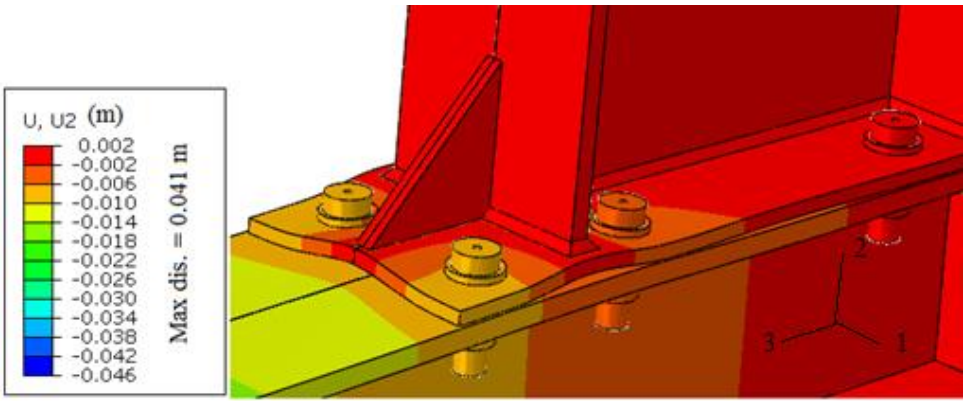

Figure 6.55. Failure mode of stiffened EEPC under lateral impact load.

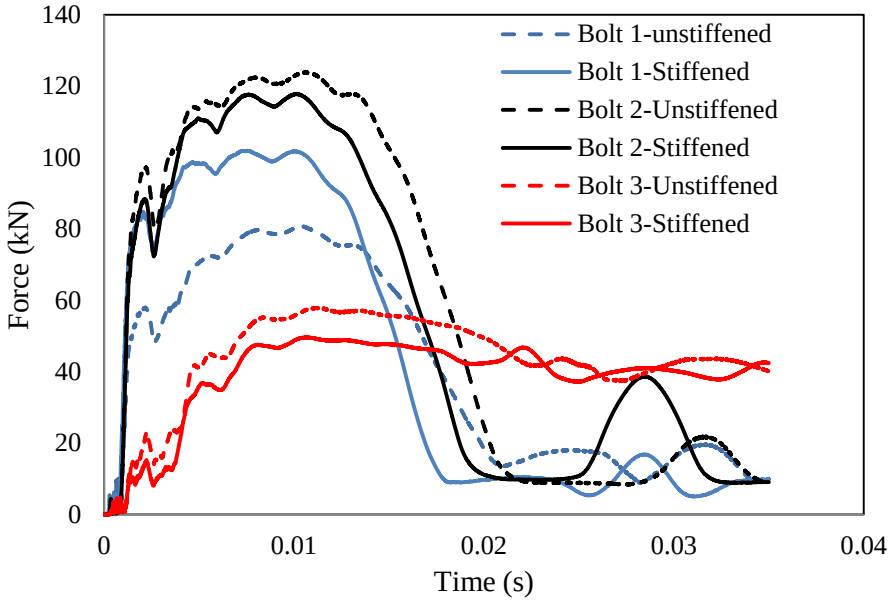

Figure 6.56. Predicted internal forces produced in the bolts of stiffened and unstiffened EEPC under lateral impact load.

6.2.7.5 Effects of boundary conditions

The validated models were employed for investigating the effect of using different boundary conditions on the connection response. In the practical situation, the column is usually connected to both its sides to the beams by appropriate connection. Hence, the symmetry about y-axis of the validated models can be exploited to achieve this task. Figure 6.57 shows the full model of column with two connections to be investigated here. It was started first by applying the impact force with two velocities of 7.5 and 12 m/s to investigate the effect of different boundary conditions on the failure mode of the connection. The numerical results showed that the deformation mode was not influenced by changing the boundary conditions and both end plate yielding and tearing failure were propagated particularly with a velocity of 12 m/s.

Figure 6.58 shows the force-displacement traces of PDEPC for the new boundary conditions adopted with two impact velocities. It can be seen that the intermittent impact still occurred and the plateau stage is almost disappeared. Therefore, the higher portion of energy was dissipated during the propagating of the initial peak force. Whilst, if the column is connected

from one end, the higher energy dissipation occurred in the plateau stage. It is important to remind that these results were obtained assuming no nut loosening failure, which might occur here, particularly with the higher energy dissipated corresponding to relatively small displacements at a short time.

The internal forces were also requested to investigate the effect of using different boundary conditions on the connection response. Figure 6.59 shows the internal time histories of the first bolt row. It is clear that the internal forces started to propagate approximately in the same way for both the boundary conditions, but it degraded faster if the column was connected from its both ends. This is attributed to the absence of the plateau stage, which in turn reduces the time of impact event. The second bolt row of both connections seems to have a different response if the column is connected to both its ends as it reaches its maximum force faster than that if connected to one end as can be seen in Figure 6.60. Also, the maximum internal force was generated in the second bolt of PDEPC if the column connected from both its ends was higher than that if the column was connected to one end by about 36 %. Moreover, the higher internal force similar to the aforementioned percentage is generated in the second bolt row of FPC, if the column is connected to one end compared with that of two connections.

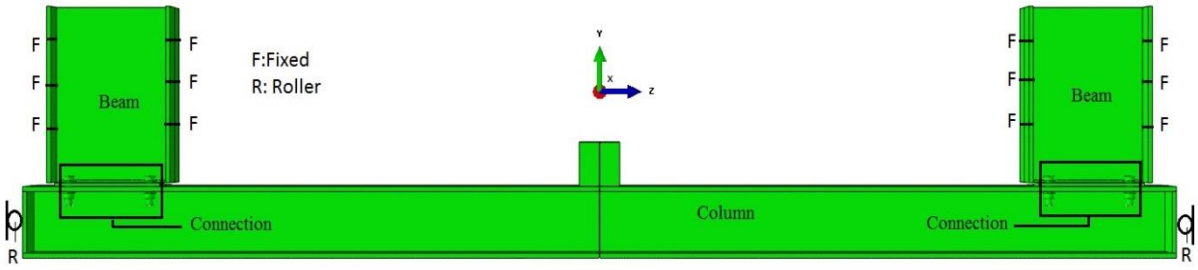

Figure 6.57. Model geometry adopted to investigate the effect of boundary conditions.

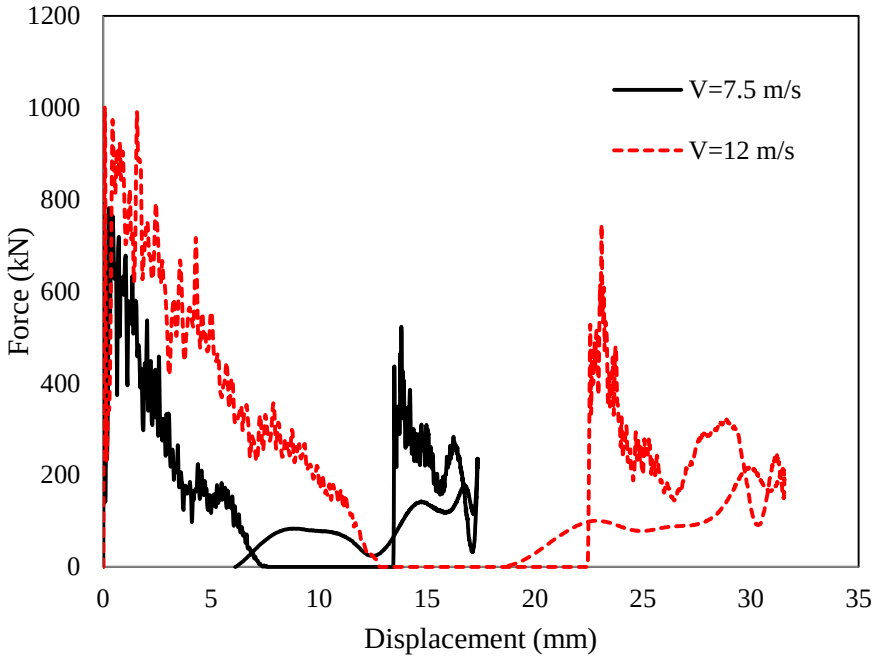

Figure 6.58. Predicted force-displacement traces of a steel column connected from its both end and impacted in the middle by a flat projectile with different velocities.

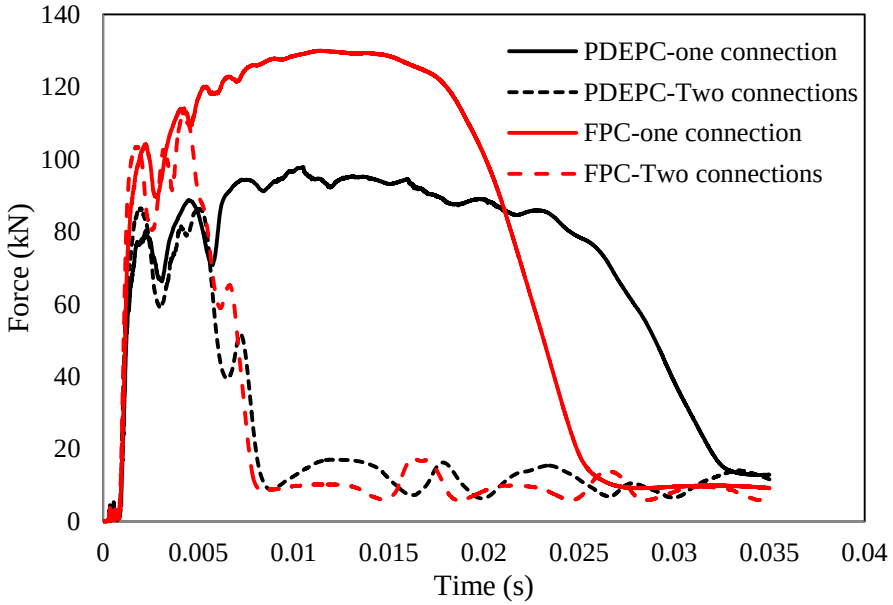

Figure 6.59. Predicted internal force time histories of first bolt row for PDEPC and FPC with different boundary conditions.

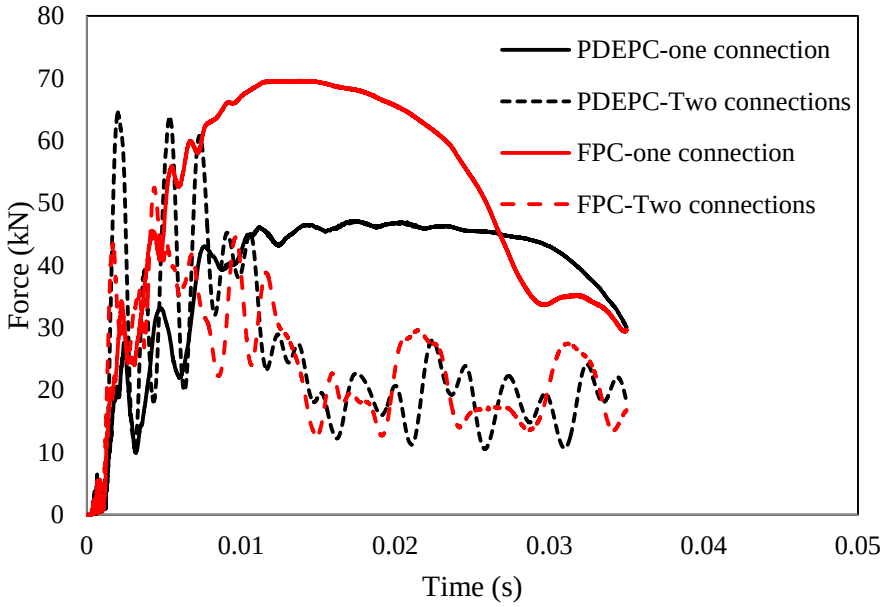

Figure 6.60. Predicted internal force time histories of second bolt row for PDEPC and FPC with different boundary conditions.

6.3 Modelling outcomes of end plate connections to CFST columns

Finite element models using ABAQUS/Explicit were developed to simulate the response of beam-to-CFST column connections using the long bolt technique under lateral impact. The geometric, loading and boundary conditions adopted in the simulation were similar to those used experimentally. The validation of the FE models is presented here against the experimental results. As one of the objectives of this thesis is to evaluate the efficiency of using the long bolt technique with an end plate to connect CFST column with steel beam, the validation process is followed by presenting a comparison study between the long bolt technique and standard connections.

6.3.1 Validation of numerical results against experimental results

The test results were used to verify the FE models in terms of failure modes, load-displacement curves and strain time histories as presented in the following sub-sections.

6.3.1.1 Validation of deformation modes

Figure 6.61 to Figure 6.68 show a comparison between the predicted and observed deformation modes of specimens tested. The model is able to predict bearing deformation of the first bolt row due to the excessive prying action of the end plate as can be seen in Figure 6.61. Also, very good correlation was obtained between the simulation and the observed plastic prying deformation of the end plate in both types of connections as shown in Figure 6.62 and Figure 6.63. The model captures the tearing failure produced in PDEPC in terms of the length and depth of the crack of tearing as shown in Figure 6.64. The damage properties of the steel defined in this study seems reasonable. If ignore such the definition the model tends to give a stiffer prediction after the onset of damage by changing its path to the dashed curve as explain before in Section 5.2.4.1. The failed elements that supposed to be removed from the model remained to be loaded, producing a stiffer model. As before, very good correlation was obtained between the predicted and observed slight prying deformation of PDEPC with a thick plate as shown in Figure 6.65. Good correlation was obtained between the observed and predicted deformations of FPC specimens with a thick plate. Also, the punching shear deformation in the steel tube around the bottom clearance holes was successfully captured in the simulation as shown in Figure 6.66. Besides, the simulation was capable to capture the deformation mode of FPC with a thick plate as shown in Figure 6.67. The failure mode of concrete infill was also verified against the experimental observations by using the scaler variable (DAMAGET) available in ABAQUS as shown in Figure 6.68. This option was used to evaluate the tensile damage state of each element, indicating a level of the softening phase in the stress-strain curve of the material.

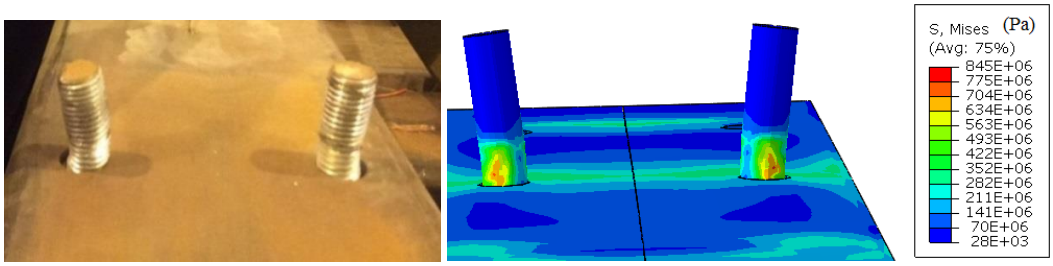

(a) Experimental (b) FE

Figure 6.61. Bearing deformation of first bolt row.

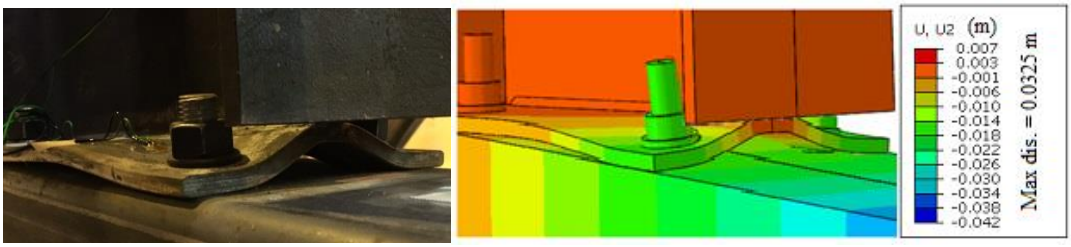

(a) Experimental (b) FE

Figure 6.62. Prying deformation of PDEPC with thin plate.

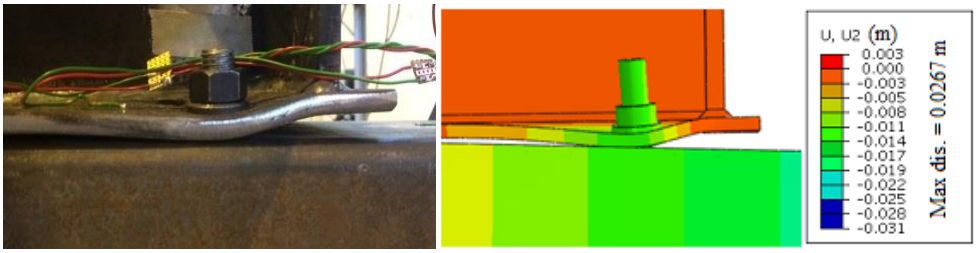

(a) Experimental (b) FE

Figure 6.63. Prying deformation of FPC with thin plate.

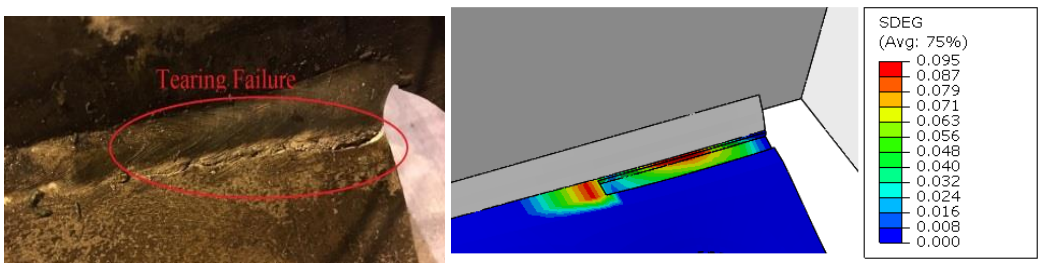

(a) Experimental (b) FE

Figure 6.64. Tearing failure of PDEPC with thin plate.

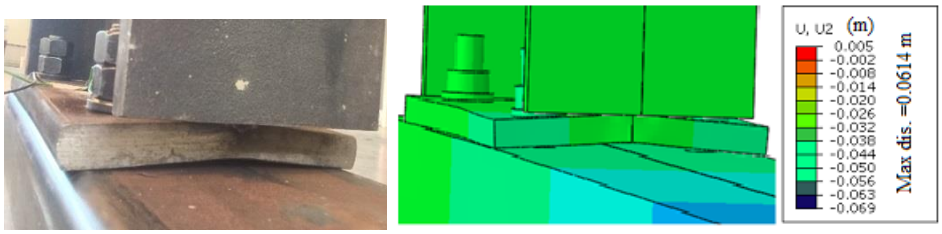

(a) Experimental (b) FE

Figure 6.65. Prying deformation of PDEPC with thick plate.

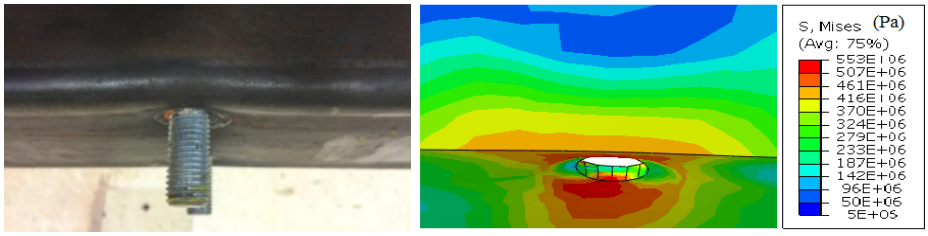

(a) Experimental (b) FE

Figure 6.66. Punching shear of CFST around first bolt row.

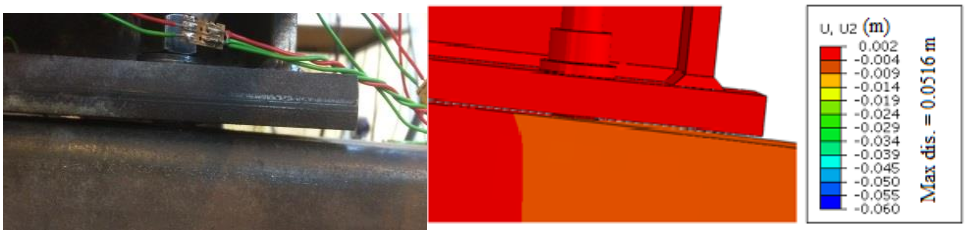

(a) Experimental (b) FE

Figure 6.67. FPC with thick plate after impact event.

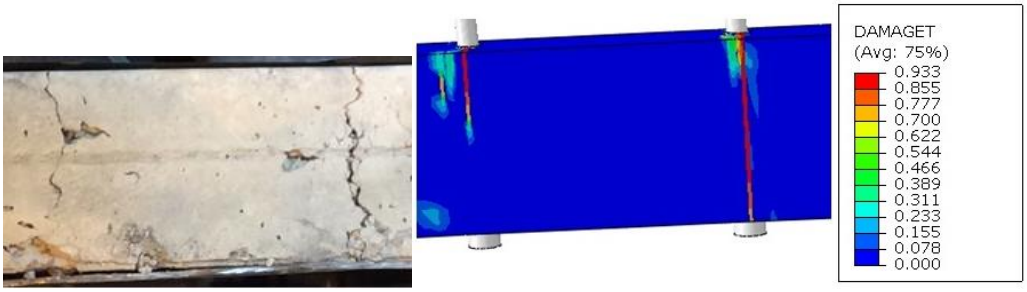

(a) Experimental (b) FE

Figure 6.68. Cracks of concrete infill around long bolts.

6.3.1.2 Validation of force-displacement traces

Figure 6.69 to Figure 6.72 show the validation of the force-displacement traces from the FE models against experimental results. The validation process includes both the load time history and displacement time history first for a specimen. Then, both experimental curves were combined to obtain the related experimental load-displacement curve. Finally, the former curves were compared with those obtained from the FE model. A good agreement is obtained, which indicates the model is capable of predicting all the stages of impact response. Also, the model is able to predict the total displacement at the free end of the column up to the separation point. However, the peak force in the simulation seems increasing faster than that in the test, which may be attributed to the assumption of the rigid projectile that has the much higher contact stiffness than the deformable steel projectile used in the test.

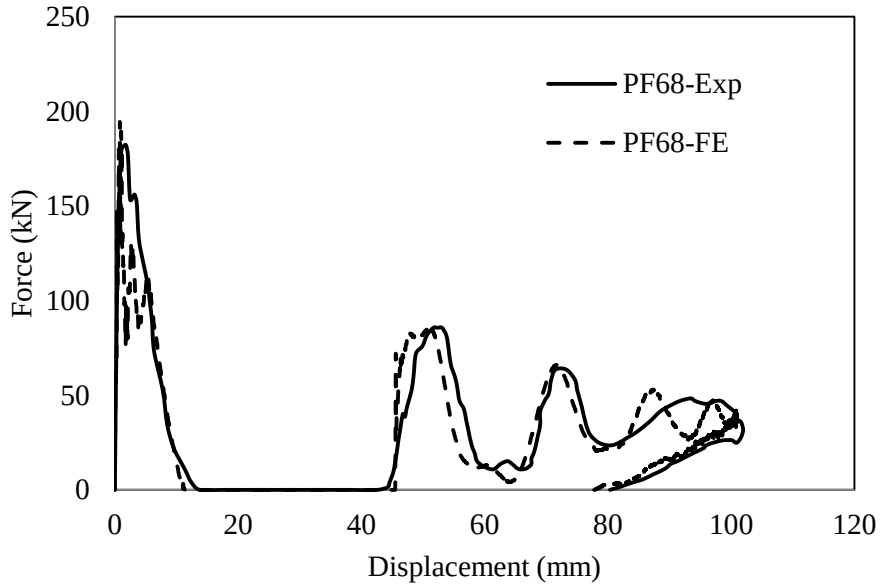

Figure 6.69. Force-displacement traces of specimen PF68 subjected to lateral impact load: comparison of experimental data with FE simulation.

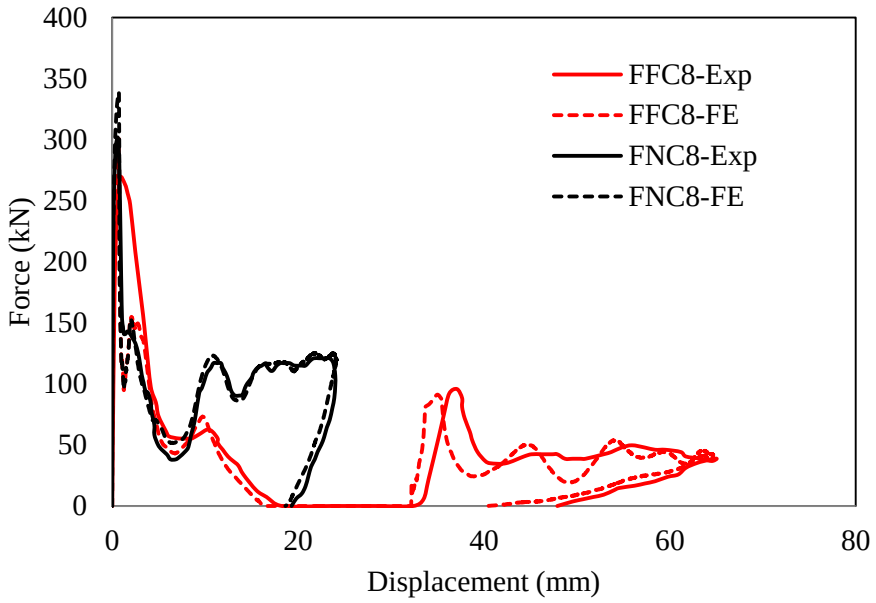

Figure 6.70. Force-displacement traces of specimen FFC8 and FNC8 subjected to lateral impact load: comparison of experimental data with FE simulation.

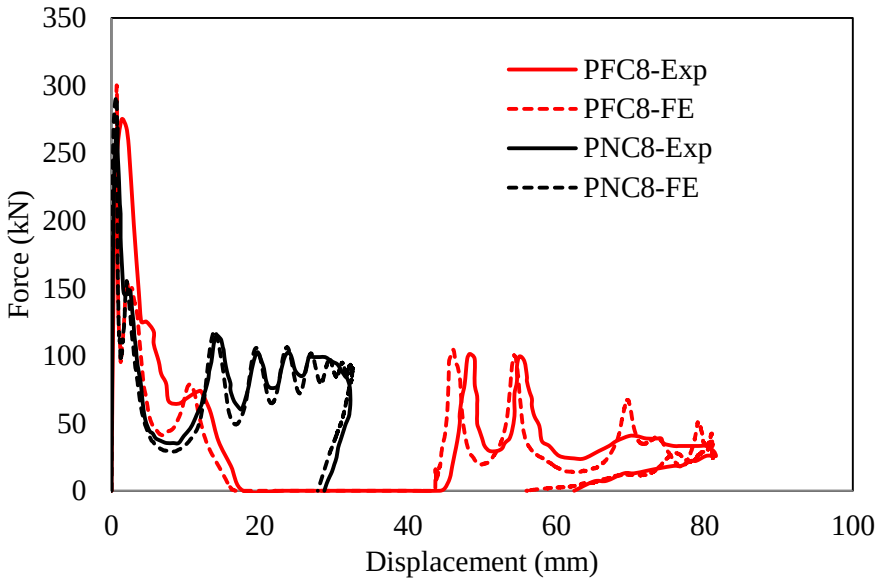

Figure 6.71. Force-displacement traces of specimen PFC8 and PNC8 subjected to lateral impact load: comparison of experimental data with FE simulation.

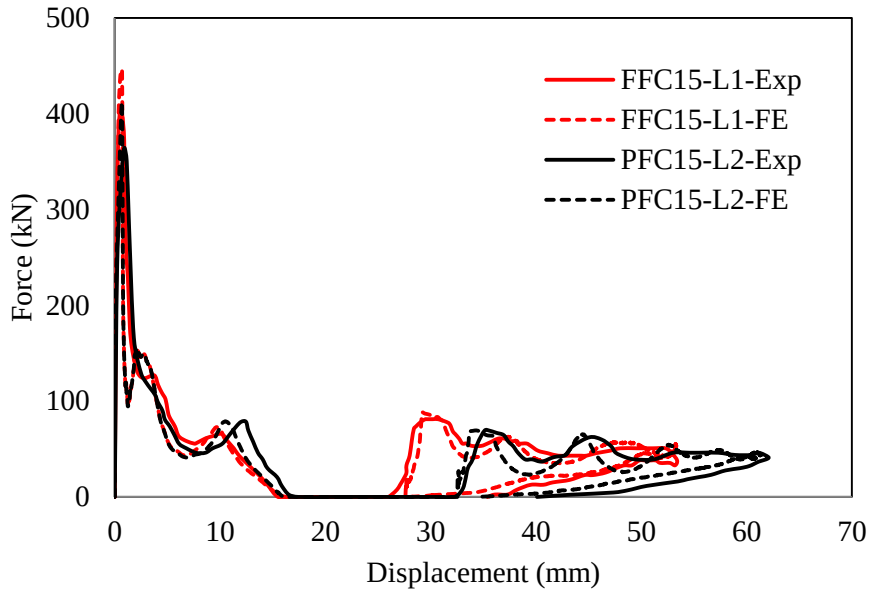

Figure 6.72. Force-displacement traces of specimen FFC15 and PFC15 subjected to lateral impact load: comparison of experimental data with FE simulation.

6.3.1.3 Validation of strain time histories

The strains were measured in four different points in each specimen tested using strain gauges that connected to oscilloscope system as explained in Section 3.4.2.3. Here, the strain time histories in these points obtained from the numerical results are verified against those obtained experimentally. Figure 6.73 to Figure 6.79 show the comparison between the experimental and predicted strain time histories for the specimens tested with CFST columns. In general, good correlation is obtained in terms of the trend of the trace, the maximum strain and the time of impact event. Some discrepancies can be seen in SG2 due to the saturation of the system after 10000 με as explained in Section 3.4.2.3 as can be seen in Figure 6.75 and Figure 6.76 in SG2. Also, it was failed to capture the strains along the entire time duration of the event in both SG1 and SG4 in specimen PNC8 as shown in Figure 6.75 due to some errors in the preparing processes of strain gauges.

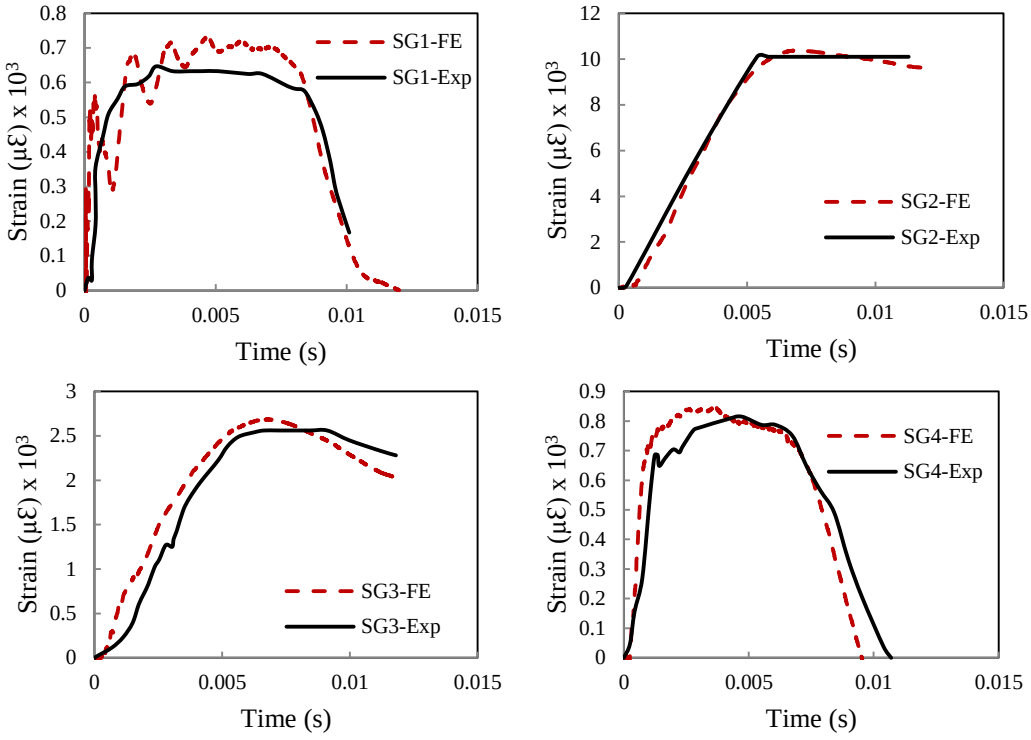

Figure 6.73. Comparison between the experimental and FE results of strain time histories of specimen FNC8.

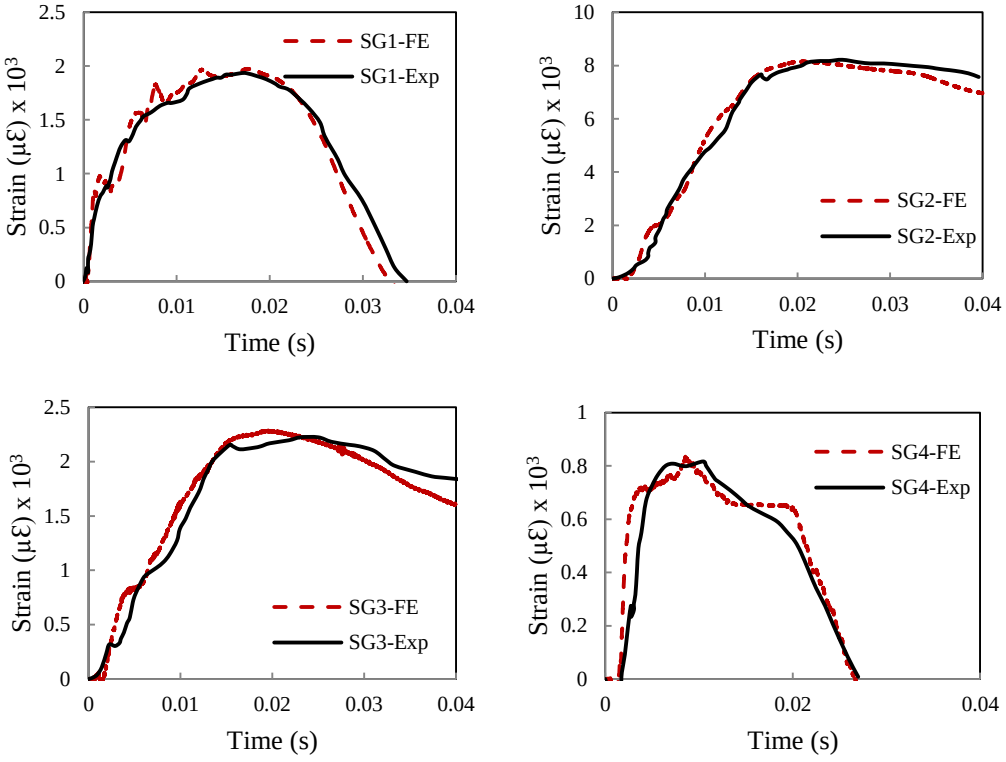

Figure 6.74. Comparison between the experimental and FE results of strain time histories of specimen FFC8

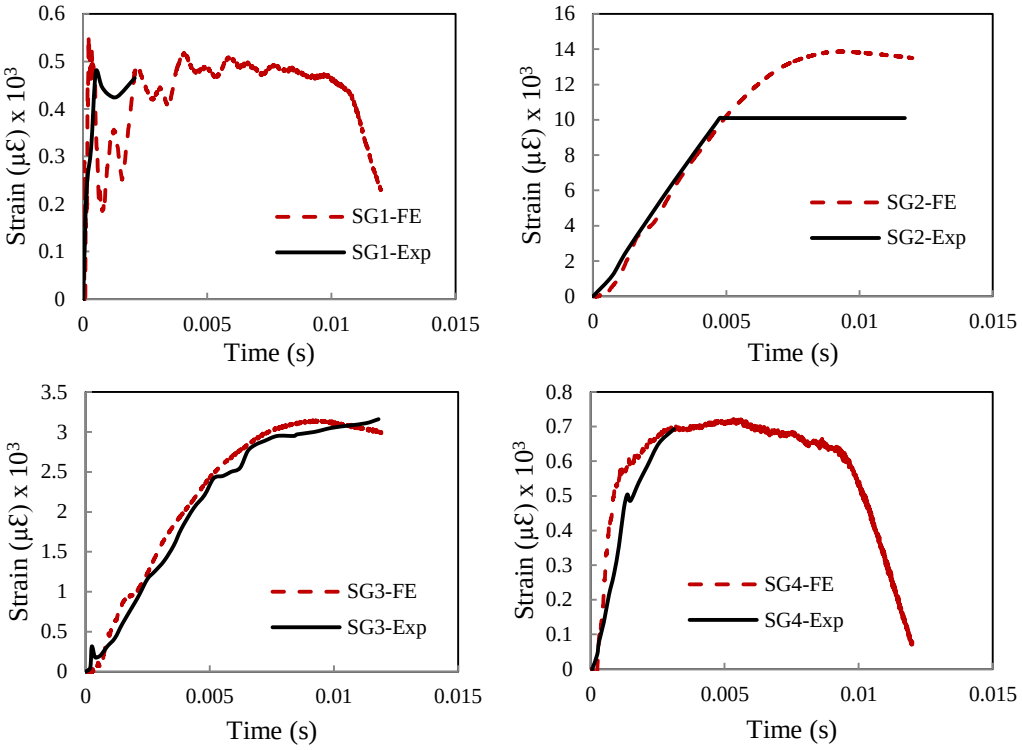

Figure 6.75. Comparison between the experimental and FE results of strain time histories of specimen PNC8.

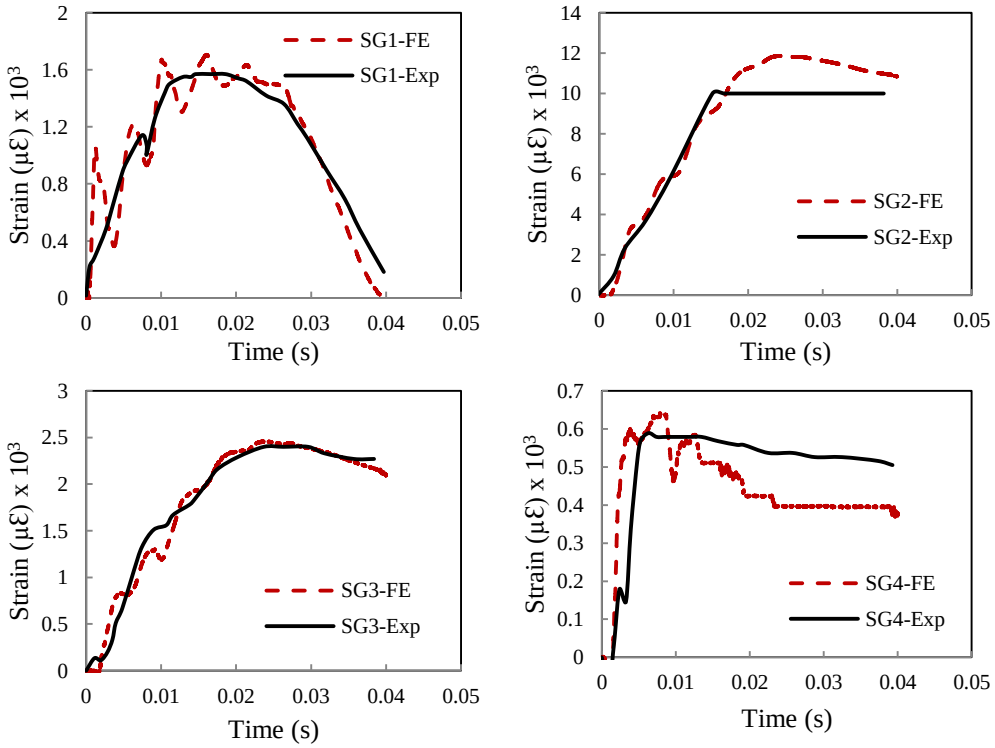

Figure 6.76. Comparison between the experimental and FE results of strain time histories of specimen PFC8.

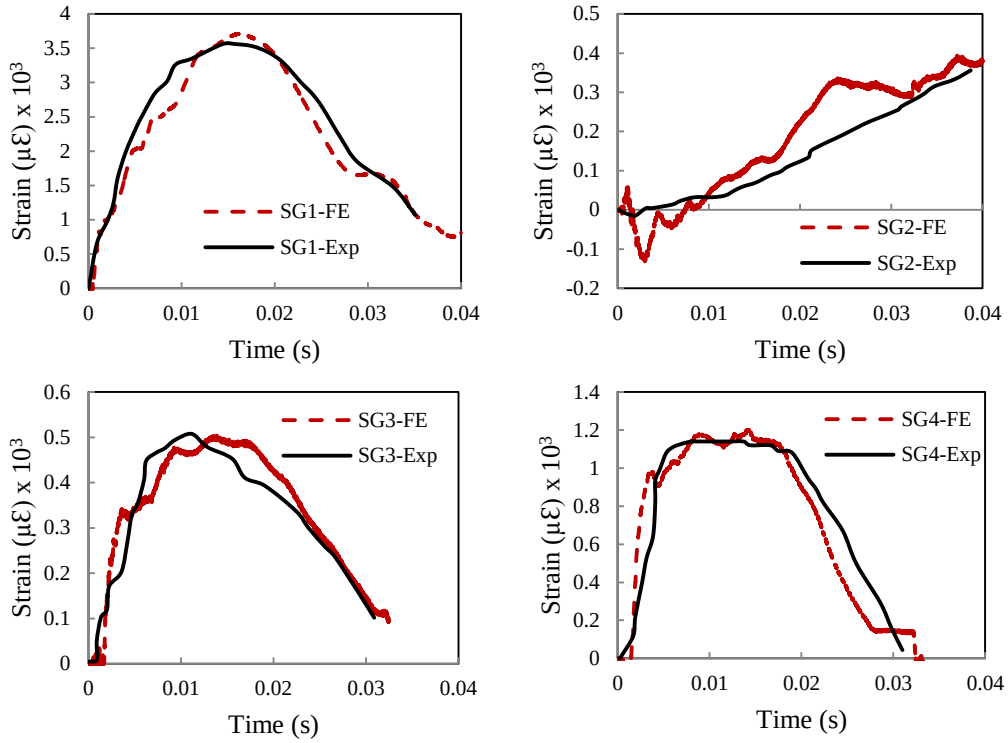

Figure 6.77. Comparison between the experimental and FE results of strain time histories of specimen FFC15.

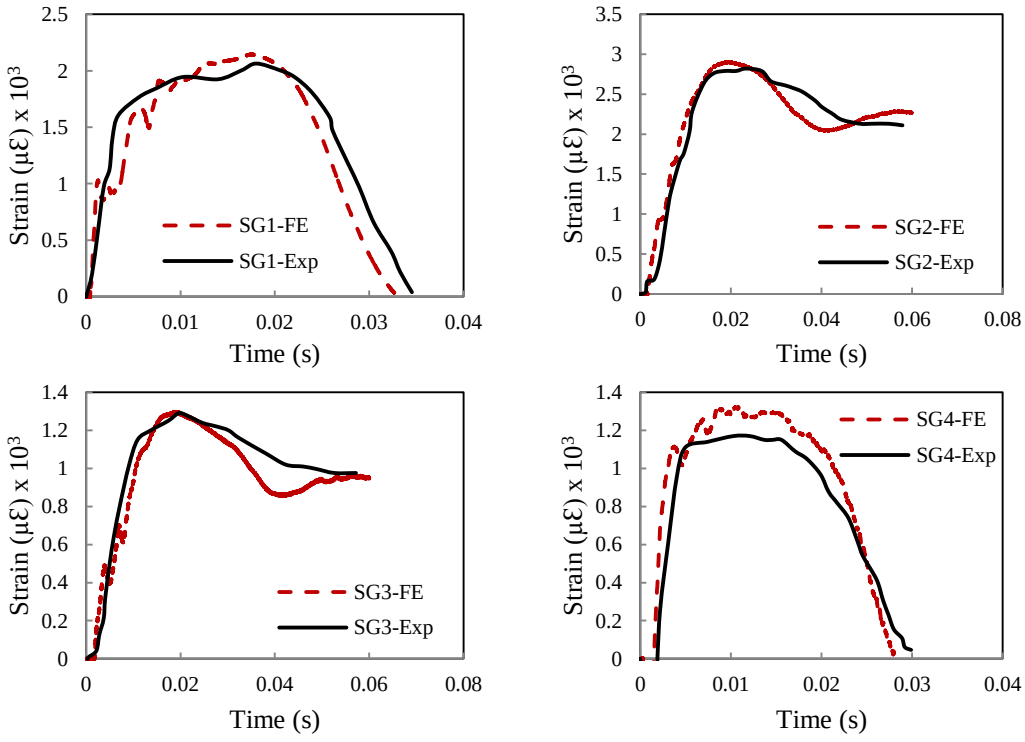

Figure 6.78. Comparison between the experimental and FE results of strain time histories of specimen PFC15.

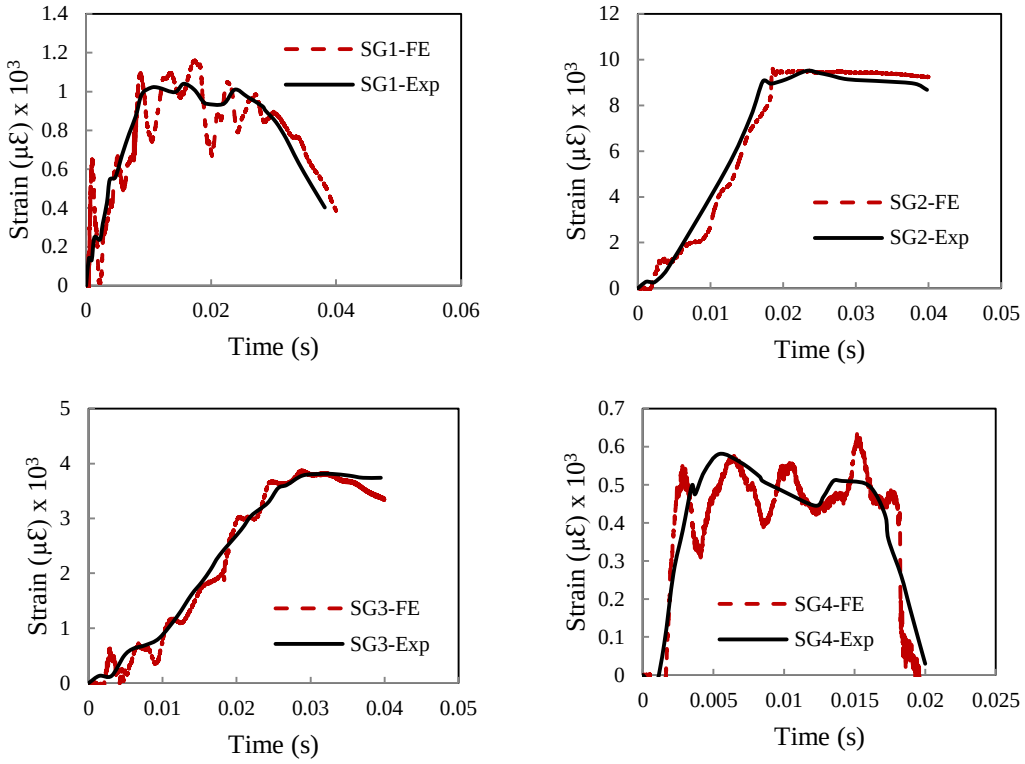

Figure 6.79. Comparison between the experimental and FE results of strain time histories of specimen PF68.

6.3.2 Full range analyses of the structural response

The validated FE models were further used to analyse the full-range response of end plate connections under lateral impact load, including the internal forces in bolts, the axial and moment resistances of the connections investigated. Also, the FE models were used to investigate the energy absorbed by connection components to give a deep understanding on their energy dissipation response.

6.3.2.1 Internal forces of bolts

The internal tensile forces on the bolt were requested in the FE model as explained before in Section 6.2.3.1. Figure 6.80 and Figure 6.81 show the internal tensile force-time histories of the first and second bolt row. Generally, continuous force flow with a few spikes can be seen for all specimens during impact event as obtained in the specimens connected to steel column using ordinary bolts. Also, for specimens connected to CFST columns, the numerical

results showed that the first bolt for all specimens exhibited a faster change in force than the second bolt after the onset of loading. The first bolt row of specimens with a thick plate demonstrated higher peak forces in a shorter time than others, which indicates that the bolt experienced a higher strain rate. This may lead to bolt thread stripping failure which is a type of failure to be avoided in connection. Mouritz [100] showed that failure load of the mild steel bolt thread under impact tension load decreased with increasing strain rate. Also, thread stripping failure was observed in a flash end plate connection subjected to the column removal scenario at which a connection exhibited a combined dynamic bending moment and shear forces [8]. However, this type of failure was not observed in all specimens tested here.

The tension resistance of M16 class 8.8 bolts is 90.4 kN, as recommended by Eurocode 3 [7]. It can be seen in Figure 6.80 that the internal tensile force of the first bolt of four specimens exceeded the recommended design value by the Eurocode. These specimens were the 8 mm flush plate specimens (FNC8 and FFC8) and the specimens with 15 mm end plate (FFC15 and PFC15). Hence, this indicates that the bolt failure may synchronize with plastic deformation on the end plate in the flush plate specimens. Also, it could be said that using a thick plate accelerates the failure of the bolt under tension, leading to a sudden loss of load carrying capacity of the connection. Besides, the specimens with a thick plate demonstrated developing another peak force on the second bolt row after the first peak, as shown in Figure 6.81. It was developed after the struck column started to rebound. In order to justify this, translations of the CFST column and thick plate were tracked in the y-axis using FE model with a deformation scale factor of 10. It was found that the CFST column region underneath the second bolt row tried to push the plate upward with developing a contact force. This could be considered as a caution of vibration that corresponding to using thick end plate, through which the possibility of developing nut loosening failure would be increased.

Figure 6.82 and Figure 6.83 show a comparison between the maximum tensile forces generated in the first and second bolt for the standard bolts (ordinary bolts) and the long

bolts. All the specimens with long bolts demonstrated lower internal tensile forces than the specimens with standard ones by 14.5 to 26.3%. The second bolt also demonstrates lower internal tensile forces but within a range from 0 to 39.5 %. This force alleviation that the long bolt experienced resulted from the higher energy that dissipated in the CFST column compared with steel column. To prove that, the plastic energies dissipated in steel and CFST column were requested from the validated models for selected specimens (FNI8 and FNC8) and compared, as shown in Figure 6.84. It can be seen that the higher energy is dissipated in the CFST column than that dissipated in steel column particularly in the early stage of the impact event. The frictional force between the long bolts and the concrete infill may assist with alleviating the internal tensile force, but the numerical results showed that it has a negligible effect as it represents less than 0.4 % of the maximum internal tensile force.

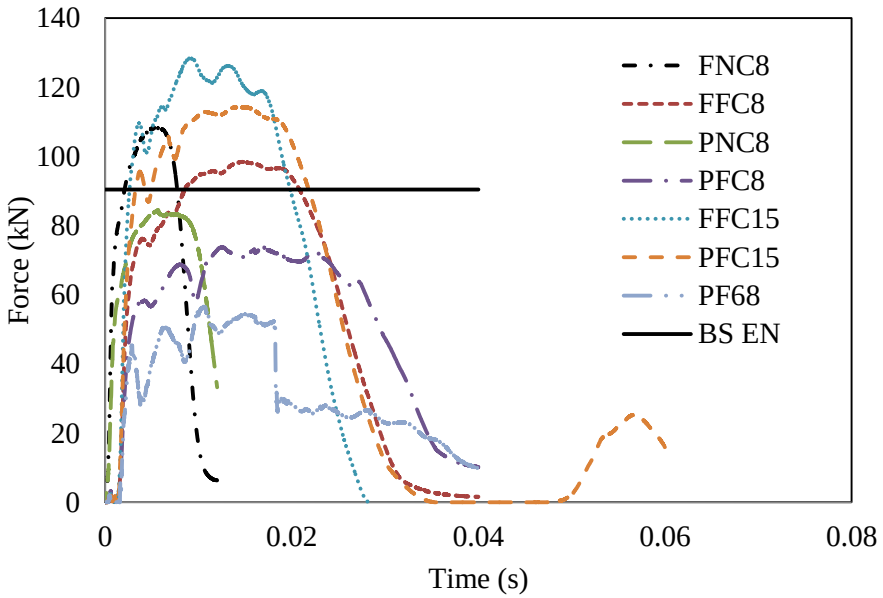

Figure 6.80. Internal tensile force time histories of the first bolt row of specimens connected to CFST column using long bolts under impact load.

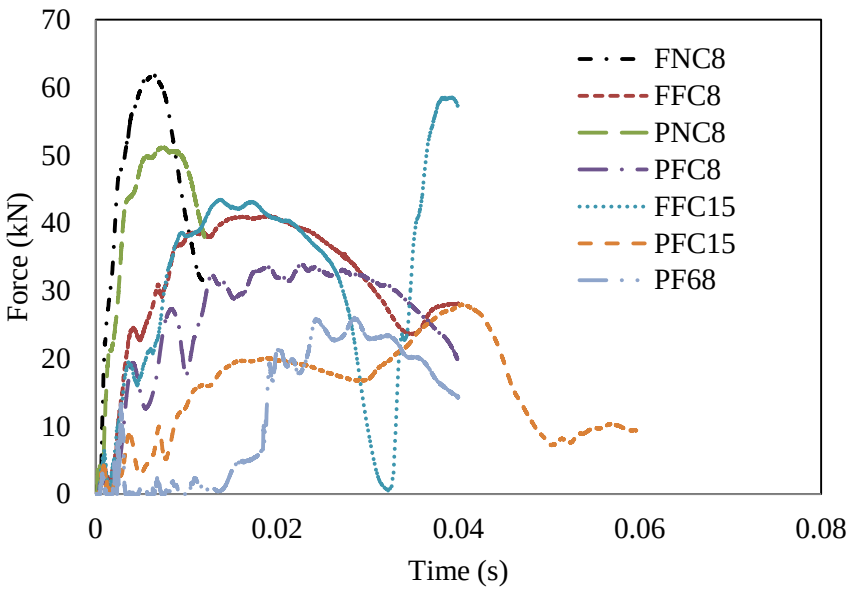

Figure 6.81. Internal tensile force time histories of the second bolt row of specimens connected to CFST column using long bolts under impact load.

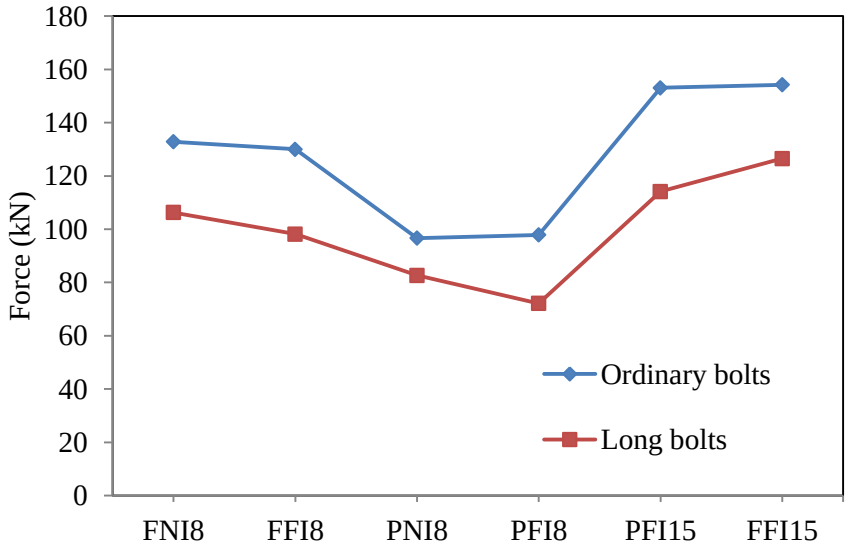

Figure 6.82. Comparison between the internal tensile forces generated in the first bolt of both bolt techniques under lateral impact load.

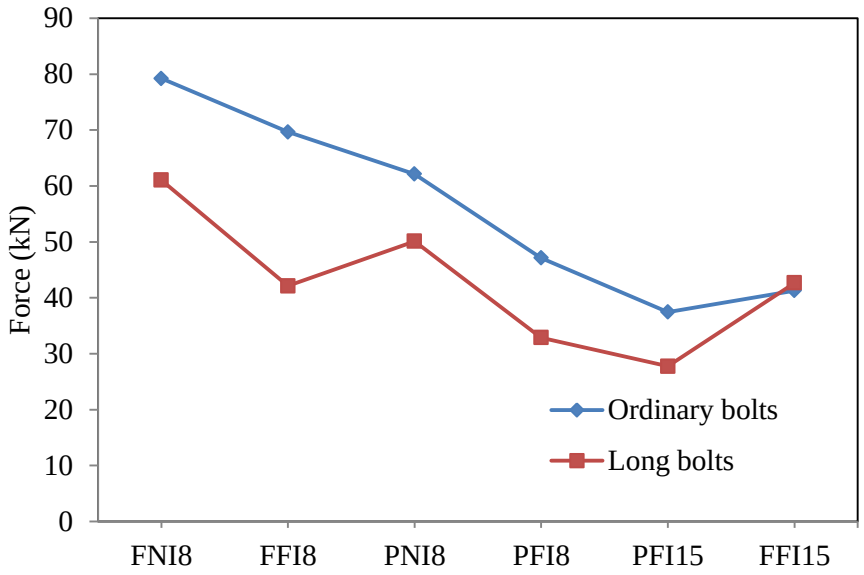

Figure 6.83. Comparison between the internal tensile forces generated in the second bolt of both bolt techniques under lateral impact load.

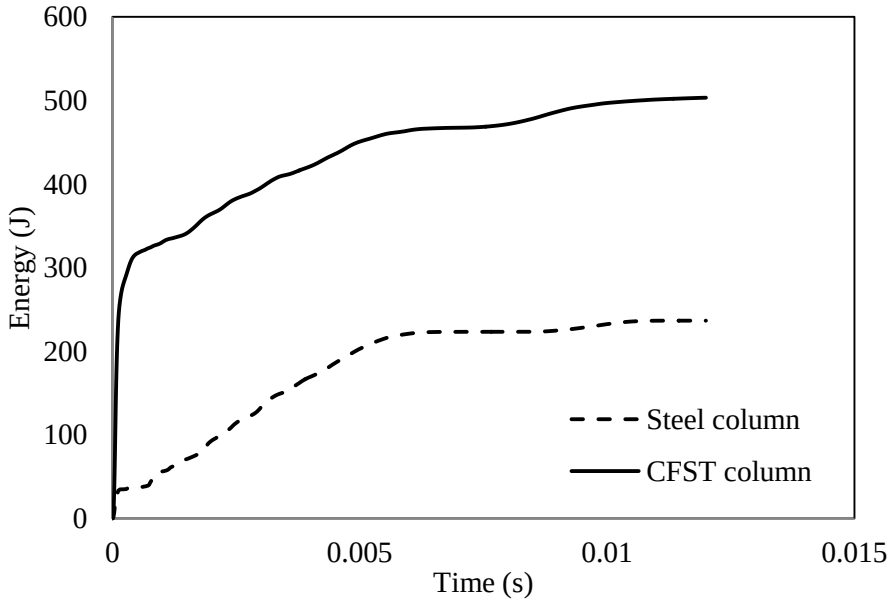

Figure 6.84. Comparison between plastic energy dissipated in steel and CFST column.

The bearing force-time histories were discussed in Section 6.2.3.1 for connections with ordinary bolts. In order to investigate the bearing resistance of the long bolts, similar

modelling procedure used for connection with ordinary bolts is adopted to obtain the bearing contact force here. A comparison between Figure 6.85 and Figure 6.31 indicates that the bearing force-time histories of both bolt techniques have similar trends along impact event. Again, the bearing forces are not developed unless the contact between the long bolts and the clearance hole of the end plate occurs as can be seen in Figure 6.85. The maximum bearing force is found to be 70.36 kN in the specimen with thin PDEP impacted far away from the connection (PFI8), while the minimum force was 0.23 kN, which was identified in specimen FFI15. The numerical results indicate that the specimens with thin PDEP (PNC8, PFC8 and PF68) exceeds the maximum bearing resistance of 54.4 kN that adopted by BS EN 1993-1-8 [7].

Comparing the bearing forces generated in both bolt techniques indicates that the long bolts experience higher bearing forces than ordinary bolts as can be seen in Figure 6.86. This difference in the forces is attributed to the restriction in translation that long bolts experienced due to the concrete infill. However, this restriction does not exist in ordinary bolts as no concrete infill is provided. Then the ordinary bolts have more translation than long bolts during the developing of the bearing forces, which then leads to generating higher forces. This restriction of the long bolt embedded in the concrete infill is the cause of concrete cracking during the impact event.

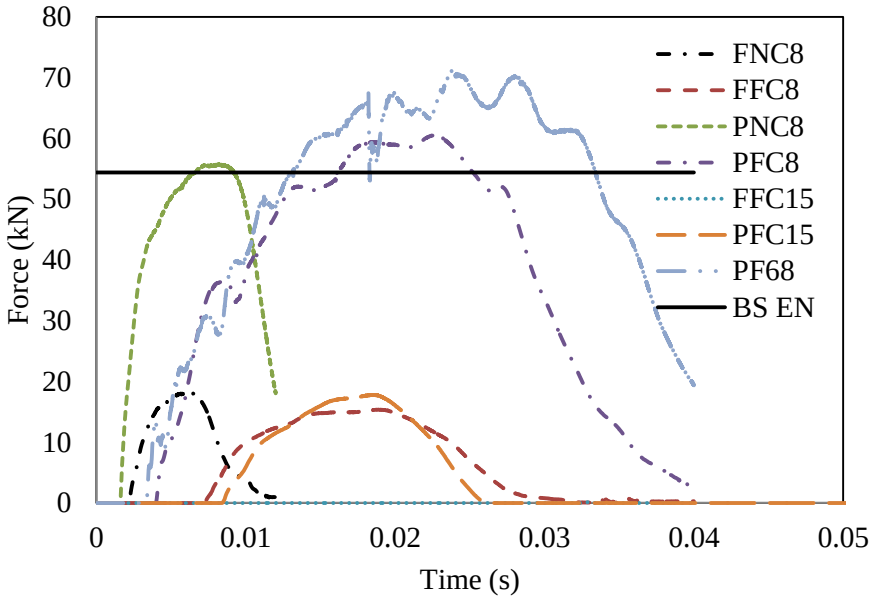

Figure 6.85. Internal tensile force time histories of the second bolt row of specimens connected to CFST column using long bolts under impact load.

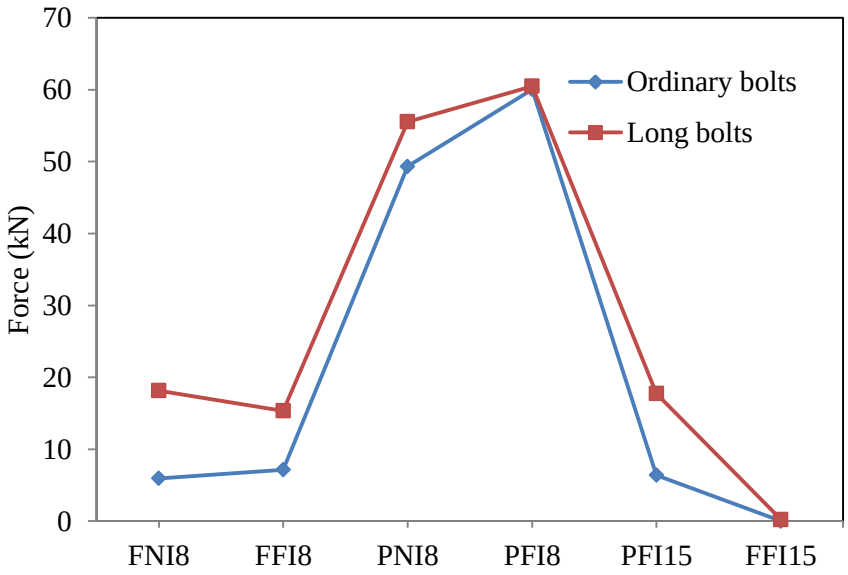

Figure 6.86. Comparison between the bearing forces generated in the first bolt of both bolt techniques under lateral impact loading.

6.3.2.2 Internal axial resistance of connections with long bolts

It was mentioned before in section 6.2.3.3 that the axial capacity of the joint plays a very important role in the progressive collapse failure, which is referred in Eurocode as a tying force. As one of requirements for the structural frame robustness, it is recommended that a

beam-to-column connection should be capable of sustaining a minimum design tensile force of 75 kN [7]. Thus, a section was made in the beam near the joint using the "free body cut" command available in the FE code ABAQUS, so that axial force versus time was requested to represent the internal tying force of the connection.

Figure 6.87 shows the internal tying force versus time curves for all specimens tested. The tying forces of specimens impacted far away from the connection (FFC8, PFC8, FFC15, PFC15 and PF68) began with a considerable negative value up to 40 kN within the first 2 ms, then jumped to its first positive peak from 2 to 3 ms. On the other hand, the negative tying forces less than 5 kN were generated in less than 0.6 ms and then it jumped to its first positive peak within 1.2 ms in specimens impacted near the connection (FNC8 and PNC8). Some fluctuations on the tying force were then developed on the first group of specimens due to the dynamic effect, which was gradually descended towards zero. On the other hand, the second group of specimens demonstrated the significantly higher internal tying forces than the first group due to the impact near the connection. In the same time, the internal tying forces generated in these specimens exceeded the minimum design tying force recommended by the BS EN 1991-1-7 [7]. Therefore, impact near the connection can be considered as the worst scenario for tying resistance of the connection.

A comparison between the tying force generated in the long bolts and ordinary bolts after impact event is presented in Figure 6.88. The tying force generated in specimens with long bolts seems to be lower than that with ordinary bolts in the maximum difference up to 14 % due to the higher contribution of CFST to dissipate the impact energy compared with steel column, as mentioned in Section 6.3.2.1. Hence, similar procedure that used in Eurocode to calculate the design tying resistance of connections with ordinary bolts can be used to predict the design tying resistance of connections with ordinary bolts considering this reduction.

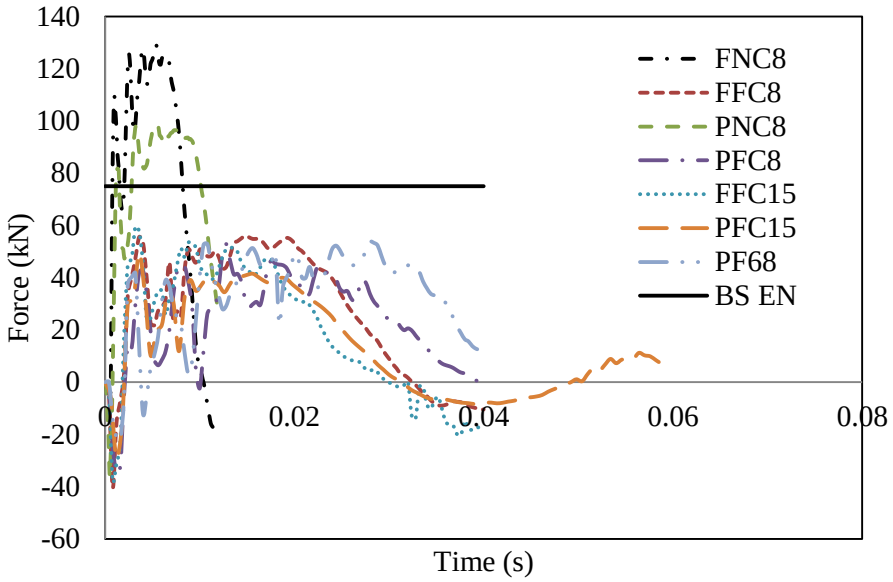

Figure 6.87. Internal tying force time histories of specimens connected to CFST column using long bolts under impact loading.

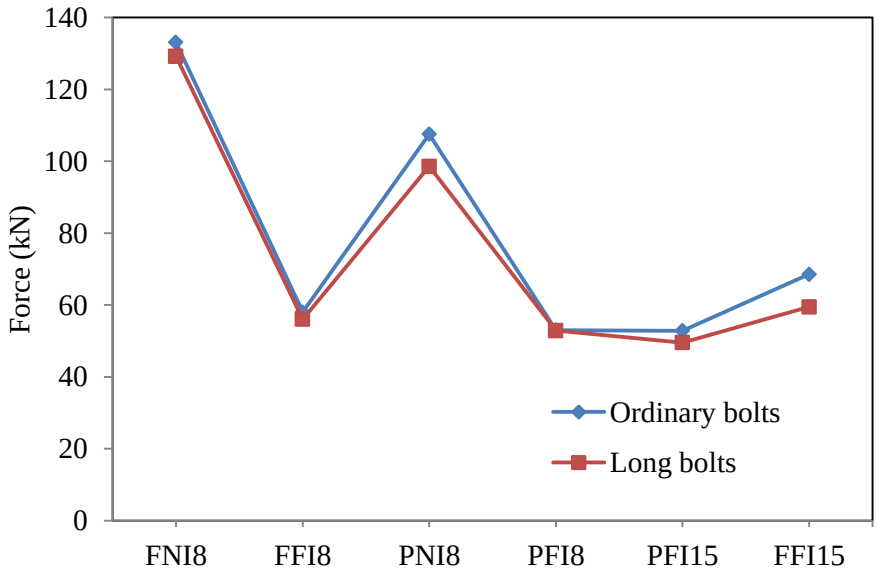

Figure 6.88. Comparison between the internal tying forces of connections under lateral impact loading.

6.3.2.3 Bending moment resistance of connections with long bolts

The "Free body cut" command available in the code was used again in the same section, which was used to investigate the internal axial force in order to examine the internal

moment. Figure 6.89 shows the internal moment versus time curves of the specimens tested. As expected, PDEPCs show a lower moment resistance than FPCs under the same applied energy as they are not classified as moment resisting connections. Also, it can be seen that specimens with a thick plate demonstrate a higher moment resistance than others. Changing the plate thickness from 8 mm to 15 mm increases the internal moment by 44 % in FPC and by 148 % in PDEPC.

The concrete infill contributes to enhance the moment resistance of the connection. Here, using concrete infill increases the internal moment by 25% which is attributed to the higher moment capacity of the CFST column compared with hollow column and the interaction between concrete and long bolts.

In addition to the lower internal forces in the bolts and the internal tying forces, the connection with long bolts shows the lower internal bending moment than that with standard bolts in a arrange from 4 to 21% as can be seen in Figure 6.90.

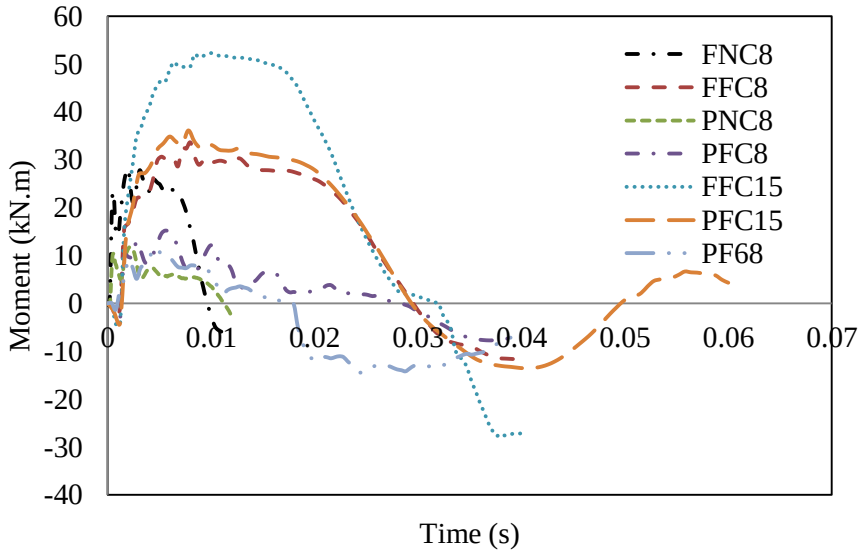

Figure 6.89. Internal moment time histories of specimens connected to CFST column using long bolts under impact load.

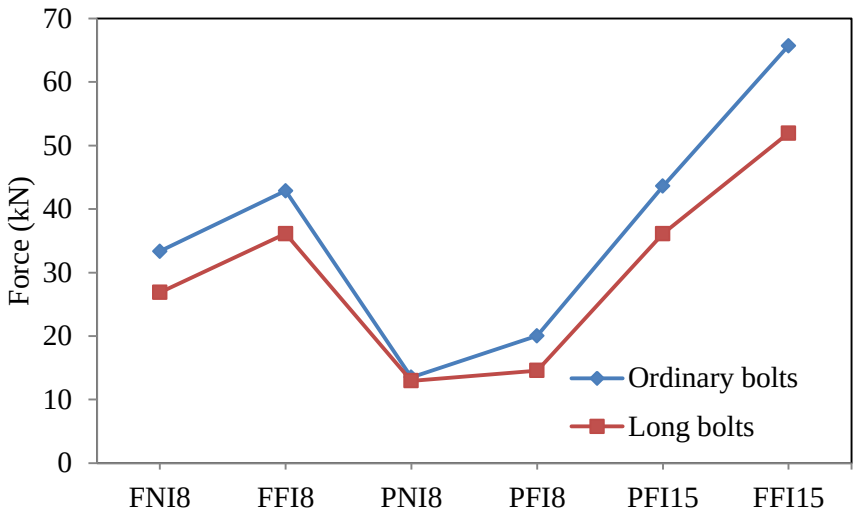

Figure 6.90. Comparison between the internal bending moment of connections under lateral impact load.

6.3.2.4 Energy dissipation

One of the important properties of a structure subjected to dynamic load is the ability to absorb energy. In order to investigate the energy absorption, the validated FE models were employed to request the time history of plastic dissipated energy for each component involved in the connection. It was found that most of the energy (more than 90% of the total plastic dissipated energy) was dissipated in the end plate and CFST column. Hence, the energy dissipation of these components is discussed here only. Figure 6.91 shows the dissipated energy by steel tube, concrete infill and end plate separately for all specimens tested. It can be seen that specimens with a thin end plate demonstrates a higher dissipated energy than those with a thick plate. Here, increasing the plate thickness from 8 to 15 mm reduces the energy dissipated significantly by about 95 % for FPCs and 26% for PDEPCs. This is attributed to the much smaller plastic deformations that the thick plate experienced compared with the thin plate for both connection types, as discussed in Section 2.4.1. The lower amount of energy dissipated by the thick plate was dissipated by the CFST column. Hence, more energy was dissipated by the CFST column of the specimens with a thick plate than those with a thin plate. In FPCs the energy dissipation in the CFST column was

increased by 54 % if the plate thickness was increased from 8mm to 15mm, while the energy dissipation increased by 29% in PDEPC. Therefore, using a thick plate leads to the more energy to be dissipated in the CFST column. This, in turn, will reduce the capacity of the CFST column, which may raise the possibility of the column failure due to preventing the connection from deforming in a ductile manner. However, a balanced end plate thickness needs to be identified for a specific connection. The effect of concrete infill on the plastic dissipated energy can be found by comparing the results of specimen PFC8 and PF68. This comparison shows that concrete infill in specimen PFC8 contributes to reduce the energy dissipated by plate and steel tube.

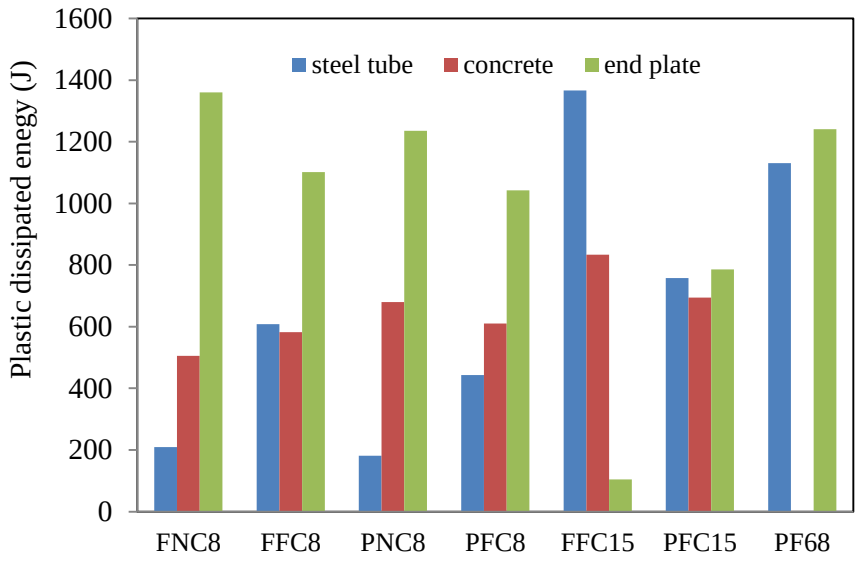

Figure 6.91. Plastic dissipation energy of connection components.

6.4 Summary

This chapter presents the results of FE simulations obtained in the current study for further understanding of the connection response against lateral impact loading. The FE models corresponding to impact and quasi-static loading were validated against the corresponding experimental results related to the load-displacement traces, strain time histories in four

selected points in addition to the deformation modes. Reasonable good agreements between the experimental results and the numerical simulations were obtained. The validated models were then exploited to perform full range analyses in which the capacity and the energy dissipation of the connections and the strain rate effect were investigated. Furthermore, the internal tensile forces produced in the bolts during the impact event were obtained and presented. It was found that using a thinner end plate alleviates the forces in the bolts then postpones the fracture of the bolts to offer the connection with a higher ductility. The full range analyses also showed that the higher connection tying force was generated if the column impacted near the connection. The numerical internal forces obtained under lateral impact and quasi-static loading were compared, DIFs being proposed. Good convergence was obtained between the DIFs calculated from the experimental results and the FE simulations.

The full range analyses were employed to evaluate the performance of end plate connections to CFST column using long bolts technique. The experimental results showed that the specimens with long bolts have the similar behaviour to that with ordinary bolts. The main difference was that the specimens with long bolts experienced slightly higher maximum displacement than those with ordinary bolts. Based on the full range analyses, the internal forces investigated were higher in specimens with ordinary bolts than those with long bolts, except for the bearing forces generated between the bolts and the clearance hole of the end plate. Moreover, the concrete infill played an important role to dissipate the impact energy, then to alleviate the tensile forces on the bolts, the axial forces and the bending moment generated in the connection.

The validated models were exploited again to investigate the effect of other parameters that were not investigated in the experimental work, such as the influence of using different impact energies, projectile configurations, boundary conditions, number of bolts in addition to predicting the lateral impact response of other type of connections, i.e. the extended end plate connection. It was found that the internal forces in the bolts and the failure modes of

the connections were not affected by changing the projectile shape. Regarding increasing the number of bolts**,** the numerical results indicated that the first bolt might still exhibit a fracture even with increasing the number of bolts. Connecting the column from both its ends had no effect on the deformation modes of the connection under lateral impact loading. Besides, more energy was dissipated during the propagation of the initial peak force if the column connected to both its ends compared with one end connections. The numerical predictions of the extended end plate response under lateral impact load indicated that the maximum tensile force was produced in the second bolt row after significant yielding of the end plate. Besides, the similar failure modes of the connection were obtained if the impact velocity increased from 7.5 to 9 m/s.

Chapter 7: Conclusions and Future Work

7.1 Introduction

This research was conducted with the aim to study the lateral impact response of a standard end plate which is used to connect steel beam to steel column using ordinary bolts. The steel beams could be connected to CFST columns in which the ordinary bolts usually used for the standard connections could not be used. The literatures showed that the long bolts technique is the best choice to connect steel beams to CFST columns. The previous studies also indicated that the connection to CFST columns using long bolts showed a good performance against seismic loadings. Therefore, it was decided in the current study to investigate the performance of connections with this technique under lateral impact loading.

The experimental work included testing series of full-scale beam-to-column connections with ordinary and long bolts under quasi-static and impact loading. Also, the material properties of concrete and steel components used in the experimental work were covered. A stiff reaction frame was also designed and fabricated to help with testing the specimens under both loading regimes. The effects of impact load locations, plate thickness for two connection types (PDEPC and FPC) were first investigated experimentally.

FE models were then developed and validated against the corresponding experimental results. The validated FE models were used to analyse the full-range response of end plate connections under quasi-static and impact loading, including the internal forces in bolts, the axial and moment resistances of the connection investigated. Based on the validated models, parametric studies were further performed to investigate the influence of different parameters. The main findings of the current study is summarised in this chapter and recommendations for future work are provided. By referring to the objectives of this study (Section 1.2), the following conclusions can be drawn:

i) To experimentally investigate the lateral impact response of standard end plate connections that used to connect steel beam to steel columns using ordinary bolts.

- The failure modes that observed in connections with standard bolts were the end plate yielding due to prying action, tearing of the PDEPC close to the weld toe, bearing deformation of the first bolt row, column flange crippling and nut loosening. It was found that the failure mode of the FPC was not influenced by changing the impact load location. However, slightly higher tearing failure occurred if the column was impacted near the connection in PDEPC.

- In spite of the higher moment resistance that obtained by connection with a thick end plate, it is not recommended according to the experimental results obtained in the current study. This is because the connections will be susceptible to lose its capacity suddenly by nut loosening or bolt fracture failure prior to the yielding of the end plate.

- During the impact event, three stages of force-displacement traces were obtained. In the first stage, the impact force reached its maximum value with less than 3 mm of displacement. Intermittent impact then occurred followed by lower peak forces. In the second stage, the impact force began to be relatively stable before it dropped in the third stage once the projectile started to rebound. On the other hand, force-displacement traces under quasi-static loading indicated bilinear behaviour with noticeable degradation on the stiffness up to failure. Comparing the force-displacement traces under both loading regimes indicated that all the static results demonstrated the lower extremes of the energy dissipated than the impact results. Also, the force values under quasi-static started to converge to that under impact loading in the plateau stage.

- The deformation modes obtained under quasi-static load were similar to the corresponding specimens tested under impact load but with a slightly higher damage for the PDEPC specimens close to the weld toe.

ii) To experimentally evaluate the lateral impact resistance of end plate connections that used to connect steel beams to CFST column using the long bolt technique by comparing with the experimental results of the standard connections.

- The end plate connection with long bolts almost showed similar behaviour of that with standard bolts under lateral impact loading. However, similar failure modes were obtained in both bolt technique specimens, except for the cracking of concrete infill, which occurred with long bolt specimens and column flange crippling which replaced the punching shear in long bolt specimens.

- The end plate connection with long bolts demonstrated slightly higher maximum displacement and lower initial peak force, compared with the standard connections. This was attributed to the higher ductility of CFST columns in comparison to steel columns.

- The end plate with the long bolt technique could be recommended to resist lateral impact loading, provided the cracks propagating around the long bolts will not affect the axial capacity of the CFST column connected.

iii) To develop the finite element models to assist with predicting the structural response of such connections subjected to quasi-static and low velocity lateral impact as well as to validate the models with the experimental results.

- Simulation of bolted connections under impact load required to consider the complexity of geometry and contact. In addition to its efficiency to model the dynamic events, ABAQUS/explicit is also an effective method to simulate bolted connections under quasi-static loading, but with ensuring the kinetic energy to internal energy ratio for each part of the model to be less than 5%. Here, using a loading rate of 0.67 mm/s with 10^6 mass scaling factor could help the analysis with

reducing computational costs without a significant dynamic effect on the numerical results.

- Concrete damage plasticity (CDP) constitutive model was adopted in the current study to model the concrete infill with neglecting the strain rate effect of the confined concrete, which provides a reasonable agreement between the FE modelling output and the experimental results. Also, the elasto-plastic and damage modelling were applied to simulate the structural response of steel, with good validation of the numerical results against the experimental measurements, in terms of failure modes.

- The FE models were validated successfully against the experimental results and a good agreement was obtained in terms of force-displacement traces, strain-time histories and deformation modes. This validation will enable to exploit the FE models for further investigation to achieve the subsequent objectives.

iv) To use the validated finite element models for further investigation of the lateral impact response of the end plate connection with ordinary bolts.

- The full range of analysis results showed that the first bolt experienced a faster change in its tensile force than the second bolt after the onset of impact loading. Also, it was concluded that the first bolt gained a considerable amount of its peak tensile force in a short time period, which indicates that the bolt experienced a higher strain rate than the second bolt.

- The full range analysis results also showed that the higher yielding of the end plate due to prying action, the higher bearing force produced. This will help enhance the ductility of the connection and prevent the sudden failure to occur. However, the numerical results showed that the bearing forces produced in connections with a

thick plate were significantly lower than those with a thin plate, which would contribute to reducing the ductility of the former connection.

- The axial impact resistance of the FPCs and PDEPCs was affected slightly for the column being struck far away from the connection. However, PDEPCs showed around 80 % of the impact axial resistance of FPCs if the column struck near the connection.

- The FPCs showed higher impact moment resistance than the PDEPCs by around 146% for thin plate specimens while this percentage reduced to 46% for thick plate specimens.

- Reducing the end plate thickness from 15 to 8 mm increased the energy dissipation of the end plate by 88%, while the energy dissipated in FPCs with a 15 mm thick end plate is almost non-existed if compared with that with 8 mm. This would prove the invalidity of using thick end plate connections to resist lateral impact loading that aforementioned in the second conclusion of the first objective.

- The FE models were used to investigate the strain rate distribution in the high deformation locations expected. It was found that higher strain rate can be obtained if the column struck near the connection. Hence, the maximum strain rates were 32.39 and 18.15 s^{-1} in PDEPCs and FPCs, respectively. The maximum strain rates in the first bolts were also obtained in specimens impacted near the connection, which were 12.5 and 8.9 s^{-1} in FPC and PDEPC, respectively. Specimens with a thick plate experienced the lowest strain rates, which will prevent the connection from the strength enhancement due to the high strain rate. Again, this to confirm the invalidity of using thick plate under lateral impact loading.

v) To use the validated finite element models for further evaluation of the use of end plate

connections that used to connect steel beams to CFST column using the long bolt technique.

- The full range analysis showed that all the internal forces produced in the connection with long bolts were lower than those with standard bolts, except for the bearing forces. This interprets the contribution of the CFST column to absorb more energy than steel columns then to alleviate the internal forces. In spite of the positive merit of CFST to absorb more energy, its concrete infill showed considerable crack patterns in the connection zone which may affect the axial capacity of the CFST negatively.

vi) To use the validated finite element models for further parametric studies to predict the effect of other parameters that might affect the lateral impact response of beam-to-column connections rather than the parameters investigated experimentally.

- The validated models were further used to investigate the effect of using different projectile configurations. Hence, in addition to the flat projectile that was used in the experiments, spherical and wedge projectiles were also examined. The parametric study results showed that the projectile shape has negligible effect on the maximum displacement. Also, specimens impacted with a flat projectile demonstrated higher impact force in all three stages of the impact event.

- Effect of increasing the number of bolts in the connection was also investigated. The results showed that the deformation mode was not influenced significantly by increasing the number of bolts, but it helps to delay the tearing failure close to the weld toe. Also, the first bolt might still experience fracture even with increasing the number of bolts, as the FE results showed that adding the centre bolt row did not decrease the maximum tensile force in the first bolt by no more than 2.2% for both connection types.

- The validated models were exploited to predict the lateral impact response of the extended end plate connections. The extended end plate connection showed a higher impact moment capacity than FPC and PDEPC with three bolts by 25 and 61 %, respectively.

- The column was connected to one end of the column in the tests. The validated models were used again to investigate the effect of connecting the column from both its ends on the connection response. No change was observed in the deformation mode for both boundary conditions. Also, the plateau stage may disappear if the column is connected from both its ends, leading to reduce the time of impact event compared with that required in specimens with one connection.

vii) To use the experimental and finite element results to propose dynamic increase factors in which the dynamic effect can be estimated.

- Dynamic increase factors (DIFs) were proposed based on the experimental results using energy principles and the FE results using the full range analyses. Based on the experimental results, the DIF varies from 1.25 to 1.38, while it varies between 1.02 to 1.45 based on the full range analyses.

7.2 The proposed future work

Based on the results obtained from the current study, following recommendations are proposed for the future work:

- The results obtained may be further used to propose a simplified model of connections to assist with predicting the response of the entire structural frame under lateral impact load. This will help to predict the critical impact energy (mass and

impact velocity), through which a structural frame with different connection configurations will begin to collapse.

- The current study has focused on the impact loading occurred perpendicular to the column. Therefore, further experimental and numerical studies can be undertaken to investigate the response of connections to lateral oblique impact with different angles.

- Further studies can be undertaken experimentally and numerically to investigate the lateral impact response of connections with axially loaded columns and/or vertically loaded beam.

- More knowledge is needed to investigate the behaviour of fully confined concrete with high strain rate (high velocity impact and blast) by assuming different confinement configurations such as square and circular confinements as the most common cases of CFST.

- The current study has investigated the lateral impact response of end plate connection. However, it will be worth to investigate the response of other types of connections that used in practice, such as fin-plate connection which represents the most common option to connect steel beam to steel column after the end plate connection.

- The response of beam-to-column connection to only one lateral impact was presented in the current study. However, it will be useful to investigate the connection response to multiple impacts as such the case may occur in practice.

References:

[1] Cook L., Events in local history-Ronan Point 1968. 2005.

[2] Pearson C. and Delatte N., Ronan point apartment tower collapse and its effect on building codes. Journal of Performance of Constructed Facilities, 2005. **19(2)**: p. 172-177.

[3] Santiago A., Silva L. S. d., Vaz G., Real P. V., and Lopes A. G., Experimental investigation of the behaviour of a steel sub-frame under a natural fire. Steel and Composite Structures, 2008. **8(3)**: p. 243–64.

[4] Y. Lu, Hao H., Ma G., and Zhou Y., Simulation of structural response under high-frequency ground excitation Earthquake engineering & structural dynamics, 2001. **30(3)**: p. 307-325.

[5] McAllister. T. and Corley. G., World Trade Center Building Performance Study: Data collection, preliminary observations, and recommendations. 2002: Fedral Emergency Management Agency.

[6] Roberts J., Safety in Tall Buildings and other Buildings with Large Occupancy. 2002, London: Institution of Structural Engineers.

[7] Way A. G., Structural robustness of steel framed buildings. 2011: SCI. 55.

[8] Yang B. and Tan K. H., Experimental tests of different types of bolted steel beam–column joints under a central-column-removal scenario. Engineering Structures, 2013. **54**: p. 112-130.

[9] Wang H., Yang B., Zhou X. H., and Kang S. B., Numerical analyses on steel beams with fin-plate connections subjected to impact loads. Journal of Constructional Steel Research, 2016. **124**: p. 101-112.

[10] Zaini S. S., Impact Resistance of Pre-Damaged Ultra-High Performance Fiber Reinforced Concrete (UHPFRC)Slabs, in School of Engineering. 2015, University of Liverpool.

[11] Zeinoddini M., Parke G. A. R., and Harding J. E., Interface Forces in Laterally Impacted Steel Tubes. Experimental Mechanics, 2008. **48**: p. 265–280.

[12] Yousuf M., Uy B., Tao Z., Remennikov A., and Liew J. R., Transverse impact resistance of hollow and concrete filled stainless steel columns. Journal of Constructional Steel Research, 2013. **82**: p. 177-189.

[13] Al-Thairy H., Behaviour and design of steel column subjected to vehicle impact, in School of Mechanical, Aerospace and Civil Engineering. 2012, University of Manchester.

[14] Al-Husainy A. S. S., Impact Response of Recycled Aggregate Concrete Filled Steel Tube Columns Strengthened with CFRP. 2017, University of Liverpool.

[15] Elchalakani M., Zhao X. L., and Grzebieta R. H., Concrete-filled circular steel tubes subjected to pure bending. Journal of Constructional Steel Research, 2001. **57(11)**: p. 1141-1168.

[16] Morino S., Uchikoshi M., and Yamaguchi I., Concrete-filled steel tube column system-its advantages. International Journal of Steel Structures, 2001. **1(1)**: p. 33-44.

[17] Shams M. and Saadeghvaziri M. A., State of the art of concrete-filled steel tubular columns. ACI Structural Journal, 1997. **94(5)**: p. 558-569.

[18] Chou C. C. and Uang C. M., Cyclic performance of a type of steel beam to steel-encased reinforced concrete column moment connection. Journal of constructional steel research, 2002. **58(5)**: p. 637-663.

[19] Li X., Wu Y., Mao W., Y. Xiao, Anderson J. C., and Guo Y., Bolted end plate connections for steel reinforced concrete composite structures. Structural Engineering and Mechanics 2006. **24(3)**: p. 291-306.

[20] Li X., Xiao Y., and Wu Y. T., Seismic behavior of exterior connections with steel beams bolted to CFT columns. Journal of Constructional Steel Research, 2009. **65(7)**: p. 1438-1446.

[21] Glenn A., Morris G. A., and Packer J. A., Beam-to-Column connection in steel frames. Canadian Journal of Civil Engineering, 1987. **14**: p. 68-76.

[22] Wilson, W. M., and Moor, H. F., Test to determine the rigidity of riveted joint in steel structures, Engineering Experimental Station, 1917,University of Illinois, Urbana, IL, Bulletin 104.

[23] Nethercot D. A., Steel beam-to-column connection a review of test data and its apllicability to the evaluation of joint behaviour in the performance of steel frames. CIRIA Project Study, 1985.

[24] Li T. Q., Choo, B. S. and Nethercot, D. A.,, Connection Element Method for the Analysis of Semi-rigid Frames. J. Construct. Steel Research, 1995. **32**: p. 143-171.

[25] Jones S. W., Kirby P. A., and Nethercot D. A., The Analysis of Frames with Semi-Rigid Connections- A State-of-the-Art Report. J. Construct. Steel Research, 1983. **3(2)**: p. 1-13.

[26] Eurocode, C.E.D.N., 1993. 3: Design of steel structures. DRAFT prEN.

[27] Faridmehr I., Tahir M. M., and Lahmer T., Classification System for Semi-Rigid Beam-to-Column Connections. Latin American Journal of Solids and Structures, 2016. **13**(11): p. 2152-2175.

[28] Murray T. M. and Shoemaker W. L., Flush and extended multiple-row moment end-plate Connections. 2002: American Institute of Steel Construction.

[29] Kidd M., Judge R., and Jones S. W., Current UK trends in the use of simple and/or semi-rigid steel connections. Case Studies in Structural Engineering, 2016. **6**: p. 63-75.

[30] Phillips J. and Packer J. A., in The Effect of Plate Thickness on Flush End-Plate Connections. 1981, International Conference on Joints in Structural Steel Work. p. 6.77–6.92.

[31] Borgsmiller J. T. and Murray T. M., Simplified Method for Design of Moment End Plate Connections. 1995, Virginia Polytechnic Institute and State University: Blacksburg, Virginia

[32] Shi G., Shi Y., and Wang Y., Behaviour of End-Plate Moment Connections under Earthquake Loading. Engineering Structures, 2007. **29/5**: p. 703–716.

[33] Shi W. L., Li G. Q., Ye Z. M., and Xiao R. Y., Hysteretic Models for Composite Joints with Flush End Plate Connections Based On Experimental Investigation, in 5th International Conference on Advances in Steel Structures, ICASS. 2007. p. 849–854. .

[34] Yu H., Burgess I. W., Davison J. B., and Plank R. J., Experimental and Numerical Investigations of the Behavior of Flush End Plate Connections at Elevated Temperatures. Journal of Structural Engineering, 2011. **137/1**: p. 80–87.

[35] Abidelah A., Bouchair A., and Kerdal D. E., Experimental and Analytical Behavior of Bolted End-Plate Connections with or without Stiffeners. Journal of Constructional Steel Research, 2012. **76**: p. 13–27.

[36] Hasan R., Kishi N., Chen W. F., and Komuro M., Evalution of rigidity of extended end-plate connections. Journal of Structural Engineering, 1997. **123(12)**: p. 1595-1602.

[37] Ribeiro J., Santiago A., Rigueiro C., and Silva L. S. d., Analytical model for the response of T-stub joint component under impact loading. Journal of Constructional Steel Research, 2015. **106**: p. 23–34.

[38] Shanmugam N. E. and Lakshmi B., State of the art report on steel–concrete composite columns. Journal of constructional steel research, 2001. **57(10)**: p. 1041-1080.

[39] D. He, Dong J., Wang Q., and Chen X., Mechanical behaviour of recycled concrete filled steel tube conlumns strengthened by CFRP, in Multimedia Technology (ICMT), 2011 International Conference. 2011, IEEE. p. 1110-1113.

[40] Sundarraja M. C. and Prabhu G. G., Investigation on strengthening of CFST members under compression using CFRP composites. Journal of Reinforced Plastics and Composites, 2011. **72**: p. 75-83.

[41] Morino S. and Tsuda K., Design and construction of concrete-filled steel tube column system in Japan. Earthquake Engineering and Engineering Seismology, 2002. **4(1)**: p. 51-73.

[42] Xu W., Han L.-H., and Li W., Seismic performance of concrete-encased column base for hexagonal concrete-filled steel tube: experimental study. Journal of Constructional Steel Research, 2016. **121**: p. 352-369.

[43] Lam D. and Testo N., Structural design of concrete filled steel elliptical hollow sections. Composite Construction 2008. **VI**: p. 20-24.

[44] Dai X. and Lam D., Numerical modelling of the axial compressive behaviour of short concrete-filled elliptical steel columns. Journal of Constructional Steel Research, 2010. **66(7)**: p. 931-942.

[45] Chen J. and Jin W. L., Experimental investigation of thin-walled complex section concrete-filled steel stub columns. Thin-Walled Structures, 2010. **48(9)**: p. 718-724.

[46] Van-Long H., Jean-Pierre J., and Jean-François D., Extended end-plate to concrete-filled rectangular column joint using long bolts. Journal of Constructional Steel Research, 2015. **113**: p. 156-168.

[47] Sheet I. S., Umarani G., and MacRae G. A., Experimental investigation of CFT column to steel beam connections under cyclic loading. Journal of Constructional Steel Research, 2013. **86**: p. 167-182.

[48] GSA U., Progressive Collapse Analysis and Design Guidelines for New Federal Office Buildings and Major Modernization Projects. 2003, Washington, DC.

[49] Menkes S. B. and Opat H. J., Tearing and shear failures in explosively loaded clamped beams. Experimental Mechanics, 1973. **13**: p. 480-486.

[50] Liu J. and Jones N., Experimental investigation of clamped beams struck transversely by a mass. International Journal of Impact Engineering, 1987. **6**: p. 303-335.

[51] Yu. J. and Jones N., Numerical simulation of a clamped beam under impact loading. computers and Structures, 1989. **32, No. 2**: p. 281-293.

[52] Yu J. and Jones N., Further experimental investigations on the failure of clamped beams under impact loads. International Journal of Solids and Structures, 1991. **27**: p. 1113-1137.

[53] Yu J. and Jones N., Numerical simulation of impact loaded steel beams and the failure criteria. International Journal of Solids and Structures, 1997. **34**: p. 3977-4004.

[54] Mannan M. N., Ansari R., and Abbas H., Failure of aluminium beams under low velocity impact. International Journal of Impact Engineering, 2008. **35**(11): p. 1201-1212.

[55] Chen F. L. and Yu T. X., Influence of Axial Pre-Load on Plastic Failure of Beams Subjected to Transverse Dynamic Load. Key Engineering Materials, 2000. **117-180**: p. 255-260.

[56] Zeinoddini M., Parke G. A. R., and Harding J. E., Axially pre-loaded steel tubes subjected to lateral impacts- an experimental study. International Journal of Impact Engineering, 2002. **27**: p. 669-690.

[57] Zeinoddini M., Harding J. E., and Parke G. A. R., Axially pre-loaded steel tubes subjected to lateral impacts (a numerical simulation). International Journal of Impact Engineering, 2008. **35**(11): p. 1267-1279.

[58] Adachi T., Tanaka T., Sastranegara A., Yamaji A., Kim S. K., and Yang I. Y., Effect of transverse impact on buckling behavior of a column under static axial compressive force. International journal of impact engineering, 2004. **30(5)**: p. 465-475.

[59] Bambach M. R., Jama H., Zhao X. L., and Grzebieta R. H., Hollow and concrete filled steel hollow sections under transverse impact loads. Engineering Structures, 2008. **30**(10): p. 2859-2870.

[60] Xiaoqing M. and Stronge W. J., Spherical missile impact and perforation of filled steel tubes. International Journal of Impact Engineering, 1985. **3(1)**: p. 1-16.

[61] Nishida M. and Tanaka K., Experimental study of perforation and cracking of water-filled aluminum tubes impacted by steel spheres. International Journal of Impact Engineering, 2006. **32(12)**: p. 2000-2016.

[62] Remennikov A. M., Kong S. Y., and Uy B., Response of foam-and concrete-filled square steel tubes under low-velocity impact loading. Journal of Performance of Constructed Facilities, 2010. **25(5)**: p. 373-381.

[63] Qu H., Li G., Chen S., Sun J., and Sozen M. A., Analysis of circular concrete-filled steel tube specimen under lateral impact. Advances in Structural Engineering. Advances in Structural Engineering, 2011. **14(5)**: p. 941-951.

[64] Deng Y., Tuan C. Y., and Xiao Y., Flexural behaviour of concrete-filled circular steel tubes under high-strain rate impact loading. Journal of Structural Engineering, 2011. **138(3)**: p. 449-456.

[65] Wang R., Han L.-H., and Hou C.-C., Behavior of concrete filled steel tubular (CFST) members under lateral impact: Experiment and FEA model. Journal of Constructional Steel Research, 2013. **80**: p. 188-201.

[66] Yousuf M., Uy B., Tao Z., Remennikov A., and Liew R., Impact Behaviour and Resistance of Hollow and Concrete Filled Mild Steel Columns. Australian Journal of Structural Engineering, 2012. **13**: p. 65-80.

[67] Yousuf M., Uy B., Tao Z., Remennikov A., and Liew J. R., Impact behaviour of pre-compressed hollow and concrete filled mild and stainless steel columns. Journal of Constructional Steel Research, 2014. **96**: p. 54-68.

[68] Han L. H., Hou C. C., Zhao X. L., and Rasmussen K. J., Behaviour of high-strength concrete filled steel tubes under transverse impact loading. Journal of Constructional Steel Research, 2014. **92**: p. 25-39.

[69] Aghdamy S., Thambiratnam D. P., Dhanasekar M., and Saiedi S., Computer analysis of impact behavior of concrete filled steel tube columns. Advances in Engineering Software, 2015. **89**: p. 52-63.

[70] Shakir A. S., Guan Z. W., and Jones S. W., Lateral impact response of the concrete filled steel tube columns with and without CFRP strengthening. Engineering Structures, 2016. **116**: p. 148-162.

[71] Izzuddin B. A., Vlassis A. G., Elghazouli A. Y., and Nethercot Obe D. A., Assessment of progressive collapse in multi-storey buildings. Proceedings of the Institution of Civil Engineers - Structures and Buildings, 2007. **160**(4): p. 197-205.

[72] Tyas A., Warren J. A., Stoddart E. P., Davison J. B., Tait S. J., and Huang Y., A Methodology for Combined Rotation-Extension Testing of Simple Steel Beam to Column Joints at High Rates of Loading. Experimental Mechanics, 2012. **52**(8): p. 1097-1109.

[73] Stoddart E. P., Byfield M. P., Davison J. B., and Tyas A., Strain rate dependent component based connection modelling for use in non-linear dynamic progressive collapse analysis. Engineering Structures, 2013. **55**: p. 35-43.

[74] Wang N., Study on the Collapse Resistance of Steel Moment Frames with Seismic Design and Improved Local Details. 2013., Hunan University.

[75] Zhang J. Q., Dynamic Behavior and Catenary Action Analysis of horizontally Restrained Steel Beam under Impact Loading. 2012, Hunan University.

[76] Rahbari R., Tyas A., Buick Davison J., and Stoddart E. P., Web shear failure of angle-cleat connections loaded at high rates. Journal of Constructional Steel Research, 2014. **103**: p. 37-48.

[77] Kang. H., Shin. J., and Kim J., Analysis of Steel Moment Frames subjected to Vehicle Impact, in APCOM & ISCM. 2013: Singapore.

[78] Grimsmo E. L., Clausen A. H., Langseth M., and Aalberg A., An experimental study of static and dynamic behaviour of bolted end-plate joints of steel. International Journal of Impact Engineering, 2015. **85**: p. 132-145.

[79] Grimsmo E. L., Clausen A. H., Aalberg A., and Langseth M., A numerical study of beam-to-column joints subjected to impact. Engineering Structures, 2016. **120**: p. 103-115.

[80] Barata P., Ribeiro J., Rigueiro C., Santiago A., and Rodrigues J. P., Assessment of T-stub joint component at ambient and elevated temperatures. Fire Safety Journal, 2014. **70**: p. 1–13.

[81] Ribeiro J., Santiago A., Rigueiro C., Barata P., and Veljkovic M., Numerical assessment of T-stub component subjected to impact loading. Engineering Structures, 2016. **106**: p. 450-460.

[82] British Standards Institution, Cement composition, specifications and conformity criteria for common cements, BS EN 197-1, 2011.

[83] British Standard Institute. Testing hardened concrete. Part 3: Compressive strength of test specimen. BS EN 12390-3-2009.

[84] British Standards Institution, Specifications for aggregates from natural sources fro concrete, BS 882, 1992.

[85] British Standard Institution, Concrete. Specification, performance, production and conformity, BS EN 206-1-2000.

[86] British Standards Institution, Metalic Materials-Tensile testing- Part 1: Method of test at ambient temperture, BS EN 10002-1, 2001. .

[87] Bridgman P. W., Studies in Large Plastic Flow and Fracture. 1952, New York: McGraw-Hil.

[88] Wang R., Han L.-H., Zhao X.-L., and Rasmussen K. J. R., Analytical behavior of concrete filled double steel tubular (CFDST) members under lateral impact. Thin-Walled Structures, 2016. **101**: p. 129-140.

[89] Liu C., Fung T. C., and Tan K. H., Dynamic Performance of Flush End-Plate Beam-Column Connections and Design Applications in Progressive Collapse. Journal of Structural Engineering, 2016. **142**(1): p. 04015074.

[90] Joints in Steel Construction simple Connections. 2002, London: The Steel Construction Institute (SCI)/ British Constructional steelwork Association.

[91] British Standards Institution, Hexagon head bolts. Product grades A and B, BS EN ISO 4014, 2011.

[92] Birch R. S. and Jones N., Measurement of Impact Loads using a Laser Doppler Velocimeter. Proceedings of the Institution of Mechanical Engineers, Part C: Journal of Mechanical Engineering Science, 1990. **204**(1): p. 1-8.

[93] DANTEC Measurement Technology, BSA/FVA Flow Software: Installation and User's Guide, Denmark, 2000: Denemark.

[94] Owens G. W. and Moore D. B., The robustness of simple connections. The Structural Engineer, 1992. **70**(3): p. 37-53.

[95] BCSA/SCI P212 Joints in steel construction: Simple connections.2002.

[96] Malver L. J. a. C., J. E., Dynamic increase factors for concrete. 28th Dept. of Defense Explosives Safety Board (DDESB) Seminar, Department of Defense Explosive Safety Board, 1998.

[97] Malver L. J. a. C., J. E., Dynamic increase factor for steel reinforcing bars. 28th Dept. of Defense Explosives Safety Board (DDESB) Seminar, Department of Defense Explosive Safety Board, 1998.

[98] Tsai M.-H. and Lin B.-H., Dynamic amplification factor for progressive collapse resistance analysis of an RC building. The Structural Design of Tall and Special Buildings, 2009. **18**(5): p. 539-557.

[99] ImPREESSion 6. NecoletTecnonlgies. Germany: Weisang GmbH & Co. KG.; 2002.

[100] Mouritz A. P., failure mechanisms of mild steel bolts under different tensile loading rates. International Journal of Impact Engineering, 1994. **15, No.3**: p. 311-324.

[101] Abaqus documontations. SIMULIA.

[102] Taverz F. A., Simulation of Behaviour of Composite Grid Reinforced Concrete Beams Using Explicit Finite Element Methods. 2001, University of Wisconsin-Madison: USA.

[103] Hooputra H., Gese H., Dell H., and Werner H., A comprehensive failure model for crashworthiness simulation of aluminium extrusions. International Journal of Crashworthiness, 2004. **9**(5): p. 449-464.

[104] Hu H. T., Huang C. S., and Wu Y. M., Nonlinear Analysis of Axially Loaded Concrete-Filled Tube column with confinement effect. Journal of Structural Engineering, 2003. **129(10)**: p. 1322-1329.

[105] Ellobody E., Young B., and Lam D., Behaviour of normal and high strength concrete-filled compact steel tube circular stub columns. Journal of Constructional Steel Research, 2006. **62**(7): p. 706-715.

[106] Dai X. and Lam D., Numerical modelling of the axial compressive behaviour of short concrete-filled elliptical steel columns. Journal of Constructional Steel Research, 2010. **66**(7): p. 931-942.

[107] Mander J. B., Priestley M. J., and Park R., Theoretical stress-strain model for confined concrete. Journal of structural engineering, 1988. **114(8)**: p. 1804-1826.

[108] Richart F. E., Brandtzaeg A., and Brown R. L., A study of the failure of concrete under combined compressive stresses, Bulletin 185, University of Illinois, Engineering Experimental Station, Champaign, III, 1928.

[109] Saenz L. P., Discussion of 'Equation for the stress-strain curve of concrete by P. Desayi, and S. Krishnan. ACI Journal, 1964. **61**: p. 1229-1235.

[110] Li Q., Duan Y., and Wang G., Behaviour of large concrete specimens in uniaxial tension. Magazine of concrete research, 2002. **54(5)**: p. 385-391.

[111] Liu J., Rehabilitation and repair of reinforced concrete short columns with external steel collars. 2008, University of Alberta.

[112] Begum M., Driver R. G., and Elwi A. E., Finite-element modeling of partially encased composite columns using the dynamic explicit method. Journal of structural engineering, 2007. **133(3)**: p. 326-334.

[113] Kono S., Watanabe F., and Kajitani A., Stress-Strain Relation of Confined Concrete under Dynamic Loading, in Fourth International Conference on Fracture Mechanics of Concrete and Concrete Structures. 2001. p. 585-592.

[114] He D., Dong J., Wang Q., and Chen X., Mechanical behaviour of recycled concrete filled steel tube conlumns strengthened by CFRP, in Multimedia Technology (ICMT), 2011 International Conference. 2011, IEEE. p. 1110-1113.

[115] Bambach M. R., Design of hollow and concrete filled steel and stainless steel tubular columns for transverse impact loads. Thin-Walled Structures, 2011. **49(10)**: p. 1251-1260.

[116] Wang Y., Qian X., Liew J. R., and Zhang M. H., Experimental behavior of cement filled pipe-in-pipe composite structures under transverse impact. International Journal of Impact Engineering, 2014. **72**: p. 1-16.

[117] Krishnamurthy N. and Graddy D. E., Correlation between 2- and 3- Dimensional Finite Element Analysis of Steel Bolted End-Plate Connections. Computers and Structures, 1976. **6**: p. 381-389.

[118] Kukreti A. R., Murray T. M., and Abolmaali A., End-Plate Connection Moment-Rotation Relationship. Journal of Constructional Steel Research, 1987. **8**: p. 137-157.

[119] Vegte G. J., Makino Y., and Sakimoto T., Numerical Research on Single Bolted Connections Using Implicit and Explicit Solution Techniques. Memoirs of the Faculty of Engineering, Kumamato University, 2002. **47**.

[120] Bursi O. S. and Jaspart J. P., Benchmarks for Finite Element Modelling of Bolted Steel Connections. Journal of Constructional Steel Research, 1997. **43**: p. 17-42.

[121] Bursi O. S. and Jaspart J. P., Calibration of a Finite Element Model for Isolated Bolted End-Plate Steel Connection. Journal of Constructional Steel Research, 1997. **44**: p. 225-262.

[122] Wheeler A. T., Clarcke M. J., and Hancock G. J., FE Modelling of Four Bolt Tubular Moment End-Plate Connections. Journal of Structural Engineering, 2000. **126**: p. 816-822.

[123] Qureshi J., Finite element modelling of steel-concrete composite structures, in School of Civil Engineering. 2010, University of Leeds.

[124] Abdullah R., Paton-Cole V. P., and Easterling W. S., Quasi-static analysis of composite slab. Malysian Journal of Civil Engineering, 2007. **19(2)**: p. 91-103.

[125] Natário P., Silvestre N., and Camotim D., Web crippling failure using quasi-static FE models. Thin-Walled Structures, 2014. **84**: p. 34-49.

[126] The Oklahoma City bombing: improving building performance though multi-hazard mitigation. 1996, Washington DC.

[127] Kurşun A., Şenel M., Enginsoy H. M., and Bayraktar E., Effect of impactor shapes on the low velocity impact damage of sandwich composite plate: experimental study and modelling. Composites Part B: Engineering, 2016. **86**: p. 143-151.

[128] Mitrevski T., Marshall I. H., R.S.Thomson, and Jones R., Low-velocity impacts on preloaded GFRP specimens with various impactor shapes. Composite structures, 2006. **76(3)**: p. 209-217.

[129] Veritas D. N., Design against accidental loads. Recommended Practice DNV-RP-C204. 2010.

[130] EN 1993 C.E.N., 2005. 1-8. Eurocode 3: design of steel structures. Part1-8: Design of Joint.

[131] Zhao W. and Tong G. S., Demand on Stiffeners in Stiffened Extended End-plate Connections. Advances in Structural Engineering, 2012. **15(8)**: p. 1455-1469.